UNIVERSITÀ DEGLI STUDI DI PISA

FACOLTÀ DI SCIENZE MATEMATICHE, FISICHE E NATURALI
CORSO DI DOTTORATO IN MATEMATICA

Variational methods and Hamiltonian perturbation theory applied to the N-body problem

A theoretical and computational approach

Relatore:
Prof. Giovanni Federico Gronchi

Candidato:
Marco Fenucci

Il coordinatore del Corso di Dottorato:
Prof. Giovanni Alberti

CYCLE XXXII

Contents

Introduction

Preface

During my Ph.D. program, I decided to study two different main topics of Celestial Mechanics. The first topic concerns variational methods applied to the N-body problem, from both the theoretical and computational point of view. This choice comes from the mathematical background that I have earned during my Bachelor and Master degree studies. The second topic is about Hamiltonian perturbation theory applied to the restricted N-body problem with orbit crossing singularities. This last choice arises from my wish of applying the mathematics that I have learned during my studies also to realistic problems in Astronomy, like the study of the long term evolution of planet crossing asteroids.

Part I: Action minimizing solutions and numerical computations

The classical Newtonian N-body problem, for its history and its challenges, is a fundamental problem in mathematical physics. The law of universal gravitation was formulated by Isaac Newton in his *Philosophiae Naturalis Principia Mathematica* in 1687, where he also solved the 2-body problem, providing a mathematical proof of the three Kepler's laws. In particular, the first Kepler law says that the motion of the planets is periodic and their trajectories are ellipses, with the Sun at one of the two foci. Since then, many mathematicians worked on this problem.

The importance of periodic solutions is well described by Henri Poincaré in his book *Les méthodes nouvelles de la mécanique céleste*, published in three volumes between 1892 and 1899.

> *Ce qui rend ces solutions périodiques aussi précieuses, c'est qu'elle sont, pour ainsi dire, la seule brèche par où nous puissions pénétrer dans une place jusqu'ici réputée inabordable.*
>
> Henri Poincaré, *Les méthodes nouvelles de la mécanique céleste.*

This means that periodic orbits are a precious tool to deeply understand the structure of the phase space, so that knowing their existence and stability properties is a fundamental issue to be investigated, not only for the N-body problem, but for general dynamical problems.

In the 3-body problem, some famous periodic solutions were found first by Leonard Euler. In 1762, he considered the circular restricted 3-body problem and proved the

existence of particular periodic solutions, in which the three particles are always collinear. Later on, Joseph-Louis Lagrange expanded and generalized the results of Euler. In 1772, he found periodic orbits where the particles are placed at the vertexes of an equilateral triangle, which uniformly rotates around its center. Nowadays these solutions are commonly known as *Lagrangian points* and they play a prominent role in planning space missions. Moreover, he discovered other particular periodic solutions for the non-restricted 3-body problem, in which every particle is placed on a 2-body ellipse. This is a particular case of a *homographic central configuration*, a notion which was extended later to the problem of N bodies. In the 19th century, Poincaré himself proved the existence of infinitely many periodic orbits in the restricted circular 3-body problem using a perturbative approach, and searching for fixed points of first return maps defined on sections transversal to the flow. Since then, some particular periodic solutions were found as relative equilibria, or by different approaches such as perturbative or topological methods.

More recently, a new and unexpected periodic solution of the 3-body problem was computed numerically by C. Moore [77] in 1993. In this orbit, three equal masses follow the same eight-shaped curve with a Dihedral symmetry, with the same time law but with a constant time-shift, see Figure 1.

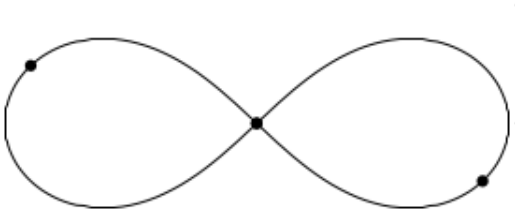

Figure 1: The Figure Eight solution of the 3-body problem.

A mathematical proof of its existence was provided in 2000 by A. Chenciner and R. Montgomery [20]. Their idea was to apply Hamilton's principle, which relates the solutions of the Euler-Lagrange equation coming from a Lagrangian $L(t, u, \dot{u})$, to the stationary points of the action functional

$$\mathcal{A}(u) = \int_0^T L(t, u(t), \dot{u}(t))\, dt,$$

where $T > 0$ is the fixed period. One can search for particular stationary points, such as minimizers. The idea of minimizing the action still goes back to Poincaré [87, 88], and he understood that collisions are the main obstruction in using the variational method, since they give a finite contribution to the action. After the work of Chenciner and Montgomery, many authors faced the N-body problem using variational techniques and many action minimizing periodic solutions were found.

Besides the theoretical work, numerical methods played an essential role in understanding and finding such solutions too. Indeed, C. Moore computed a Figure Eight

solution using a numerical method implementing the minimization of the action. In the early 2000s, C. Simó was able to compute many solutions in which N equal masses share a common planar trajectory, which is followed with the same time law and a constant time-shift. He named *choreographies* these particular solutions. Figures and videos of his solutions can be found at the websites [94, 95]. Moreover, the increasing computational power available nowadays led also to the development of rigorous numerical techniques, which have been used to provide computer-assisted proofs of existence and stability (or instability) of choreographies.

Part I of this thesis is structured as follows. In Chapter 1, we review the Calculus of Variation techniques and recall the proof of the existence of periodic orbits sharing the symmetry of a Platonic polyhedron, following [40]. Moreover, we provide an algorithm to enumerate them, in order to produce a list of periodic orbits.

In Chapter 2, we modify the previous problem by adding a massive body at the center. Imposing both symmetry and topological constraints, we are still able to prove the existence of periodic orbits, found as minimizers of the action. Moreover, we apply Γ-convergence theory to understand their asymptotic behaviour as the value of the central mass goes to infinity.

In Chapter 3, we introduce the theory of local minimizers for periodic problems. The theory for fixed-ends problems is a classical topic in Calculus of Variations and it is essentially well known. Here we discuss its extension to the case of periodic boundary conditions, underlying the difficulties that arise. Moreover, we test the theory applying it to the Kepler problem and the periodic orbits found in Chapter 1.

Chapter 4 is devoted to the description of numerical methods used to compute periodic orbits, both rigorous and non-rigorous. The basic idea to search for minimizers of the action is to consider a finite dimensional loop space, such as the space of truncated Fourier series, and then apply an iterative method to reduce the value of the action. Furthermore, the periodic orbit is refined using a multiple shooting method. On the other hand, rigorous methods aim at producing computer-assisted proofs and they are based on interval arithmetics, useful to control the numerical errors.

In Chapter 5, we apply numerical methods to the compute periodic orbits described in Chapters 1 and 2. In particular, we were able to provide a computer-assisted proof of the instability for a few of them. Moreover, we considered a system composed by charged particles, which reminds the Rutherford model of the atom. Here we were still able to compute periodic orbits, analyzing their stability. Using the theory of local minimizers introduced in Chapter 3, we studied their variational nature. It turns out that these orbits are not minimizers of the action, not even directionally, but rather saddle points.

Part II: The full and the averaged CR3BP

In many physical problems it may happen that the quantities involved do not evolve significantly on the same timescale. We can find some examples of this behaviour in Celestial Mechanics. For instance, the rotation axis of the Earth shifts its orientation periodically, with a period of approximately 25 772 years, with a behaviour similar to a spinning top. This has the effect of changing our view of the fixed stars during the years:

indeed, Earth's rotation axis is currently pointing towards Polaris (commonly known as the North Star), while it will point towards Vega in about 13 000 years (see Figure 2). This process is also called *precession of the equinoxes* and it was already known by the ancient Greeks.

Another example, coming from astronomy, is the precession of the perihelia of the planets, due to their mutual gravitational interactions. This has been relevant in the history of Science, since it has played an important role in the development of general relativity. Indeed, the observed precession rate of the perihelion of Mercury was in disagreement with the predictions coming from classical Celestial Mechanics. The precession of the perihelion was computed using averaging methods and taking into account only the Newtonian gravitation. The discrepancy between the predictions and the observations was explained later with the introduction of general relativity by Albert Einstein, providing the first experimental proof of the validity of his new gravitational theory. However, hereafter we will not consider relativistic dynamical effects.

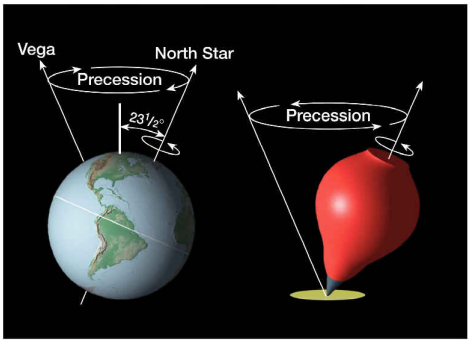

Figure 2: The precession of Earth's rotation axis.

The above results are typically obtained by averaging out all the short periodic perturbations, in order to capture only the long term behaviour of the system. This idea dates back to the 18th century, when Lagrange formulated the gravitational 3-body problem as a perturbation of the 2-body problem. Indeed, he took into account a system composed by the Sun, a planet and a small body (that we are going to call asteroid, for the sake of simplicity), which does not influence the motion of the larger bodies. The Sun and the planet move on circular orbits with a 2-body motion, while the asteroid undergoes the gravitational attraction of the two other objects. If the mass of the planet is small, compared to the mass of the Sun, the motion of the asteroid can be considered as a 2-body motion around the Sun, plus a small perturbation due to the presence of the planet itself. This problem is also known as *circular restricted* 3*-body problem* and it is the system that we take into account in this second part of the thesis. The fast variables involved are the two mean anomalies ℓ, ℓ' of the asteroid and the planet, respectively. The averaged evolution is obtained by averaging the vector field over ℓ, ℓ'. The *averaging principle* tells us that the solution of the averaged problem is a good approximation of the solution of the full problem. However, due to its physical nature, this is not a theorem and it cannot be applied in any situation.

In this second part, we study the relation between the solutions of the full circular restricted 3-body problem and the solutions of the averaged equations, even when the averaging principle can not be applied. In the averaged problem, the semimajor axis of the asteroid is a constant of motion: the averaging principle fails when, in the full problem, this value changes. This typically happens because of two reasons: close encounters between the planet and the asteroid, which deeply modify the value of the semimajor axis in a short time, or mean motion resonances, which periodically vary it over a long timescale. In this second case we can define a resonant normal form, which keeps all the resonant terms in the Hamiltonian, and use this model to make a comparison with the solutions of the full equations of motion.

Part II is structured as follows. In Chapter 6, we first recall the formulation of the averaged problem, focusing on the problematics produced by its singularities. Indeed, when the orbit of the asteroid crosses the orbit of the planet, the averaged Hamiltonian is infinite and the vector field is not defined. However, we can extend it introducing a discontinuity in the derivatives, and in this way we are able to continue a solution beyond an orbit crossing. Later, we introduce the resonant normal form, which aims to capture the long term behaviour of the system in presence of mean motion resonances between the planet and the asteroid. Finally, we recall the Kustaanheimo-Stiefel regularization, used to accurately integrate the full circular restricted 3-body problem near close encounters. This is needed to make a comparison between the two systems.

In Chapter 7 we show the results obtained from our numerical experiments. Taking into account many solutions of the full equations, all with the same initial conditions for the slow variables, numerical simulations show a relation between them and the solution of the equations of motion of the normal form, in the sense that the solutions obtained through the normal form give statistical information on the solutions of the full circular restricted 3-body problem. However, a mathematical proof of this evidence is still lacking.

Part I

Action minimizing solutions and numerical computations

Chapter 1

Variational approach to the N-body problem

The existence of several periodic orbits of the Newtonian N-body problem has been proved by means of variational methods, see e.g. [20, 21, 38, 103, 104]. In all these works, periodic orbits are found as minimizers of the Lagrangian action functional and the bodies have all the same mass. In [18], periodic orbits with different values for the masses are found. One difficulty with the variational approach is that the action is not coercive on the whole space of T-periodic loops, for which a natural choice is the Sobolev space of T-periodic loops in H^1, denoted with $H^1_T(\mathbb{R}, \mathbb{R}^n)$. We can overcome this problem by restricting the domain of the action to symmetric loops or by adding topological constraints, e.g. as done in [31, 11, 44]. Another difficulty is to prove that the minimizers are free of collisions. For this purpose we can use different techniques, like level estimates or local perturbations, see for example [65, 19, 17].

In this chapter, we first recall the direct method of Calculus of Variations, providing the general setting of the variational formulation of the N-body problem and discussing the main obstructions mentioned above. Then we focus on periodic motions of N equal masses, sharing the symmetry of Platonic polyhedra (that is, *Tetrahedron, Cube, Octahedron, Dodecahedron* and *Icosahedron*), which minimize the Lagrangian action on suitable sets of T-periodic loops, for a given $T > 0$. A proof of the existence of these orbits is given in [40], and here we recall the main fundamental steps. Later, we present an algorithm to enumerate all the orbits that can be found following this proof. Part of this work has been published in [37].

1.1 The direct method of Calculus of Variations

Let X be a set endowed with a notion of convergence and $\mathcal{A} : X \to \overline{\mathbb{R}} := \mathbb{R} \cup \{\pm\infty\}$ be a functional. With the term *direct method of Calculus of Variation* we mean a set of mathematical tools aimed to prove the existence of

$$\min\{\mathcal{A}(u) : u \in X\}.$$

Here we recall the fundamental tools to state a first theorem, which are the *lower semicontinuity* and the *coercivity*. For an extensive treatment of the direct method of Calculus of Variations, the interested reader can refer, for instance, to [25].

Definition 1.1. A functional $\mathcal{A} : X \to \overline{\mathbb{R}}$ is said to be *lower semicontinuous* if for every sequence $\{u_n\}_{n\in\mathbb{N}} \subseteq X$ such that

$$\lim_{n\to\infty} u_n = u_\infty,$$

we have that

$$\liminf_{n\to\infty} \mathcal{A}(u_n) \geq \mathcal{A}(u_\infty).$$

Definition 1.2. A functional $\mathcal{A} : X \to \overline{\mathbb{R}}$ is said to be *coercive* if for every $t \in \mathbb{R}$ there exists a closed and sequentially compact set $K_t \subseteq X$ such that the t sub-level of $\mathcal{A}$ is contained in K_t, i.e.

$$\{u \in X : \mathcal{A}(u) \leq t\} \subseteq K_t.$$

Theorem 1.3 (Tonelli's Theorem)**.** *Let $\mathcal{A} : X \to \overline{\mathbb{R}}$ be a lower semicontinuous coercive functional. Then there exists a minimum point $u^* \in X$.*

Proof. If $\mathcal{A}$ is always equal to $+\infty$, there is nothing to prove. Suppose that $I = \inf_X \mathcal{A} \in \mathbb{R} \cup \{-\infty\}$. Then there exists a minimizing sequence $\{u_n\}_{n\in\mathbb{N}} \subseteq X$ such that

$$\lim_{n\to\infty} \mathcal{A}(u_n) = I.$$

Therefore, there exists $L \in \mathbb{R}$ such that

$$\mathcal{A}(u_n) \leq L, \quad \forall n \in \mathbb{N},$$

hence $\{u_n\}_{n\in\mathbb{N}}$ is completely contained in a sequentially compact set, since $\mathcal{A}$ is coercive. Thus the sequence $\{u_n\}_{n\in\mathbb{N}}$ admits a subsequence $\{u_{n_k}\}_{k\in\mathbb{N}}$ which converges to a point $u^* \in X$. From the lower semicontinuity of $\mathcal{A}$ we have that

$$I \leq \mathcal{A}(u^*) \leq \liminf_{k\to\infty} \mathcal{A}(u_{n_k}) = \lim_{k\to\infty} \mathcal{A}(u_k) = I,$$

hence $I \in \mathbb{R}$ and u^* is a minimum point. □

Let us observe that the two hypotheses of Tonelli's Theorem are in some kind of conflict, since to have the lower semicontinuity we need a rather strong topology, while for the coercivity we need a rather weak topology. The direct method of Calculus of Variations consists in determine the right topology on the set X which satisfies both conditions, ensuring the existence of the minimum of $\mathcal{A}$.

Let us consider an integral functional, i.e. suppose that $\mathcal{A}$ is of the type

$$\mathcal{A}(u) = \int_a^b L(t, u, \dot{u})dt,$$

where $[a, b] \subseteq \mathbb{R}$ is an interval, $L : [a, b] \times \Omega \to \mathbb{R}$ is a C^2 function usually called *Lagrangian*, $\Omega \subseteq \mathbb{R}^n \times \mathbb{R}^n$ is an open set and $u : [a, b] \to \mathbb{R}^n$ is a C^1 curve. We consider $\mathcal{A}$ defined on a subset Y such that

$$Y \subseteq C^1([a, b], \mathbb{R}^n).$$

Defined in this way, $\mathcal{A}$ is usually not coercive on Y endowed with the uniform convergence, since in general the sublevels

$$\{u \in Y : \mathcal{A}(u) \leq t\},$$

are not sequentially compact. This problem can be faced by assuming that $\mathcal{A}$ is defined on a subset of the *Sobolev space* $H^1([a, b], \mathbb{R}^n)$, endowed with the H^1 topology, which have further compactness properties (see for example [22] for an extensive treatment about Sobolev spaces). What is usually done, is to extend $\mathcal{A}$ to a functional $\tilde{\mathcal{A}} : X \to \overline{\mathbb{R}}$, where X is such that $Y \subseteq X \subseteq H^1([a, b], \mathbb{R}^n)$, and $\tilde{\mathcal{A}}$ satisfies

(i) $\tilde{\mathcal{A}}(u) \leq \mathcal{A}(u)$ for all $u \in Y$,

(ii) $\tilde{\mathcal{A}}$ is lower semicontinuous and coercive on X,

(iii) the minimum point u^* of $\tilde{\mathcal{A}}$ belongs to Y and $\tilde{\mathcal{A}}(u^*) = \mathcal{A}(u^*)$.

In these hypotheses, it is straightforward that u^* is a minimum point for the original functional $\mathcal{A}$. It is worth noting that, in this extension process, we have to be particularly careful at the step (iii). In fact, at step (ii) Tonelli's Theorem provides us a minimizer u^* which belongs to the Sobolev space H^1, therefore the proof that u^* is in fact regular has to be done separately.

1.1.1 The N-body problem as a variational problem

Consider N point masses $m_1, \ldots, m_N$ subjected to their mutual gravitational attraction and let $u_i \in \mathbb{R}^3$ be the position of the i-th particle, $i = 1, \ldots, N$. Here we choose the units so that the gravitational constant G is unitary. The equations of motion for this problem are

$$m_i \ddot{u}_i = \frac{\partial U}{\partial u_i}(u), \quad i = 1, \ldots, N, \tag{1.1}$$

where

$$U(u) = \sum_{1 \leq h < k \leq N} \frac{m_h m_k}{|u_h - u_k|}, \tag{1.2}$$

is the potential. The map $\mathbb{R} \ni t \mapsto u = (u_1, \dots, u_N) \in \mathbb{R}^{3N}$ describes the evolution of the N particles in the three-dimensional space. The kinetic energy of the problem is given by

$$K(\dot{u}) = \frac{1}{2} \sum_{i=1}^{N} m_i |\dot{u}_i|^2.$$

Hence the Euler-Lagrange equations

$$\frac{d}{dt}\left(\frac{\partial L}{\partial \dot{u}_i}\right) - \frac{\partial L}{\partial u_i} = 0, \quad i = 1, \dots, N,$$

associated to the Lagrangian function

$$L(u, \dot{u}) = K(\dot{u}) + U(u), \tag{1.3}$$

correspond to the equations of motion (1.1) of the N-body problem. Fixed the period $T > 0$, using the variational formulation of the classical mechanics, we have that periodic orbits of (1.1) are stationary points of the Lagrangian action functional

$$\mathcal{A}(u) = \int_0^T L(u, \dot{u}) dt, \tag{1.4}$$

which, in a classical setting, is defined on the set of collision-less C^1 T-periodic loops

$$Y = \left\{ u \in C^1_T(\mathbb{R}, \mathbb{R}^{3N}) : u_i(t) \neq u_j(t) \ \forall t \in [0, T],\ 1 \leq i < j \leq N \right\}.$$

In particular, we can search for periodic solutions which are minimum points of $\mathcal{A}$, using the direct method of Calculus of Variations.

Extension of the functional

It is well known that for these type of problems, it is natural to extend the above functional on a subset which is contained in the Sobolev space of T-periodic loops $H^1_T(\mathbb{R}, \mathbb{R}^{3N})$, endowed with the norm

$$\|u\|_{H^1_T} = \left[\int_0^T |u(t)|^2 + |\dot{u}(t)|^2 dt \right]^{1/2},$$

where $\dot{u} \in L^2$ is the weak derivative of u in H^1. Using the integral of the center of mass we can assume $\sum_{h=1}^{N} m_h u_h = 0$ and consider the *configuration space*

$$\mathcal{X} = \left\{ x = (x_1, \dots, x_N) \in \mathbb{R}^{3N} : \sum_{h=1}^{N} m_h x_h = 0 \right\}.$$

In this way we extend the domain of (1.4) to the loop space

$$\Lambda = H^1_T(\mathbb{R}, \mathcal{X}).$$

The extension of $\mathcal{A}$ to Λ is simply done using the same formula (1.4), since the square of the weak derivative of a function $u \in H^1$ is integrable. Note also that $\mathcal{A}(u)$ can be $+\infty$, since Λ contains loops with collisions. Therefore, for the sake of simplicity, we still denote with $\mathcal{A}$ the extended functional, instead of $\tilde{\mathcal{A}}$.

Lower semicontinuity

The functional (1.4) is lower-semicontinuous on Λ. Indeed, if $\{u^{(k)}\}_{k\in\mathbb{N}} \subseteq \Lambda$ is a sequence such that $u^{(k)} \to u^\infty$ in H^1, then by the Ascoli-Arzelà Theorem $u^{(k)} \to u^\infty$ uniformly in $[0,T]$, up to subsequences. Moreover $\dot{u}^{(k)} \rightharpoonup \dot{u}^\infty$ in L^2, since the sequence is bounded in norm. Then from the Cauchy-Schwartz inequality we have

$$\liminf_{k\to\infty} \|\dot{u}^{(k)}\|_{L^2}^2 \geq \|\dot{u}^\infty\|_{L^2}^2,$$

hence the kinetic term of $\mathcal{A}$ is lower-semicontinuous. Furthermore, the uniform convergence of $\{u^{(k)}\}_{k\in\mathbb{N}}$, together with the continuity of the potential U, ensures that

$$\lim_{k\to\infty} \int_0^T U(u^{(k)}(t))dt = \int_0^T U(u^\infty(t))dt,$$

hence the functional (1.4) is lower-semicontinuous on Λ.

Coercivity

Note that on Λ, which is endowed with the H^1 norm, Definition 1.2 is equivalent to the following.

Definition 1.4. The functional $\mathcal{A} : \Lambda \to \overline{\mathbb{R}}$ is *coercive* if for every sequence $\{u^{(k)}\}_{k\in\mathbb{N}} \subseteq \Lambda$ such that

$$\lim_{k\to\infty} \|u^{(k)}\|_{H^1} = +\infty,$$

we have that

$$\lim_{k\to\infty} \mathcal{A}(u^{(k)}) = +\infty.$$

However, $\mathcal{A}$ is not coercive on the whole set of loops Λ. Consider for example the problem of 4 bodies and take the sequence

$$u^{(n)}(t) = (u_1^{(n)}(t), u_2^{(n)}(t), u_3^{(n)}(t), u_4^{(n)}(t)),$$

defined by

$$\begin{cases} u_1^{(n)}(t) = \left(n + \frac{1}{n}\cos\frac{2\pi t}{T}, n + \frac{1}{n}\sin\frac{2\pi t}{T}, 0\right), \\ u_2^{(n)}(t) = \left(-n + \frac{1}{n}\cos\frac{2\pi t}{T}, n + \frac{1}{n}\sin\frac{2\pi t}{T}, 0\right), \\ u_3^{(n)}(t) = \left(n + \frac{1}{n}\cos\frac{2\pi t}{T}, -n + \frac{1}{n}\sin\frac{2\pi t}{T}, 0\right), \\ u_4^{(n)}(t) = \left(-n + \frac{1}{n}\cos\frac{2\pi t}{T}, -n + \frac{1}{n}\sin\frac{2\pi t}{T}, 0\right). \end{cases}$$

They represent four circular trajectories of radius $1/n$ centered at the points $(\pm n, \pm n)$, covered in a time T with uniform motion: in this way we have that $\|u^{(n)}\|_{H^1_T} \to +\infty$. Since the mutual distances between the particles become larger and larger, the contribute of the potential part to the action is zero in the limit $n \to +\infty$. Furthermore, for the kinetic part we can compute directly that

$$|\dot{u}_i^{(n)}|^2 = \frac{4\pi^2}{n^2 T^2}, \quad i = 1, 2, 3, 4,$$

and then also the kinetic part tends to zero as $n \to \infty$: this is enough to show the lack of coercivity of $\mathcal{A}$. Later we shall see that we can recover the coercivity introducing some constraints on the space of admissible loops: in particular we will use both symmetry and topological constraints.

Collisions and regularity

Another obstruction is that minimizers of $\mathcal{A}$ may have collisions: indeed if u^* is a solution with a collision at time t_c, then from Sundman's estimates [110], we have that

$$|u^*(t)| = O(|t_c - t|^{2/3}), \quad |\dot{u}^*(t)| = O(|t_c - t|^{-1/3}),$$

for t near t_c, so that

$$K = O(|t_c - t|^{-2/3}), \quad U = O(|t_c - t|^{-2/3}).$$

Therefore the contribution of collisions to the action is finite, that is $\mathcal{A}(u^*) < +\infty$: hence to find minimizers that are solution of the classical N-body problem, we must exclude both partial and total collisions.

However, if we are able to prove that a minimizer $u^* \in \Lambda$ is collision-free, then we are also able to prove that it is smooth, and therefore a classical solution of the gravitational N-body problem. Indeed, in general, let us consider a functional $\mathcal{A} : \Lambda \to \mathbb{R}$ defined by

$$\mathcal{A}(u) = \int_0^T L(u(t), \dot{u}(t))dt,$$

where $\Lambda \subseteq H^1_T(\mathbb{R}, \mathbb{R}^n)$ is a set of T-periodic loops, where the period $T > 0$ is fixed. Moreover, assume that we have a mechanical system, so that the Lagrangian is of the form

$$L(u, \dot{u}) = \frac{\dot{u} \cdot M\dot{u}}{2} + U(u), \quad M = \mathrm{diag}(m_1, \dots, m_n),$$

where the potential U is defined on $\mathbb{R}^n \setminus \Gamma$, for a certain set $\Gamma \subseteq \mathbb{R}^n$, and it is regular enough (it will be sufficient continuous differentiable) and $m_i > 0$, $i = 1, \dots, n$. In the N-body problem, the set Γ plays the role of the collision set. Let us assume that $u^* \in \Lambda$ is a minimizer of $\mathcal{A}$ and it is "collision free", i.e. $u^*([0, T]) \cap \Gamma = \emptyset$: we want to show that, under these conditions, $u^* \in C^\infty_T(\mathbb{R}, \mathbb{R}^n)$. If we take as set of variations

$$\tilde{V} = \{v \in C^2_T(\mathbb{R}, \mathbb{R}^n) : v(0) = v(T) = 0\},$$

then fixed $v \in \tilde{V}$, the curve $u^* + \lambda v$ is still T-periodic and collision free for small values of λ, therefore we assume it belongs to the loop space Λ. Since u^* is a minimizer, its first variation is zero, that is

$$\frac{d}{d\lambda}\mathcal{A}(u^* + \lambda v)\Big|_{\lambda=0} = \int_0^T \left[(M\dot{u}^*(t)) \cdot \dot{v}(t) + \frac{\partial U(u^*(t))}{\partial u} \cdot v(t)\right] dt = 0, \quad \text{for all } v \in \tilde{V}.$$

Integrating by parts the second term of the integral and using the periodic boundary conditions, we obtain

$$\int_0^T \left[M\dot{u}^*(t) - \int_0^t \frac{\partial U(u^*(s))}{\partial u} ds\right] \cdot \dot{v}(t) dt = 0, \quad \text{for all } v \in \tilde{V}.$$

Since v is zero at the extrema, the integral mean over the period of its time derivative $\dot{v}$ is zero, then from the Du Bois-Reymond Lemma [43], we have that the integrating function is constant, that is

$$M\dot{u}^*(t) - \int_0^t \frac{\partial U(u^*(s))}{\partial u} ds = c \in \mathbb{R},$$

and finally we get

$$\dot{u}^*(t) = M^{-1}\big(F(t) + c\big), \quad F(t) = \int_0^t \frac{\partial U(u^*(s))}{\partial u} ds.$$

Since we have assumed that U is a continuous differentiable function, its derivative $\partial U/\partial u$ is a continuous function, and since u_* is a Lipschitz function, $F(t)$ is differentiable. From this we get that $\dot{u}^* \in C^1_T(\mathbb{R}, \mathbb{R}^n)$ and therefore $u^* \in C^2_T(\mathbb{R}, \mathbb{R}^n)$. Furthermore, by induction we obtain that $u^* \in C^\infty_T(\mathbb{R}, \mathbb{R}^n)$.

1.2 Minimizers with the symmetry of Platonic polyhedra

We recall here the steps of the proof of the existence of periodic orbits given in [40]. Let us fix $T > 0$ and let $\mathcal{R}$ be the rotation group of one of the five Platonic polyhedra. We recall that the pairs (Cube, Octahedron) and (Dodecahedron, Icosahedron) share the same rotation group, that we call $\mathcal{O}$ and $\mathcal{I}$ respectively. Moreover, we denote by $\mathcal{T}$ the rotation group of the Tetrahedron, therefore $\mathcal{R} \in \{\mathcal{T}, \mathcal{O}, \mathcal{I}\}$. We consider the motion of $N = |\mathcal{R}|$ particles with unitary mass, hence $N = 12, 24, 60$ for $\mathcal{R} = \mathcal{T}, \mathcal{O}, \mathcal{I}$ respectively. Let us denote by

$$u_I : \mathbb{R} \to \mathbb{R}^3,$$

the map describing the motion of one of these particles, arbitrarily selected, that we call *generating particle*. Assume that

(a) the motion u_R, $R \in \mathcal{R} \setminus \{I\}$ of the other particles fulfills the relation

$$u_R = Ru_I, \tag{1.5}$$

(b) the trajectory of the generating particle belongs to a given non-trivial free-homotopy class of $\mathbb{R}^3 \setminus \Gamma$, where

$$\Gamma = \cup_{R \in \mathcal{R} \setminus \{I\}} r(R),$$

with $r(R)$ the rotation axis of R.

(c) there exist $R \in \mathcal{R}$ and $M > 0$ such that

$$u_I(t + T/M) = R u_I(t), \tag{1.6}$$

for all $t \in \mathbb{R}$.

Imposing the symmetry (1.5), the action functional of the N-body problem depends only on the motion of the generating particle and it is expressed by

$$\mathcal{A}(u_I) = N \int_0^T \left(\frac{1}{2} |\dot{u}_I|^2 + \frac{1}{2} \sum_{R \in \mathcal{R} \setminus \{I\}} \frac{1}{|(R - I)u_I|} \right) dt. \tag{1.7}$$

We search for periodic motions by minimizing $\mathcal{A}$ on subsets $\mathcal{K}$ of a Sobolev space of T-periodic maps. More precisely, we choose the cones

$$\mathcal{K} = \{u_I \in H^1_T(\mathbb{R}, \mathbb{R}^3) : (b), (c) \text{ hold}\}. \tag{1.8}$$

1.2.1 Encoding $\mathcal{K}$ and proving the existence of minimizers

We describe two ways to encode the topological constraints defining the cones $\mathcal{K}$. Let $\tilde{\mathcal{R}}$ be the full symmetry group (including reflections) related to $\mathcal{R}$. The reflection planes induce a tessellation of the unit sphere $\mathbb{S}^2$, as shown in Figure 1.1, with $2N$ spherical triangles. Each vertex of such triangles corresponds to a pole $p \in \mathcal{P} = \Gamma \cap \mathbb{S}^2$. Let us

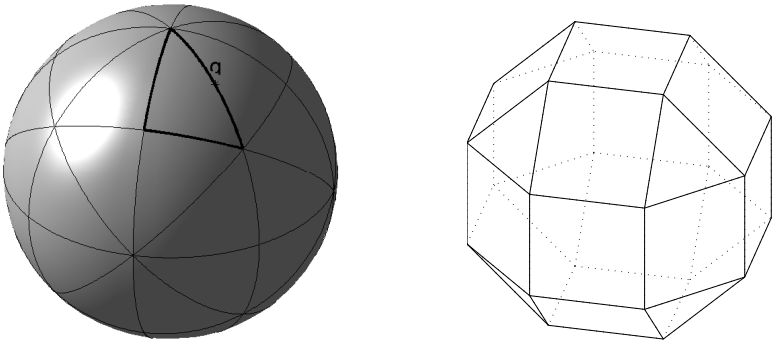

Figure 1.1: Tessellation of $\mathbb{S}^2$ for $\mathcal{R} = \mathcal{O}$ and the Archimedean polyhedron $\mathcal{Q}_{\mathcal{O}}$.

select one triangle, say τ. By a suitable choice of a point $q \in \partial\tau$ (see Figure 1.1) we can define an Archimedean polyhedron $\mathcal{Q}_{\mathcal{R}}$, which is the convex hull of the orbit of q under $\mathcal{R}$, and therefore it is strictly related to the symmetry group $\mathcal{R}$. For details see [40].
We can characterize a cone $\mathcal{K}$ by a periodic sequence $\mathfrak{t} = \{\tau_k\}_{k \in \mathbb{Z}}$ of triangles of the tessellation such that τ_{k+1} shares an edge with τ_k and $\tau_{k+1} \neq \tau_{k-1}$ for each $k \in \mathbb{Z}$. This

sequence is uniquely determined by $\mathcal{K}$ up to translations, and describes the homotopy class of the admissible paths followed by the generating particle (see Figure 1.2, left). We can also characterize $\mathcal{K}$ by a periodic sequence $\nu = \{\nu_k\}_{k\in\mathbb{Z}}$ of vertexes of $\mathcal{Q}_\mathcal{R}$ such that the segment $[\nu_k, \nu_{k+1}]$ is an edge of $\mathcal{Q}_\mathcal{R}$ and $\nu_{k+1} \neq \nu_{k-1}$ for each $k \in \mathbb{Z}$. Also the sequence ν is uniquely determined by $\mathcal{K}$ up to translations, and with it we can construct a piecewise linear loop v, joining consecutive vertexes ν_k with constant speed, that represents an element of the cone $\mathcal{K}$ (see Figure 1.2, right).

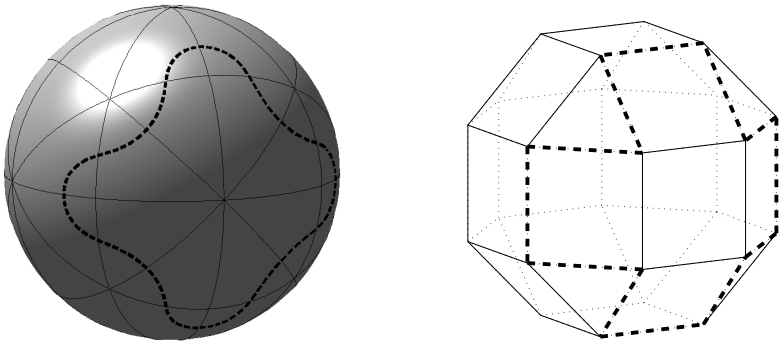

Figure 1.2: Encoding a cone $\mathcal{K}$. Left: the dashed path on $\mathbb{S}^2$ describes the periodic sequence $\mathfrak{t}$ of triangles of the tessellation. Right: the dashed piecewise linear path describes the corresponding periodic sequence ν of vertexes of $\mathcal{Q}_\mathcal{O}$.

The existence of a minimizer u_I^* of $\mathcal{A}$ restricted to a cone $\mathcal{K} = \mathcal{K}(\nu)$ can be shown by Tonelli's Theorem 1.3, provided that

$$\bigcap_{\tau_j\in\mathfrak{t}} \overline{\tau_j} = \emptyset, \tag{1.9}$$

where $\mathfrak{t}$ is the sequence of spherical triangles corresponding to $\mathcal{K}$. Indeed, we have already seen that the action functional is lower-semicontinuous. The coercivity is recovered from the fact that, by condition 1.9, there exists $c_\mathcal{K} > 0$ such that

$$|u_I(t)| \leq (1/c_\mathcal{K} + 1) \max_{t_1,t_2\in[0,T]} |u_I(t_1) - u_I(t_2)|,$$

for all $t \in [0, T]$ and $u_I \in \mathcal{K}$. This is sufficient to conclude that the integral of the kinetic energy goes to plus infinity as a sequence of periodic loops goes to infinity in H^1 norm. Note that condition (1.9) means that the trajectory of the generating particles does not wind around one rotation axis only.

For later use we introduce the following definitions.

Definition 1.5. We say that a cone $\mathcal{K}$ is *simple* if the corresponding sequence $\mathfrak{t}$ does not contain a string $\tau_k \dots \tau_{k+2\mathfrak{o}}$ such that

$$\bigcap_{j=0}^{2\mathfrak{o}} \overline{\tau_{k+j}} = p,$$

where $p \in \mathcal{P}$ and $\mathfrak{o}$ is the order of p, which corresponds to the order of its associated rotation.

Definition 1.6. We say that a cone $\mathcal{K}$ *winds around two coboundary axes* if

(i) the corresponding sequence $\mathfrak{t}$ is the union of two strings, $\tau_{k_j} \dots \tau_{k_j+2\mathfrak{o}_j-1}$, $j = 1, 2$, such that
$$\bigcap_{h=0}^{2\mathfrak{o}_j-1} \overline{\tau_{k_j+h}} = p_j,$$
where $\mathfrak{o}_j$ is the order of p_j, for two different poles p_1, p_2;

(ii) there exists $\tau_k \in \mathfrak{t}$ such that $p_1, p_2 \in \overline{\tau_k}$.

To show that for a suitable choice of $\mathcal{K}$ the minimizers are collision-free we consider total and partial collisions separately.

1.2.2 Total collisions

To exclude total collisions we use *level estimates*, i.e. first we prove that there exists $a \in \mathbb{R}$ such that if u^* is a solution with total collisions, then $\mathcal{A}(u^*) \geq a$. Then we search for an admissible loop u such that $\mathcal{A}(u) < a$, hence minimizers do not have total collisions. The fundamental estimate, that can be adapted depending on the problem we are dealing with, is the following.

Proposition 1.7. *Let $u : [0, \mathrm{T}] \to \mathbb{R}^{3N}$ be a motion of N masses $m_1, \dots, m_N$ connecting a total ejection at time $t = 0$ to a total collision at time $t = \mathrm{T}$. Then for the action*
$$\mathcal{A}(u) = \int_0^{\mathrm{T}} \Big(\frac{1}{2} \sum_{i=1}^{N} m_i |\dot{u}_i|^2 + \sum_{1 \leq i < j \leq N} \frac{1}{|m_i - m_j|} \Big) dt,$$
we have the estimate
$$\mathcal{A}(u) \geq \frac{3}{2} \mathcal{M} (\pi U_0)^{2/3} \mathrm{T}^{1/3}, \quad \mathcal{M} = \sum_{i=1}^{N} m_i, \tag{1.10}$$
where
$$U_0 = \min_{\rho(u)=1} U(u), \quad U(u) = \frac{1}{\mathcal{M}} \sum_{\substack{i,j=1 \\ i \neq j}}^{N} \frac{1}{|u_i - u_j|}, \quad \rho(u) = \Big(\sum_{i=1}^{N} \frac{m_i}{\mathcal{M}} |u_i|^2 \Big)^{1/2}.$$

Proof. For the function ρ we have that
$$\sum_{i=1}^{N} \frac{m_i}{\mathcal{M}} |\dot{u}_i|^2 \geq \dot{\rho}^2(u).$$
Therefore we have that
$$\mathcal{A}(u) \geq \frac{\mathcal{M}}{2} \int_0^{\mathrm{T}} \Big(\dot{\rho}^2(u) + \frac{1}{\rho(u)} U\Big(\frac{u}{\rho(u)} \Big) \Big) dt \geq \frac{\mathcal{M}}{2} \int_0^{\mathrm{T}} \Big(\dot{\rho}^2 + \frac{U_0}{\rho} \Big) dt.$$

The right hand side of the inequality corresponds to the action of the Kepler problem, in which the gravitational constant is equal to U_0. From the estimates given by [44] for the Kepler problem, we have

$$\mathcal{A}(u) \geq \frac{3}{2}\mathcal{M}(\pi U_0)^{2/3}\mathrm{T}^{1/3}.$$

□

We note that a total collision of the N particles occurs at time t_c if and only if $u_I(t_c) = 0$. If there is a total collision then, by condition (c), there are M of them per period. For a minimizer u_I^* with a total collision, *a priori* estimates for its action are found using Proposition 1.7 as

$$\mathcal{A}(u_I^*) \geq \alpha_{\mathcal{R},\mathcal{M}}, \tag{1.11}$$

where $\alpha_{\mathcal{R},\mathcal{M}}$ depends only on M and T. Rounded values of $\alpha_{\mathcal{R},\mathcal{M}}$ for $T = 1$ are computed in [40] and reported in Table 1.1. For some sequences ν, the action of the related

$\mathcal{R} \diagdown M$	1	2	3	4	5
$\mathcal{T}$	132.695	210.640	276.017	/	/
$\mathcal{O}$	457.184	725.734	950.981	1152.032	/
$\mathcal{I}$	2296.892	3646.089	4777.728	/	6716.154

Table 1.1: Lower bounds $a_{\mathcal{R},M}$ for loops with M total collisions ($T = 1$).

piecewise linear loop v is lower than $\alpha_{\mathcal{R},\mathcal{M}}$. Therefore, minimizing the action over the cones $\mathcal{K}$ defined by such sequences yields minimizers without total collisions. The action of the piecewise linear loop v can be computed explicitly and for $T = 1$ it is given by

$$\mathcal{A}(v) = \frac{3}{2 \cdot 4^{1/3}} N\ell^{2/3}(k_1\zeta_1 + k_2\zeta_2)^{2/3}, \tag{1.12}$$

where k_1, k_2 are the numbers of sides of the two different kinds (i.e. separating different pairs of polygons) in the trajectory of v, ℓ is the length of the sides (assuming $\mathcal{Q}_{\mathcal{R}}$ is inscribed in the unit sphere) and ζ_1, ζ_2 are the values of explicitly computable integrals, see Table 1.2. Relations (1.11) and (1.12) will be useful later in Section 1.3.

$\mathcal{R}$	$\mathcal{T}$	$\mathcal{O}$	$\mathcal{I}$
ℓ	1.0	0.7149	0.4479
ζ_1	9.5084	20.3225	53.9904
ζ_2	9.5084	19.7400	52.5762

Table 1.2: Numerical values of ℓ, ζ_1, ζ_2.

1.2.3 Partial collisions

Because of the symmetry, a partial collision occurs at time t_c if and only if $u_I(t_c) \in \Gamma\backslash\{0\}$, that is when the generating particle passes through a rotation axis r. Indeed, in this case all the particles collide in separate clusters, each containing as many particles as the order of r. We summarize below the technique used in [40] to deal with partial collisions.

Assume that the minimizer $u^* \in \overline{\mathcal{K}}$ has a partial collision at time $t = t_c$. From results presented in [38], we can assume that the collision is isolated in time. Since u^* is a minimizer, if (t_1, t_2) is an interval of regularity, then the generating particle u_I^* solves the Euler-Lagrange equation of (1.7), which is

$$\ddot{w} = \sum_{R\in\mathcal{R}\backslash\{I\}} \frac{(R-I)w}{|(R-I)w|^3}, \quad t \in (t_1, t_2). \tag{1.13}$$

Let r be the rotation axis on which the generating particle collides and let $\mathcal{C}$ be the subgroup (of order $\mathfrak{o}_\mathcal{C}$) of the rotations with axis r. We can rewrite equation (1.13) and the first integral of the energy in the form

$$\ddot{w} = \alpha\frac{(R_\pi - I)w}{|(R_\pi - I)w|^3} + V_1(w), \quad \alpha = \sum_{j=1}^{\mathfrak{o}_\mathcal{C}-1} \frac{1}{\sin\left(\frac{j\pi}{\mathfrak{o}_\mathcal{C}}\right)}, \tag{1.14}$$

$$|\dot{w}|^2 - \alpha\frac{1}{|(R_\pi - I)w|} - V(w) = h, \tag{1.15}$$

where R_π is the rotation of π around r, $V_1(w)$ and $V(w)$ are smooth functions defined in an open set $\Omega \subseteq \mathbb{R}^3$ that contains $r \setminus \{0\}$. Moreover, if $\tilde{R} \in \tilde{\mathcal{R}}$ is a reflection such that $\tilde{R}r = r$, then V_1, V satisfy the conditions

$$V_1(\tilde{R}w) = \tilde{R}V_1(w), \quad V(\tilde{R}w) = V(w). \tag{1.16}$$

The form (1.14) of Newton's equation is well suited for the analysis of partial collisions occurring on r and, in particular, it implies that all the partial collisions a minimizer $u^* \in \overline{\mathcal{K}}$ may present can be regarded as binary collisions. Note that, every time we are in this situation, partial collisions can be excluded with the same technique that we are going to summarize.

From [40] (see, alternatively Appendix B), we can associate to a partial collision two unit vectors $\mathsf{n}^+, \mathsf{n}^-$, orthogonal to the collision axis r, corresponding to the ejection and collision limit directions, respectively. The angle formed by these two directions is called *collision angle*. Moreover, we say that a collisions is of type $(\rightrightarrows)$ if

(i) $\mathsf{n}^+ = \mathsf{n}^-$, and

(ii) the plane $\pi_{r,\mathsf{n}}$ generated by r and $\mathsf{n} = \mathsf{n}^\pm$ is fixed by some reflection $\tilde{R} \in \tilde{\mathcal{R}}$.

A useful tool which helps in constructing local perturbations, which are free of collisions, is the *Marchal Lemma*, appearing in several papers [65, 19, 38, 76]. Here we recall the version given in [40].

Lemma 1.8 (Marchal's Lemma)**.** *Let $u_A, u_B \in \mathbb{R}^2 \setminus \{0\}$ such that $|u_A| = |u_B|$, let $u_0 : [-\tau, \tau] \to \mathbb{R}^2$ be the parabolic collision-ejection solution such that*

$$u_0(-\tau) = u_A, \quad u_0(\tau) = u_B, \quad u_0(0) = 0,$$

and set

$$\mathtt{n}^- = \frac{u_A}{|u_A|}, \quad \mathtt{n}^+ = \frac{u_B}{|u_B|}.$$

Denote with

$$\mathcal{A}(u) = \int_{-\tau}^{\tau} \Big(\frac{|\dot{u}|^2}{2} + \frac{\kappa}{|u|} \Big) dt, \quad \kappa > 0,$$

the Keplerian action. Then

(i) if $\mathtt{n}^+ \cdot \mathtt{n}^- \neq 1$ there exist exactly two Keplerian arcs $u_d, u_i : [-\tau, \tau] \to \mathbb{R}^2$, called direct and indirect arcs, such that

$$u_d(-\tau) = u_i(-\tau) = u_A, \quad u_d(\tau) = u_i(\tau) = u_B,$$

and

$$\begin{cases} u_d([-\tau, \tau]) \subseteq \{a_1\mathtt{n}^- + a_2\mathtt{n}^+, a_i > 0\}, \\ u_i([-\tau, \tau]) \subseteq \mathit{Span}\{\mathtt{n}^+, \mathtt{n}^-\} \setminus \{a_1\mathtt{n}^- + a_2\mathtt{n}^+, a_i \geq 0\}. \end{cases}$$

Moreover

$$\mathcal{A}(u_d) < \mathcal{A}(u_0), \quad \mathcal{A}(u_i) < \mathcal{A}(u_0).$$

(ii) if $\mathtt{n}^+ \cdot \mathtt{n}^- = 1$ (i.e. $\mathtt{n}^+ = \mathtt{n}^- := \mathtt{n}$ and $u_A = u_B$), there exists only the direct arc $u_d : [-\tau, \tau] \to \mathbb{R}^2$, such that

$$u_d(-\tau) = u_A, \quad u_d(\tau) = u_A,$$

and

$$u_d([-\tau, \tau]) \subseteq \{a\mathtt{n}, a > 0\}.$$

Moreover

$$\mathcal{A}(u_d) < \mathcal{A}(u_0).$$

It turns out that, if u_I^* is a solution with a partial collision and the cone $\mathcal{K}$ is simple, then necessarily the collision is of type ($\rightrightarrows$). Indeed, if that would not be the case, then the collision angle θ is such that

$$-\frac{\pi}{\mathfrak{o}_r} \leq \theta < 2\pi.$$

Moreover, using the *blow-up technique* (see [108, 38]), u_I^* can be treated as a parabolic collision-ejection solution, near the collision. More specifically, let us suppose that

the collision takes place at $t_c = 0$. Up to translations, we can also suppose that $\lim_{t\to 0^+} u_I^*(t) = 0$. Rescaling the generating particle as

$$w^\lambda : [0,1] \to \mathbb{R}^3, \quad w^\lambda(t) = \lambda^{2/3} u_I^*(t/\lambda),$$

we have that $\{w^\lambda\}_\lambda$ converges uniformly in $[0,1]$ as $\lambda \to +\infty$. The limit is the parabolic ejection motion

$$s^\alpha(t)\mathtt{n}^+, \quad s^\alpha(t) = \frac{3^{3/2}}{2}\alpha^{1/3}t^{1/3}.$$

Therefore, local perturbations of u_I^* which are collision-free can be constructed using the direct and indirect arcs, see Figure 1.3 for a sketch of the construction. By Marchal's Lemma, the action of these local perturbations is lower than the action of the collision solution u_I^*, then we have a contradiction.

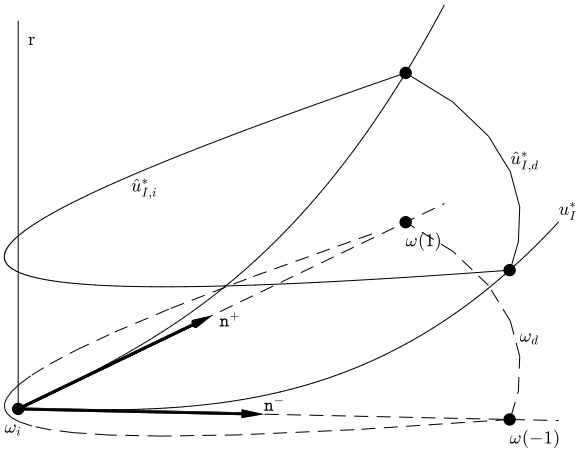

Figure 1.3: The construction of a local perturbation without collisions

In case of collision of type ($\rightrightarrows$), by a uniqueness result (see Appendix B or, alternatively, [40], Proposition 5.9), it turns out that the generating particle must move on a reflection plane, between two rotation axes. This contradicts the membership to the cone $\mathcal{K}$, except for the cones defined by sequences ν winding around two coboundary axes.

In conclusion, provided that $\mathcal{K}$ is simple and it does not wind around two coboundary axes, the minimizer u_I^* of the action $\mathcal{A}$ restricted to $\mathcal{K}$ is free of partial collisions, hence it is a smooth periodic solution of the N-body problem.

1.3 Enumerating the collision-free minimizers

Here we introduce an algorithm to generate all the sequences ν of length l, for some admissible integer l. Then we select only the periodic ones, and check whether they satisfy all the conditions ensuring the existence of collision-free minimizers of (1.7) in the corresponding cone $\mathcal{K} = \mathcal{K}(\nu)$. Precisely, our algorithm is based on the following steps:

1. Find the maximal admissible length $l_{\max}$ and other constraints on the length l.

2. Construct all the periodic sequences ν of vertexes of the Archimedean polyhedron $\mathcal{Q}_{\mathcal{R}}$.

3. Exclude the sequences that wind around one axis only or around two coboundary axes.

4. Exclude the sequences that do not respect the additional choreography symmetry (1.6).

5. Exclude the sequences that give rise to non-simple cones.

1.3.1 Constraints on the length

To exclude total collisions we use (1.11) and (1.12). If v is the linear piecewise loop defined by the sequence ν, the relation $\mathcal{A}(v) < \alpha_{\mathcal{R},M}$ can be rewritten as

$$k_1\zeta_1 + k_2\zeta_2 < \left(\alpha_{\mathcal{R},M}\frac{2\cdot 4^{1/3}}{3}\frac{1}{N}\frac{1}{\ell^{2/3}}\right)^{3/2} =: K. \tag{1.17}$$

Since the coefficients ζ_1 and ζ_2 are positive, for each M there exist only a finite number of positive integers (k_1, k_2) fulfilling (1.17). Given $\mathcal{R} \in \{\mathcal{T}, \mathcal{O}, \mathcal{I}\}$, taking the maximal value of $k_1 + k_2$ we get a constraint on the maximal length $l_{\max} = l_{\max}(M)$ of the sequence ν, see Table 1.3.

$\mathcal{R}\backslash M$	1	2	3	4	5
$\mathcal{T}$	4	8	12	/	/
$\mathcal{O}$	6	12	19	25	/
$\mathcal{I}$	10	21	32	/	54

Table 1.3: Values of $l_{\max}(M)$ for the different symmetry groups.

On the other hand, we can also give a constraint on the minimal length $l_{\min}$. Indeed, a periodic sequence of length $l \leq 5$ either winds around one axis only or encloses two coboundary axes. However, for all the five Platonic polyhedra there exists at least a good sequence ν of length 6: for this reason we set $l_{\min} = 6$.

Furthermore, in the case of $\mathcal{R} = \mathcal{T}, \mathcal{O}$ we cannot have $M = 1$. In fact:

- if $\mathcal{R} = \mathcal{T}$, $l_{\max}(1) = 4$, therefore we cannot construct any good sequence ν.

- if $\mathcal{R} = \mathcal{O}$, $l_{\max}(1) = 6$, and the only sequences of length 6 that do not wind around two coboundary axes have $M = 2$.

1.3.2 Periodic sequences construction

To know which vertexes are reachable from a fixed vertex V_j of $\mathcal{Q}_\mathcal{R}$, we interpret the polyhedron as a connected graph: in this manner we have an *adjacency matrix* A associated to the graph. In this matrix we want to store the information about the kind of sides connecting two different vertexes. The generic entry of A is

$$A_{ij} = \begin{cases} 1 & \text{if the vertex } i \text{ and the vertex } j \text{ are connected by a side of type 1,} \\ 2 & \text{if the vertex } i \text{ and the vertex } j \text{ are connected by a side of type 2,} \\ 0 & \text{otherwise.} \end{cases} \quad (1.18)$$

For a fixed length $l \in \{l_{\min}, \dots, l_{\max}\}$, we want to generate all the sequences of vertexes with that length, starting from vertex 1. Because of the symmetry, we can select the first side arbitrarily, while in the other steps we can choose only among 3 different vertexes, since we do not want to travel forward and backward along the same side. Therefore, the total number of sequences with length l is 3^{l-1}. To generate all these different sequences we produce an array of choices $c = (c_1, \dots, c_l)$ such that $c_1 = 1$ and $c_j \in \{1, 2, 3\}, j = 2, \dots, l$. Each entry tells us the way to construct the sequence: if v_1, v_2, v_3 are the number of the vertexes reachable from ν_j (with v_i sorted in ascending order), then $\nu_{j+1} = v_{c_j}$. All the different 3^{l-1} arrays of choices can be generated using an integer number $k \in \{0, \dots, 3^{l-1} - 1\}$, through its base 3 representation.

1.3.3 Winding around one axis only or two coboundary axes

To check whether a closed sequence winds around one axis only we have to take into account the type of Archimedean polyhedron $\mathcal{Q}_\mathcal{R}$. In the cases $\mathcal{R} = \mathcal{T}, \mathcal{O}$ it is sufficient to count the number m of different vertexes appearing in ν. If $m = 3, 4$ then ν winds around one axis only. The case of $\mathcal{R} = \mathcal{I}$ is different, since also pentagonal faces appear. If $m = 5$, to check this property we can take the arithmetic mean of the coordinates of the touched vertexes and control whether it coincides with a rotation axis or not.

We note that for M different from 1, a periodic sequence satisfying the choreography condition (1.19), introduced in the next paragraph, cannot wind around two coboundary axes. For this reason we decided to avoid performing this additional control, since $M = 1$ is possible only in the case of $\mathcal{R} = \mathcal{I}$. In this case we exclude the non-admissible sequences in a non-automated way, looking at them one by one. We point out that such sequences can be of three different types:

1. a pentagonal face and a triangular face sharing a vertex;
2. a pentagonal face and a square face sharing a side;
3. a square face and a triangular face sharing a side.

The sequences that travel along the boundary of two square faces sharing a vertex winds around two axes too, but these axes are not coboundary, thus we have to keep them.

1.3.4 Choreography condition

Condition (1.6) is satisfied if and only if there exists a rotation $R \in \mathcal{R}$ such that

$$\eta_R \nu_j = \nu_{j+k}, \tag{1.19}$$

for some integer k, where η_R denotes the permutation of the vertexes of $\mathcal{Q}_\mathcal{R}$ induced by R. To check condition (1.19), we have to construct η_R. Let $V_1, \dots, V_N \in \mathbb{R}^3$ be the coordinates of all the vertexes of $\mathcal{Q}_\mathcal{R}$: since each rotation R leaves $\mathcal{Q}_\mathcal{R}$ unchanged, it sends vertexes into vertexes. Therefore, we construct the matrices η_R such that

$$(\eta_R)_{ji} = \begin{cases} 1 & \text{if } RV_i = V_j, \\ 0 & \text{otherwise.} \end{cases}$$

It results that each $\eta_R \in \mathbb{R}^{N \times N}$ is a *permutation matrix*. The product of η_R with the vector $\mathbf{v} = (1, \dots, N)^T$ provides the permutation of $\{1, \dots, N\}$. At this point, given a rotation R, we are able to write the permuted sequence $\eta_R \nu$: we can simply check that (1.19) holds by comparing the sequences ν and $\eta_R \nu$. Moreover, if the condition is satisfied, we compute the value $M = k_\nu / k$, where k_ν is the minimal period of ν.

1.3.5 Simple cone control

Definition 1.5 of simple cones is given by using the tessellation of the sphere induced by the reflection planes of the Platonic polyhedra. To decide whether a cone $\mathcal{K}$ is simple or not, we must translate this definition into a condition on the sequence of vertexes. We observe that the only way to produce a non-simple cone is by traveling all around the boundary of a face $\mathcal{F}$ of $\mathcal{Q}_\mathcal{R}$: for the cone $\mathcal{K}$, being simple or not depends on the order of the pole associated to $\mathcal{F}$ and on the way the oriented path defined by ν gets to the boundary of $\mathcal{F}$ and leaves it. We discuss first the case of a triangular face, pointing out that it is associated to a pole p of order three. Suppose that ν contains a subsequence $[\nu_k, \nu_{k+1}, \nu_{k+2}, \nu_{k+3}]$ that travels all around a triangular face $\mathcal{F}$, that is $\nu_k = \nu_{k+3}$. Let ν_{k-1} and ν_{k+4} be the vertexes before and after accessing the boundary of $\mathcal{F}$. Four different cases can occur:

(i) ν_{k+4} is a vertex of the triangular face $\mathcal{F}$ (Figure 1.4, top left);

(ii) the path defined by ν accesses and leaves $\mathcal{F}$ through the same side, i.e. $[\nu_{k-1}, \nu_k] = [\nu_{k+3}, \nu_{k+4}]$ (Figure 1.4, top right);

(iii) the path defined by ν accesses and leaves $\mathcal{F}$ through two different sides describing an angle $\theta > \pi$ around p (Figure 1.4, bottom left);

(iv) the path defined by ν accesses and leaves $\mathcal{F}$ through two different sides describing an angle $\theta < \pi$ around p (Figure 1.4, bottom right).

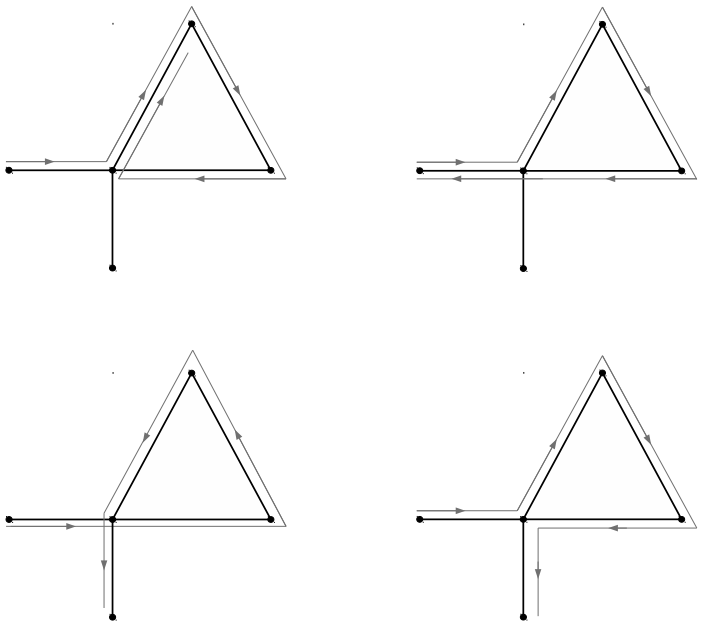

Figure 1.4: The different cases occurring for a path around a triangular face of $\mathcal{Q}_{\mathcal{R}}$.

In the first three cases, the sequence ν defines a non-simple cone, while case iv) is the only admissible situation for a simple cone. Cases iii) and iv) can be distinguished by the sign of $\vec{a} \times \vec{d} \cdot \vec{b} \times \vec{c}$ where

$$\vec{a} = [\nu_{k-1}, \nu_k], \quad \vec{b} = [\nu_k, \nu_{k+1}], \quad \vec{c} = [\nu_{k+2}, \nu_{k+3}], \quad \vec{d} = [\nu_{k+3}, \nu_{k+4}].$$

If this sign is positive we have case iii), if negative case iv). This argument concludes the discussion about triangular faces. Actually, we can see that a similar argument can be used for square and pentagonal faces, provided that the associated poles have order greater than two. However, in the case $\mathcal{R} = \mathcal{O}$, we can find poles of order two associated to square faces. In this situation there is no way to travel all around the square face and get a simple cone.

1.3.6 Summary of the procedure

Now we summarize the procedure that we adopt. For each admissible value of M (see Table 1.1) we observe that M divides the possible lengths $l \in \{l_{\min}, \ldots, l_{\max}(M)\}$ of the sequence ν. Then, for each integer $h \in \{0, \ldots, 3^{l/M-1} - 1\}$ we perform the following steps:

(1) construct the array of choices c corresponding to h;

(2) generate the sequence $\hat{\nu}$ on the basis of c, starting from vertex number 1. Note that $\hat{\nu}$ is a sequence with length $l/M + 1$;

(3) control whether $\eta_R\hat{\nu}_1 = \hat{\nu}_{l/M+1}$ for some $R \in \mathcal{R}$. In this case we extend $\hat{\nu}$ to a sequence ν with length $l+1$, using the choreography condition (1.19);

(4) check whether ν is periodic or not;

(5) compute the minimal period k_ν of ν;

(6) check whether ν winds around one axis only or not;

(7) check whether (1.19) holds or not; if it holds, check whether the ratio k_ν/k is equal to M or not;

(8) compute the values of k_1, k_2 and check whether (1.17) holds or not;

(9) check whether the cone $\mathcal{K} = \mathcal{K}(\nu)$ is simple or not.

If the sequence ν passes all the controls above, then there exists a collision-free minimizer of the action $\mathcal{A}$ restricted to $\mathcal{K}$. Recall that, in the case $\mathcal{R} = \mathcal{I}$, we also have to check the sequences with $M = 1$, excluding the ones winding around two coboundary axes.

1.3.7 Results

The lists of good sequences found by the algorithm described in Section 1.3.6 for the three groups $\mathcal{T}, \mathcal{O}, \mathcal{I}$ are available at the webpage [34]. Here we list only the total number of good sequences (i.e. leading to collision-free minimizers and then classical periodic orbits) for the different polyhedra, in Table 1.4. All the periodic orbits listed in [40]

M	Total number
2	3
3	6
	9

M	Total number
2	24
3	18
4	15
	57

M	Total number
1	28
2	386
3	455
5	573
	1442

Table 1.4: Total number of sequences ν found for $\mathcal{Q}_\mathcal{T}, \mathcal{Q}_\mathcal{O}, \mathcal{Q}_\mathcal{I}$ respectively, from the left to the right.

were found again with this procedure. We point out that we can identify two different sequences $\nu, \tilde{\nu}$ if there exists a symmetry S of the polyhedron $\mathcal{Q}_\mathcal{R}$ such that $\eta_R\nu = \tilde{\nu}$, where η_R still denotes the permutation of the vertexes induced by the symmetry S. The results are presented using this identification.

Chapter 2

Symmetric constellations of satellites

The $(1+N)$-body problem has been introduced by Maxwell [68] to study the dynamical structure of Saturn's ring, and more recently it has been reviewed in [70, 73]. In this chapter we consider an $(1+N)$-body problem, composed by a massive particle of mass $m_0 \gg 1$, which is fixed at a point of the space, plus N equal particles of mass $m = 1$, moving around the massive body. All these particles interact through the gravitational force. This system can be thought as a big planet possessing some small satellites. Imposing symmetry and topological constraints on the possible configurations of these satellites, we are able to find periodic orbits using variational techniques, as minimizers of the Lagrangian action functional. Moreover, as the mass m_0 of the planet increases, we study the asymptotic behaviour of the minimizers, making use of Γ-convergence theory, that we recall below.

2.1 Definition of Γ-convergence and its properties

Many mathematical problems appearing in different branches of applied mathematics depend on a parameter, small or large, that can have different origins (constructive, coming from an approximation process, specific of the problem). As this parameter varies, it is often possible to understand a certain limit behaviour, and guess that we may substitute the full problem we started with, with a new and simpler one, where the parameters have disappeared. If we are studying a problem with variational techniques, this often means that we have a sequence of minimum problems

$$\min\{\mathcal{A}_\varepsilon(u) : u \in X\},$$

depending on a real parameter ε, where X is a set endowed with a notion of convergence. Γ-convergence is a notion of convergence for sequences of functionals, which was introduced by E. De Giorgi in the mid 70s in a series of paper, see for example [28, 29, 30]. Its purpose is to describe the asymptotic behaviour of families of minimum problems

depending on a parameter, and guess a limit problem whose minima are the limit of the sequence of minima of the full problem.

In the literature about Γ-convergence, we can find many equivalent definitions, as reported for example in [26]. Here we recall the definition adopted in [13], and state the main properties that we are going to use in this chapter.

Definition 2.1. We say that a sequence $\mathcal{A}_j : X \to \overline{\mathbb{R}}$ of functionals Γ-*converges* in X to $\mathcal{A}_\infty : X \to \overline{\mathbb{R}}$ if for all $u \in X$ we have

(i) (lim inf inequality) for every sequence $\{u_j\}_{j\in\mathbb{N}}$ converging to u in X

$$\mathcal{A}_\infty(u) \leq \liminf_{j\to\infty} \mathcal{A}_j(u_j); \tag{2.1}$$

(ii) (lim sup inequality) there exists a sequence $\{u_j\}_{j\in\mathbb{N}}$ converging to u such that

$$\mathcal{A}_\infty(u) \geq \limsup_{j\to\infty} \mathcal{A}_j(u_j). \tag{2.2}$$

We usually refer to such a sequence as *recovery sequence*.

The function $\mathcal{A}_\infty$ is called the Γ-limit of $\{\mathcal{A}_j\}_{j\in\mathbb{N}}$, and we write $\Gamma\text{-}\lim_{j\to\infty} \mathcal{A}_j = \mathcal{A}_\infty$.

Remark 2.2. If we have a family of functionals $\mathcal{A}_\varepsilon : X \to \overline{\mathbb{R}}$ depending on a small continuous parameter $\varepsilon > 0$, we have to better specify the definition. We say that $\{\mathcal{A}_\varepsilon\}_{\varepsilon>0}$ Γ-converges to $\mathcal{A}_0$ if for all sequences $\{\varepsilon_j\}_{j\in\mathbb{N}} \subseteq \mathbb{R}$ converging to 0 we have $\Gamma\text{-}\lim_{j\to\infty} \mathcal{A}_{\varepsilon_j} = \mathcal{A}_0$. If this is the case, we write $\Gamma\text{-}\lim_{\varepsilon\to 0} \mathcal{A}_\varepsilon = \mathcal{A}_0$.

It is worth noting that Γ-convergence is indeed a different kind of notion of convergence, and it differs from the usual known notions of convergence. Consider for example $X = \mathbb{R}$ and the sequence

$$\mathcal{A}_j : \mathbb{R} \to \mathbb{R}, \quad \mathcal{A}_j(u) = \sin(ju), \quad j \in \mathbb{N}.$$

It is known that the pointwise limit of $\{\mathcal{A}_j\}_{j\in\mathbb{N}}$ does not exist, however we have that

$$\Gamma\text{-}\lim_{j\to\infty} \mathcal{A}_j(u) = -1.$$

Indeed

(i) the (lim inf inequality) is trivial, since we always have

$$-1 \leq \mathcal{A}_j(u), \quad \forall\, u \in \mathbb{R}, \quad \forall\, j \in \mathbb{N}.$$

(ii) for the (lim sup inequality) we can construct the recovery sequences explicitly. Let $u \in \mathbb{R}$ be a point, and set

$$u_j = -\frac{\pi}{2j} + \frac{2\pi}{j}\left[\frac{ju}{2\pi}\right], \quad j \in \mathbb{N},$$

where $[\,\cdot\,]$ denotes the integer part. Then we have that $\lim_{j\to\infty} u_j = u$ and

$$\limsup_{j\to\infty} \mathcal{A}_j(u_j) = \lim_{j\to\infty} A_j(u_j) = -1.$$

Definition 2.3. Let (X, d) be a metric space. A sequence $\mathcal{A}_j : X \to \overline{\mathbb{R}}$, $j \in \mathbb{N}$ is said to be *equi-coercive* if there exists a compact set $K \subseteq X$ such that

$$\inf_X \mathcal{A}_j = \inf_K \mathcal{A}_j,$$

for every $j \in \mathbb{N}$.

When the sequence of functionals is equi-coercive, then Γ-convergence can be used to study the asymptotic behaviour of the minimizers.

Theorem 2.4 (Convergence of minima and minimizers)**.** *Assume that*

$$\Gamma\text{-}\lim_{j\to\infty} \mathcal{A}_j = \mathcal{A}_\infty,$$

and the sequence $\{\mathcal{A}_j\}_{j\in\mathbb{N}}$ *is equi-coercive, and let* K *be the compact set of Definition 2.3. Then*

(i) $\mathcal{A}_\infty$ *has a minimum in* X*;*

(ii) the sequence of infimum values converges, that is

$$\lim_{j\to\infty} \left(\inf_X \mathcal{A}_j\right) = \min_X \mathcal{A}_\infty; \tag{2.3}$$

(iii) if $\{u_j\}_{j\in\mathbb{N}} \subseteq K$ *is a sequence such that*

$$\lim_{j\to\infty} \left(\mathcal{A}_j(u_j) - \inf_X \mathcal{A}_j\right) = 0,$$

then from every subsequence $\{u_{j_k}\}_{k\in\mathbb{N}}$ *converging to* $u_\infty \in X$ *we have*

$$\mathcal{A}_\infty(u_\infty) = \min_X \mathcal{A}_\infty.$$

Proof. Consider the sequence of the inf values, i.e.

$$I_j = \inf_X A_j, \quad j \in \mathbb{N},$$

and let

$$I_\infty = \liminf_{j\to\infty} I_j$$

be its inferior limit. Then there exists a subsequence $j_k \to \infty$ such that

$$\lim_{k\to\infty} I_{j_k} = I_\infty.$$

Let $u_{j_k} \to u_\infty$ be a sequence as in (iii), then we can prove that u_∞ is a minimum point for $\mathcal{A}_\infty$. Indeed, if $v \in X$, let $\{v_j\}_{j\in\mathbb{N}}$ be a recovery sequence for v, provided by the definition of Γ-convergence. Then

$$\mathcal{A}_\infty(v) \geq \limsup_{j\to\infty} \mathcal{A}_j(v_j) \geq \limsup_{j\to\infty} I_j \geq \liminf_{j\to\infty} I_j = I_\infty. \tag{2.4}$$

Moreover,

$$I_\infty = \lim_{k\to\infty} I_{j_k} = \lim_{k\to\infty} \left(\mathcal{A}_{j_k}(u_{j_k}) + I_{j_k} - \mathcal{A}_{j_k}(u_{j_k})\right) = \lim_{k\to\infty} \mathcal{A}_{j_k}(u_{j_k}) \geq \mathcal{A}_\infty(u_\infty). \quad (2.5)$$

The last inequality follows from the lim inf property of Γ-convergence.

Combining (2.4) and (2.5) we obtain that, for every $v \in X$,

$$\mathcal{A}_\infty(v) \geq \mathcal{A}_\infty(u_\infty),$$

hence u_∞ is a minimizer for the Γ-limit $\mathcal{A}_\infty$. This proves (i) and (iii). From (2.5) and (2.4) with $v = u_\infty$ we obtain

$$\liminf_{j\to\infty} I_j \geq \mathcal{A}_\infty(u_\infty) \geq \limsup_{j\to\infty} I_j,$$

that yields (ii). □

It is worth noting that the converse of the above theorem is not true, i.e. we can have a situation in which a minimizer of $\mathcal{A}_\infty$ is not the limit of minimizers of $\{\mathcal{A}_j\}_{j\in\mathbb{N}}$, and in general $\mathcal{A}_\infty$ can have several minimum points. Moreover, Γ-convergence does not imply the convergence of the local minimizers. As a simple example of this, choose $X = \mathbb{R}$ and

$$\mathcal{A}_j : \mathbb{R} \to \mathbb{R}, \quad \mathcal{A}_j(u) = u^2 + \sin(ju), \quad j \in \mathbb{N}.$$

These functions have a global minimum and local minima, but the Γ-limit

$$\mathcal{A}_\infty : \mathbb{R} \to \mathbb{R}, \quad \mathcal{A}_\infty(u) = t^2 - 1,$$

has only a global minima.

2.2 The $(1 + N)$-body problem with symmetries

Let us consider a system of N particles with mass $m_1 = \cdots = m_N = 1$, plus a particle with mass $m_0 \gg 1$, and denote their positions with $u_i \in \mathbb{R}^3, i = 0, \ldots, N$. We assume that

(1) the center of mass of the whole system corresponds to the origin of the reference frame:

$$\sum_{i=0}^{N} m_i u_i \equiv 0;$$

(2) the central body is in equilibrium at the origin:

$$u_0 \equiv 0.$$

We introduce the configuration space

$$\mathcal{X} = \left\{ u = (u_0, \dots, u_N) \in \mathbb{R}^{3(1+N)} : u_0 = 0, \sum_{i=1}^{N} u_i = 0 \right\}.$$

The particles move under the force generated by potentials of the form $1/r^\alpha$, where $\alpha \in [1, 2)$ and r is the distance between two particles. Note that for $\alpha = 1$ we obtain the usual Newtonian gravitational potential. We write the potential separating the contribution of the central body from the interaction among the satellites:

$$U_\alpha(u) = \sum_{i=1}^{N} \frac{m_0}{|u_i|^\alpha} + \sum_{1 \le i < j \le N} \frac{1}{|u_i - u_j|^\alpha}. \tag{2.6}$$

Since m_0 is at rest, the kinetic energy contains only terms due to the motion of the small particles, that is

$$K = \frac{1}{2} \sum_{i=1}^{N} |\dot{u}_i|^2, \tag{2.7}$$

and the Lagrangian is given by the sum

$$L_\alpha = K + U_\alpha.$$

Fixed the period $T > 0$, consider the set of T-periodic loops $\Lambda = H^1_T(\mathbb{R}, \mathcal{X})$, and define the Lagrangian action functional

$$\mathcal{A}^\alpha(u) = \int_0^T L_\alpha(u, \dot{u})\, dt,$$

for $u \in \Lambda$. As already done in Chapter 1, in the following we restrict $\mathcal{A}^\alpha$ to sets of loops which are invariant under an action of a group of rotations. Let us denote with $\mathcal{G}$ a subgroup of the 3-D orthogonal group $O(3)$, containing as many elements as the number of satellites, i.e. $|\mathcal{G}| = N$. Then, labeling the satellites with the elements of $\mathcal{G}$, we introduce the space of symmetric loops

$$\Lambda_\mathcal{G} = \{ u \in \Lambda : u_R(t) = R u_I(t),\ R \in \mathcal{G},\ t \in \mathbb{R} \},$$

where $u_I : [0, T] \to \mathbb{R}^3$ is the motion of an arbitrarily selected satellite, that we call the *generating particle*. If we restrict the action to $\Lambda_\mathcal{G}$, then $\mathcal{A}^\alpha$ depends only on the motion of u_I, hence

$$\mathcal{A}^\alpha(u_I) = N \int_0^T \left(\frac{|\dot{u}_I|^2}{2} + \frac{m_0}{|u_I|^\alpha} + \frac{1}{2} \sum_{R \in \mathcal{G} \setminus \{I\}} \frac{1}{|(R - I) u_I|^\alpha} \right) dt. \tag{2.8}$$

Note that a collision occurs if and only if there exist $R \in \mathcal{G} \setminus \{I\}$ and $t_c \in [0, T]$ such that

$$u_I(t_c) = R u_I(t_c).$$

We denote with

$$\Gamma = \{ x \in \mathbb{R}^3 : Rx = x \text{ for some } R \in \mathcal{G} \setminus \{I\} \},$$

the set of collisions. What we want to do in the following, is

(i) impose some additional topological constraints, defining a new set of loops, in order to recover the coercivity of $\mathcal{A}^\alpha$;

(ii) prove that, for this chosen set, there exists a collision-free minimizer for every value of m_0 large enough;

(iii) find the Γ-limit and study the properties of its minimizers.

2.2.1 The $(1+N)$-body problem and Γ-convergence

Let us discuss first the point (iii). If we consider the limit $m_0 \to \infty$, the integrand function in the action (2.8) tends to $+\infty$, and it is not clear what the Γ-limit is. In these situations, the usual technique adopted is a suitable rescaling of the motion. We consider

$$u_I(t) = m_0^\beta v_I(t), \quad t \in \mathbb{R},$$

and get

$$\mathcal{A}^\alpha(u_I) = N \int_0^T \left(m_0^{2\beta} \frac{|\dot{v}_I|^2}{2} + \frac{m_0^{1-\alpha\beta}}{|v_I|^\alpha} + \frac{1}{2m_0^{\alpha\beta}} \sum_{R \in \mathcal{G}\setminus\{I\}} \frac{1}{|(R-I)v_I|^\alpha} \right) dt.$$

We choose β in a way to balance the exponent in the kinetic energy and the exponent in the term of the potential energy containing the mass of the central body, i.e we set $2\beta = 1 - \alpha\beta$, so that

$$\beta = \frac{1}{2+\alpha}.$$

Using this value, the action functional becomes

$$\begin{aligned}\mathcal{A}^\alpha(u_I) &= N \int_0^T \left(m_0^{\frac{2}{2+\alpha}} \frac{|\dot{v}_I|^2}{2} + \frac{m_0^{\frac{2}{2+\alpha}}}{|v_I|^\alpha} + \frac{1}{2m_0^{\frac{\alpha}{2+\alpha}}} \sum_{R \in \mathcal{G}\setminus\{I\}} \frac{1}{|(R-I)v_I|^\alpha} \right) dt \\ &= N m_0^{\frac{2}{2+\alpha}} \int_0^T \left(\frac{|\dot{v}_I|^2}{2} + \frac{1}{|v_I|^\alpha} + \frac{1}{2m_0} \sum_{R \in \mathcal{G}\setminus\{I\}} \frac{1}{|(R-I)v_I|^\alpha} \right) dt.\end{aligned}$$

Setting

$$\varepsilon = \frac{1}{m_0},$$

and discarding the constants in front of the integral, we can study the functional

$$\mathcal{A}^\alpha_\varepsilon(v_I) = \int_0^T \left(\frac{|\dot{v}_I|^2}{2} + \frac{1}{|v_I|^\alpha} + \frac{\varepsilon}{2} \sum_{R \in \mathcal{G}\setminus\{I\}} \frac{1}{|(R-I)v_I|^\alpha} \right) dt. \tag{2.9}$$

Note that this is the action of a Kepler problem plus a perturbation, that becomes smaller and smaller as the mass of the central body increases and, in the limit $\varepsilon \to 0$, we obtain the action of the Kepler problem itself

$$\mathcal{A}^\alpha_0(v_I) = \int_0^T \left(\frac{|\dot{v}_I|^2}{2} + \frac{1}{|v_I|^\alpha} \right) dt.$$

This is an hint of what the Γ-limit is. Note that, at step (i) we are restricting the loop space $\Lambda_{\mathcal{G}}$ in order to recover the coercivity. Therefore, let us denote with

$$\mathcal{K} \subseteq H^1_T(\mathbb{R}, \mathbb{R}^3 \setminus \Gamma),$$

the set where $\mathcal{A}^\alpha_\varepsilon$ is defined and coercive. We assume that $\mathcal{K}$ is open in the H^1 topology, and the loops belonging to $\mathcal{K}$ are all collision-free. Collision loops necessarily belong to the boundary

$$\partial\mathcal{K} = \overline{\mathcal{K}}^{H^1} \setminus \mathcal{K},$$

where $\overline{\mathcal{K}}^{H^1}$ denotes the H^1-closure of $\mathcal{K}$. Moreover, we assume the following property on the loops belonging to $\mathcal{K}$, which will be satisfied in all the examples that we are going to consider: there exists a constant $c_{\mathcal{K}} > 0$ such that, for every $u_I \in \mathcal{K}$ and for every $\tau \in [0,T]$, we have

$$|u_I(\tau)| \le c_{\mathcal{K}} \max_{t,s\in[0,T]} |u_I(t) - u_I(s)|. \tag{2.10}$$

Then we define [1]

$$\mathcal{A}^\alpha_\varepsilon(v) = \begin{cases} \displaystyle\int_0^T \left(\frac{|\dot v|^2}{2} + \frac{1}{|v|^\alpha} + \frac{\varepsilon}{2} \sum_{R\in\mathcal{G}\setminus\{I\}} \frac{1}{|(R-I)v|^\alpha} \right) dt, & v \in \overline{\mathcal{K}}^{H^1}, \\ +\infty, & v \in \overline{\mathcal{K}}^{L^2} \setminus \overline{\mathcal{K}}^{H^1}, \end{cases} \tag{2.11}$$

and

$$\mathcal{A}^\alpha_0(v) = \begin{cases} \displaystyle\int_0^T \left(\frac{|\dot v|^2}{2} + \frac{1}{|v|^\alpha} \right) dt, & v \in \overline{\mathcal{K}}^{H^1}, \\ +\infty, & v \in \overline{\mathcal{K}}^{L^2} \setminus \overline{\mathcal{K}}^{H^1}, \end{cases} \tag{2.12}$$

where $\overline{\mathcal{K}}^{L^2}$ denotes the L^2-closure of $\mathcal{K}$.

Theorem 2.5. *For every $\alpha \ge 1$, we have*

i)

$$\Gamma\text{-}\lim_{\varepsilon\to 0} \mathcal{A}^\alpha_\varepsilon = \mathcal{A}^\alpha_0;$$

ii) the sequence $\{\mathcal{A}^\alpha_\varepsilon\}_{\varepsilon>0}$ is equicoercive.

Proof. To prove i) we first show that the lim inf inequality holds. Let $\{\varepsilon_j\}_{j\in\mathbb{N}} \subseteq \mathbb{R}$ be a sequence converging to 0 and let $\{v_j\}_{j\in\mathbb{N}} \subseteq \overline{\mathcal{K}}^{L^2}$ such that $v_j \to v$ in L^2. If $\liminf_j \mathcal{A}^\alpha_{\varepsilon_j}(v_j) = +\infty$ there is nothing to prove. Therefore we assume that

$$\liminf_{j\to\infty} \mathcal{A}^\alpha_{\varepsilon_j}(v_j) < +\infty. \tag{2.13}$$

[1] for simplicity, here we write v instead of v_I.

Then, up to subsequences, there exists $M > 0$ such that

$$\int_0^T \frac{|\dot{v}_j|^2}{2} dt \leq \mathcal{A}^\alpha_{\varepsilon_j}(v_j) \leq M, \tag{2.14}$$

hence $\{\|v_j\|_{H^1}\}_{j\in\mathbb{N}}$ is bounded and, again up to subsequences, $v_j \rightharpoonup v$ in H^1. From Hölder's inequality and (2.14) it follows that for all $t, s \in [0,T]$ and for all $j \in \mathbb{N}$ we have

$$|v_j(t) - v_j(s)| \leq \int_s^t |\dot{v}_j(\tau)| d\tau \leq \sqrt{2TM}.$$

Moreover, the functions are all bounded by the same constant, since for every $\tau \in [0,T]$, by assumption (2.10), we have

$$|v_j(\tau)| \leq c_{\mathcal{K}} \max_{t,s\in[0,T]} |v_j(t) - v_j(s)| \leq c_{\mathcal{K}}\sqrt{2TM}.$$

Then, by the Ascoli-Arzelà theorem, $v_j \to v$ uniformly in $[0,T]$, up to subsequences. We conclude that there exists a subsequence $\{v_{j_k}\}_{k\in\mathbb{N}} \subseteq \overline{\mathcal{K}}^{H^1}$ such that

(i) $\lim_k \mathcal{A}^\alpha_{\varepsilon_{j_k}}(v_{j_k}) = \liminf_j \mathcal{A}^\alpha_{\varepsilon_j}(v_j)$;

(ii) $v_{j_k} \rightharpoonup v$ in H^1;

(iii) $v_{j_k} \to v$ uniformly in $[0,T]$.

It follows that

$$\begin{aligned}
\liminf_{j\to\infty} \mathcal{A}^\alpha_{\varepsilon_j}(v_j) &= \lim_{k\to\infty} \mathcal{A}^\alpha_{\varepsilon_{j_k}}(v_{j_k}) \\
&= \liminf_{k\to\infty} \int_0^T \left(\frac{|\dot{v}_{j_k}|^2}{2} + \frac{1}{|v_{j_k}|^\alpha} + \frac{\varepsilon_{j_k}}{2} \sum_{R\in\mathcal{G}\setminus\{I\}} \frac{1}{|(R-I)v_{j_k}|^\alpha} \right) dt \\
&\geq \liminf_{k\to\infty} \int_0^T \left(\frac{|\dot{v}_{j_k}|^2}{2} + \frac{1}{|v_{j_k}|^\alpha} \right) dt \\
&\geq \int_0^T \frac{|\dot{v}|^2}{2} dt + \int_0^T \left(\liminf_{k\to\infty} \frac{1}{|v_{j_k}|^\alpha} \right) dt \\
&\geq \int_0^T \left(\frac{|\dot{v}|^2}{2} + \frac{1}{|v|^\alpha} \right) dt \\
&= \mathcal{A}^\alpha_0(v),
\end{aligned}$$

where we used the lower semicontinuity of the L^2 norm with respect to the weak convergence and Fatou's lemma. This proves the lim inf inequality.

Next we prove the lim sup inequality. Let $v \in \overline{\mathcal{K}}^{L^2}$ and let $\{\varepsilon_j\}_{j\in\mathbb{N}} \subseteq \mathbb{R}$ be a sequence converging to 0. Without loss of generality we can assume that $\varepsilon_j \searrow 0$. If $\mathcal{A}^\alpha_0(v) = +\infty$ there is nothing to prove. Therefore we assume that $\mathcal{A}^\alpha_0(v) < +\infty$, hence necessarily $v \in \overline{\mathcal{K}}^{H^1}$. We show that there exist $\{v_j\}_{j\in\mathbb{N}} \subseteq \overline{\mathcal{K}}^{L^2}$ such that $v_j \xrightarrow{L^2} v$ and

$$\lim_{j\to\infty} \mathcal{A}_{\varepsilon_j}(v_j) = \mathcal{A}_0(v). \tag{2.15}$$

Let us consider $\{w_k\}_{k\in\mathbb{N}} \subseteq \mathcal{K}$ such that $w_k \overset{H^1}{\to} v$, which exists because v belongs to the H^1 closure of $\mathcal{K}$. The loops in $\mathcal{K}$ are collision-free, therefore we can set

$$a_k = \int_0^T \sum_{R\in\mathcal{G}\setminus\{I\}} \frac{1}{|(R-I)w_k|^\alpha} dt < +\infty.$$

We can find an increasing sequence $\{h_k\}_{k\in\mathbb{N}} \subseteq \mathbb{N}$ such that

$$\lim_{k\to\infty} \varepsilon_{h_k} a_k = 0.$$

Let us define a sequence $\{v_j\}_{j\in\mathbb{N}} \subseteq \mathcal{K}$ such that, for each $k \in \mathbb{N}$,

$$v_j = w_k, \quad j \in \{h_k, \dots, h_{k+1} - 1\}.$$

Thus we have

$$\varepsilon_j \int_0^T \sum_{R\in\mathcal{G}\setminus\{I\}} \frac{1}{|(R-I)v_j|^\alpha} dt \le \varepsilon_{h_k} a_k, \quad j \in \{h_k, \dots, h_{k+1} - 1\}, \quad \forall k \in \mathbb{N},$$

hence this term tends to zero as k (and therefore j) increases. From $v_j \overset{H^1}{\to} v$ we obtain

$$\lim_{j\to\infty} \int_0^T |\dot{v}_j|^2 dt = \int_0^T |\dot{v}|^2 dt, \qquad \lim_{j\to\infty} \int_0^T \frac{1}{|v_j|^\alpha} dt = \int_0^T \frac{1}{|v|^\alpha} dt. \tag{2.16}$$

The second relation in (2.16) follows from the uniform convergence of $\{v_j\}_{j\in\mathbb{N}}$ to v, up to subsequences.

Thus we proved that for each sequence $\{\varepsilon_j\}_{j\in\mathbb{N}}$ converging to zero there exists a subsequence $\{j_k\}_{k\in\mathbb{N}}$ of integers such that $\varepsilon_{j_k} \searrow 0$ and

$$\lim_{k\to\infty} \mathcal{A}^\alpha_{\varepsilon_{j_k}}(v_{j_k}) = \mathcal{A}^\alpha_0(v).$$

This yields (2.15) and i) is proved.

Let us prove ii), i.e. that the sequence $\{\mathcal{A}^\alpha_\varepsilon\}_{\varepsilon>0}$ is equi-coercive. The functional $\mathcal{A}^\alpha_0$ is coercive in $\overline{\mathcal{K}}^{L^2}$ and weakly lower semicontinuous in H^1, hence a minimizer exists. We observe that the sequence $\{\mathcal{A}^\alpha_\varepsilon(v)\}_{\varepsilon>0} \subseteq \mathbb{R}$ is decreasing with ε for each $v \in \overline{\mathcal{K}}^{L^2}$ and

$$\mathcal{A}^\alpha_0(v) \le \mathcal{A}^\alpha_\varepsilon(v), \quad 0 < \varepsilon \le \varepsilon_0, \tag{2.17}$$

where $\varepsilon_0 > 0$. Given $s \in \mathbb{R}$, we introduce the sub-levels

$$\mathcal{K}^{\varepsilon,\alpha}_s = \{v \in \overline{\mathcal{K}}^{L^2} : \mathcal{A}^\alpha_\varepsilon(v) \le s\}, \tag{2.18}$$

$$\mathcal{K}^{0,\alpha}_s = \{v \in \overline{\mathcal{K}}^{L^2} : \mathcal{A}^\alpha_0(v) \le s\}. \tag{2.19}$$

From (2.17) we have $\mathcal{K}^{\varepsilon,\alpha}_s \subseteq \mathcal{K}^{0,\alpha}_s$ for all $\varepsilon > 0$ and for $s \in \mathbb{R}$ large enough they are all non-empty. Moreover, the sub-levels $\mathcal{K}^{0,\alpha}_s$ are weakly compact since $\mathcal{A}^\alpha_0$ is coercive and weakly lower semicontinuous. Therefore, the set $\mathcal{K}^{0,\alpha}_s$, for a fixed $s \in \mathbb{R}$ large enough, satisfies Definition 2.3 of equi-coercivity for the sequence $\{\mathcal{A}^\alpha_\varepsilon\}_{\varepsilon>0}$. □

It follows that, to understand the asymptotic behaviour of the minimizers, we can simply study the minimizers of the Γ-limit functional $\mathcal{A}_0^\alpha$. It is worth noting that, as already remarked, at step (i) we are restricting the loop space, and this set is unchanged as ε decreases. This means that the action functional of the Kepler problem is defined on the same set of definition of $\{\mathcal{A}_\varepsilon\}_{\varepsilon>0}$. In particular, this set of loops may not contain Keplerian orbits or, more in general, planar loops whose plane of motion passes through the origin. As a consequence, the minimizers of the Γ-limit may not coincide with Keplerian orbits, as one would expect: we will clarify this behaviour in the following, showing concrete examples.

2.3 $\mathbb{Z}_4$ symmetry: Hip-Hop constellations

In this section we consider $N = 4$ and discuss the existence of periodic orbits called *Hip-Hop solutions*, appearing in [21] in the case without central body. These solutions oscillates between the square central configuration and the tetrahedral one.

Here we consider only the Keplerian case $\alpha = 1$. The rotation group of the Hip-Hop solution is isomorphic to

$$\mathbb{Z}_4 = \{I, \mathsf{R}, \mathsf{R}^2, \mathsf{R}^3\}, \quad \mathsf{R} = \begin{pmatrix} 0 & -1 & 0 \\ 1 & 0 & 0 \\ 0 & 0 & -1 \end{pmatrix}. \tag{2.20}$$

Moreover, the collision set Γ corresponds to the vertical axis

$$\Gamma = \{x \in \mathbb{R}^3 : x \cdot e_3 = 0\},$$

where $e_3 \in \mathbb{R}^3$ is the unit vector corresponding to the third coordinate axis. To obtain the coercivity of the action functional, we restrict its domain to the loops $u \in \Lambda_{\mathbb{Z}_4}$ such that

$$u_I\left(t + \frac{T}{2}\right) = -u_I(t), \quad t \in \mathbb{R}. \tag{2.21}$$

Relation (2.21) is often called the *Italian symmetry*, because it was introduced in [31, 24]. Therefore, the set of admissible loops is

$$\mathcal{K} = \left\{u_I \in H^1_T(\mathbb{R}, \mathbb{R}^3 \setminus \Gamma) : u_I(t + T/2) = -u_I(t),\, t \in \mathbb{R}\right\}.$$

The action (2.8) is coercive on $\mathcal{K}$, in fact if $\{u_I^{(k)}\}_{k\in\mathbb{N}} \subset \mathcal{K}$ is such that $\|u_I^{(k)}\|_{H^1} \to +\infty$, then the kinetic part goes to infinity along this sequence, and so does the action. Therefore, for each value of $m_0 \geq 0$, there exists a minimizer in the H^1 closure of $\mathcal{K}$, possibly with collisions. The next step is the exclusion of collisions, in order to obtain a sequence of classical solutions, depending on the parameter m_0, of the Newtonian $(1 + 4)$-body problem.

Note that in $\mathcal{K}$ there exists a T-periodic solution of the $(1+4)$-body problem with the satellites placed at the vertexes of a square, which uniformly rotates around the central

body with period T. Let us denote with $u_I^{\square}(t)$ this solution. With straightforward computations we get that

$$u_I^{\square}(t) = \begin{pmatrix} a\cos(\omega t) \\ a\sin(\omega t) \\ 0 \end{pmatrix}, \quad a = \left(\frac{T}{2\pi}\right)^{2/3}\left(\frac{1}{\sqrt{2}} + \frac{1}{4} + m_0\right)^{1/3}, \quad \omega = \frac{2\pi}{T}. \tag{2.22}$$

Lemma 2.6. *The solution $u_I^{\square} \in \mathcal{K}$ given by (2.22) is not a local minimizer of the action.*

Proof. To prove this result, it is sufficient to compute the second variation $\delta^2\mathcal{A}(u_I^{\square})$ of the action and see that there exists a periodic variation $w : [0, T] \to \mathbb{R}^3$ for which

$$\delta^2\mathcal{A}(u_I^{\square})(w) < 0. \tag{2.23}$$

To this end we will consider vertical variations, i.e. we take

$$w(t) = \begin{pmatrix} 0 \\ 0 \\ w_z(t) \end{pmatrix},$$

with $w_z : [0, T] \to \mathbb{R}$. Using the symmetries, the potential

$$U(u_I) = \frac{m_0}{|u_I|} + \frac{1}{2}\sum_{R\in\mathbb{Z}_4\setminus\{I\}} \frac{1}{|(R-I)u_I|},$$

can be written as

$$U(u_I) = \frac{m_0}{\sqrt{x^2+y^2+z^2}} + \frac{1}{2}\Big[\frac{\sqrt{2}}{\sqrt{x^2+y^2+2z^2}} + \frac{1}{2\sqrt{x^2+y^2}}\Big],$$

where we have set $u_I = (x, y, z)$. The second variation $\delta^2\mathcal{A}$ is given by

$$\delta^2\mathcal{A}(u_I^{\square})(w) = \int_0^T \left(|\dot{w}(t)|^2 + w(t)\cdot\frac{\partial^2 U(u_I^{\square}(t))}{\partial u^2} w(t)\right)dt.$$

Since we consider vertical variations, we only need to consider the following second derivatives

$$\begin{aligned}
\frac{\partial^2 U}{\partial z\partial x} &= 3\sqrt{2}\frac{xz}{(x^2+y^2+2z^2)^{5/2}} + 3m_0\frac{xz}{(x^2+y^2+z^2)^{5/2}}, \\
\frac{\partial^2 U}{\partial z\partial y} &= 3\sqrt{2}\frac{yz}{(x^2+y^2+2z^2)^{5/2}} + 3m_0\frac{yz}{(x^2+y^2+z^2)^{5/2}}, \\
\frac{\partial^2 U}{\partial z^2} &= -\frac{\sqrt{2}}{(x^2+y^2+2z^2)^{3/2}} - \frac{m_0}{(x^2+y^2+z^2)^{3/2}} \\
&\quad + 3\sqrt{2}\frac{2z^2}{(x^2+y^2+2z^2)^{5/2}} + 3m_0\frac{z^2}{(x^2+y^2+z^2)^{5/2}}.
\end{aligned}$$

When we evaluate them at $u_I^{\square}(t)$ the only non-zero derivative is

$$\frac{\partial^2 U(u_I^{\square}(t))}{\partial z^2} = -\frac{\sqrt{2}+m_0}{a^3}.$$

Therefore, substituting in the second variation and using the expressions of a and ω given in (2.22) we obtain

$$\delta^2\mathcal{A}(u_I^{\square})(w) = \int_0^T \left(\dot{w}_z(t)^2 - w_z(t)^2 \frac{\sqrt{2}+m_0}{\frac{1}{\sqrt{2}}+\frac{1}{4}+m_0}\omega^2\right)dt.$$

Using as vertical variation the function

$$w_z(t) = \cos(\omega t)$$

we get

$$\delta^2\mathcal{A}(u_I^{\square})(w) = \frac{\omega^2 T}{2}\left(1 - \frac{\sqrt{2}+m_0}{\frac{1}{\sqrt{2}}+\frac{1}{4}+m_0}\right) < 0,$$

hence $u_I^{\square}$ is not a local minimizer. □

From this lemma and from the following discussion we can conclude that minimizers of $\mathcal{A}$ are not planar, in a way similar to [21].

2.3.1 Total collisions

To exclude total collisions we use level estimates. From Proposition 2.8 we can estimate the action of a solution with a total collision. Indeed, the total mass is

$$\mathcal{M} = 4 + m_0,$$

and, if $u \in \Lambda_{\mathbb{Z}_4}$ and (2.21) is satisfied, the distance between two satellites satisfy

$$|u_h - u_k| \le 2|u_I|, \quad h,k = 1,\dots,4, \quad h \neq k,$$

where u_j stands for u_{R^j}, with $j = 1,\dots,4$. Therefore, following Proposition 2.8, we obtain

$$\begin{aligned} U(u) &= \frac{1}{4+m_0}\left(\sum_{\substack{h,k=1\\h\neq k}}^{4} \frac{1}{|u_h-u_k|} + 2\sum_{i=1}^{4}\frac{m_0}{|u_i|}\right) \\ &= \frac{1}{4+m_0}\left(\sum_{\substack{h,k=1\\h\neq k}}^{4} \frac{1}{|u_h-u_k|} + \frac{8m_0}{|u_I|}\right) \\ &\ge \frac{1}{4+m_0}\left(\frac{6}{|u_I|} + \frac{8m_0}{|u_I|}\right). \end{aligned}$$

Moreover, we have

$$\rho(u) = \Big(\sum_{i=1}^{4} \frac{|u_i|^2}{4+m_0} \Big)^{1/2} = \frac{2}{\sqrt{4+m_0}} |u_I|.$$

The minimum of $U(u)$ restricted to $\rho(u) = 1$ satisfies

$$U_0 := \min_{\rho(u)=1} U(u) \geq \frac{4}{(4+m_0)^{3/2}} (3+4m_0).$$

Consider now a solution $u_I^* \in \overline{\mathcal{K}}$ with a total collision. Because of the symmetry (2.21), there are at least two total collisions per period, therefore, from Proposition 2.8, the action functional satisfies

$$\begin{aligned} \mathcal{A}(u_I^*) &\geq 2 \cdot \frac{3}{2} (4+m_0)(\pi U_0)^{2/3} \Big(\frac{T}{2} \Big)^{1/3} \\ &\geq 3 \cdot 2^{1/3} (2\pi)^{2/3} (3+4m_0)^{2/3} T^{1/3}. \end{aligned} \tag{2.24}$$

Note also that the action of the rotating square solution $u_I^{\square}$ given by (2.22) is

$$\begin{aligned} \mathcal{A}(u_I^{\square}) &= \Big(\frac{3+6\sqrt{2}}{2} + 6m_0 \Big) \frac{(2\pi)^{2/3}}{\Big(\frac{1}{\sqrt{2}} + \frac{1}{4} + m_0 \Big)^{1/3}} T^{1/3} \\ &= \frac{3}{2^{1/3}} \big(1 + 2\sqrt{2} + 4m_0\big)^{2/3} (2\pi)^{2/3} T^{1/3}. \end{aligned} \tag{2.25}$$

Set

$$f(m_0) = 3 \cdot 2^{1/3} \big(3+4m_0\big)^{2/3}, \quad g(m_0) = \frac{3}{2^{1/3}} \big(1 + 2\sqrt{2} + 4m_0\big)^{2/3}.$$

With this notation, the action of a solution with total collisions u_I^* and the action of the rotating square solution $u_I^{\square}$ can be written as

$$\mathcal{A}(u_I^*) = f(m_0)(2\pi)^{2/3} T^{1/3}, \quad \mathcal{A}(u_I^{\square}) = g(m_0)(2\pi)^{2/3} T^{1/3},$$

respectively. The equation $f(m_0) = g(m_0)$ has a unique real solution

$$m_0 = \frac{2\sqrt{2} - 5}{4} < 0,$$

and $f(0) > g(0)$. This means that

$$f(m_0) > g(m_0), \quad \forall m_0 \geq 0,$$

hence we obtain

$$\mathcal{A}(u_I^*) > \mathcal{A}(u_I^{\square}). \tag{2.26}$$

Therefore, minimizers of this problem are free of total collisions, for all the values of the mass $m_0 \geq 0$.

2.3.2 Partial collisions

The method used to exclude partial collisions is similar to the one used in [21], where the central body is missing. Using cylindrical coordinates for the generating particle

$$u_I(t) = \frac{1}{2}\begin{pmatrix} \rho(t)\cos\varphi(t) \\ \rho(t)\sin\varphi(t) \\ \zeta(t) \end{pmatrix}, \tag{2.27}$$

the Lagrangian of the functional (2.8) is $L = K + U$, where

$$K = \frac{\dot\rho + \rho^2\dot\varphi^2 + \dot\zeta^2}{2}, \qquad U = \frac{4\sqrt{2}}{\sqrt{\rho^2+2\zeta^2}} + \frac{2}{\rho} + \frac{8m_0}{\sqrt{\rho^2+\zeta^2}}. \tag{2.28}$$

Let us consider a solution $u_I^* \in \overline{\mathcal{K}}$ which has a partial collision at time $t = 0$. Since partial collisions can occur only on the vertical axis, we have

$$\rho^*(0) = \rho^*(T/2) = 0, \quad \zeta^*(0) = -\zeta^*(T/2) \neq 0.$$

Moreover, since the total energy and $\Phi = \rho^2\dot\varphi$ are first integrals, we can easily deduce that $\Phi = 0$ for a solution with partial collisions, hence it is contained on a vertical plane. Without loss of generality, we can assume that $\varphi = 0$, hence

$$u_I^*(t) = \frac{1}{2}\begin{pmatrix} \rho^*(t) \\ 0 \\ \zeta^*(t) \end{pmatrix}.$$

Lemma 2.7. *If the trajectory of a solution $u_I^*(t)$ lies in a vertical plane, then it does not minimize the action.*

Proof. We show that the action decreases if we rotate the orbit about the x axis by a small angle γ. Let us denote with $\bar u_I$ the rotated orbit and with $\bar\rho, \bar\varphi, \bar\zeta$ the corresponding cylindrical coordinates. The kinetic part remains unchanged:

$$K(\dot{\bar u}_I) = \frac{1}{2}\left(\dot{\bar\rho}^2 + \bar\rho^2\dot{\bar\varphi}^2 + \dot{\bar\zeta}^2\right) = \frac{1}{2}(\dot\rho^2 + \dot\zeta^2) = K(\dot u_I^*).$$

On the other hand, the potential becomes

$$\begin{aligned} U(\bar u_I) &= \frac{4\sqrt{2}}{\sqrt{\bar\rho^2+2\bar\zeta^2}} + \frac{2}{\bar\rho} + \frac{8m_0}{\sqrt{\bar\rho^2+\bar\zeta^2}} \\ &= \frac{4\sqrt{2}}{\sqrt{\rho^2+\zeta^2-\zeta^2\sin^2\gamma}} + \frac{2}{\sqrt{\rho^2+\zeta^2\sin^2\gamma}} + \frac{8m_0}{\sqrt{\rho+\zeta^2}}. \end{aligned}$$

The difference between the actions of the two loops is

$$\mathcal{A}(\bar u_I) - \mathcal{A}(u_I^*) = 2\int_0^{T/2} (U(\bar u_I) - U(u_I^*))dt,$$

and the term $U(\bar{u}_I) - U(u_I^*)$ in the integral does not contain the part of the attraction due to the central body, like in the case with $m_0 = 0$. Hence, to prove that

$$\mathcal{A}(\bar{u}_I) - \mathcal{A}(u_I^*) < 0,$$

we can simply use the same proof given in [21, Lemma 4]. □

From Lemma 2.7, we can conclude that minimizers are free of collisions for every value of the mass $m_0 \geq 0$, hence they are classical periodic solutions of the $(1+4)$-body problem.

2.3.3 Minimizers of the Γ-limit

In this setting, circular Keplerian orbits are compatible with the set $\mathcal{K}$ of admissible loops. Indeed, fixed a plane $\Pi \subseteq \mathbb{R}^3$ passing through the origin, there exists a unique (up to phase shifts and inversions of time) circular Keplerian orbit $u_I^\Pi : \mathbb{R} \to \mathbb{R}^3$ with period T lying on Π and satisfying (2.21), hence it is an element of $\mathcal{K}$. Therefore, there is an infinite number of minimizers of the Γ-limit functional in $\mathcal{K}$, represented by circular motions. Indeed, from [44] it is known that all the T-periodic Keplerian ellipses (including the circular and the degenerate ones) are minimizers of the action of the Kepler problem in the set of planar T-periodic loops winding around the origin only once, either clockwise or counter-clockwise. Moreover non-circular orbits are not compatible with relation (2.21).

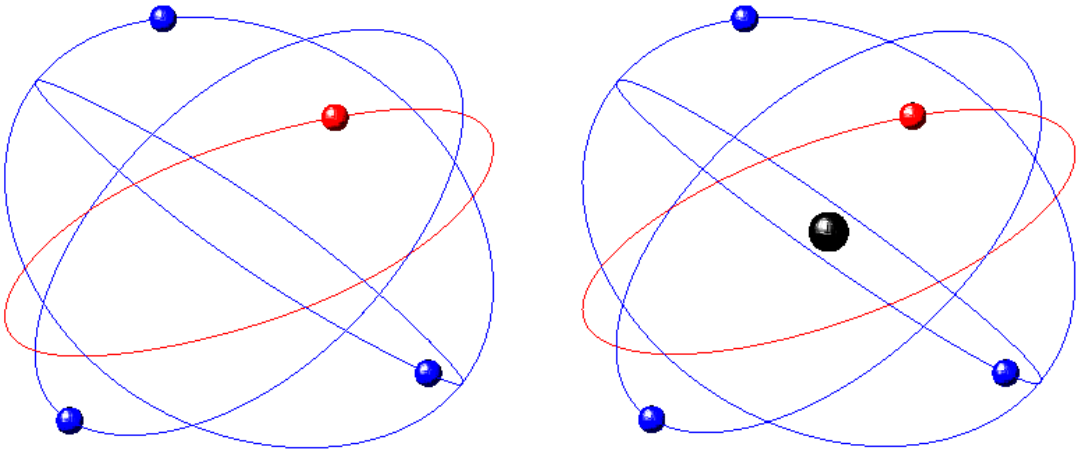

Figure 2.1: The Hip-Hop solution. On the left we show the solution without central body, on the right the solution with a central body of mass $m_0 = 100$. The red curve represents the trajectory of the generating particle u_I.

Note also that a solution with collisions cannot be a minimizer. Indeed, because of relation (2.21), there are at least two collisions per period. In [44] these are called multiple *legs* solutions and it is shown that their action is strictly larger than the action of a circular orbit with minimal period T. This also means that all the minimizers in a sequence $\{u_{m_0}^*\}_{m_0 \geq 0}$ are bounded away from the origin. In Figure 2.1 we show two

orbits, computed without a central body (on the left) and with a central body of mass $m_0 = 100$ (on the right). Since the orbit with no mass in the center is almost circular, the difference in the trajectories of the satellites cannot be really appreciated in the two pictures.

2.3.4 Constellations with $2N$ satellites

In [7, 104] the Hip-Hop solution has been generalized to the case of $2N$ equal masses. Here we do the same in the case of the $(1 + 2N)$-body problem, with a massive central body at the origin. The computations become longer, but techniques and arguments are similar to the ones used above. The symmetry group $\mathcal{G}$ in this case is

$$\mathbb{Z}_{2N} = \{I, \mathsf{R}, \dots, \mathsf{R}^{2N-1}\},$$

where the generator is

$$\mathsf{R} = \begin{pmatrix} \cos\frac{\pi}{N} & -\sin\frac{\pi}{N} & 0 \\ \sin\frac{\pi}{N} & \cos\frac{\pi}{N} & 0 \\ 0 & 0 & -1 \end{pmatrix}.$$

As before, the collision set Γ corresponds to the vertical axis

$$\Gamma = \{x \in \mathbb{R}^3 : x \cdot e_3 = 0\}.$$

The loop set $\mathcal{K}$ is still defined imposing the symmetry (2.21):

$$\mathcal{K} = \{u_I \in H^1_T(\mathbb{R}, \mathbb{R}^3 \setminus \Gamma) : u_I(t + T/2) = -u_I(t),\, t \in \mathbb{R}\},$$

and the argument used to prove the coercivity of the action functional on $\mathcal{K}$ is the same as before. The action of a solution u_I^* with total collisions can be estimated with the results of Proposition 2.8. Then we can compare it with the action of the solution where the satellites are placed at the vertexes of a planar regular $2N$-gon, which rotates uniformly around the origin, and check that the latter is lower. Moreover, this problem is invariant under rotations around the vertical axis, therefore solutions with partial collisions must lie on a vertical plane. Hence, we only have to find a small perturbation $\bar{u}_I$ without collisions and with a lower value of the action. This is obtained in a way similar to [21, Lemma 4] by applying a rotation of a small angle γ to the collision solution u_I^*. In this case we have

$$\mathcal{A}(\bar{u}_I) - \mathcal{A}(u_I^*) = 2\int_0^{T/2} (A + B)dt,$$

with

$$A = 2\sqrt{2}N \sum_{h=1}^{N} \left(\frac{1}{\sqrt{\rho^2\big(1 - \cos\frac{(2h-1)\pi}{N}\big) + \zeta^2\big(1 - \sin^2\gamma\cos\frac{(2h-1)\pi}{N}\big)}} - \frac{1}{\sqrt{\rho^2\big(1 - \cos\frac{(2h-1)\pi}{N}\big) + \zeta^2}} \right),$$

$$B = 2\sqrt{2}N \sum_{h=1}^{N-1} \left(\frac{1}{\sqrt{(\rho^2 + \zeta^2\sin^2\gamma)\big(1 - \cos\frac{2h\pi}{N}\big)}} - \frac{1}{\sqrt{\rho^2\big(1 - \cos\frac{2h\pi}{N}\big)}} \right).$$

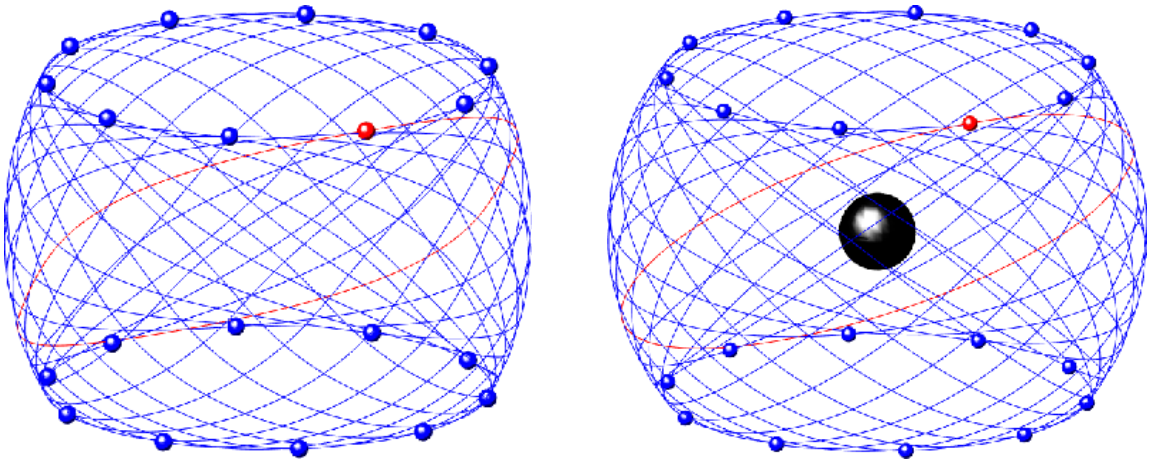

Figure 2.2: The Hip-Hop solution for 20 bodies. On the left it is shown the solution without central body, on the right the solution with a central body of mass $m_0 = 100$. The red curve represents the trajectory of the generating particle u_I. Note that here the difference between the trajectory of the satellites can be appreciated in the two pictures.

The discussion for the Γ-limit is the same as in Section 2.3.3, since the generating particle still moves on a circular orbit. An example of these orbits for $N = 10$ is shown in Figure 2.2, together with an approximation of the minimizer of the Γ-limit.

2.4 $\mathbb{Z}_2 \times \mathbb{Z}_2$ symmetry

In this section we consider $N = 4$, $\alpha = 1$ and discuss the existence of periodic orbits with the symmetry of the Klein group $\mathcal{G} = \mathbb{Z}_2 \times \mathbb{Z}_2$, appearing in [40] in the case without a central body. Using the rotations in $\mathbb{R}^3$, the Klein group can be written as

$$\mathbb{Z}_2 \times \mathbb{Z}_2 = \{I, R_2, R_3, R_4\},$$

where

$$R_2 = \begin{pmatrix} 1 & 0 & 0 \\ 0 & -1 & 0 \\ 0 & 0 & -1 \end{pmatrix}, \quad R_3 = \begin{pmatrix} -1 & 0 & 0 \\ 0 & 1 & 0 \\ 0 & 0 & -1 \end{pmatrix}, \quad R_4 = \begin{pmatrix} -1 & 0 & 0 \\ 0 & -1 & 0 \\ 0 & 0 & 1 \end{pmatrix}$$

are the rotations of π around the three coordinate axes. Moreover, the collisions set Γ corresponds to the union of the three coordinate axes:

$$\Gamma = \bigcup_{i=1}^{3} \{\alpha e_i,\ \alpha \in \mathbb{R}\},$$

where $e_i \in \mathbb{R}^3$ is the unit vector corresponding to the i-th coordinate axis.

We consider loops $u \in \Lambda_{\mathbb{Z}_2 \times \mathbb{Z}_2}$ with the additional symmetry

$$\begin{cases} u_I(t) = \widetilde{R}_3 u_I(-t), \\ u_I(t) = \widetilde{R}_2 u_I(T/2 - t), \end{cases} \tag{2.29}$$

where $\widetilde{R}_j$ is the reflection with respect to the plane $\{x_j = 0\}$. Moreover, we restrict the action functional to the set

$$\mathcal{K} = \Big\{ u_I \in H^1_T(\mathbb{R}, \mathbb{R}^3 \setminus \Gamma) : u_I \text{ satisfies (2.29) and } u_I(0) \in S_1, u_I(T/4) \in S_2 \Big\},$$

where

$$S_1 = \{\alpha e_1 + \beta e_2, \alpha, \beta > 0\}, \qquad S_2 = \{-\alpha e_1 + \beta e_3, \alpha, \beta > 0\}$$

are two quadrants of the planes $\{x_3 = 0\}$, $\{x_2 = 0\}$, respectively. Note that $\mathcal{A}$ is coercive on $\mathcal{K}$, therefore minimizers exist, for every value of $m_0 \geq 0$.

2.4.1 Exclusion of collisions

Total collisions. To exclude total collisions we still use the results of Proposition 2.8. With a notation similar to Section 2.3 we have $\mathcal{M} = 4 + m_0$ and

$$\begin{aligned} U(u) &= \frac{1}{4+m_0}\Big(\sum_{\substack{h,k=1 \\ h\neq k}}^{4} \frac{1}{|u_h - u_k|} + 2\sum_{i=1}^{4} \frac{m_0}{|u_i|} \Big) \\ &= \frac{1}{4+m_0}\Big(2\sum_{j=1}^{3} \frac{1}{|u_I \times e_j|} + \frac{8m_0}{|u_I|} \Big) \\ &= \frac{2}{4+m_0}\Big(\sum_{j=1}^{3} \frac{1}{|u_I \times e_j|} + \frac{4m_0}{|u_I|} \Big). \end{aligned}$$

Moreover, $\rho(u) = 1$ if and only if

$$|u_I| = \frac{\sqrt{4+m_0}}{2},$$

hence

$$U_0 := \min_{\rho(u)=1} U(u) = \frac{4}{(4+m_0)^{3/2}}\Big(3\sqrt{\frac{3}{2}} + 4m_0 \Big).$$

Let $u_I^* \in \overline{\mathcal{K}}$ be a solution with a total collision. Because of the symmetries (2.29), there are at least two total collisions per period, therefore, from Proposition 2.8, its action satisfies

$$\begin{aligned} \mathcal{A}(u_I^*) &\geq 2 \cdot \frac{3}{2}(4+m_0)(\pi U_0)^{2/3}\Big(\frac{T}{2}\Big)^{1/3} \\ &= \frac{3}{2^{1/3}}\pi^{2/3}4^{2/3}\Big(3\sqrt{\frac{3}{2}} + 4m_0\Big)^{2/3} T^{1/3} \\ &= 6\pi^{2/3}\Big(3\sqrt{\frac{3}{2}} + 4m_0\Big)^{2/3} T^{1/3}. \end{aligned} \tag{2.30}$$

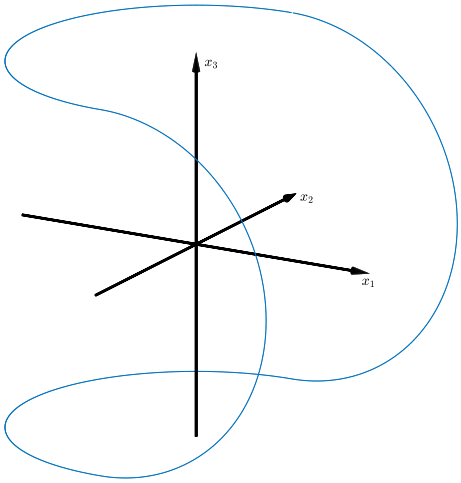

Figure 2.3: The shape of the generating particle of the loop v used to exclude total collisions.

We search for a collision-less loop whose action is less than the lower bound in (2.30). To do that, let $\rho > 0$ and take a loop $v_I \in \mathcal{K}$ such that the generating particle moves with uniform velocity on a closed curve constructed as union of four half circles $C_1^{\pm}, C_2^{\pm}$ of radius ρ. $C_1^{\pm}$ lies on the plane $\{x_3 = \pm\rho\}$, with its center on the axis x_3, and $C_2^{\pm}$ lies on the plane $\{x_2 = \pm\rho\}$, with its center on the axis x_2, see Figure 2.3 for a sketch. From the definition of v_I we have

$$|(R - I)v_I(t)| \geq 2\rho,$$

for all $R \in \mathcal{R} \setminus \{I\}$ and $t \in \mathbb{R}$, and $|v_I(t)| = \sqrt{2}\rho$, for all $t \in \mathbb{R}$. Hence for the action we have the estimate

$$\mathcal{A}(v_I) \leq 32\frac{\pi^2\rho^2}{T} + \frac{3 + 2\sqrt{2}m_0}{\rho}T. \tag{2.31}$$

Choosing

$$\rho = \left(\frac{3 + 2\sqrt{2}m_0}{64\pi^2}T^2\right)^{1/3}$$

we minimize the value of the right hand side of (2.31), therefore

$$\begin{aligned}\mathcal{A}(v_I) &\leq \left(\frac{32\pi^2}{(64\pi^2)^{2/3}} + (64\pi^2)^{1/3}\right)(3 + 2\sqrt{2}m_0)^{2/3}T^{1/3} \\ &= 6\pi^{2/3}(3 + 2\sqrt{2}m_0)^{2/3}T^{1/3}.\end{aligned}$$

Comparing this estimate with (2.30) we see that

$$\mathcal{A}(v_I) < \mathcal{A}(u_I^*),$$

for every value of $m_0 \geq 0$. Hence minimizers are always free of total collisions.

Partial collisions. Let $u_I^* \in \overline{\mathcal{K}}$ be a minimizer with partial collisions and (t_1, t_2) be an interval of regularity. Then u_I^* is a solution of the equation

$$\ddot{w} = \sum_{R \in \mathbb{Z}_2 \times \mathbb{Z}_2 \setminus \{I\}} \frac{(R-I)w}{|(R-I)w|^3} - m_0 \frac{w}{|w|^3}, \quad t \in (t_1, t_2). \tag{2.32}$$

Partial collisions can be excluded as in [40]. Indeed, they can only occur on a coordinate axes and, using the blow-up technique [38], they can be seen locally as parabolic double collisions in a perturbed Kepler problem. The term due to the presence of the central body with mass m_0 turns out to be irrelevant for the discussion (as for the case of the Hip-Hop solution of Section 2.3), since it is included in the perturbation, and does not play any relevant role in the estimates. The situation is similar to the one recalled in Section 2.5.2, where the symmetry of Platonic polyhedra is considered.

Therefore, for every choice of the mass $m_0 \geq 0$, there exists a collision-free minimizer, hence a classical solution of the $(1+4)$-body problem.

2.4.2 Minimizers of the Γ-limit

Let $u_I^* \in \overline{\mathcal{K}}$ be a minimizer of the Γ-limit functional (2.12). We note that there exists $\bar{u}_I \in \partial\mathcal{K}$ such that $\bar{u}_I([0,T])$ is a Keplerian circle with center at the origin, hence we can exclude total collisions in u_I^* like in Section 2.3. It follows that, up to translations of time, $(0, T/4)$ is an interval of regularity of the solution, and u_I^* solves the Keplerian equations of motion. Therefore $u_I^*([0,T/4]) \subseteq \Pi$ where $\Pi \subset \mathbb{R}^3$ is a plane passing through the origin. Moreover

$$u_I^*(0) \in \overline{S}_1, \quad u_I^*(T/4) \in \overline{S}_2. \tag{2.33}$$

By conditions (2.33) and (2.29), we have that Π coincides with a coordinate plane

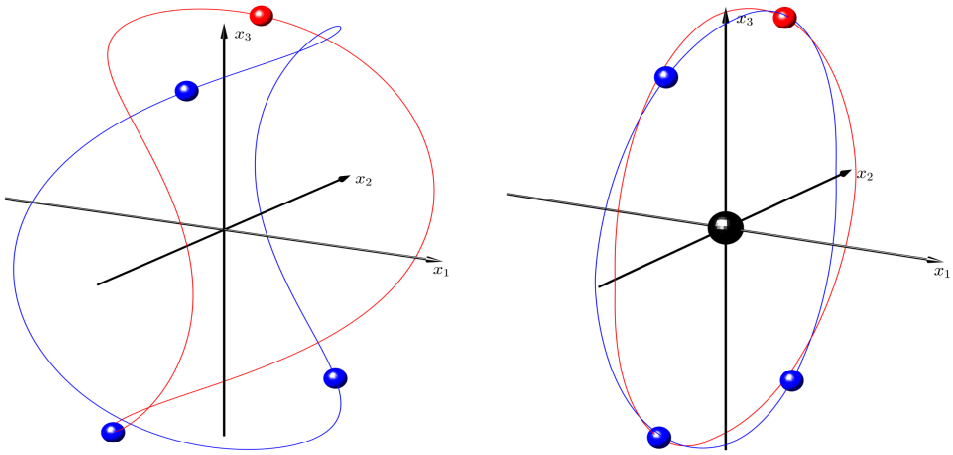

Figure 2.4: Two minimizers of the action functional with the $\mathbb{Z}_2 \times \mathbb{Z}_2$ symmetry. On the left $m_0 = 0$, on the right $m_0 = 1000$. The blue curve is the trajectory of the generating particle.

$\{x_1 = 0\}, \{x_2 = 0\}$ or $\{x_3 = 0\}$. In fact, if this were not the case, then u_I^* would lie on

the same plane also for times $t > T/4$, so that it would not belong to $\overline{\mathcal{K}}$. Moreover, Π cannot be $\{x_2 = 0\}$ or $\{x_3 = 0\}$. Indeed, loops in $\overline{\mathcal{K}}$ are entirely contained in these two planes and satisfying (2.29) are necessarily multiple legs solutions, which contain at least two collisions per period, therefore they cannot be minimizers. The only possibility is that $\Pi = \{x_1 = 0\}$, and extending the minimizer to the whole time interval $[0, T]$ using reflections, we obtain that u_I^* lies entirely on Π. Moreover, $u_I^*([0, T])$ cannot be an ellipse, since ellipses do not satisfy (2.29). The only remaining possibility is that u_I^* is circular, hence the minimizer $u_I^* \in \partial\mathcal{K}$ is

$$u_I^*(t) = r\big(\cos(\omega t)e_2 + \sin(\omega t)e_3\big), \quad \omega = \frac{2\pi}{T},$$

where

$$r = \left(\frac{T}{2\pi}\right)^{\frac{2}{3}}$$

is given by the third Kepler's law. In Figure 2.4 we draw the trajectories of a minimizer for different values of the mass m_0. As m_0 increases, the trajectory of the generating particle becomes closer and closer to the circular loop lying in the plane $\{x_1 = 0\}$, and the four satellites pass closer and closer to two simultaneous double collisions.

It is worth noting that, in the limit $m_0 \to \infty$, the satellites do not bounce back and forth at double collisions, as it happens when we regularize the Keplerian equations of motion (see, for instance, [69]). Instead, they continue moving on the same circular trajectory and cross each other at collisions.

2.5 Symmetry of the Platonic polyhedra

In this section we use the setting of Chapter 1, hence we take the group of rotation $\mathcal{R} \in \{\mathcal{T}, \mathcal{O}, \mathcal{I}\}$ of one of the five Platonic polyhedra. The number of particles N can be either $12, 24$ or 60, accordingly to the choice of the group $\mathcal{R}$. Here we take into account an exponent $\alpha \in [1, 2)$ for potential energy, defining the force of attraction. Still imposing constraints (a), (b) and (c) of Chapter 1, we search for minimizers in the subset of H^1_T defined by (1.8). The coercivity of the action functional $\mathcal{A}^\alpha$ is recovered imposing that the homotopy class fixed by condition (b) is not represented by a loop winding around one axis only. Indeed in this case, if we take a sequence of loops going to infinity in the H^1 norm, then the kinetic energy goes to infinity along this sequence. Therefore, minimizers exist, possibly with collisions, for every value $m_0 \geq 0$ of the central mass. In the following, we state sufficient conditions to exclude partial and total collisions, depending on the selected free-homotopy class.

2.5.1 Total collisions

A priori estimates for the action of a solution with total collisions can be obtained also in the case of α-homogeneous potentials.

Proposition 2.8. *Let $\alpha \in [1,2)$ and let $u : [0,\mathrm{T}] \to \mathbb{R}^{3N}$ be a motion of N masses $m_1, ..., m_N$ connecting a total ejection at time $t = 0$ to a total collision at time $t = \mathrm{T}$. Then for the action*

$$\mathcal{A}^\alpha(u) = \int_0^{\mathrm{T}} \Big(\frac{1}{2}\sum_{h=1}^{N} m_h|\dot u_h|^2 + \sum_{1\le h<k\le N} \frac{m_h\, m_k}{|u_h - u_k|^\alpha}\Big)dt,$$

we have the estimate

$$\mathcal{A}^\alpha(u) \ge \mathcal{M}\bar c^\alpha_{U_{\alpha,0}}(\mathrm{T}), \quad \mathcal{M} = \sum_{h=1}^{N} m_h,$$

where

$$U_{\alpha,0} = \min_{\rho(u)=1} U_\alpha(u), \quad U_\alpha(u) = \frac{1}{\mathcal{M}} \sum_{\substack{h,k=1\\ h\ne k}}^{N} \frac{m_h m_k}{|u_h - u_k|^\alpha}, \quad \rho(u) = \Big(\sum_{h=1}^{N} \frac{m_h}{\mathcal{M}}|u_h|^2\Big)^{1/2},$$

and

$$\bar c^\alpha_{U_{\alpha,0}}(\mathrm{T}) = \mathrm{T}^{\frac{2-\alpha}{2+\alpha}} \frac{2+\alpha}{2-\alpha}(2\alpha^2)^{-\frac{\alpha}{2+\alpha}} \left(\frac{U_{\alpha,0}}{2}\right)^{\frac{2}{2+\alpha}} \left(\int_0^{2\pi} |\sin t|^{\frac{2}{\alpha}}\right)^{\frac{2\alpha}{2+\alpha}}. \tag{2.34}$$

Proof. Using the Cauchy-Schwartz inequality for the scalar product

$$\langle x, y\rangle = \sum_{h=1}^{N} \frac{m_h}{\mathcal{M}} x_h \cdot y_h, \qquad x, y \in \mathbb{R}^{3N},$$

we obtain the inequality

$$\sum_{h=1}^{N} \frac{m_h}{\mathcal{M}}|\dot u_h|^2 \ge \dot\rho^2(u).$$

Then, using the α-homogeneity of the potential, it follows that

$$\mathcal{A}^\alpha(u) \ge \frac{\mathcal{M}}{2}\int_0^{\mathrm{T}} \Big(\dot\rho^2(u) + \frac{1}{\rho^\alpha(u)} U_\alpha\Big(\frac{u}{\rho(u)}\Big)\Big)\, dt \ge \frac{\mathcal{M}}{2}\int_0^{\mathrm{T}} \Big(\dot\rho^2 + \frac{U_{\alpha,0}}{\rho^\alpha}\Big)dt.$$

Then the result follows from the relation

$$\bar c^\alpha_a(\mathrm{T}) = \inf_{\mathfrak{S}} \int_0^{\mathrm{T}} \left(\frac{1}{2}|\dot u|^2 + \frac{a}{|u|^\alpha}\right) dt, \quad \text{for } a > 0,$$

where

$$\mathfrak{S} = \{u \in H^1_T(\mathbb{R}, \mathbb{R}^3) : u(t) = 0 \text{ for some } t\},$$

see [90]. □

Corollary 2.9. *In the same hypotheses of Proposition 2.8 we have*

$$\mathcal{A}^\alpha(u) > \frac{2+\alpha}{2-\alpha}\frac{\mathcal{M}}{2}\left[U_{\alpha,0}\Big(\frac{\pi}{\alpha}\Big)^\alpha\right]^{\frac{2}{2+\alpha}} \mathrm{T}^{\frac{2-\alpha}{2+\alpha}}. \tag{2.35}$$

Proof. The inequality (2.35) follows immediately from Proposition 2.8 and the estimate

$$\int_0^{2\pi} |\sin t|^{\frac{2}{\alpha}} dt > \pi, \quad \forall\, \alpha \in (1,2).$$

□

A priori estimates The total mass is $\mathcal{M} = N + m_0$ and, imposing the symmetry (a), the potential becomes

$$U_\alpha(u) = \frac{N}{N+m_0}\Big(\sum_{R\in\mathcal{R}\setminus\{I\}} \frac{1}{|(R-I)u_I|^\alpha} + \frac{m_0}{|u_I|^\alpha}\Big).$$

Let $p_j \in \mathcal{P}$, $j = 1,2,3$ be the vertexes of a triangle τ of the tessellation of the sphere $\mathbb{S}^2$, recalled in Section 1.2.1. For each pole $p \in \mathcal{P}$, let $\mathfrak{o}_p$ be its order and set

$$k_{\alpha,p} = \sum_{j=1}^{\mathfrak{o}_p - 1} \frac{1}{\sin^\alpha(\frac{j\pi}{\mathfrak{o}_p})}. \tag{2.36}$$

Then the potential can be written as

$$U_\alpha(u) = \frac{N}{N+m_0}\Big(\frac{1}{4}\sum_{p\in\mathcal{P}} \frac{k_{\alpha,p}}{|u_I \times p|^\alpha} + \frac{m_0}{|u_I|^\alpha}\Big). \tag{2.37}$$

Since the loops have the symmetry (a), we also have that

$$\rho(u) = \sqrt{\frac{N}{N+m_0}}|u_I|,$$

hence $\rho(u) = 1$ if and only if $|u_I| = \sqrt{\frac{N+m_0}{N}}$. Therefore, restricting to $\rho(u) = 1$ and using the fact that U_α is an α-homogeneous function, we have

$$\begin{aligned}
U_{\alpha,0} &= \min_{|u_I|=\sqrt{\frac{N+m_0}{N}}} U_\alpha(u) \\
&= \Big(\frac{N}{N+m_0}\Big)^{\frac{\alpha}{2}} \min_{|u_I|=1} U_\alpha(u) \\
&= \Big(\frac{N}{N+m_0}\Big)^{\frac{\alpha+2}{2}} \Big(\frac{1}{4}\min_{|u_I|=1}\sum_{p\in\mathcal{P}} \frac{k_{\alpha,p}}{|u_I\times p|^\alpha} + m_0\Big) \\
&= \Big(\frac{N}{N+m_0}\Big)^{\frac{\alpha+2}{2}} \Big(\frac{1}{4}\min_{u_I\in\overline{\tau}}\sum_{p\in\mathcal{P}} \frac{k_{\alpha,p}}{|u_I\times p|^\alpha} + m_0\Big).
\end{aligned}$$

Since

$$\max_{u_I \in \overline{\tau}} |u_I \times p| = \max_{j\in\{1,2,3\}} |u_I \times p_j|,$$

and

$$\frac{k_{\alpha,p}}{\max_{j\in\{1,2,3\}} |p_j \times p|^\alpha} > \frac{k_{1,p}}{\max_{j\in\{1,2,3\}} |p_j \times p|}, \quad \forall \alpha \in (1,2),$$

we obtain that

$$U_{\alpha,0} \geq \left(\frac{N}{N+m_0}\right)^{\frac{\alpha+2}{2}} (\tilde{U}_0 + m_0), \tag{2.38}$$

where

$$\tilde{U}_0 = \frac{1}{4} \sum_{p\in\mathcal{P}} \frac{k_{1,p}}{\max_{j\in\{1,2,3\}} |p_j \times p|}. \tag{2.39}$$

Consider now a solution $u_I^* \in \overline{\mathcal{K}}$ with M total collisions per period. From Corollary 2.9 and from the above computations we have

$$\begin{aligned} \mathcal{A}^\alpha(u_I^*) &> \frac{2+\alpha}{2-\alpha} \frac{(N+m_0)}{2} U_{\alpha,0}^{\frac{2}{2+\alpha}} \left(\frac{M\pi}{\alpha}\right)^{\frac{2\alpha}{2+\alpha}} T^{\frac{2-\alpha}{2+\alpha}} \\ &\geq \frac{2+\alpha}{2-\alpha} \frac{N}{2} (\tilde{U}_0 + m_0)^{\frac{2}{2+\alpha}} \left(\frac{M\pi}{\alpha}\right)^{\frac{2\alpha}{2+\alpha}} T^{\frac{2-\alpha}{2+\alpha}}. \end{aligned} \tag{2.40}$$

The values of $\tilde{U}_0$ are reported in Table 2.2 and they can be used to compute the right hand side of inequality (2.40). Note that, as the value m_0 of the central mass increases, the term containing $\tilde{U}_0$ becomes irrelevant, since we are mostly interested in the existence of the orbits for large values of m_0.

	$\mathcal{T}$	$\mathcal{O}$	$\mathcal{I}$
$\tilde{U}_0$	6.37126	14.40566	41.03905

Table 2.1: The values of $\tilde{U}_0$ for the three different rotation groups.

Constructing test loops Let ν be the closed sequence of vertexes on $\mathcal{Q}_\mathcal{R}$, used to identify the free-homotopy class fixed in condition (b), and let v_I^ν be the linear piecewise loop, travelling on the edges of the Archimedean polyhedron $\mathcal{Q}_\mathcal{R}$ defined by ν. Its action is given by $\mathcal{A}^\alpha(v_I^\nu) = A_{U_\alpha} + A_K$, where

$$\begin{aligned} A_K &= \frac{N}{2} \int_0^T |\dot{v}_I^\nu|^2 dt = \frac{N}{2} \frac{\ell^2 k_\nu^2}{T}, \\ A_{U_\alpha} &= \frac{N}{2} \int_0^T \Big(\sum_{R\in\mathcal{R}\setminus\{I\}} \frac{1}{|(R-I)v_I^\nu|^\alpha} + \frac{2m_0}{|v_I^\nu|^\alpha} \Big) dt. \end{aligned}$$

Here ℓ is the length of a side of $\mathcal{Q}_{\mathcal{R}}$, k_ν is the minimal period of ν and we have used that $|\dot v_I^\nu| = \ell\frac{k_\nu}{T}$. Rescaling the test loop and using the α-homogeneity of the potential, we have

$$\mathcal{A}^\alpha(\lambda v_I^\nu) = \lambda^2 A_K + \frac{1}{\lambda^\alpha} A_{U_\alpha},$$

and the minimum is attained at $\bar\lambda = \left(\frac{\alpha A_{U_\alpha}}{2A_K}\right)^{\frac{1}{2+\alpha}}$. For this value, the action is

$$\mathcal{A}^\alpha(\bar\lambda v_I^\nu) = (2+\alpha)\left[\left(\frac{A_{U_\alpha}}{2}\right)^2\left(\frac{A_K}{\alpha}\right)^\alpha\right]^{\frac{1}{2+\alpha}}. \tag{2.41}$$

The term A_{U_α} can be expressed through integrals. Indeed, let $\mathcal{L}_{\mathcal{R}}$ be the set of the sides of $\mathcal{Q}_{\mathcal{R}}$, which corresponds to the union of the two orbits $\{R[q,q_i]\}_{R\in\mathcal{R}}$, $i=1,2$, of the segments $[q,q_i]$, $i=1,2$. It follows that we can associate to each $j\in\mathbb{Z}$ a uniquely determined pair $(R_j,i_j)\in\mathcal{R}\times\{1,2\}$ such that $[\nu_{j-1},\nu_j] = R_j[q,q_{i_j}]$. For each given $R'\in\mathcal{R}$, set

$$\zeta_{\alpha,i}(R') = \int_0^1 \sum_{R\in\mathcal{R}\setminus\{I\}} \frac{ds}{|(R-I)R'[(1-s)q+sq_i]|^\alpha}, \qquad i=1,2.$$

Since

$$\big|(R-I)R'[(1-s)q+sq_i]\big| = \big|((R')^{-1}RR'-I)[(1-s)q+sq_i]\big|,$$

and the map $R\mapsto (R')^{-1}RR'$ is an isomorphism of $\mathcal{R}$ onto itself, we have

$$\zeta_{\alpha,i}(R') = \zeta_{\alpha,i}(I) \overset{def}{=} \zeta_{\alpha,i}, \quad i=1,2.$$

We define also

$$\begin{aligned}\zeta_{\alpha,0} &= \int_0^1 \frac{2}{|(1-s)q+sq_1|^\alpha} ds \\ &= \int_0^1 \frac{2}{|(1-s)q+sq_2|^\alpha} ds.\end{aligned}$$

Since v_I^ν travels along each side $[\nu_{j-1},\nu_j]$ in a time interval of size T/k_ν, it follows that

$$\begin{aligned}A_{U_\alpha} &= \frac{N}{2}\frac{T}{k_\nu}\sum_{j=1}^{k_\nu}\int_0^1\Big(\sum_{R\in\mathcal{R}\setminus\{I\}}\frac{1}{|(R-I)R_j[(1-s)q+sq_{i_j}]|^\alpha} + \frac{2m_0}{|(1-s)q+sq_{i_j}|^\alpha}\Big)ds \\ &= \frac{N}{2}\frac{T}{k_\nu}\big(k_1\zeta_{\alpha,1}+k_2\zeta_{\alpha,2}+m_0(k_1+k_2)\zeta_{\alpha,0}\big),\end{aligned}$$

where k_i, $i=1,2$ is the number of sides $[\nu_{j-1},\nu_j]$ in the orbit of $[q,q_i]$, $i=1,2$. From (2.41) we finally obtain

$$\mathcal{A}^\alpha(\bar\lambda v_I^\nu) = \frac{2+\alpha}{2}N\left[\frac{\ell^{2\alpha}\big(k_1\zeta_{\alpha,1}+k_2\zeta_{\alpha,2}+m_0(k_1+k_2)\zeta_{\alpha,0}\big)^2 k_\nu^{2(\alpha-1)}}{4\alpha^\alpha}\right]^{\frac{1}{2+\alpha}} T^{\frac{2-\alpha}{2+\alpha}}. \tag{2.42}$$

Note that, for the Keplerian case, the integrals defining $\zeta_{1,0}, \zeta_{1,1}, \zeta_{1,2}$ can be actually expressed by elementary functions, see [40]. The values of $\zeta_{1,1}, \zeta_{1,2}$ are provided in Table 1.2, while those of $\zeta_{1,0}$ are reported in Table 2.2. For the non-Keplerian case $\alpha \in (1,2)$, we can estimate $\zeta_{\alpha,i}$, $i = 0,1,2$ using the values for the Keplerian case. Indeed, let

$$d_i(R) = \frac{1}{2}|(R - I)(q + q_i)|, \quad i = 1,2,$$

be the minimal distance between the particle v_I^ν travelling along $[q, q_i]$, and the particle v_R^ν travelling along $R[q, q_i]$. We introduce the minimal distance

$$\delta_i = \min_{R \in \mathcal{R} \setminus \{I\}} d_i(R), \quad i = 1,2. \tag{2.43}$$

The values of δ_1, δ_2 are reported in Table 2.2. Note that we can estimate $\zeta_{\alpha,1}$, $\zeta_{\alpha,2}$ using

$$\zeta_{\alpha,i} < \frac{\zeta_{1,i}}{\delta_i^{\alpha-1}} < \frac{\zeta_{1,i}}{\delta_i}, \quad i = 1,2, \tag{2.44}$$

where the last inequality follows from the relations $\delta_i < 1$, $i = 1,2$ (see Table 2.2). The coefficients $\zeta_{\alpha,0}$ can be estimated as follow

$$\zeta_{\alpha,0} < \frac{2}{\left(1 - \frac{\ell^2}{4}\right)^{\frac{\alpha}{2}}} < \frac{8}{4 - \ell^2}. \tag{2.45}$$

In conclusion, in the Keplerian case we can use equation (2.42) to compute the action of the test loop. Instead, in the non-Keplerian case $\alpha \in (1,2)$, we can only estimate it, using inequalities (2.44) and (2.45), and get

$$\mathcal{A}^\alpha(\bar{\lambda} v_I^\nu) < \frac{2+\alpha}{2} N \left[\frac{\ell^{2\alpha} \left(k_1 \frac{\zeta_{1,1}}{\delta_1} + k_2 \frac{\zeta_{1,2}}{\delta_2} + \frac{8 m_0}{4 - \ell^2}(k_1 + k_2)\right)^2 k_\nu^{2(\alpha-1)}}{4\alpha^\alpha} \right]^{\frac{1}{2+\alpha}} T^{\frac{2-\alpha}{2+\alpha}}. \tag{2.46}$$

	$\mathcal{T}$	$\mathcal{O}$	$\mathcal{I}$
δ_1	0.35740	0.35740	0.36230
δ_2	0.35740	0.50544	0.22391
$\zeta_{1,0}$	2.19722	2.09234	2.03446
$\frac{8}{4-\ell^2}$	2.66666	2.29297	2.10560

Table 2.2: Values of $\delta_1, \delta_2, \zeta_{1,0}$ and the upper bound for $\zeta_{\alpha,0}$, for the three different rotation groups.

Using the expressions (2.40), (2.42) and (2.46), for certain free-homotopy classes we have

$$\mathcal{A}^\alpha(\bar{\lambda} v_I^\nu) < \mathcal{A}^\alpha(u_I^*), \tag{2.47}$$

for values of m_0 large enough, and therefore minimizers are free of total collisions. It is worth noting that $\mathcal{A}^\alpha(\bar{\lambda} v_I^\nu)$ and $\mathcal{A}^\alpha(u_I^*)$ goes to $+\infty$ as $m_0 \to \infty$ with the same

asymptotic behaviour. Therefore, to conclude the proof of inequality 2.47, we have to compare the constants in front of the main terms containing the central mass m_0. For this reason, it can happen that the action of the test loop is greater than the action of a solution with total collision for large m_0, provided that the sequence ν is long enough. This suggests that, if the free-homotopy class chosen is complicate enough, it would be more convenient for a minima to undergo a total collision rather than continuing winding around the rotation axes, even if the central mass is large.

2.5.2 Partial collisions

As seen before, partial collisions take place only on the rotation axes $\Gamma \setminus \{0\}$. Let $u_I^* \in \overline{\mathcal{K}}$ be a collision solution and (t_1, t_2) an interval of regularity. Then it is a solution of the Euler-Lagrange equation

$$\ddot{w} = \alpha \sum_{R \in \mathcal{R} \setminus \{I\}} \frac{(R-I)w}{|(R-I)w|^{\alpha+2}} - \alpha m_0 \frac{w}{|w|^{\alpha+2}}, \quad t \in (t_1, t_2). \tag{2.48}$$

Let r be the rotation axis on which the generating particle collides and let $\mathcal{C}$ be the subgroup (of order $\mathfrak{o}_{\mathcal{C}}$) of the rotations with axis r. We can rewrite equation (2.48) and the first integral of the energy in the form

$$\ddot{w} = \alpha c_\alpha \frac{(R_\pi - I)w}{|(R_\pi - I)w|^{2+\alpha}} + V_1(w), \quad c_\alpha = \sum_{j=1}^{\mathfrak{o}_{\mathcal{C}}-1} \frac{1}{\sin^\alpha\left(\frac{j\pi}{\mathfrak{o}_{\mathcal{C}}}\right)}, \tag{2.49}$$

$$|\dot{w}|^2 - c_\alpha \frac{1}{|(R_\pi - I)w|^\alpha} - V(w) = h, \tag{2.50}$$

where R_π is the rotation of π around r, $V_1(w)$ and $V(w)$ are smooth functions defined in an open set $\Omega \subseteq \mathbb{R}^3$ that contains $r \setminus \{0\}$. Moreover, if $\tilde{R} \in \tilde{\mathcal{R}}$ is a reflection such that $\tilde{R}r = r$, then V_1, V satisfy the conditions

$$V_1(\tilde{R}w) = \tilde{R}V_1(w), \quad V(\tilde{R}w) = V(w). \tag{2.51}$$

Therefore, also in this case partial collisions can be seen as binary collisions and asymptotic collision and ejection directions $\mathtt{n}^\pm$, orthogonal to r, can be defined (see Appendix B). Moreover, we can associate an angle θ to the minimizer u_I^* at the collision time t_c. This angle is the same for all the loops in a minimizing sequence converging to u_I^*. It represents the angle between the two asymptotic directions $\mathtt{n}^+, \mathtt{n}^-$ taking into account the (signed) number of revolutions of the trajectories of the minimizing sequence converging to u_I^* around the collision axis r.

In particular, it follows that in the Keplerian case $\alpha = 1$, partial collisions can be excluded as in Subsection 1.2.3, provided that the cone $\mathcal{K}$ is simple and the sequence ν defining the cone does not wind around two coboundary axes. For $\alpha \in (1, 2)$ the discussion has to be adapted, and it is worth to see this case more accurately.

Non-Keplerian case

In Subsection 1.2.3, we have seen the key tools used to exclude partial collisions in the Keplerian case: the blow-up technique and Marchal's Lemma.

Blow-up The blow-up technique remains valid also in the case of α-homogeneous potential (see [38]) and the collision corresponds, asymptotically, to a parabolic collision-ejection solution. Indeed, let us consider an ejection solution of (2.48), i.e. such that

$$\lim_{t\to t_c^+} w(t) = w(t_c) \in r \setminus \{0\},$$

for some $t_c \in [0, T]$ and some rotation axis r. Up to translations of time and space, we can assume that $w(t_c) = 0$, $t_c = 0$ and let $\mathtt{n}$ be the limit ejection direction (see Appendix B). Let $(0, \bar{t})$ the maximal interval of definition of w. Then the rescaled functions

$$w^\lambda : [0, 1] \to \mathbb{R}^3, \quad w^\lambda(\tau) = \lambda^{2/(2+\alpha)} w(\tau/\lambda), \quad \lambda > 1/\bar{t},$$

satisfy

$$\lim_{\lambda\to+\infty} w^\lambda(t) = s^\alpha(\tau)\mathtt{n} \text{ uniformly in } [0, 1],$$
$$\lim_{\lambda\to+\infty} \dot{w}^\lambda(t) = \dot{s}^\alpha(\tau)\mathtt{n} \text{ uniformly in } [\delta, 1],\ 0 < \delta < 1,$$

where

$$s^\alpha(\tau) = \frac{(2+\alpha)^{2/(2+\alpha)}}{2} c_\alpha^{1/(2+\alpha)} \tau^{2/(2+\alpha)}, \quad \tau \in [0, +\infty), \tag{2.52}$$

is the parabolic ejection motion, solution to the equation

$$\dot{s} = \sqrt{\frac{c_\alpha}{(2s)^\alpha}}.$$

Marchal's Lemma Marchal's Lemma for $\alpha \in (1, 2)$ can be found in the literature, see for example [19, 38, 76]. However, the statement commonly found (reported in Appendix A, Lemma A.1) tells us that the minimizer among the arcs connecting two points in the space in a given time is free of collision. In particular, it does not give any information on the action of other critical points, different from the minimizer, as done for the version proved in [40] for the Keplerian case (i.e. Lemma 1.8). For $\alpha \in (1, 2)$ a similar statement, suitable four our purposes, is reported in Appendix A, Lemma A.3. This version can be directly deduced from results present is [10] (see Appendix A, Theorem A.2.

Constructing local perturbations Here we see how to use the above mentioned tools to exclude partial collisions for our problem. Denoting by $\varphi \in [0, 2\pi)$ the angle between any two points in the plane (with the same distance from the origin), the total angle swept by a connecting arc is

$$\varphi + 2k\pi,$$

where $k \in \{k_{\max}, \dots, k_{\max}\}$. The values $k_{\min}, k_{\max} \in \mathbb{Z}$ depend on α and φ and are given by Lemma A.4, formulas (A.19), (A.20) respectively.

Note that, in the Keplerian case, the maximal number of arcs is always two, provided that the angle between the points is not 0. The notion of simple cone is given in order to always have these two arcs available: indeed, if $\mathcal{K}$ is simple and we have a solution with a partial collision which is not of type ($\rightrightarrows$), the possibility of choosing between the two arcs permits to construct a local perturbation, belonging to $\mathcal{K}$ itself, which removes the collision and lowers the action.

The notion of simple cone should be generalized to α-homogeneous potentials trying to reproduce this property, i.e. in always having the possibility of choosing between connecting arcs with the same winding number, independently from the value of the angle φ. For $\alpha \in (1,2)$, the arcs which are always available have winding number k such that

$$\max_{\varphi\in(0,2\pi)} k_{\min} \le k \le \min_{\varphi\in(0,2\pi)} k_{\max}.$$

Note that

$$\max_{\varphi\in(0,2\pi)} k_{\min} = -\left[\frac{1}{2-\alpha}\right], \quad \min_{\varphi\in(0,2\pi)} k_{\max} = \left[\frac{1}{2-\alpha}\right] - 1,$$

hence the total number of arcs always available is $2\big[1/(2-\alpha)\big]$. This suggests that, intuitively, a cone can be defined to be α-*simple* if its loops, for every rotation axis r, do not wind around r more than $[1/(2-\alpha)]$ times. More precisely, a possible rigorous definition is the following.

Definition 2.10. A cone $\mathcal{K}$ is said to be α-*simple* cone if the sequence σ corresponding to $\mathcal{K}$ does not contain any string $\tau_k, \cdots, \tau_{k+2[\frac{1}{2-\alpha}]\mathfrak{o}}$ such that

$$\mathrm{Span}\Big(\bigcap_{j=0}^{2[\frac{1}{2-\alpha}]\mathfrak{o}} \overline{\tau_{k+j}}\Big) = r(R),$$

for some $R \in \mathcal{R} \setminus \{I\}$, where $\mathfrak{o}$ is the order of the pole $r(R)$ determined by R.

Assuming that the cone $\mathcal{K}$ is α-simple, we have

$$-\frac{\pi}{\mathfrak{o}_{\mathcal{C}}} \le \theta \le 2\pi\left[\frac{1}{2-\alpha}\right],$$

where $[\,\cdot\,]$ denotes the integer part. Let $\bar\theta \in [-\frac{\pi}{\mathfrak{o}_{\mathcal{C}}}, 2\pi]$ and $h \in \mathbb{Z}$ such that

$$\theta = \bar\theta + 2\pi h.$$

Note that $h \le [1/(2-\alpha)]$. Let us suppose that the collision is not of type ($\rightrightarrows$), hence we can always assume

$$\theta \neq 2\pi\left[\frac{1}{2-\alpha}\right],$$

from which it follows that $h < [1/(2-\alpha)]$. From Lemma A.4, the arcs which are always available (i.e. independently from the angle between the two points) sweep a total angle of $\bar{\theta} + 2\pi k$, where

$$\max_{\varphi\in(0,2\pi)} k_{\min} \le k \le \min_{\varphi\in(0,2\pi)} k_{\max},$$

and $k_{\min}, k_{\max}$ are given by (A.19), (A.20), respectively. Note that

$$\max_{\varphi\in(0,2\pi)} k_{\min} = -\left[\frac{1}{2-\alpha}\right], \quad \min_{\varphi\in(0,2\pi)} k_{\max} = \left[\frac{1}{2-\alpha}\right] - 1,$$

hence the total number of arcs always available is $2\big[1/(2-\alpha)\big]$. The exclusion of collisions of type different from ($\rightrightarrows$) can be done in the same way as before. Indeed, we can choose a suitable connecting arc and construct a local perturbation $\hat{u}_I^*$, which removes the collision and belongs to the cone $\mathcal{K}$. Moreover, by Lemma A.4, the action of $\hat{u}_I^*$ is lower than the action of the colliding solution u_I^*.

On the other hand, if the collision is of type ($\rightrightarrows$), then

$$\theta = 2\pi\left[\frac{1}{2-\alpha}\right],$$

and it cannot be excluded as before, because one arc is missing. However, Proposition B.2 still holds for $\alpha \in (1,2)$, hence partial collisions are excluded provided that $\mathcal{K}$ does not wind around to two coboundary axes.

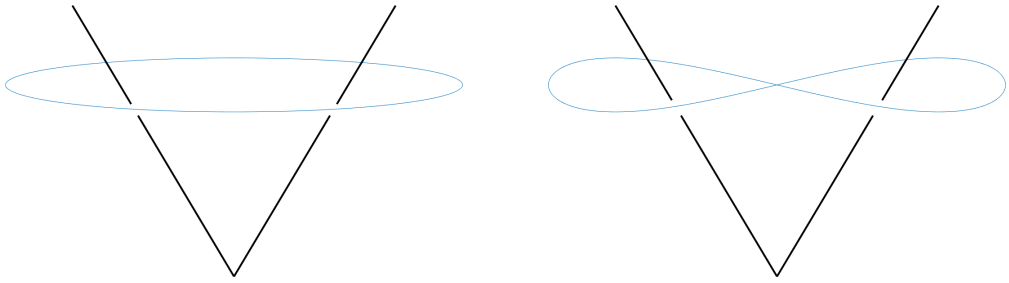

Figure 2.5: Two loops winding around two axes only, having different free-homotopy class. The loop on the left belongs to a cone which is simple in the Keplerian case. The loop on the right is not admissible for the Keplerian case, however it belongs to an α-simple cone for some $\alpha \in (1,2)$.

Note that Definition 1.6 has to be modified properly, to take into account a larger set of cones, including the α-simple one. However, cones of this type can be simply recognized by eye, see Figure 2.5 for an example.

2.5.3 Minimizers of the Γ-limit

The minimizers of the Γ-limit belong to the boundary $\partial\mathcal{K}$, which means that the satellites pass closer and closer to partial collisions as the mass m_0 increases, and they collide in the limit, as we have already seen in the example of Section 2.4 with the Klein group symmetry. However, as opposite to the previous case, here it can happen that the

minimizers of the Γ-limit are not C^1, as we shall see in the examples below. The following statement provides information about the shape of the minimizers.

Theorem 2.11. *Assume $\mathcal{K}$ is not central and $M > 1$. Let $v_I^* \in \overline{\mathcal{K}}$ be a minimizer of the Γ-limit functional $\mathcal{A}_0^\alpha$. Then only one of the following statements holds:*

(i) v_I^* has at least M total collisions per period;

(ii) its trajectory $v_I^*([0,T])$ is composed by circular arcs passing through some rotation axes, hence $v_I^* \in \partial\mathcal{K}$. Moreover, these arcs are swept with uniform motion.

Proof. Let us suppose that v_I^* is a minimizer without total collisions. By contradiction, if v_I^* did not pass through the rotation axes, then it would be a classical smooth solution of

$$\ddot{v_I} = -\alpha \frac{v_I}{|v_I|^{2+\alpha}}. \tag{2.53}$$

In particular, v_I^* would lie on a plane passing through the origin, and this would imply that $\mathcal{K}$ is central. Therefore, we can associate to v_I^* a sequence $\hat{r}_1, \dots, \hat{r}_m$ of rotation semi-axes and a sequence $0 \le \tau_1 < \cdots < \tau_m < T$ of collision times, such that

$$v_I^*(\tau_i) \in \hat{r}_i, \quad i = 1, \dots, m.$$

In the intervals (τ_i, τ_{i+1}) the minimizer solves equation (2.53) with the boundary conditions

$$\begin{cases} \dot{v}_I^*(\tau_i^+) \perp \hat{r}_i, \\ \dot{v}_I^*(\tau_{i+1}^-) \perp \hat{r}_{i+1}. \end{cases} \tag{2.54}$$

Therefore, in these intervals, its trajectory can be either a circular arc, or an arc joining two points where the radial velocity of the orbit vanishes (inversion points). In both cases the energy $E = |\dot{v}_I|^2/2 - 1/|v_I|^\alpha$ of the arc is negative, since positive energies correspond to unbounded solutions, that do not fulfill condition (2.54). However, non-circular orbits are such that the angle between two inversion points is equal to π if $\alpha = 1$, or greater than π if $\alpha \in (1,2)$. We observe that the angle between two rotation semi-axes is at most π. Hence, for $\alpha = 1$, only circular arcs are allowed since elliptic arcs are excluded by condition $M > 1$. For $\alpha > 1$ we can have only circular arcs, even without assuming $M > 1$.

Without loss of generality, we can assume that $0 = \tau_1 < \tau_2 < \cdots < \tau_m < T$ and set $\tau_{m+1} = T$. Set $\hat{r}_{m+1} = \hat{r}_1$ and let θ_i be the angle between the half lines $\hat{r}_i$ and $\hat{r}_{i+1}$, for $i = 1, \dots, m$. Let ρ be the radius of the piecewise circular loop v_I^* passing through the half lines $\hat{r}_1, \cdots, \hat{r}_m$ at the times $\tau_1, \cdots, \tau_m$, respectively, and let ω be its angular velocity, which does not depend on i. Then we have that

$$\omega = \frac{\Delta\theta}{T}, \quad \Delta\theta = \sum_{i=1}^{m} \theta_i, \tag{2.55}$$

Imposing that v_I^* is a solution of the equation on motion (2.53) in $(\tau_i, \tau_{i+1}), i = 1, \dots, m$, we obtain that the radius is

$$\rho = \left(\frac{\alpha}{\omega^2}\right)^{\frac{1}{2+\alpha}}. \tag{2.56}$$

The action of v_I^* is therefore

$$\mathcal{A}_0^\alpha(v_I^*) = \sum_{i=1}^m \int_{\tau_i}^{\tau_{i+1}} \left(\frac{\omega^2\rho^2}{2} + \frac{1}{\rho^\alpha}\right) dt = \frac{2+\alpha}{2}\frac{T}{\rho^\alpha} = \frac{2+\alpha}{2\alpha^{\frac{\alpha}{2+\alpha}}} \Delta\theta^{\frac{2\alpha}{2+\alpha}} T^{\frac{2-\alpha}{2+\alpha}}. \tag{2.57}$$

Note that the action depends only on the sum of the angles $\Delta\theta$ between the intersected half lines. Hence v_I^* minimizes this quantity, and this is equivalent to minimize the length of this piecewise circular loop. □

Remark 2.12. The minimizers of the Γ-limit can have total collisions, and in such case they are necessarily multiple legs solutions, with at least M total collisions per period. A priori estimates for them can be found in [44] for the Keplerian case and in [90] for the non-Keplerian case. For the examples we shall consider here (see Table 2.3), it can be easily verified that multiple leg solutions are not minimizers, since $M > 1$, hence total collisions are excluded.

2.5.4 Examples

Here we discuss some examples, gathering the discussions of Sections 2.5.1, 2.5.2, 2.5.3. to prove the existence of collision-free minimizers of $\mathcal{A}_\varepsilon^\alpha$ for $\varepsilon > 0$. In Table 2.3 we report the list of the selected free-homotopy classes. In Figure 2.6, the trajectories of some of them are displayed, for different values of the mass m_0. More images and videos can be found at the website [35].

Theorem 2.13. *For each sequence ν and the corresponding value of the exponent α listed in Table 2.3, there exists a sequence $\{v_{I,\varepsilon}^*\}_{\varepsilon>0}$ of collision-free minimizers of $\mathcal{A}_\varepsilon^\alpha$ on the cone $\mathcal{K} = \mathcal{K}(\nu)$ such that*

i) each $v_{I,\varepsilon}^*$ is a classical T-periodic solution of the $(1+N)$-body problem with α-homogeneous potential;

ii) as $\varepsilon \to 0$, the sequence $\{v_{I,\varepsilon}^*\}_{\varepsilon>0}$ converges to a minimizer v_I^* of the Kepler problem (2.12) which is of the form described in Theorem 2.11.

Proof. Sequences of Table 2.3 do not wind around one axis only, hence the action functional $\mathcal{A}_\varepsilon^\alpha$ is coercive in the cone $\mathcal{K}(\nu)$, independently from the value of m_0, and minimizers therefore exist.

We use the estimates of Section 2.5.1 to exclude that minimizers have total collisions. Let us distinguish two cases: $\alpha = 1$ and $\alpha \in (1, 2)$. If $\alpha = 1$ the action (2.42) of the test

$\mathcal{R}$	ν	M	k_1	k_2	α
$\mathcal{T}$	$\nu_1 = [1,5,2,6,11,3,12,9,1]$	2	8	/	1
	$\nu_2 = [1,5,8,3,12,4,9,7,1]$	2	8	/	1
	$\nu_3 = [1,5,8,3,10,11,3,12,4,9,12,8,1]$	3	12	/	1
	$\nu_4 = [1,7,6,2,7,9,12,4,9,1,5,8,1]$	3	12	/	1.7
	$\nu_5 = [1,9,7,2,5,1,7,2,10,5,1,7,2,5,1]$	2	14	/	1.8
	$\nu_6 = [1,9,4,12,9,4,12,9,7,2,10,3,11,10,3,11,10,5,1]$	2	18	/	1.85
$\mathcal{O}$	$\nu_1 = [1,3,7,20,24,12,4,9,2,5,1]$	2	4	6	1
	$\nu_2 = [1,3,8,18,13,12,4,9,2,19,11,14,1]$	2	4	8	1
	$\nu_3 = [1,3,7,20,18,8,15,4,6,10,16,5,1]$	3	6	6	1
	$\nu_4 = [1,3,8,15,4,9,2,5,1]$	4	4	4	1
	$\nu_5 = [1,3,10,8,15,6,4,9,22,2,5,16,1]$	4	8	4	1
	$\nu_6 = [1,3,8,10,3,7,20,18,7,14,11,23,14,1,16,5,1]$	4	12	2	1.6
	$\nu_7 = [1,14,7,20,23,14,7,3,1,16,10,3,1]$	2	4	8	1.7
	$\nu_8 = [1,14,7,20,23,14,7,3,1,14,7,3,1,16,10,3,1,14,7,3,1]$	2	4	16	1.8
	$\nu_9 = [1,16,22,6,10,16,5,1,3,7,14,1,16,5,11,19,2,5,1]$	3	6	12	1.75
$\mathcal{I}$	$\nu_1 = [1,3,6,11,48,15,25,26,33,47,7,12,52,59,54,50,1]$	2	6	10	1
	$\nu_2 = [1,3,59,54,51,36,35,46,10,17,57,56,60,5,4,8,14,24,38,34,48,28,11,19,1]$	3	9	15	1
	$\nu_3 = [1,3,7,12,21,39,30,44,2,4,8,20,31,45,19,1]$	5	5	10	1
	$\nu_4 = [1,3,59,7,3,6,47,15,6,11,48,28,11,19,45,43,19,1,50,54,1]$	5	15	5	1

Table 2.3: Sequences of vertexes of $\mathcal{Q}_{\mathcal{R}}$, defining the free-free homotopy classes. The enumeration of the vertexes for $\mathcal{Q}_{\mathcal{O}}$ is referred to the one in Figure 1.2. Images with the enumeration of the vertexes of the other two Archimedean polyhedra can be found at [35]. Note that, for $\mathcal{R} = \mathcal{T}$, the distinction between the two kind of sides is not relevant, so only one value is reported.

loop v_I^ν, associated to the sequence ν, can be computed through elementary functions. Therefore, we use the estimates (2.40) and (2.42), checking that

$$\mathcal{A}^\alpha(\bar{\lambda} v_I^\nu) < \mathcal{A}^\alpha(u_I^*). \tag{2.58}$$

After some computations we find that the above inequality is satisfied if and only if

$$k_1\zeta_{1,1} + k_2\zeta_{1,2} + m_0(k_1+k_2)\zeta_{1,0} < \frac{4\pi M}{\ell}(\tilde{U}_0 + m_0). \tag{2.59}$$

Note that inequality (2.59) is verified for every value of $m_0 \geq 0$ if and only if

$$\begin{cases} k_1\zeta_{1,1} + k_2\zeta_{1,2} < \dfrac{4\pi M}{\ell}\tilde{U}_0, \\ (k_1+k_2)\zeta_{1,0} < \dfrac{4\pi M}{\ell}. \end{cases} \tag{2.60}$$

Values of the members of the above inequalities for the sequences of Table 2.3 are reported in Table 2.4.

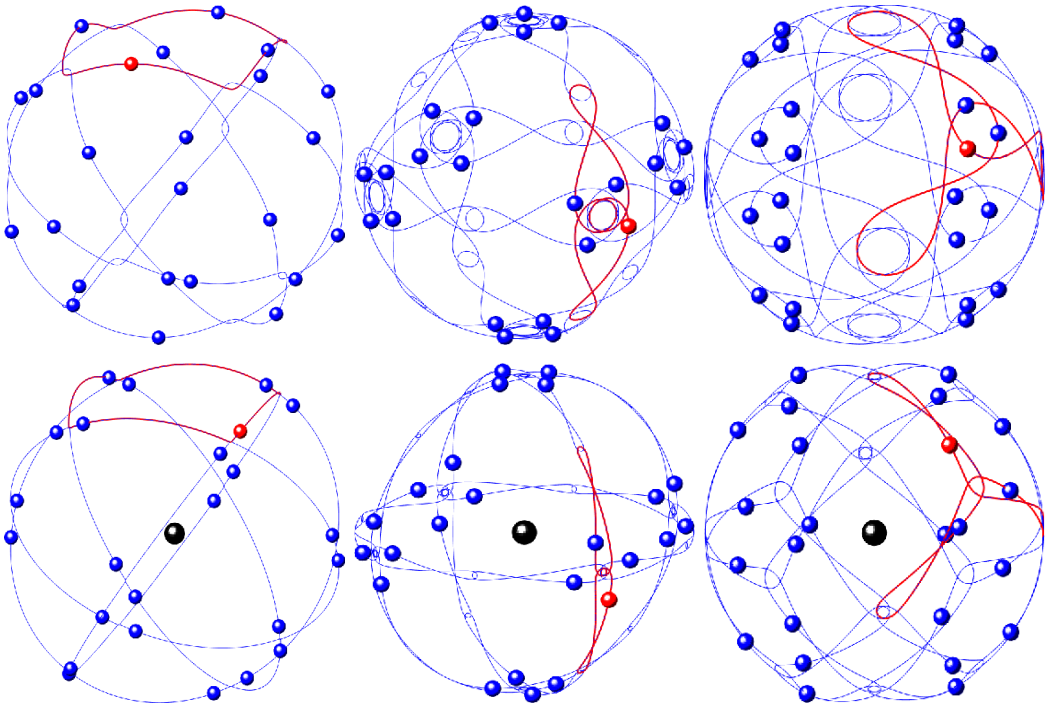

Figure 2.6: Some periodic orbits with the symmetry of the Cube. The topological constraints are given, from the left to the right, by the sequences ν_5, ν_8, ν_9 of Table 2.3. Orbits in the same column belong to the same free-homotopy class. The mass of the central body for the figures on the top is $m_0 = 0$, while $m_0 = 100$ for the figures on the bottom. As the value of m_0 increases, the minimizer approaches an orbit composed by circular arcs, joined at some points on the rotation axes, where partial collisions occur.

In the case $\alpha \in (1, 2)$, the action of the test loop v_I^ν has to be estimated. To this purpose we use (2.46) to estimate the left hand side of (2.58). A sufficient condition to exclude total collisions is therefore

$$k_1 \frac{\zeta_{1,1}}{\delta_1} + k_2 \frac{\zeta_{1,2}}{\delta_2} + \frac{8(k_1 + k_2)\zeta_{1,0}}{4 - \ell^2} m_0 < C(\tilde{U}_0 + m_0), \tag{2.61}$$

where

$$C = \frac{2k_\nu}{(2 - \alpha)^{\frac{2+\alpha}{2}}} \left(\frac{\pi M}{\alpha^{1/2} \ell k_\nu} \right)^\alpha. \tag{2.62}$$

Condition (2.61) is verified for every value of $m_0 \geq 0$ if and only if

$$\begin{cases} k_1 \dfrac{\zeta_{1,1}}{\delta_1} + k_2 \dfrac{\zeta_{1,2}}{\delta_2} < C\tilde{U}_0, \\ \dfrac{8(k_1 + k_2)\zeta_{1,0}}{4 - \ell^2} < C. \end{cases} \tag{2.63}$$

Values of the members of the above inequalities for the sequences of Table 2.3 are reported in Table 2.5. In all the cases, the inequality (2.58) holds true, hence the minimizers are free of total collisions for all the values of $m_0 \geq 0$.

$\mathcal{R}$	ν	$k_1\zeta_{1,1} + k_2\zeta_{1,2}$	$\frac{4\pi M\tilde{U}_0}{\ell}$	$(k_1+k_2)\zeta_{1,0}$	$\frac{4\pi M}{\ell}$
$\mathcal{T}$	ν_1	76.6704	160.1272	17.5776	25.1327
	ν_2	76.6704	160.1272	17.5776	25.1327
	ν_3	115.0056	240.1908	26.3664	37.6991
$\mathcal{O}$	ν_1	199.7300	506.4397	20.9230	35.1556
	ν_2	239.2100	506.4397	25.1076	35.1556
	ν_3	240.3750	759.6595	25.1076	53.7334
	ν_4	160.2500	1012.8793	16.7384	70.3112
	ν_5	241.5400	1012.8793	25.1076	70.3112
$\mathcal{I}$	ν_1	849.7033	2302.7993	32.5513	56.1123
	ν_2	1274.5550	3454.1990	48.8270	84.1685
	ν_3	795.7130	5756.9983	30.5169	140.2809
	ν_4	1072.7354	5756.9983	40.6892	140.2809

Table 2.4: Values of the terms in the inequalities (2.60) corresponding to the sequences of Table 2.3, valid for $\alpha = 1$.

$\mathcal{R}$	ν	$k_1\frac{\zeta_{1,1}}{\delta_1} + k_2\frac{\zeta_{1,2}}{\delta_2}$	$C\tilde{U}_0$	$\frac{8(k_1+k_2)\zeta_{1,0}}{4-\ell^2}$	C
$\mathcal{T}$	ν_4	321.7839	599.1471	70.3104	94.0390
	ν_5	375.4146	528.9010	82.0288	83.0136
	ν_6	482.5759	714.1623	105.4656	112.0912
$\mathcal{O}$	ν_6	838.5492	1914.3903	76.7614	132.8915
	ν_7	539.8787	1203.0097	57.5710	83.5095
	ν_8	852.3135	1644.8228	95.9518	114.1789
	ν_9	809.8181	1804.5146	86.3566	125.2642

Table 2.5: Values of the terms in the inequalities (2.63) corresponding to the sequences of Table 2.3, valid for $\alpha \in (1, 2)$.

Partial collisions are excluded by the results of Section 2.5.2. Indeed, the sequences in Table 2.3 correspond to α-simple cones, for the listed values of α. Moreover, they are not tied to two coboundary axes. Hence, for each sequence ν of Table 2.3, there exists a sequence $\{v^*_{I,\varepsilon}\}_{\varepsilon>0}$ of collision-free minimizers of $\mathcal{A}^\alpha_\varepsilon$, corresponding to a classical T-periodic solution of the $(1+N)$-body problem.

Finally, since the cones $\mathcal{K}$ identified by the sequences of Table 2.3 are all central, the convergence of the sequence to a minimizer of the Kepler problem (2.12) is ensured by Theorem 2.11. □

Chapter 3

Local minimizers for periodic problems

In the following (see Chapter 5), we compute periodic orbits using numerical methods. In particular, we shall compute periodic orbits of Chapters 1 and 2, which are found as minimizers of the action. However, the used numerical methods does not ensure that what we compute is actually a minimizer (see Chapter 4). Despite that, we can check numerically the minimality, at least the local one, after computing the orbits, provided that we have a suitable theory of minimizers, to be implemented in a computer program. The theory of local minimizers for variational problems with fixed endpoints is a well known topic in Calculus of Variations, and it can be found in classical books such as [25, 43, 85]. For other types of boundary conditions, definitions and proofs have to be adapted. A theory for quadratic functionals, with general boundary conditions, can be found in [33] and [113]. A theory of local minimizers for disjoined endpoints has been developed in [111] and further improvements led to a theory for general boundary conditions [112].

Here we present a theory of local minimizers for the case of periodic boundary conditions, adapting some proofs of the classical fixed endpoints problem, and taking inspiration from the results present in the mentioned literature. We also discuss how these results can be used when we want to check the minimality with numerical computations.

3.1 Definitions of minimizers

Fixed $T > 0$, let us consider a functional

$$\mathcal{A}(u) = \int_0^T L(t, u, \dot{u})dt, \tag{3.1}$$

where $L : [0, T] \times \Omega \to \mathbb{R}$ is a C^2 function, T-periodic in the variable t, and $\Omega \subseteq \mathbb{R}^n \times \mathbb{R}^n$ is an open set. We define the space of T-periodic functions

$$V = \{u \in C^1([0, T], \mathbb{R}^n) : u(0) = u(T)\},$$

and assume that $\mathcal{A}$ is defined on a set $X \subseteq V$. We say that $u_0 \in X$ is a

(GM) *global minimum point* if $\mathcal{A}(u) \geq \mathcal{A}(u_0)$ for all $u \in X$;

(SLM) *strong local minimum point* if there exists $\varepsilon > 0$ such that for all $u \in X$ satisfying

$$\|u - u_0\|_\infty < \varepsilon;$$

we have that $\mathcal{A}(u) \geq \mathcal{A}(u_0)$.

(WLM) *weak local minimum point* if there exists $\varepsilon > 0$ such that for all $u \in X$ satisfying

$$\|u - u_0\|_\infty + \|\dot{u} - \dot{u}_0\|_\infty < \varepsilon;$$

we have that $\mathcal{A}(u) \geq \mathcal{A}(u_0)$.

(DLM) *directional local minimum point* if the function $\varphi(s) = \mathcal{A}(u_0 + sv)$ has a local minimum point at $s = 0$ for all $v \in V$. Note that, fixed $v \in V$, $\varphi : (-\delta, \delta) \to \mathbb{R}$ is a function of the real variable s.

We want to state necessary and sufficient conditions to establish whether a given function $u_0 \in X$ is a (DLM), (WLM), (SLM) or none of them. From the classical theory of Calculus of Variations it is well known that, if u_0 is a C^2 minimum point, then it solves the Euler-Lagrange equation associated to (3.1), i.e.

$$\frac{d}{dt} L_{\dot{u}}(t, u_0(t), \dot{u}_0(t)) = L_u(t, u_0(t), \dot{u}_0(t)), \tag{3.2}$$

Moreover, u_0 also satisfies a periodic condition on the derivative, i.e.

$$L_{\dot{u}}(0, u_0(0), \dot{u}_0(0)) = L_{\dot{u}}(T, u_0(T), \dot{u}_0(T)), \tag{3.3}$$

which leads to

$$\dot{u}_0(0) = \dot{u}_0(T). \tag{3.4}$$

Note that u_0 is a (DLM) if and only if the second variation

$$\delta^2 \mathcal{A}(v) = \int_0^T \left(v(t) \cdot \hat{L}_{uu}(t) v(t) + 2\dot{v}(t) \cdot \hat{L}_{u\dot{u}}(t) v(t) + \dot{v}(t) \cdot \hat{L}_{\dot{u}\dot{u}}(t) \dot{v}(t)\right) dt, \tag{3.5}$$

is non-negative, where

$$\begin{aligned} \hat{L}_{uu}(t) &= L_{uu}(t, u_0(t), \dot{u}_0(t)), \\ \hat{L}_{u\dot{u}}(t) &= L_{u\dot{u}}(t, u_0(t), \dot{u}_0(t)), \\ \hat{L}_{\dot{u}\dot{u}}(t) &= L_{\dot{u}\dot{u}}(t, u_0(t), \dot{u}_0(t)). \end{aligned}$$

Since $\delta^2 \mathcal{A}$ is a quadratic functional, defined on the whole space of T-periodic functions V, we are interested in studying these particular type of functionals first.

3.2 Quadratic functionals

We consider a quadratic functional

$$\mathcal{Q}(v) = \int_0^T (v \cdot P(t)v + 2\dot{v} \cdot Q(t)v + \dot{v} \cdot R(t)\dot{v})dt, \tag{3.6}$$

defined on the whole space V, where $P, Q, R : [0,T] \to \mathbb{R}^{n\times n}$ are C^1 matrix functions such that[1] $P(t) = P^T(t)$, $R(t) = R^T(t)$ for all $t \in [0,T]$. The Euler-Lagrange equation associated to (3.6) is

$$\frac{d}{dt}(R\dot{y} + Qy) = Q^T\dot{y} + Py, \tag{3.7}$$

and it is usually called *Jacobi differential equation*. If $\det R(t) \neq 0$ for all $t \in [0,T]$, setting $z = R\dot{y} + Qy$, we can write the system as

$$\begin{cases} \dot{y} = Ay + Bz, \\ \dot{z} = Cy - A^T z, \end{cases} \tag{3.8}$$

where

$$A = -R^{-1}Q, \quad B = R^{-1}, \quad C = P - Q^T R^{-1} Q.$$

Note that B and C are symmetric matrices. It is also useful to introduce the matrix version of equation (3.8), i.e.

$$\begin{cases} \dot{Y} = AY + BZ, \\ \dot{Z} = CY - A^T Z, \end{cases} \tag{3.9}$$

where $Y, Z : [0,T] \to \mathbb{R}^{n\times n}$ are matrix functions.

Remark 3.1. Note that, if $(Y_1, Z_1), (Y_2, Z_2)$ are two solutions of (3.9), then

$$Y_1^T(t)Z_2(t) - Z_1^T(t)Y_2(t) \equiv K, \tag{3.10}$$

where $K \in \mathbb{R}^{n\times n}$ is a constant matrix. This is obtained simply by differentiating the expression on the left hand side of (3.10), and substituting the derivatives given by (3.9).

Definition 3.2. A solution (Y, Z) of (3.9) is said to be *self-conjoined* if

$$Y^T Z - Z^T Y \equiv 0. \tag{3.11}$$

Self-conjoined solutions are particularly useful to write the general solution of the Jacobi differential equation (3.9).

[1] The character T is already used to denote the period. However, when we use the superscript T for a matrix, we mean the transpose of the matrix itself. This notation will not be confusing in the following, since it is always clear when we intend to transpose a matrix.

Proposition 3.3. *Let (Y_0, Z_0) be a self-conjoined solution of (3.9) such that $\det Y_0(t) \neq 0$ for all $t \in [0,T]$. Then all solutions (Y,Z) of (3.9) are given by the formula*

$$\begin{aligned} Y(t) &= Y_0(t)(M + S_0(t)N), \\ Z(t) &= Z_0(t)(M + S_0(t)N) + Y_0^{-T}(t)N, \end{aligned} \tag{3.12}$$

where $M, N \in \mathbb{R}^{n\times n}$ are arbitrary constant matrices and

$$S_0(t) = \int_a^t Y_0^{-1}(s)B(s)Y_0^{-T}(s)\,ds, \tag{3.13}$$

for some $a \in [0,T]$. Moreover

$$\begin{aligned} Y_0^T(t)Z(t) - Z_0^T(t)Y(t) &= N, \\ Y^T(t)Z(t) - Z^T(t)Y(t) &= M^TN - N^TM. \end{aligned} \tag{3.14}$$

Proof. Differentiating (3.12) and using the fact that (Y_0, Z_0) is a self-conjoined solution, we can verify that (Y,Z) defined by (3.12) solves (3.9). Indeed,

$$\begin{aligned} \dot{Y} &= (AY_0 + BZ_0)(M + S_0N) + BY_0^{-T}N \\ AY + BZ &= AY_0(M + S_0N) + BZ_0(M + S_0N) + BY_0^{-T}N \\ \dot{Z} &= (CY_0 - A^TZ_0)(M + S_0N) + Z_0Y_0^{-1}BY_0^{-T}N - Y_0^{-T}(AY_0 + BZ_0)Y_0^{-T}N \\ CY - A^TZ &= CY_0(M + S_0N) - A^TZ_0(M + S_0N) - A^TY_0^{-T}N, \end{aligned}$$

where we have used that

$$\frac{d}{dt}(Y^{-1}) = -Y^{-1}\dot{Y}Y^{-1}.$$

Moreover, since

$$Y(a) = Y_0(a)M, \quad Z(a) = Z_0(a)M + Y_0^{-T}(a)N,$$

the matrices M, N can be chosen in one and only one way so that they satisfy arbitrary initial conditions. Then (3.14) are easily verified evaluating at the left hand sides for $t = a$. □

We introduce now some conditions and give some definitions, useful for later discussions.

(L) The *Legendre condition* holds if $R(t) \geq 0$ [2] for all $t \in [0,T]$.

(L') The *strengthened Legendre condition* holds if $R(t) > 0$ for all $t \in [0,T]$.

[2] In the following, when we write $A > 0$ (resp. $A \geq 0$), where $A \in \mathbb{R}^{n\times n}$ is a symmetric matrix, we mean that A is positive definite (resp. positive semi-definite).

(R) The *regularity condition* holds if

$$v \cdot \int_0^T P(t)dt\, v \geq 0,$$

for all $v \in \mathbb{R}^n$.

(R') The *strengthened regularity condition* holds if

$$v \cdot \int_0^T P(t)dt\, v > 0,$$

for all $v \in \mathbb{R}^n \setminus \{0\}$.

Definition 3.4. Let (y, z) be a solution of system (3.8) such that $y(0) = 0$. A point $c \in (0, T]$ is said to be *conjugate* with 0 if

$$y(c) = 0.$$

Remark 3.5. For later use, it is worth noting that $c \in (0, T]$ is conjugate with 0 if and only if

$$\det Y_0(c) = 0.$$

Definition 3.6. Let (y, z) be a solution of system (3.8). A point $c \in (0, T]$ is said to be *semicoupled* with 0 if

$$\begin{cases} y(0) = y(c), \\ z(0) = z(c) + \displaystyle\int_c^T P(t)dt\, y(c). \end{cases} \tag{3.15}$$

Moreover, if $y(t) \neq y(c)$ for all $t \in (c, T]$, c is said to be *coupled* with 0.

We introduce the following definitions:

(J) The *Jacobi condition* (J) holds if every solution (y, z) of (3.8) with initial condition $y(0) = 0$ does not have any conjugate point $c \in (0, T)$ with 0.

(J') The *strengthened Jacobi condition* (J') holds if every solution (y, z) of (3.8) with initial condition $y(0) = 0$ does not have any conjugate point $c \in (0, T]$ with 0.

(C) Condition (C) holds if every solution (y, z) of (3.8) does not have any semicoupled point $c \in (0, T)$ with 0.

(C') Condition (C') holds if every solution (y, z) of (3.8) does not have any semicoupled point $c \in (0, T]$ with 0.

First we focus on necessary conditions to have a non-negative quadratic functional. In the classical setting of the fixed endpoints problem, it is known that (L) is a necessary condition, moreover, if (L') holds, then (J) is necessary. The interested reader can refer to classical books of Calculus of Variations, such as [43], for detailed proofs of these facts. Here we can prove similar statements, as done in the following lemmas.

Lemma 3.7. *If $\mathcal{Q}(v) \geq 0$ for all $v \in V$, then conditions* (L) *and* (R) *hold.*

Proof. The proof that (L) holds is the same as in the fixed endpoints problem, since we can restrict ourself to local variations vanishing at the extrema of the interval. The regularity condition (R) follows taking constant variations $v(t) \equiv v_0 \in \mathbb{R}^n$, since in this case

$$\mathcal{Q}(v) = v_0 \cdot \int_0^T P(t)\, dt\, v_0 \geq 0,$$

and this is exactly condition (R). □

Lemma 3.8. *If $\mathcal{Q}(v) \geq 0$ for all $v \in V$ and condition* (L′) *holds, then* (C) *holds.*

Proof. Since (L') holds, we can write equation (3.7) as a first order system, in the form (3.8). Suppose that the system has a coupled point, i.e. there exist a non-zero solution (y, z) such that for a certain $c \in (0, T]$ we have $y(c) = y(0)$ and

$$z(0) = z(c) + \int_c^T P(t)\, dt\, y(c).$$

We define

$$v_c(t) = \begin{cases} y(t) & t \in [0, c], \\ y(c) & t \in [c, T]. \end{cases}$$

Note that v_c is T-periodic, then evaluating the quadratic functional and integrating by parts we obtain

$$\begin{aligned}
\mathcal{Q}(v_c) &= \int_0^c (y \cdot Py + 2\dot{y} \cdot Qy + \dot{y} \cdot R\dot{y})dt + y(c) \cdot \int_c^T P(t)\, dt\, y(c) \\
&= \int_0^c (y \cdot (Py + Q^T\dot{y}) + \dot{y} \cdot (Qy + R\dot{y}))dt + y(c) \cdot \int_c^T P(t)\, dt\, y(c) \\
&= \int_0^c (y \cdot \dot{z} + \dot{y} \cdot z)dt + y(c) \cdot \int_c^T P(t)\, dt\, y(c) \\
&= [y \cdot z]_0^c + y(c) \cdot \int_c^T P(t)\, dt\, y(c) \\
&= y(c) \cdot \left(z(c) - z(0) + \int_c^T P(t)\, dt\, y(c) \right) \\
&= 0.
\end{aligned}$$

This means that v_c is a minimizer of $\mathcal{Q}$. However, by condition (L'), the minimizers solve the Jacobi differential equation (3.8) and, moreover, the theorem of uniqueness of the solutions holds. In this case, we would obtain that $v_c(t)$ is constant, which is a contradiction. □

Let us now focus on sufficient conditions. In the classical setting, it is known that conditions (L') and (J') imply that the quadratic functional is non-negative. In [33], a theory for quadratic functionals with general boundary conditions is provided. The authors stated that, if (L'), (R') and (C') hold, then the quadratic functional is non-negative, i.e. the absence of coupled points joined with the regularity condition are sufficient to ensure the non-negativity. The non-negativity of a quadratic functional can be also described in terms of the existence of a particular solution of the Riccati equation that we are going to introduce. This approach can be found, for example, in [111, 112]. Here we present both approaches, describing the main differences between them. In particular, we will see that we obtain necessary and sufficient conditions using the first approach, while with the second one we obtain only sufficient conditions. In the following, we shall remark the difficulties in finding necessary conditions with this approach.

We associate to the quadratic functional (3.6) the *Riccati matrix equation*, which is defined as

$$\dot{W} - C + WA + A^T W + WBW = 0. \tag{3.16}$$

For this purpose we note, that if (Y, Z) is a solution of (3.9) such that $Y(t)$ is non-singular on $[0, T]$, then $W(t) = Z(t)Y^{-1}(t)$ is a solution of (3.16) defined on the whole interval $[0, T]$. Indeed

$$\begin{aligned}
\frac{dZ}{dt}Y^{-1} + Z\frac{dY^{-1}}{dt} - C + ZY^{-1}A + A^T ZY^{-1} + ZY^{-1}BZY^{-1} = \\
(CY - A^T Z)Y^{-1} - ZY^{-1}\dot{Y}Y^{-1} - C + ZY^{-1}A + A^T ZY^{-1} + ZY^{-1}BZY^{-1} = \\
-ZY^{-1}\dot{Y}Y^{-1} + ZY^{-1}(A + BZY^{-1}) = \\
-ZY^{-1}\dot{Y}Y^{-1} + ZY^{-1}\dot{Y}Y^{-1} = 0
\end{aligned}$$

Moreover, if (Y, Z) is also self-conjoined, then W is symmetric.

3.2.1 The approach based on coupled points

In [33], the authors provide a theory of quadratic functionals for general boundary conditions. Given an interval $[a, b] \subseteq \mathbb{R}$, consider the functional

$$\mathcal{Q}(v) = \int_a^b (v \cdot P(t)v + 2\dot{v} \cdot Q(t)v + \dot{v} \cdot R(t)\dot{v})dt,$$

defined on functions $v : [a, b] \to \mathbb{R}^n$ satisfying the boundary conditions

$$D \begin{pmatrix} v(a) \\ v(b) \end{pmatrix} = 0, \tag{3.17}$$

where D is a constant matrix of order $2n$. In this setting, we can still define conditions (J), (C) and (R) (together with their strengthened versions) in an almost analogue way

as above, simply by following the proofs of the lemmas for necessary conditions. The main theorem of [33] states that the absence of coupled points together with the regularity condition (R'), ensures the non-negativity of the quadratic functional. Moreover, this condition is equivalent to the absence of conjugate points plus a condition of non-negativity of a matrix, constructed using particular solutions of the Riccati equation.

Theorem 3.9 ([33], Theorem 3)**.** *Assume that condition* (L′) *holds. Then the following properties are equivalent*

(i) $\mathcal{Q}(v) > 0$ *for all non-zero admissible functions* v*.*

(ii) Conditions (C′) *and* (R′) *hold.*

(iii) Condition (J′) *holds and*

$$\alpha \cdot \begin{pmatrix} -W_b(a) & -Y_a^{-1}(b) \\ -Y_a^{-T}(b) & W_a(b) \end{pmatrix} \alpha > 0, \tag{3.18}$$

for all nonzero $\alpha \in \mathbb{R}^{2n}$ *such that* $D\alpha = 0$*. Here* (Y_a, Z_a)*,* (Y_b, Z_b) *are the solutions of* (3.9) *given by the initial conditions*

$$\begin{cases} Y_a(a) = 0, \\ Z_a(a) = I, \end{cases} \qquad \begin{cases} Y_b(b) = 0, \\ Z_b(b) = -I, \end{cases}$$

and $W_a = Z_a Y_a^{-1}$*,* $W_b = Z_b Y_b^{-1}$*.*

Let us focus on the case of periodic boundary conditions. Then $[a, b] = [0, T]$ and the matrix D results to be

$$D = \begin{pmatrix} I & -I \\ 0 & 0 \end{pmatrix} \in \mathbb{R}^{2n \times 2n}.$$

The vectors $\alpha \in \mathbb{R}^{2n}$ such that $D\alpha = 0$ are of the form

$$\alpha = \begin{pmatrix} \beta \\ \beta \end{pmatrix},$$

where $\beta \in \mathbb{R}^n$. Therefore, condition (3.18) becomes

$$\beta \cdot (W_0(T) - W_T(0) - Y_0^{-1}(T) - Y_0^{-T}(T))\beta > 0, \tag{3.19}$$

for all $\beta \in \mathbb{R}^n \setminus \{0\}$, which means that the matrix within the parentheses is positive definite. From the numerical point of view, we have to choose which conditions are suitable to be verified with numerical computations. It is clear that we can check (R') by computing an integral and see if the resulting matrix is positive definite, but condition (C') is impossible to check numerically, since it takes into account all the solutions of (3.8). Instead, conditions (J') and (3.19) can be managed numerically. Indeed, what we have to do is

(1) compute the solution (Y_0, Z_0) of (3.9) integrating the differential equation using the initial conditions $Y_0(0) = 0$, $Z_0(0) = I$ on $[0, T]$. Then we check whether $\det Y_0(t) \neq 0$ for all $t \in (0, T]$ to check (J');

(2) compute the solution (Y_T, Z_T) of (3.9) integrating the differential equations on $[0, T]$ backwards in time, using the initial conditions $Y_T(T) = 0$, $Z_T(T) = -I$;

(3) invert the matrices $Y_0(T)$, $Y_T(0)$, compute $W_0(T), W_T(0)$ and construct the matrix in (3.19);

(4) compute the eigenvalues of the matrix in (3.19) and check whether they are all positive or not.

3.2.2 The approach based on Riccati equation with boundary conditions

Here we describe an approach based on the existence of solutions of the Riccati equation with particular boundary conditions, similar to the ones present in [111, 112]. We point out that we discuss both approaches also because sufficient conditions for the strong local minimality are given in these terms, and not in terms of coupled points, as we will see in Section 3.4. We introduce the following condition.

(SR) Condition (SR) is satisfied if there exists a symmetric solution $W(t)$ of the Riccati equation (3.16), defined on the whole interval $[0, T]$, such that

$$W(T) - W(0) > 0. \tag{3.20}$$

This condition is sufficient to have a positive definite quadratic functional in the case of periodic boundary conditions. For other types of boundary conditions, the inequality (3.20) has to be adapted, see for example [112].

Theorem 3.10. *Let conditions* (L′) *and* (SR) *hold. Then we have that* $\mathcal{Q}(v) \geq 0$ *for all* $v \in V$.

Proof. Let W be the symmetric solution of the Riccati equation (3.16) defined on the whole interval $[0, T]$, such that $W(T) - W(0)$ is positive definite. Given $v \in V$, we have that

$$\begin{aligned}
\mathcal{Q}(v) &= \int_0^T \Big(v \cdot Pv + 2\dot{v} \cdot Qv + \dot{v} \cdot R\dot{v} - \frac{d}{dt}(v \cdot Wv) + \frac{d}{dt}(v \cdot Wv) \Big) dt \\
&= v(t) \cdot W(t)v(t)\Big|_0^T + \int_0^T (R\dot{v} + Qv - Wv) \cdot B(R\dot{v} + Qv - Wv) dt \\
&= v(0) \cdot (W(T) - W(0))v(0) + \int_0^T (R\dot{v} + Qv - Wv) \cdot B(R\dot{v} + Qv - Wv) dt,
\end{aligned}$$

where we have used that $v(0) = v(T)$ in the last equality. Since $B(t) = R^{-1}(t)$, from condition (L'), B is positive definite for all $t \in [0, T]$, then the function in the integral is non-negative. Since also $W(T) - W(0)$ is positive definite, we have that $\mathcal{Q}(v) \geq 0$. □

One could try to match the sufficient conditions of Theorem 3.9 with the (SR) condition on the existence of a symmetric solution of the Riccati equation with boundary conditions. Indeed, these conditions are equivalent for the classical case of the fixed endpoints problem, since it is known that the absence of conjugate points leads to the existence of a symmetric solution of the Riccati equation which is positive definite. More in general, the same can be done when the endpoints are disjoined [111]. However, when the endpoints are joined, as in the case of the periodic boundary conditions, the existence of a symmetric solution of the Riccati equation with boundary conditions is sufficient but not necessary to have a positive quadratic functional (see [112], pag. 599). To show the problems arising in finding necessary conditions for the case of periodic boundary conditions, let us prove first the following result.

Lemma 3.11. *Let conditions* (L′) *and* (J′) *hold. Let* (Y_0, Z_0), (Y_T, Z_T) *be the solutions of* (3.9) *with initial conditions*

$$\begin{cases} Y_0(0) = 0, \\ Z_0(0) = I, \end{cases} \qquad \begin{cases} Y_T(T) = 0, \\ Z_T(T) = -I, \end{cases}$$

and $W_0 = Z_0 Y_0^{-1}$, $W_T = Z_T Y_T^{-1}$. *If*

$$W_0(T) - \left(Y_0(T) Y_0^T(T)\right)^{-1} - W_T(0) - I > 0, \tag{3.21}$$

then condition (SR) holds.

Proof. Since condition (J') holds, by Remark 3.5 $Y_0(t)$ is invertible for $t \in (0, T]$ and $Y_T(t)$ is invertible for $t \in [0, T)$. Let $M = Y_0(T)^{-T}$ and $(Y_1, Z_1) = (Y_T M, Z_T M)$. The solutions (Y_0, Z_0), (Y_1, Z_1) are self-conjoined, and by Remark 3.1 we have that

$$Y_1^T Z_0 - Z_1^T Y_0 = I.$$

Let (Y, Z) be the solution of (3.9) defined by

$$\begin{cases} Y = Y_0 + Y_1, \\ Z = Z_0 + Z_1. \end{cases}$$

Using the above observations, evaluating at $t = T$ we obtain that

$$Y^T Z - Z^T Y \equiv 0,$$

i.e. the solution (Y, Z) is self-conjoined.

Let us prove first that $Y(t)$ is invertible for $t \in [0, T]$. By Proposition 3.3, we have $Y_0(t) = Y_1(t) S_1(t)$ for $t \in [0, T)$, where

$$S_1(t) = \int_0^t Y_1^{-1}(s) B(s) Y_1^{-T}(s)\, ds \geq 0.$$

Then, $Y(T) = Y_0(T)$ is invertible, and the relation

$$Y(t) = Y_1(t)\big(I + S_1(t)\big), \quad t \in [0, T),$$

shows that $Y(t)$ is invertible in $[0, T)$, hence $Y(t)$ is invertible on the whole $[0, T]$.

Hence $W = YZ^{-1}$ is a symmetric solution of the Riccati equation, defined on the whole $[0, T]$, such that

$$\begin{aligned}
W(0) &= \big(Z_0(0) + Z_T(0)M\big)\big(Y_0(0) + Y_T(0)M\big)^{-1} \\
&= \big(I + Z_T(0)M\big)M^{-1}Y_T(0)^{-1} \\
&= M^{-1}Y_T(0)^{-1} + W_T(0), \\
&= M^{-1}Y_0(T)^{-T} + W_T(0), \\
&= I + W_T(0), \\
W(T) &= \big(Z_0(T) + Z_T(T)M\big)\big(Y_0(T) + Y_T(T)M\big)^{-1} \\
&= \big(Z_0(T) - M\big)Y_0(T)^{-1} \\
&= W_0(T) - MY_0(T)^{-1} \\
&= W_0(T) - \big(Y_0(T)Y_0^T(T)\big)^{-1}.
\end{aligned}$$

Then $W(T) - W(0)$ has the expression given in the left hand side of (3.21), and it is positive definite by the hypothesis, therefore condition (SR) holds. □

Remark 3.12. Note that the matrices in (3.19) and in (3.21) look similar. Therefore, one is tempted to deduce the (SR) condition assuming that (J') and (3.19) hold, and then follow the steps of the proof of the above lemma, proving that condition (SR) is also necessary. The idea is to construct a solution W of the Riccati equation such that

$$W(T) - W(0) = W_0(T) - W_T(0) - Y_0^{-1}(T) - Y_0^{T-1}(T),$$

which is positive definite if we assume (3.19). Such solution can be obtained using the solution (Y, Z) of (3.9) defined as

$$\begin{cases} Y = Y_0 + Y_T, \\ Z = Z_0 + Z_T, \end{cases}$$

where (Y_0, Z_0), (Y_T, Z_T) are as above. Using similar arguments, one can prove that $\det Y(t) \neq 0$ for all $t \in [0, T]$, hence $W = ZY^{-1}$ is defined on the whole $[0, T]$. However, some problems arise when we try to prove that (Y, Z) is self-conjoined, which is equivalent to saying that W is symmetric. Indeed, evaluating in $t = 0$ the relation (3.10), the invariant matrix results to be

$$\begin{aligned}
Y^T(0)Z(0) - Z^T(0)Y(0) &= Y_T^T(0) - Y_T(0) \\
&= Y_0(T) - Y_0^T(T).
\end{aligned} \tag{3.22}$$

In dimension $n = 1$ this is actually zero, hence (SR) condition is equivalent to (J') joined with (3.19). However, this is a very special situation, since the transpose sign has no effects in dimension one. In higher dimension, equation (3.22) is not zero in general, hence we cannot conclude the equivalence between the two conditions with the above approach. Moreover, if we subtract the two matrices in (3.19) and (3.21), we obtain

$$W_0(T) - W_T(0) - Y_0^{-1}(T) - Y_0^{T-1}(T) - W_0(T) + W_T(0) + \left(Y_0(T)Y_0^T(T)\right)^{-1} + I = \\ (Y_0^{-1}(T) - I)^T(Y_0^{-1}(T) - I) \geq 0.$$

This means that the sufficient condition (3.19) does not necessarily imply condition (3.21), which ensures the (SR) condition. However, it is not clear if it is possible to obtain a solution of the Riccati equation satisfying condition (SR) with other strategies.

The following lemma relates the dimension and the sign of the determinant of $Y_0(t)$ with the (SR) condition. This could be useful to search for a symmetric solution W of the Riccati equation satisfying the boundary condition $W(T) - W(0) > 0$ when we cannot use Lemma 3.11.

Lemma 3.13. *Let conditions (L') and (J') hold. Let (Y_0, Z_0) be the solution of (3.9) with initial conditions*

$$\begin{cases} Y_0(0) = 0, \\ Z_0(0) = I. \end{cases}$$

Then

(i) if n is even and $\det Y_0(t) > 0$ for $t \in (0, T]$, then condition (SR) holds;

(ii) if n is odd and $\det Y_0(t) < 0$ for $t \in (0, T]$, then condition (SR) holds.

Proof. From condition (J'), we have that the solution (Y_0, Z_0) of (3.9) is such that $\det Y_0(t) \neq 0$ for all $t \in (0, T]$, then we can define $W_0(t) = Z_0(t)Y_0^{-1}(t)$. Let $(Y_\varepsilon, Z_\varepsilon)$ be the solution of (3.9) with initial conditions

$$\begin{cases} Y_\varepsilon(0) = -\varepsilon I, \\ Z_\varepsilon(0) = I. \end{cases}$$

From the continuous dependence of the solutions with respect to the initial conditions, we know that $(Y_\varepsilon, Z_\varepsilon) \to (Y_0, Z_0)$ uniformly in $[0, T]$. Moreover,

$$\det Y_\varepsilon(0) = (-\varepsilon)^n,$$

hence in the hypotheses (i) or (ii) we have that $\det Y_0(t)$ and $\det Y_\varepsilon(t)$ have the same sing for t near zero. Therefore, for ε small enough, we have that $\det Y_\varepsilon(t) \neq 0$ for all $t \in [0, T]$. Moreover, evaluating (3.10) for $t = 0$, we obtain that $(Y_\varepsilon, Z_\varepsilon)$ is self-conjoined, hence $W_\varepsilon(t) = Z_\varepsilon(t)Y_\varepsilon^{-1}(t)$ is a symmetric solution of (3.16) defined on the whole $[0, T]$.

Now we prove that $W_\varepsilon(T) - W_\varepsilon(0)$ is positive definite for ε small enough. First we note that

$$W_\varepsilon(0) = Z_\varepsilon(0)Y_\varepsilon^{-1}(0) = -\frac{1}{\varepsilon}I.$$

Let $w \in \mathbb{R}^n$ be a nonzero vector, then

$$\lim_{\varepsilon\to 0^+} w \cdot W_\varepsilon(T)w = w \cdot W_0(T)w \in \mathbb{R},$$

$$\lim_{\varepsilon\to 0^+} w \cdot W_\varepsilon(0)w = \lim_{\varepsilon\to 0^+} \frac{-|w|^2}{\varepsilon} = -\infty,$$

hence the thesis. □

3.3 Weak local minimizers

Using the theory of quadratic functionals, we can find sufficient conditions to have a (WLM) for the case of periodic boundary conditions. Since the approach based on symmetric solutions of the Riccati equation with boundary condition does not fully match the necessary and sufficient conditions of Theorem 3.9, we discuss the theory of weak local minimizers using the approach based on coupled points.

Lemma 3.14. *Let $\mathcal{Q}$ be a quadratic functional defined on V. Then there exists $C > 0$ such that*

$$|\mathcal{Q}(v)| \le C \int_0^T \Big(|v|^2 + |\dot v|^2\Big)dt, \tag{3.23}$$

for all $v \in V$.

Proof. It is sufficient to note that

$$2|v||\dot v| \le |v|^2 + |\dot v|^2,$$

Then we have that

$$|\mathcal{Q}(v)| \le C_1 \int_0^T |\dot v|^2 dt + C_2 \int_0^T |v|^2 dt,$$

where the constants C_1, C_2 are

$$C_1 = \|Q\|_\infty + \|R\|_\infty, \quad C_2 = \|Q\|_\infty + \|P\|_\infty.$$

Then taking $C = \max\{C_1, C_2\}$ the thesis follows. □

Remark 3.15. Note that the coefficient C is small if C_1 and C_2 are both small. This happens when the matrix functions P, Q, R are small in the sup norm.

Lemma 3.16. *Let $\mathcal{Q}$ be a positive definite quadratic functional defined on V and satisfying* (L′). *Then there exists $\varepsilon_0 > 0$ such that*

$$\mathcal{Q}(v) \ge \varepsilon_0 \int_0^T \Big(|v|^2 + |\dot v|^2\Big)dt \tag{3.24}$$

for all $v \in V$.

Proof. Consider the functional

$$\begin{aligned}\hat{\mathcal{Q}}_\varepsilon(v) &:= \mathcal{Q}(v) - \varepsilon \int_0^T \Big(|v|^2 + |\dot{v}|^2\Big) dt \\ &= \int_0^T \Big(v \cdot (P - \varepsilon I)v + 2\dot{v} \cdot Qv + \dot{v} \cdot (R - \varepsilon I)\dot{v}\Big) dt \\ &= \int_0^T \Big(v \cdot \hat{P}v + 2\dot{v} \cdot \hat{Q}v + \dot{v} \cdot \hat{R}\dot{v}\Big) dt,\end{aligned}$$

where $\hat{P} = P - \varepsilon I$, $\hat{Q} = Q$, $\hat{R} = R - \varepsilon I$. We verify that $\hat{\mathcal{Q}}_\varepsilon$ is still positive definite for ε small enough, using the equivalent conditions given by Theorem 3.9. For ε small enough, $\hat{\mathcal{Q}}_\varepsilon$ verifies (L'), (J') and (3.19).

(L') holds since, from condition (L') on R, we have that $R \geq kI$ for some $k > 0$. Hence $\hat{R} \geq (k - \varepsilon)I$. For ε small enough we have that $k - \varepsilon > 0$.

(J') holds because of the uniform convergence of the solutions of (3.9) as $\varepsilon \to 0$.

(3.19) holds for the same reason above, since the eigenvalues are continuous functions with respect to the entries of the matrix.

Therefore, for ε small enough, the quadratic functional $\hat{\mathcal{Q}}_\varepsilon$ is positive definite and the thesis follows. □

Lemma 3.17. *Let $\mathcal{Q}_0$ be a positive definite quadratic functional defined on V, with coefficients P_0, Q_0, R_0, satisfying* (L′). *Let $\mathcal{Q}$ be a quadratic functional defined on V with coefficients P, Q, R. If*

$$\|P - P_0\|_\infty, \quad \|Q - Q_0\|_\infty, \quad \|R - R_0\|_\infty,$$

are small enough, then $\mathcal{Q}$ is positive definite.

Proof. Let us write

$$\mathcal{Q}(v) = \mathcal{Q}_0(v) + \hat{\mathcal{Q}}(v),$$

where

$$\hat{\mathcal{Q}}(v) = \int_0^T \Big(v \cdot (P - P_0)v + 2\dot{v} \cdot (Q - Q_0)v + \dot{v} \cdot (R - R_0)\dot{v}\Big) dt.$$

From Lemma 3.16 we have that

$$\mathcal{Q}_0(v) \geq \varepsilon_0 \int_0^T \Big(|v|^2 + |\dot{v}|^2\Big) dt.$$

From Lemma 3.14, there exists C such that

$$|\hat{\mathcal{Q}}(v)| \leq C \int_0^T \Big(|v|^2 + |\dot{v}|^2\Big) dt.$$

Then

$$\mathcal{Q}(v) \geq \varepsilon_0 \int_0^T \Big(|v|^2 + |\dot{v}|^2\Big)dt - C\int_0^T \Big(|v|^2 + |\dot{v}|^2\Big)dt,$$

and the coefficient C, from Remark 3.15, is smaller than ε_0 for $\|P - P_0\|_\infty$, $\|Q - Q_0\|_\infty$, $\|R - R_0\|_\infty$ small enough, hence $\mathcal{Q}$ is positive definite. □

Theorem 3.18. *Let $u_0 \in X$ be a periodic solution of the Euler-Lagrange equation* (3.2) *and let conditions* (L′), (C′) *and* (R′) *hold for the second variation associated to u_0. Then u_0 is a* (WLM).

Proof. Let $u \in X$ and set $v = u - u_0 \in V$. Consider

$$\varphi(s) := \mathcal{A}(u_0 + sv).$$

Then

$$\mathcal{A}(u) = \varphi(1) = \varphi(0) + \varphi'(0) + \frac{1}{2}\varphi''(s_0) = \mathcal{A}(u_0) + \frac{1}{2}\varphi''(s_0), \quad s_0 \in (0,1).$$

We have that

$$\begin{aligned}\varphi''(s_0) = \int_0^T \Big(& v(t)\cdot L_{uu}(t, u_0(t) + s_0 v(t), \dot{u}_0(t) + s_0\dot{v}(t))v(t) \\ & + 2\dot{v}(t)\cdot L_{\dot{u}u}(t, u_0(t) + s_0 v(t), \dot{u}_0(t) + s_0\dot{v}(t))v(t) \\ & + \dot{v}(t)\cdot L_{\dot{u}\dot{u}}(t, u_0(t) + s_0 v(t), \dot{u}_0(t) + s_0\dot{v}(t))\dot{v}(t)\Big)dt.\end{aligned}$$

Note that $\varphi''(s_0)$ is a quadratic functional. If $\|v\|_\infty + \|\dot{v}\|_\infty$ is small enough, by the continuity of the second derivatives of L, the coefficients of $\varphi''(s_0)$ are near to the coefficients of the second variation associated to u_0, in the sup norm. Therefore, from Lemma 3.17 we conclude that $\varphi''(s_0) \geq 0$ and u_0 is a (WLM). □

3.4 Strong local minimizers

To discuss the strong local minimizers, we need a few other definitions and conditions. We define the *Weierstrass excess function* as

$$E(t, u, v, w) := L(t, u, w) - L(t, u, v) - (w - v)\cdot L_{\dot{u}}(t, u, v). \tag{3.25}$$

Let $u_0 \in X$ be a solution of the Euler-Lagrange equation (3.2). To simplify the notations in the following, we define the *tube* around u_0 of radius $\varepsilon > 0$ as

$$T(u_0, \varepsilon) = \big\{(t, y) \in [0, T] \times \mathbb{R}^n : |y - u_0(t)| < \varepsilon\big\},$$

and the *restricted tube* as

$$RT(u_0, \varepsilon) = \big\{(t, y, v) \in [0, T] \times \mathbb{R}^n \times \mathbb{R}^n : |y - u_0(t)| < \varepsilon,\ |v - \dot{u}_0(t)| < \varepsilon\big\}.$$

We introduce also additional conditions.

(W) The *Weierstrass condition* holds if

$$E(t, u_0(t), \dot{u}_0(t), w) \geq 0, \tag{3.26}$$

for all $t \in [0, T]$ and for all $w \in \mathbb{R}^n$.

(W') The *strengthened Weierstrass condition* holds if

$$E(t, y, v, w) \geq 0, \tag{3.27}$$

for $(t, y, v) \in RT(u_0, \varepsilon)$ and for all $w \in \mathbb{R}^n$.

(HJ) A C^1 function $V(t, y)$ is said to satisfy the *Hamilton-Jacobi inequality* for $v \in \mathbb{R}^n$ if

$$\begin{aligned} V_t(t, y) + V_y(t, y) \cdot v - L(t, y, v) \leq \\ V_t(t, u_0(t)) + V_y(t, u_0(t)) \cdot \dot{u}_0(t) - L(t, u_0(t), \dot{u}_0(t)). \end{aligned} \tag{3.28}$$

Remark 3.19. Note that condition (W') is satisfied whenever L is globally convex in $\dot{u}$, that is when $L_{\dot{u}\dot{u}} \geq 0$. In classical mechanics, the latter condition is fulfilled because the term of the kinetic energy which is quadratic in $\dot{u}$ is positive definite.

In the classical setting of the fixed endpoints problem, it is known that a necessary condition for a solution of the Euler-Lagrange equation to be a (SLM) is that condition (W) holds. This is true also in the case of periodic boundary conditions: we can use the same proof, taking into account only the competitors that are zero at the extrema of the time interval. Moreover, it is known that, if a solution of the Euler-Lagrange equation satisfy conditions (L'), (J') and (W'), then it is a strong local minimizer. We refer again to classical books of Calculus of Variations for proofs of this fact [43, 85]. Here we prove the strong local minimality under the (SR) condition and the Weierstrass condition (W'), adapting the proof for the classical problem of fixed endpoints given in [23]. It is not clear whether conditions (C') and (R'), sufficient to have weak local minimizers, can be used to prove the strong local minimality, in such a way to have a unified view of directional, weak and strong local minimizers.

Theorem 3.20. *Let $u_0 \in X$ be a periodic solution of the Euler-Lagrange equation* (3.2)*. Suppose that conditions* (L′) *and* (SR) *are satisfied for the second variation associated to u_0, and that condition* (W′) *holds. Then u_0 is a* (SLM)*.*

Proof. By the (SR) condition, there exists a symmetric solution $W(t)$ of the Riccati differential equation (3.16), defined on the whole $[0, T]$ and such that $W(T) - W(0) > 0$. From the embedding theorem of differential equations (see for instance Theorem 4.1 in [55]), there exists $\varepsilon_0 > 0$ and a symmetric matrix function $\widetilde{W} : [0, T] \to \mathbb{R}^{n \times n}$ such that

$$\dot{\widetilde{W}} - C + \widetilde{W}A + A^T\widetilde{W} + \widetilde{W}B\widetilde{W} = -\varepsilon_0 I,$$

and $\widetilde{W}(T) - \widetilde{W}(0) > \varepsilon_0 I$. We set

$$p(t) = L_{\dot{u}}(t, u_0(t), \dot{u}_0(t)),$$
$$V(t,y) = p(t)\cdot y + \frac{1}{2}(y - u_0(t))\cdot \widetilde{W}(t)(y - u_0(t)).$$

Assume for the moment that $V(t,y)$ satisfies condition (HJ) for all $(t,y) \in T(u_0,\varepsilon)$ and for all $v \in \mathbb{R}^n$, and let $u \in X$ be another T-periodic competitor such that $\|u - u_0\|_\infty < \varepsilon$. Hence, substituting $(t, u(t), \dot{u}(t))$ for (t,y,v) in (3.28) and integrating on $[0,T]$, we get

$$\int_0^T L(t,u(t),\dot{u}(t))\,dt + \big(V(0,u(0)) - V(T,u(T))\big) \geq$$
$$\int_0^T L(t,u_0(t),\dot{u}_0(t))\,dt + \big(V(0,u_0(0)) - V(T,u_0(T))\big).$$

Note that, since $u(t)$, $u_0(t)$ and $L(t,\cdot,\cdot)$ are T-periodic functions, then also $p(t)$ is T-periodic. Therefore, we have that

$$\begin{aligned} V(0,u_0(0)) - V(T,u_0(T)) &= p(0)\cdot u_0(0) + \frac{1}{2}(u_0(0) - u_0(0))\cdot \widetilde{W}(0)(u_0(0) - u_0(0)) \\ &\quad - p(T)\cdot u_0(T) - \frac{1}{2}(u_0(T) - u_0(0))\cdot \widetilde{W}(T)(u_0(T) - u_0(0)) \\ &= 0, \end{aligned}$$

$$\begin{aligned} V(0,u(0)) - V(T,u(T)) &= p(0)\cdot u(0) + \frac{1}{2}(u(0) - u_0(0))\cdot \widetilde{W}(0)(u(0) - u_0(0)) \\ &\quad - p(T)\cdot u(T) - \frac{1}{2}(u(T) - u_0(0))\cdot \widetilde{W}(T)(u(T) - u_0(0)) \\ &= \frac{1}{2}\Big((u(0) - u_0(0))\cdot \widetilde{W}(0)(u(0) - u_0(0)) \\ &\quad - (u(0) - u_0(0))\cdot \widetilde{W}(T)(u(0) - u_0(0))\Big) \\ &\leq 0. \end{aligned}$$

Hence, the inequality above becomes

$$\int_0^T L(t,u_0(t),\dot{u}_0(t))\,dt \leq \int_0^T L(t,u(t),\dot{u}(t))\,dt,$$

i.e. u_0 is a (SLM).

It remains to prove that $V(t,y)$ satisfies (HJ). Consider the equation

$$p(t) + \widetilde{W}(t)(y - u_0(t)) = L_{\dot{u}}(t,y,\zeta). \tag{3.29}$$

Note that the left hand side of the equation corresponds to $V_y(t,y)$. A solution is $\zeta = \dot{u}_0(\gamma)$ when $t = \gamma, y = u_0(\gamma)$, and moreover $L_{\dot{u}\dot{u}}(\gamma, u_0, \dot{u}_0) > 0$ by condition (L'). From the implicit function theorem, there exists a C^1 function $\zeta(t,y)$ defining near

$(\gamma, u_0(\gamma))$ the solution of (3.29). We can suppose that ζ is defined on a tube $T(u_0, \varepsilon_1)$. We can also suppose that

$$L_{\dot{u}\dot{u}}(t, y, v) > 0, \tag{3.30}$$

on $RT(u_0, \varepsilon_2)$, where $|\zeta(t, y) - \dot{u}_0(t)| < \varepsilon_2$ for all $(t, y) \in T(u_0, \varepsilon_1)$. Then, for a fixed $(t, y) \in T(u_0, \varepsilon_1)$, the function

$$v \mapsto V_y(t, y) \cdot v - L(t, y, v)$$

is concave on the set $|v - \dot{u}_0(t)| < \varepsilon_2$ and has zero gradient at $v = \zeta(t, y)$. We deduce that

$$\begin{aligned} \max_{|v-\dot{u}_0|<\varepsilon_2} \big(V_t(t, y) + V_y(t, y) \cdot v - L(t, y, v)\big) &:= F(t, y) \\ &= V_t(t, y) + V_y(t, y) \cdot \zeta(t, y) - L(t, y, \zeta(t, y)). \end{aligned} \tag{3.31}$$

Substituting the expression of $p(t)$ and using (3.29), we obtain that F_y, F_{yy} are continuous in (t, y) and satisfy

$$\begin{cases} F_y(t, u_0(t)) = 0, \\ F_{yy}(t, u_0(t)) = \dot{\widetilde{W}} - C + \widetilde{W}A + A^T\widetilde{W} + \widetilde{W}B\widetilde{W} < 0. \end{cases}$$

From Taylor's formula follows that for every $(t, y) \in T(u_0, \varepsilon_3)$ we have

$$F(t, y) \leq F(t, u_0(t)) = V_t(t, u_0(t)) + V_y(t, u_0(t)) \cdot \dot{u}_0(t). \tag{3.32}$$

Set $\varepsilon = \min(\varepsilon_1, \varepsilon_2, \varepsilon_3)$, let $(t, y) \in T(u_0, \varepsilon)$ and $v \in \mathbb{R}^n$. Then, using (3.29), (3.31), (3.32) and condition (W'), we obtain

$$\begin{aligned} V_t(t, y) + V_y(t, y) \cdot v - L(t, y, v) &= V_t(t, y) + L_{\dot{u}}(t, y, \zeta(t, y)) \cdot v - L(t, y, v) \\ &\leq V_t(t, y) + L_{\dot{u}}(t, y, \zeta(t, y)) \cdot \zeta(t, y) - L(t, y, \zeta(t, y)) \\ &= F(t, y) \\ &\leq F(t, u_0(t)) \\ &= V_t(t, u_0(t)) + V_y(t, u_0(t)) \cdot \dot{u}_0(t) - L(t, u_0(t), \dot{u}_0(t)), \end{aligned}$$

i.e. the function $V(t, y)$ satisfies (HJ). □

Remark 3.21. Note that, if in the above proof we drop the Weierstrass condition (W'), we arrive to the conclusion that (HJ) is true only on a restricted tube $RT(u_0, \varepsilon)$, for some $\varepsilon > 0$. Therefore, we can state that u_0 is only a (WLM). This proves that the theory of weak local minimizers can be also formulated in terms of the (SR) condition, instead of using the approach of Section 3.3 based on coupled points.

3.5 Examples

In this last part of the chapter we show some examples of application of the above theory, focusing also on the differences on the two approaches presented. The first example is a simple 1-dimensional problem, useful to recall the results described. The second one is the Kepler problem, which is a well known 2-dimensional problem, useful to test the theory. As last example, we apply the theory to the periodic orbits of the N-body problem with the symmetry of Platonic polyhedra, discussed in Section 1.2. In this case, even if we know that the minimizer exists, the solution is computed with numerical methods, which does not ensure that the orbit they produce is actually a minimizer of the action.

Example 1. Fixed a period $T > 0$, consider the functional

$$\mathcal{A}(u) = \int_0^T \frac{\dot{u}^2 + u^2}{2} dt,$$

defined on the set of the C^1 T-periodic functions $u : [0, T] \to \mathbb{R}$. Note that $\mathcal{A}$ is itself a quadratic functional and it is trivial that $\mathcal{A}(u) \geq 0$ and $\mathcal{A}(u) = 0$ if and only if $u(t) \equiv 0$. But still, we can check the sufficient conditions given by Theorem 3.9. The Jacobi differential equation is

$$\begin{cases} \dot{y} = z, \\ \dot{z} = y, \end{cases}$$

and the general solution is given by

$$\begin{cases} y(t) = Ae^t + Be^{-t}, \\ z(t) = Ae^t - Be^{-t}, \end{cases}$$

where $A, B \in \mathbb{R}$. With straightforward computations, we obtain that the solutions (y_0, z_0), (y_T, z_T) and the corresponding solutions of the Riccati equation are

$$y_0(t) = \frac{e^t - e^{-t}}{2}, \qquad z_0(t) = \frac{e^t + e^{-t}}{2}, \qquad w_0(t) = \frac{e^t + e^{-t}}{e^t - e^{-t}},$$
$$y_T(t) = \frac{-e^{t-T} + e^{-t+T}}{2}, \quad z_T(t) = \frac{-e^{t-T} - e^{-t+T}}{2}, \quad w_T(t) = \frac{-e^{t-T} - e^{-t+T}}{-e^{t-T} + e^{-t+T}}.$$

The Legendre condition (L') is trivially satisfied since $L_{\dot{u}\dot{u}} = 1$, hence we can check the validity of Theorem 3.9 by verifying one of the equivalent properties. From the expression of $y_0(t)$, we can directly verify that it does not vanish in $(0, T]$, hence there are no conjugate points and (J') holds. Moreover, the expression in (3.19) is a scalar number, and with simple computations, we see that it has the form

$$\frac{2(e^T + e^{-T} - 2)}{e^T - e^{-T}},$$

and this is positive for $T > 0$. Property (iii) of Theorem 3.9 is therefore satisfied, hence $\mathcal{A}$ is positive definite.

Example 2 (Kepler problem)**.** Fixed the period $T > 0$, we consider the action of the Kepler problem

$$\mathcal{A}(u) = \int_0^T \left(\frac{1}{2}|\dot{u}|^2 + \frac{1}{|u|}\right)dt, \tag{3.33}$$

defined on the set of the C^1 T-periodic curves $u : [0, T] \to \mathbb{R}^2$ which wind around but do not intersect the origin. From [44], it is known that (3.33) attains its global minimum at the elliptical T-periodic functions u which satisfy the Keplerian equations of motion, i.e.

$$\ddot{u} = -\frac{u}{|u|^3}, \tag{3.34}$$

and for which T is the minimum period. This problem has a degeneration, since all the elliptical solutions are minimizers. However, we can see what happens in case of circular orbits. Circular orbits are given by

$$u_0(t) = (a\cos(nt), a\sin(nt)), \quad n = \frac{2\pi}{T}, \quad a = \frac{1}{n^{2/3}}.$$

Let us discuss first the second variation of the action. The second derivatives of the Lagrangian are

$$L_{\dot{u}\dot{u}} = I, \quad L_{u\dot{u}} = 0, \quad L_{uu} = -\frac{I}{|u|^3} + 3\frac{uu^T}{|u|^5}.$$

The Legendre condition (L') is trivially satisfied. When we evaluate the derivatives along the circular solution, the only non-trivial one is

$$L_{uu}(u_0(t), \dot{u}_0(t)) = \frac{1}{a^3}\begin{pmatrix} 3\cos^2(nt) - 1 & 3\cos(nt)\sin(nt) \\ 3\cos(nt)\sin(nt) & 3\sin^2(nt) - 1 \end{pmatrix}.$$

Since this matrix depends directly on the time, to solve the Jacobi differential equation (3.9) we use numerical integration. We have done the computations for three different values of the period, namely $T = 0, 2\pi, 4\pi$, and see the changes in the results.

The Jacobi condition (J') can be verified numerically integrating the with initial conditions $Y_0(0) = 0, Z_0(0) = I$, and then checking that $\det Y_0(t) \neq 0$. The determinant of Y_0 is shown in Figure 3.1. As we can see, in all the cases there are no conjugate points, hence condition (J') holds.

To check property (iii) of Theorem 3.9, we have to integrate the Jacobi differential equation backward in time, using as initial condition $Y_T(T) = 0, Z_T(T) = -I$, then compute the matrices $W_0(T)$, $W_T(0)$ and construct the matrix in (3.19). Moreover, these matrices can be used to construct also the matrix in (3.21). Therefore we check the hypotheses of Lemma 3.11, in order to apply Theorem 3.10, and see the differences. To simplify the discussion of the results, let us call D_1 the matrix in (3.19) and D_2 the one in (3.21). Since we have to check whether D_1, D_2 are positive definite or not, we compute their eigenvalues. The results, for the different values of the period T examined, are reported in Table 3.1. As we can see, the eigenvalues of matrix D_1 are always positive, therefore by Theorem 3.9 circular orbits are directional local minimizers.

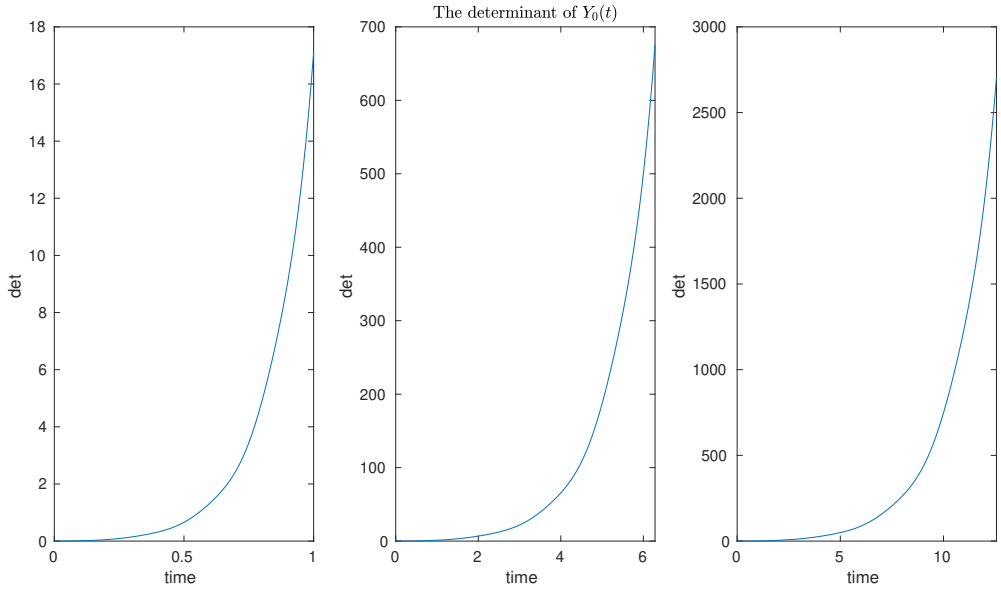

Figure 3.1: The determinant of the matrix $Y_0(t)$ for the circular orbits with period, from the left to the right, $T = 1, 2\pi, 4\pi$ respectively.

Moreover, by Theorem 3.18 we can state that they are also weak local minimizers. On the other hand, the matrix D_2 is positive definite only for $T = 1$, instead for $T = 2\pi, 4\pi$ negative eigenvalues arise. This means that, if we want to find a solution W or the Riccati equation satisfying condition (SR), Lemma 3.11 is not always effective. Moreover, following Remark 3.12, we computed the solution $(Y, Z) = (Y_0 + Y_T, Z_0 + Z_T)$ and constructed the solution $W = ZY^{-1}$ of the Riccati equation. From the computations performed, we verified directly that W is not a symmetric matrix, confirming that the approach of Remark 3.12 cannot be used in general situations.

T	eigs(D_1)	eigs(D_2)
1	9.8024	9.4457
	2.9775	2.1684
2π	1.5601	0.6872
	0.4738	−0.4923
4π	0.7800	−0.7459
	0.2369	−0.1552

Table 3.1: The eigenvalues of the two matrices D_1 and D_2 for the different values of the period.

However, in this case Lemma 3.13 can help to find a symmetric solution of the Riccati equation satisfying condition (SR). Indeed, we already verified that (L') and (J') hold, moreover the determinant $Y_0(t)$ is positive in $(0, T]$. Since the dimension of the Kepler problem is $n = 2$, we are in the hypotheses (i) of Lemma 3.13, hence condition (SR)

holds. Therefore, the directional local minimality is verified also by Theorem (3.10).

Concerning the strong local minimality, we have to use the approach based on the solutions of Riccati equation, and check the hypotheses of Theorem 3.20. Since the second derivative $L_{\dot{u}\dot{u}}$ is globally positive definite, by Remark 3.19, the strong Weierstrass condition (W') holds. Since we already saw that condition (SR) holds, by Theorem 3.20, the circular orbits taken into account are strong local minimizers of the Kepler problem.

Example 3. We take into account the orbits whose existence has been proved in Section 1.2. We know that these orbits exist, so that we assume for the moment that we are able to compute a periodic solution $u_0 \in \mathcal{K}$, without knowing if they are the actual global minimizers. We want to check whether what we compute is at least a local minimizer or not. The numerical methods used for the computation of the orbits are described in Chapter 4.

We take into account the four different solutions $\nu_1, \nu_{16}, \nu_{27}, \nu_{43}$, with the symmetry of the Cube and period $T = 1$. The enumeration is referred to the one used in the list at the website [34] and the sequences can be found in Table 5.1. The steps we perform are similar to the ones used for the Kepler problem. First of all, we note that the Legendre condition (L') is satisfied, hence we try to check property (iii) of Theorem 3.9. From the computation of $Y_0(t)$, we can compute its determinant and check whether the solution has a conjugate point or not. From Figure 3.2 we can see that solutions ν_1 and ν_{43} do not have any conjugate point, therefore condition (J') holds. On the contrary, solutions ν_{16} and ν_{27} have a conjugate point near $t = 1$, hence these are not local minimizers. Therefore, for the orbits ν_1 and ν_{43}, we construct the matrix in (3.19), which we still call D_1 and compute its eigenvalues. For the reasons explained before, we also compute the matrix in (3.21) and call it D_2. The computed eigenvalues are reported in Table 3.2. From these values we see that in both cases the matrix D_1 is positive definite, even if we note the presence of a very small eigenvalues. We can conclude that these orbits satisfy property (iii) of Theorems 3.9 and the hypotheses of Theorem 3.18, therefore ν_1 and ν_{43} are weak local minimizers. On the other hand, the matrix D_2 is not positive definite, since negative eigenvalues appear, hence Lemma 3.11 is not useful to deduce (SR) condition. Moreover, since here the dimension of the space is odd and the sign of the determinant of $Y_0(t)$ is positive, we can neither use Lemma 3.13, and we are not able to conclude if they are also strong local minimizers or not.

orbit	eigs(D_1)	eigs(D_2)
ν_1	$0.33487314 \times 10^{-7}$	0.87715310×10^{1}
	0.99721256×10^{1}	$-0.26741239 \times 10^{1}$
	0.62518499×10^{1}	0.53061290×10^{0}
ν_{43}	0.18803264×10^{2}	$-0.13136236 \times 10^{3}$
	0.29126208×10^{1}	$-0.16911298 \times 10^{1}$
	$0.12147953 \times 10^{-9}$	0.17842526×10^{2}

Table 3.2: The eigenvalues of the matrices D_1 and D_2 for the solutions ν_1 and ν_{43}.

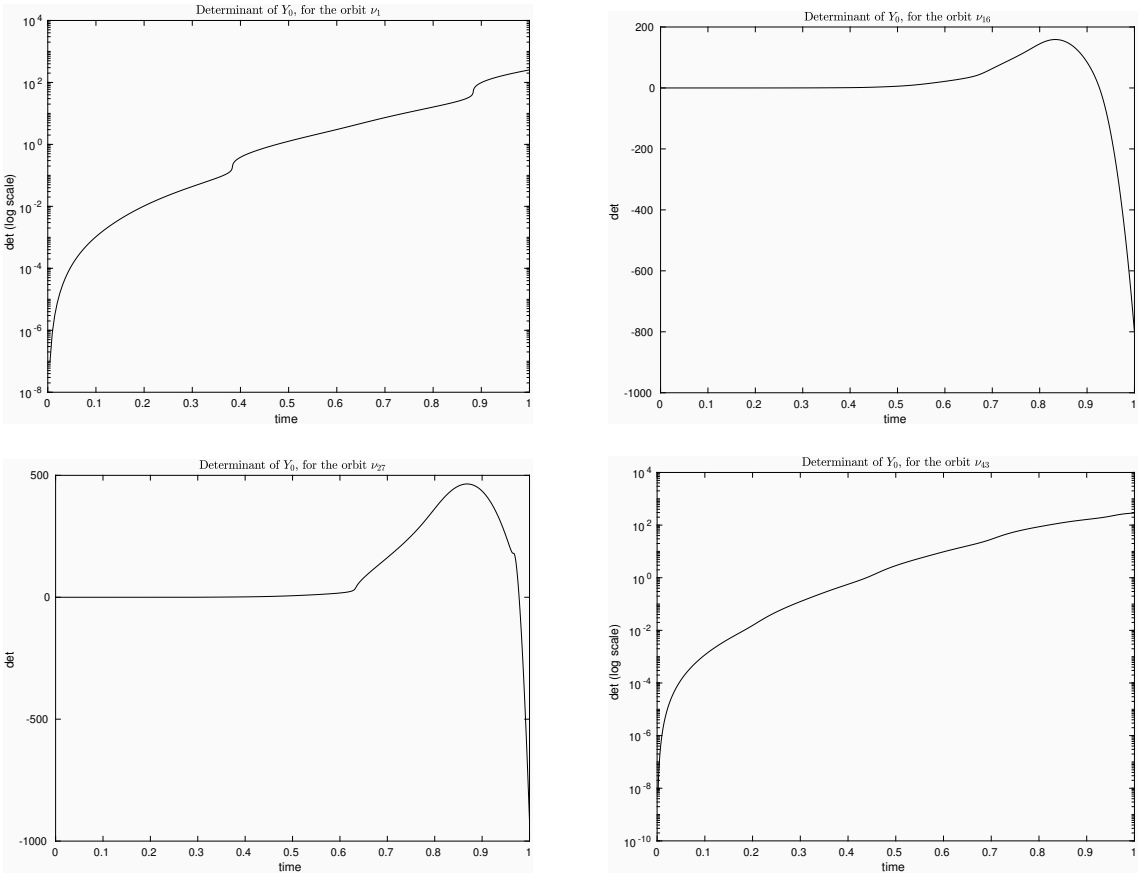

Figure 3.2: The determinant of the matrix Y_0 in the interval $[0, 1]$, for the four orbits $\nu_1, \nu_{16}, \nu_{27}, \nu_{43}$, with the symmetry of the Cube.

As a remark, we want to emphasize that solutions in Section 1.2 are found as minimizers of the action. Instead here we have seen that some solutions computed (namely ν_{16} and ν_{27}) are not minimizers, not even directional, and this seems to be a contradiction. This can be due to the fact that numerical methods do not ensure that what we compute is a minimizer, and actually we computed another type of stationary point. On the other hand, as we will see in Chapter 5, these orbits are computed using an implementation of the direct method of Calculus of Variations, i.e. the gradient method, whose aim is to modify the orbit in order to decrease the action. For this reason, it is not likely that we end up in computing an orbit which is not a local minimizer.

However, we want to point out that minimizers of Section 1.2 are obtained imposing an additional symmetry on the loop set, i.e. the choreography condition (1.6). Instead, the theory developed in this chapter is done using the complete space of the T-periodic loops: this means that we also allow non-symmetric variations for the orbit, that destroys the symmetry condition (1.6). For this reason, it is possible that we can choose a non-symmetric variation that reduces the value of the action, and this is not in contradiction of being a minimizer on the loop set that includes condition (1.6). What we can do is

try to adapt the above theory of local minimizers, taking into account the symmetry.

Including the symmetry in the theory Here we include the symmetry in the space of loops. We are not going to do again the theory of local minimizers, but we underline the major changes that have to be done in the proofs. From now on, we always assume that condition (L') holds. For the sake of simplicity, we assume that the dimension of the system is $n = 3$, since this is the case we need. Let us suppose that the loops taken into account satisfy the symmetry constrain

$$u\left(t + \frac{T}{M}\right) = Ru(t), \quad t \in [0, T],$$

where $R \in SO(3)$ and M is an integer number. To make the discussion simpler, we suppose that L does not depend on the time, and suppose that

$$\int_0^T L(u, \dot{u})\, dt = M \int_0^{\frac{T}{M}} L(u, \dot{u})\, dt. \tag{3.35}$$

We consider the functional

$$\bar{\mathcal{A}}(u) = \int_0^{T/M} L(u, \dot{u})\, dt.$$

defined on the set of loops

$$u : \left[0, \frac{T}{M}\right] \longrightarrow \mathbb{R}^3,$$

such that $Ru(0) = u(T/M)$. Note that, by means of (3.35), if $u_0 : [0, T] \to \mathbb{R}^3$ is a minimizer of the functional $\mathcal{A}$, then the restriction

$$u_0|_{[0,T/M]} : \left[0, \frac{T}{M}\right] \longrightarrow \mathbb{R}^3,$$

is a minimizer of $\bar{\mathcal{A}}$. Vice versa, if $u_0 : [0, T/M] \to \mathbb{R}^3$ is a minimizer of $\bar{\mathcal{A}}$, then we can extend it to a closed loop $u_0 : [0, T] \to \mathbb{R}^3$, simply by using the rotation R, and we obtain a minimizer for $\mathcal{A}$.

Therefore, we study the minimality of u_0, restricted to the interval $[0, T/M]$, as stationary point for the functional $\bar{\mathcal{A}}$. We first discuss the positivity of the quadratic functional, adapting Theorem 3.9. Note that the matrix D defining the boundary conditions for the admissible curves for the second variation is

$$D = \begin{pmatrix} R & -I \\ 0 & 0 \end{pmatrix} \in \mathbb{R}^{6\times 6}.$$

Therefore, a vector $\alpha \in \mathbb{R}^6$ satisfying $D\alpha = 0$ is of the form

$$\alpha = \begin{pmatrix} \beta \\ R\beta \end{pmatrix},$$

where $\beta \in \mathbb{R}^3$. Inserting this relation in (3.18), we obtain that the second variation associated to a solution u_0 of the Euler-Lagrange equation, is positive definite if and only if (J') holds in the interval $[0, T/M]$ and the 3×3 matrix

$$- W_{T/M}(0) - Y_0^{-1}(T/M)R - R^T Y_0^{T-1}(T/M) + R^T W_0(T/M)R, \tag{3.36}$$

is positive definite. Then, the proof that u_0 is also a weak local minimizer can be done in the same way as before.

Regarding the approach that uses the symmetric solution W of the Riccati equation with boundary condition, we can look at the proof of Theorem 3.10. We still write the quadratic functional using the solution W, and integrating by parts, the term outside the integral becomes

$$\begin{aligned} v(t) \cdot W(t)v(t)\Big|_0^{T/M} &= v(T/M) \cdot W(T/M)v(T/M) - v(0) \cdot W(0)v(0) \\ &= v(0) \cdot \Big(R^T W(T/M)R - W(0)\Big)v(0). \end{aligned}$$

Therefore, a symmetric solution W of the Riccati equation satisfying the boundary condition

$$R^T W(T/M)R - W(0) > 0, \tag{3.37}$$

is sufficient to ensure a non-negative quadratic functional. Then, in the definition of (SR) condition, (3.20) is replaced by (3.37). For the strong local minimality, the proof of Theorem 3.20 is the same if we have assume that

$$p(0) - R^T p\Big(\frac{T}{M}\Big) = 0. \tag{3.38}$$

Note that, if the derivative $L_{\dot{u}}$ is such that $L_{\dot{u}}(Ru, Rv) = RL_{\dot{u}}(u, v)$ for all (u, v), condition (3.38) is verified, hence the remaining part of the proof of Theorem 3.20 is the same.

Further computations For the case that we are studying, hypotheses (3.35) and (3.38) are satisfied, hence we can check the modified conditions described above. We take into account the two orbits ν_{16} and ν_{27}, for which the value of M is 2 and 3 respectively. Condition (J') is satisfied, since from Figure 3.2 we see that there are no conjugate points in the interval $[0, 1/2]$ for ν_{16} and in the interval $[0, 1/3]$ for ν_{27}. Moreover, integrating backwards the Jacobi differential equation (3.9), starting from $t = T/M$, we can construct the matrix in (3.36), which we call D_1 for the sake of simplicity. Therefore we compute the eigenvalues of D_1, in order to see whether it is positive definite or not. The values of the computed eigenvalues are reported in Table 3.3. As we can see, D_1 is positive definite, with a small eigenvalue appearing. Therefore, we can conclude that these solutions are weak local minimizers, if restricted to symmetric variations. To state the strong local minimality, we have to search for a symmetric solution W of the Riccati

orbit	eigs(D_1)
ν_{16}	$0.14210855 \times 10^{-13}$
	0.14377455×10^{2}
	0.21020856×10^{2}
ν_{27}	$0.12768453 \times 10^{-10}$
	0.15912220×10^{2}
	0.21086023×10^{2}

Table 3.3: The eigenvalues of the matrices D_1 for the solutions ν_{16} and ν_{27}.

equation satisfying (3.37). To this end, we can prove statements similar to Lemma 3.11 and Lemma (3.13), modifying the proofs taking into account the form of the boundary condition for the Riccati equation. However, as before, we are not able to verify the hypotheses of these lemmas, and so we cannot conclude that they are strong minimizers.

Chapter 4

Numerical methods

In this chapter we describe the numerical methods, both non-rigorous and rigorous, used in the following. In particular we focus on the computation of periodic orbits with given period $T > 0$, on the continuation with respect to a parameter and on the rigorous numerical techniques used to make computer-assisted proofs.

From now on, we assume that the equations of motion are given by a Lagrangian $L : [a, b] \times \Omega \to \mathbb{R}$, where $\Omega \subseteq \mathbb{R}^n \times \mathbb{R}^n$ is an open set. The dynamics is defined by the Euler-Lagrange equation

$$\frac{d}{dt}\left(\frac{\partial L}{\partial \dot{u}}\right) - \frac{\partial L}{\partial u} = 0. \tag{4.1}$$

We assume also that we can write this equation in normal form, i.e. if we set $x = (u, \dot{u})$, then we are able to write equation (4.1) as a first order differential system of the form

$$\dot{x} = f(x, t). \tag{4.2}$$

We also define the Lagrangian action

$$\mathcal{A}(u) = \int_a^b L(t, u(t), \dot{u}(t))\, dt, \tag{4.3}$$

where $u : [a, b] \to \mathbb{R}^n$ is a curve in $H^1([a, b], \mathbb{R}^n)$. The set X of curves on which (4.3) is defined depends on the problem one wants to study. In the case of periodic orbits with fixed period $T > 0$, the time interval $[a, b]$ is $[0, T]$ and

$$X \subseteq \{u \in H^1([0, T], \mathbb{R}^n) : u(0) = u(T)\} =: H^1_T(\mathbb{R}, \mathbb{R}^n),$$

is a subset of T-periodic loops in H^1. We recall that by Hamilton's principle, it is known that classical solutions of equation (4.1) are stationary points of the action (4.3).

4.1 Approximation with Fourier polynomials

A first method to compute periodic orbits is to use Hamilton's principle: in particular, we can search for minimizers of the action $\mathcal{A}$. Following [78] and [96], we search for an

approximation of the minimizers by discretizing the action $\mathcal{A}$ and considering it defined on a finite dimensional loop space. To discretize the infinite dimensional set of T-periodic loops, we take into account the truncated Fourier series at some order F_M. We consider only loops $u : [0, T] \to \mathbb{R}^n$ of the form

$$u(t) = \frac{a_0}{2} + \sum_{k=1}^{F_M} \left[a_k \cos\left(\frac{2\pi k}{T} t\right) + b_k \sin\left(\frac{2\pi k}{T} t\right) \right], \tag{4.4}$$

where $a_k, b_k \in \mathbb{R}^n$ are the Fourier coefficients. Restricting $\mathcal{A}$ to loops of the form (4.4) we obtain a function $A : \mathbb{R}^{n(2F_M+1)} \to \mathbb{R}$ that discretizes the action functional. This function is defined simply by composition

$$A(a_0, a_1, \ldots, a_{F_M}, b_1, \ldots, b_{F_M}) = \int_0^T L(t, u, \dot{u})\, dt \tag{4.5}$$

The derivatives with respect to the Fourier coefficients are

$$\begin{aligned}
\frac{\partial A}{\partial a_k} &= \int_0^T \left(\frac{\partial L}{\partial u}(t, u(t), \dot{u}(t)) \frac{\partial u}{\partial a_k} + \frac{\partial L}{\partial \dot{u}}(t, u(t), \dot{u}(t)) \frac{\partial \dot{u}}{\partial a_k} \right) dt \\
&= \int_0^T \left(\frac{\partial L}{\partial u}(t, u(t), \dot{u}(t)) \cos\left(\frac{2\pi k}{T} t\right) - \frac{2\pi k}{T} \frac{\partial L}{\partial \dot{u}}(t, u(t), \dot{u}(t)) \sin\left(\frac{2\pi k}{T} t\right) \right) dt, \\
\frac{\partial A}{\partial b_k} &= \int_0^T \left(\frac{\partial L}{\partial u}(t, u(t), \dot{u}(t)) \frac{\partial u}{\partial b_k} + \frac{\partial L}{\partial \dot{u}}(t, u(t), \dot{u}(t)) \frac{\partial \dot{u}}{\partial b_k} \right) dt \\
&= \int_0^T \left(\frac{\partial L}{\partial u}(t, u(t), \dot{u}(t)) \sin\left(\frac{2\pi k}{T} t\right) + \frac{2\pi k}{T} \frac{\partial L}{\partial \dot{u}}(t, u(t), \dot{u}(t)) \cos\left(\frac{2\pi k}{T} t\right) \right) dt.
\end{aligned}$$

If, as in our case, we assume that the Lagrangian L is of the form

$$L(t, u, \dot{u}) = K(\dot{u}) + U(t, u),$$

where

$$K(\dot{u}) = \frac{1}{2} \dot{u} \cdot M\dot{u}, \quad M = \operatorname{diag}(m_1, \ldots, m_n), \quad m_i > 0, \quad i = 1, \ldots, n,$$

is the kinetic energy and U is the potential, we can explicitly compute the second term of the integrals, and the partial derivatives become

$$\frac{\partial A}{\partial a_k} = \frac{2(\pi k)^2}{T} M a_k + \int_0^T \frac{\partial U}{\partial u}(t, u(t)) \cos\left(\frac{2\pi k}{T} t\right) dt, \quad k \geq 0, \tag{4.6}$$

$$\frac{\partial A}{\partial b_k} = \frac{2(\pi k)^2}{T} M b_k + \int_0^T \frac{\partial U}{\partial u}(t, u(t)) \sin\left(\frac{2\pi k}{T} t\right) dt, \quad k > 0. \tag{4.7}$$

Note that these derivatives may be large for high frequencies because of the term k^2, and this leads to instability of the classical gradient method (see [78]). In [78] the authors propose a variant of the gradient method avoiding this problem. If a_k is the k-th Fourier

coefficient at some iteration, we obtain the new coefficient a'_k for the successive step by adding

$$\delta a_k = a'_k - a_k = -\delta\tau_k \frac{\partial A}{\partial a_k}, \tag{4.8}$$

and similarly for the coefficients b_k. This means that the decay rate in the Fourier coefficients is controlled by a parameter $\delta\tau_k$ which depends also on the order k of the harmonic. If we set

$$\delta\tau_k = \frac{T}{2(\pi k)^2}\delta, \tag{4.9}$$

where $\delta > 0$ is a small positive constant, this removes the high frequency instability.

To stop the iterations we could check the value of the residual acceleration, i.e. the difference between the acceleration computed from $u(t)$ and the vector field $f(u(t))$. However, this in practice can be done only when there are no singularities in the equations. In the case of the N-body problem, when a passage near a collision occurs, we have to choose a very large value of F_M (see [96]) to obtain a better approximation, and this slows down the computations. For this reason we choose to stop the iterations also when the increments $\delta a_k, \delta b_k$ become small, as suggested in [78].

4.1.1 Gradient method on the sphere

Suppose now that the dynamics is constrained to be on the sphere $\mathbb{S}^2 \subseteq \mathbb{R}^3$. To simplify the discussion we suppose that $\Omega = [0,T] \times \mathbb{S}^2 \times \mathbb{R}^3$, the general case $\Omega = \mathbb{R} \times (\mathbb{S}^2)^n \times \mathbb{R}^{3n}$ being similar. Denote with

$$\Pi : \mathbb{R}^3 \setminus \{0\} \to \mathbb{S}^2, \quad \Pi(x) = \frac{x}{|x|},$$

the projection on the sphere. The gradient method explained above can be adapted to work in this setting simply by using this projection. Indeed, if $u : [0,T] \to \mathbb{S}^2$ is a periodic loop on the sphere with Fourier coefficients $a_k, b_k \in \mathbb{R}^3$, $k = 0, \ldots, F_M$, we still use equation (4.8) to obtain new coefficients $a'_k, b'_k \in \mathbb{R}^3$, $k = 0, \ldots, F_M$ and a new loop $u'(t)$. However, $u'(t)$ will not be on the sphere in general, but we can project it, obtaining a new loop on the sphere $\bar{u} : [0,T] \to \mathbb{S}^2$, defined by $\bar{u} := \Pi \circ u'$. Then we can compute its corresponding Fourier coefficients $\bar{a}_k, \bar{b}_k \in \mathbb{R}^3$, $k = 0, \ldots, F_M$, either by using the classical formula

$$\bar{a}_k = \frac{2}{T}\int_0^T \bar{u}(t)\cos\left(\frac{2\pi k}{T}t\right)dt,$$
$$\bar{b}_k = \frac{2}{T}\int_0^T \bar{u}(t)\sin\left(\frac{2\pi k}{T}t\right)dt,$$

or by using the FFT algorithm (see for example [89]), and continue with the iterations. Note that the same manner to update the Fourier coefficients can be used every time we have loops constrained to be on an embedded manifold $M \subseteq \mathbb{R}^n$, provided that we have a projection from the embedding space to the manifold itself.

We remark that the natural way to define the gradient method on a manifold M would be by using local charts $\varphi : U \to M$, where $U \subseteq \mathbb{R}^s$ is an open set and s is the dimension of the manifold. Composing the action $\mathcal{A}$ with the charts φ, we reduce ourself to the previous setting explained at the beginning of this chapter, then we can simply use the same formulation of the gradient method. Note that this method has been effectively used in [74, 75] to compute choreographies on the sphere and on the hyperbolic plane. However, in the simple case of the sphere, the method proposed here is an effective and fast-to-code alternative that we have used successfully.

4.2 Shooting method

Another method to compute periodic orbits is to use the *shooting method*. We describe this method for general systems of ODEs, that are not necessarily of Euler-Lagrange type. The goal is to solve the boundary value problem

$$\begin{cases} \dot{x} = f(x), \\ x(T/M) = Sx(0), \end{cases} \tag{4.10}$$

where $x \in \mathbb{R}^n$, $f : \Omega \to \mathbb{R}^n$ is a vector field, $\Omega \subseteq \mathbb{R}^n$ is an open set, $S \in O(n)$, and $M > 0$ is an integer number. This formulation takes into account also possible rotation or reflection symmetries of the periodic orbit. Note that if there are no symmetries at all, we can set $M = 1$ and $S = I$ and obtain the usual periodic boundary conditions.

Fixed $m + 1$ time points $0 = \tau_0 < \tau_1 < \cdots < \tau_m = T/M$, we define the function

$$G : \mathbb{R}^{nm} \to \mathbb{R}^{nm},$$

as

$$\begin{cases} G_i = \phi^{\tau_i - \tau_{i-1}}(x_{i-1}) - x_i, & i = 1, \dots, m-1 \\ G_m = \phi^{\tau_m - \tau_{m-1}}(x_{m-1}) - Sx_0, \end{cases} \tag{4.11}$$

where $x_0, \dots, x_{m-1} \in \mathbb{R}^n$ are points in the space. If $x(t)$ is a T-periodic solution satisfying (4.10), the function G evaluated at

$$X = (x(\tau_0), \dots, x(\tau_{m-1})) \in \mathbb{R}^{nm},$$

vanishes. Then, the equation

$$G(X) = 0, \tag{4.12}$$

is solved using the Newton method. The Jacobian matrix of G is

$$\begin{bmatrix} M_1 & -I & & \\ & M_2 & \ddots & \\ & & \ddots & -I \\ -S & & & M_m \end{bmatrix}, \tag{4.13}$$

where

$$M_i = \frac{\partial}{\partial x}\phi^{\tau_i-\tau_{i-1}}(x_{i-1}), \quad i = 1, \dots, m.$$

If X' denotes the new value of X at some iteration of the Newton method and $\Delta X = X' - X$, at each step we solve the linear system

$$\frac{\partial G}{\partial X}(X)\Delta X = -G(X). \tag{4.14}$$

However, the Jacobian matrix is singular at the minimum points, since we are free to choose the initial point along the periodic orbit. This degeneracy can be avoided as in [1], by adding the condition on the first shooting point

$$f(x_0) \cdot \Delta x_0 = 0, \tag{4.15}$$

to the system (4.14), where $x_0, \Delta x_0$ are the first components of $X, \Delta X$ respectively. The system of equations (4.14), (4.15) has $nm + 1$ equations and nm unknowns, and we can solve it through the SVD decomposition, obtaining the value of ΔX. Note that, if the system has the Jacobi integral, as in the case of autonomous Lagrangian systems, the additional degeneracy given by the conservation of this quantity is automatically removed since we have fixed the period. Moreover, to increase the stability of the method, we use a damping factor, i.e. the new value X' at a generic iteration is obtained as

$$X' = X + \gamma \Delta X. \tag{4.16}$$

The damping parameter γ is adaptive and it is computed as

$$\gamma = \frac{\gamma_{\min}}{\max\left\{\gamma_{\min,} \|\Delta X\|_\infty\right\}},$$

where $\|\Delta X\|_\infty = \max_i |\Delta X_i|$.

4.2.1 Least squares approach

To search for the zeros of G we can also use a least-squares approach. We set

$$F(X) = \frac{|G(X)|^2}{2},$$

and search for the absolute minimum points by a modified Newton method. The derivatives of F are

$$\frac{\partial F}{\partial x_j} = \sum_{i=1}^{n} \frac{\partial G_i}{\partial x_j} \cdot G_i, \tag{4.17}$$

$$\frac{\partial^2 F}{\partial x_j \partial x_h} = \sum_{i=1}^{n} \left[\frac{\partial G_i}{\partial x_j}\frac{\partial G_i}{\partial x_h} + \frac{\partial^2 G_i}{\partial x_j \partial x_h} G_i\right]. \tag{4.18}$$

If X' denotes the new value of X at some iteration and $\Delta X = X' - X$, at each step we solve the linear system

$$A(X)\Delta X = -\frac{\partial F}{\partial X}(X), \tag{4.19}$$

where the entries of the matrix A are

$$A_{jh} = \sum_{i=1}^{n} \frac{\partial G_i}{\partial x_j}\frac{\partial G_i}{\partial x_h},$$

i.e. we consider an approximation of the second derivatives (4.18) of F, neglecting the terms containing the second derivatives of G_i. For the same reasons explained above, we have to add condition (4.15) to system (4.19) and still use the SVD method to compute the corrections ΔX.

4.3 Continuation method

Suppose now that the vector field in (4.10) depends also on a real parameter, say λ, that is $f = f(x, \lambda)$. In this manner, also the function G in (4.11) depends on λ: $G = G(X, \lambda)$. Given a couple $(X_i, \lambda_i)^T$ such that $G(X_i, \lambda_i) = 0$, we want to continue this solution with respect to the varying parameter λ, in order to find a curve of solutions, parametrized with λ. To do this, we add to system (4.11) an equation to displace the entire couple $(X, \lambda)^T$. The system that we solve is therefore

$$\begin{cases} G(X, \lambda) = 0, \\ \\ \dfrac{1}{2}\left| \begin{pmatrix} X_i \\ \lambda_i \end{pmatrix} - \begin{pmatrix} X \\ \lambda \end{pmatrix} \right|^2 - \delta^2 = 0, \end{cases} \tag{4.20}$$

where $\delta > 0$ is a positive value, determining the displacement along the curve of solutions.

The solution $(X_{i+1}, \lambda_{i+1})^T$ of system (4.20) is computed using again a Newton method, solving at each step a linear system given by the matrix

$$\begin{bmatrix} \dfrac{\partial G}{\partial X} & \dfrac{\partial G}{\partial \lambda} \\ X - X_i & \lambda - \lambda_i \end{bmatrix}. \tag{4.21}$$

Since we are searching for periodic solutions, for the reasons explained above, we add the transversality condition (4.15). The final system we solve at each step is non-squared, and we use again the SVD decomposition. Since this is a pseudo arc-length method, the starting guess to compute $(X_{i+1}, \lambda_{i+1})^T$ should be constructed starting from the known solution (X_i, λ_i), taking a tangent displacement along the curve of solutions. Here we construct the starting guess approximating the tangent line using two previous different solutions, say $(X_i, \lambda_i)^T$ and $(X_{i-1}, \lambda_{i-1})^T$, as

$$\begin{pmatrix} \hat{X} \\ \hat{\lambda} \end{pmatrix} = \begin{pmatrix} X_i \\ \lambda_i \end{pmatrix} + \gamma \begin{pmatrix} X_i - X_{i-1} \\ \lambda_i - \lambda_{i-1} \end{pmatrix}, \qquad \gamma = \frac{2\delta}{|(X_i, \lambda_i)^T - (X_{i-1}, \lambda_{i-1})^T|}.$$

Note also that, since G is defined through the flow of an ordinary differential equation and we need to compute the derivatives of G with respect to the parameter λ, we have to compute the derivatives of the flow with respect to λ. To do this, the system of differential equations that we have to solve numerically is

$$\begin{cases} \dot{x} = f(x, \lambda), \\ \dot{A} = \dfrac{\partial f(x, \lambda)}{\partial x} A, \\ \dot{w} = \dfrac{\partial f(x, \lambda)}{\partial x} w + \dfrac{\partial f(x, \lambda)}{\partial \lambda}, \end{cases} \tag{4.22}$$

where $x, w \in \mathbb{R}^n$, $A \in \mathbb{R}^{n \times n}$ and $\lambda \in \mathbb{R}$. Indeed, the second equation gives the derivatives of the flow ϕ^t with respect to the initial condition x, while the third equation gives the derivatives of the flow ϕ^t with respect to the parameter λ.

4.4 Starting guess for the shooting method

Despite the introduction of the dumping factor makes Newton's method more stable and can force the convergence in some cases, the choice of a good initial condition is still fundamental to obtain a fast convergence. However, this choice strongly depends on the features of the specific problem one is facing.

When the problem has a variational formulation and the action functional is coercive, things become simpler. Indeed, we can first discretize and minimize the action using the gradient method, as explained in Section 4.1, obtaining a rough approximation of the solution, and then use this curve as starting guess for Newton's method. Note that this is still effective even if we do not have a theoretical proof of the existence of minimizers, as long as the process of minimization of the action converges. We will see how to apply this computation scheme in Chapter 5, applying the above methods to the N-body problem.

However, it can also happen that the gradient method fails, because the problem we are facing does not have minima; it can also happen that the problem does not have a variational formulation at all and therefore we cannot use the minimization of the action. A general strategy that can be used in these cases makes use of continuation. It consists in using an auxiliary differential problem

$$\dot{x} = g(x, t, \lambda), \tag{4.23}$$

depending on a real parameter $\lambda \in \mathbb{R}$, and possibly on the time t, such that for $\lambda = 0$ corresponds to the original problem (4.10), i.e. $g(x, t, 0) = f(x)$. The idea is to make the system simpler for $\lambda = 1$: if we are able to find easily a solution for this value of the parameter, then we can use continuation and try to reach a value close to $\lambda = 0$. At that point, we can switch to the original problem and use the output of the continuation method as starting guess for the Newton method. In the next chapter we will see an example where the minimization of the action fails and instead this method is effective.

4.5 Computer-assisted proofs and rigorous numerics

The methods described above are all non-rigorous, in the sense that we always compute an approximation of the initial condition x_0 of a periodic orbit with fixed period $T > 0$, without providing any estimate of the errors done during the computation. In this section we mention tools and methods that we used to produce rigorous computer-assisted proofs, which means that, together with the computations, we also provide the information on the errors done.

4.5.1 Introduction to computer-assisted proofs

Since the mid 60s, the computational power of electronic calculators experienced an enormous and fast development. Indeed, according to the now famous Moore's law [79], the number of transistors in integrated chips doubles every two years. This availability of computing power led to the development of new mathematical techniques, aimed to assist the human being in proving mathematical statements in a rigorous way, i.e. theorems. The first computer-assisted proof goes back to the year 1977, in which a proof of the *Four Color Theorem* [3, 4] was provided, even if it was rather controversial. The Four Color Problem was first formulated in 1852 by Francis Guthrie, a student of Augustus De Morgan, when, while trying to color the map of countries of England, he noticed that four colors were sufficient [109]. An intuitive statement of this theorem says that "given any separation of a plane into contiguous regions, the regions can be colored using at most four colors so that no two adjacent regions have the same color". Another famous theorem, which has been proved with the help of a computer, is the so called *Kepler conjecture* about sphere packaging. The statement was first formulated by Johannes Kepler in 1611, in his essay *Strena seu de nive sexangula*. Intuitively, it says that "the best way to pack equally sized spheres is in a pyramid". The pyramid packaging, represented in Figure 4.1, is also called face-centered cubic packaging. The

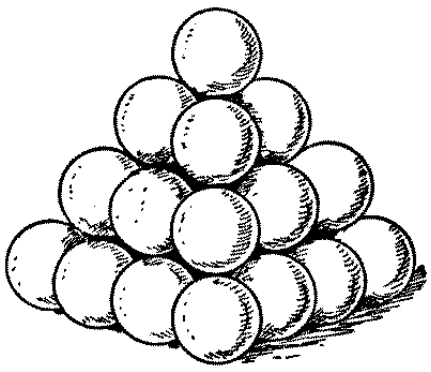

Figure 4.1: The face-centered cubic packaging.

first computer-assisted proof of this conjecture can be found in [53, 54].

One of the most famous problems of dynamics studied with computer-assisted methods is the Lorenz attractor and its chaotic nature [72, 105]. The understanding of the

dynamics of this system was included in the list of open mathematical problems proposed by Stephen Smale [98], as the 14-th problem. The proof has been given in [106], with the aim of rigorous computational methods. Computer-assisted methods have also been used to study solutions of the N-body problem, see for example [62, 60, 61, 37]. With computers we are able to check inequalities, using rigorous finite approximations of numbers. If hypotheses of theorems are formulated as a finite number of inequalities, here is where the role of computers becomes important and can help to verify them. In the following, we will explain the tools and the methods needed to perform computer-assisted proofs in dynamics.

4.5.2 Interval arithmetic and Interval Newton Theorem

Since the precision of floating point numbers is finite due to truncation, we use interval arithmetic to take into account rounding-off errors. This means that all the basic operations between floating point numbers are replaced by the corresponding operations on closed intervals, producing a superset of the true result. Interval computations are also extended to all elementary functions. For a detailed explanation of interval arithmetic and its implementation, the reader can refer to [80]. In the following, for any set B we denote by $[B]$ the interval hull of B, i.e. the smallest product of intervals containing B. Moreover, for any interval set B we denote with $\mathrm{mid}(B)$ the center of B.

The main tool to rigorously prove the existence of a zero of a function is the Interval Newton Theorem.

Theorem 4.1 (Interval Newton)**.** *Let $f : \mathbb{R}^n \to \mathbb{R}^n$ be a C^1 function and let $B \subseteq \mathbb{R}^n$ be a product of intervals. Assume that the interval hull of the Jacobian $df(B)$, denoted by $[df(B)]$, is invertible. Let $x_0 \in B$ and define the interval Newton operator as*

$$N(x_0, B, f) = x_0 - [df(B)]^{-1} f(x_0). \tag{4.24}$$

Then

1. *if*
$$N(x_0, B, f) \subseteq B, \tag{4.25}$$
then there exists a unique $x^* \in B$ such that $f(x^*) = 0$;
2. *if $x_1 \in B$ and $f(x_1) = 0$, then $x_1 \in N(x_0, B, f)$;*
3. *if $N(x_0, B, f) \cap B = \emptyset$, then $f(x) \neq 0$ for all $x \in B$.*

This theorem can be used to construct a Newton-like algorithm to find rigorous enclosures of zeros of a function, as proposed in [62]. Given a first guess $x_0 \in \mathbb{R}^n$, usually computed with non-rigorous methods, we choose an interval set B containing x_0 and then perform the following algorithm.

Step 1 Compute $N(x_0, B, f)$.

Step 2 If $N(x_0, B, f) \subseteq B$, then return success.

Step 3 If $B \cap N(x_0, B, f) = \emptyset$, then return failure, there are no zeros of f in B.

Step 4 If $B \subseteq N(x_0, B, f)$, then modify the computation parameters and go to Step 1.

Step 5 Define a new interval set B by $B := B \cap N(x_0, B, f)$ and a new x_0 by $x_0 := \mathrm{mid}(B)$ and then go to Step 1.

4.5.3 Computation of periodic orbits

To rigorously integrate a system of ODEs and compute rigorous enclosures of the partial derivatives with respect to the initial conditions, we use the C^1-Lohner algorithm [114]. This algorithm is based on the Taylor integration method (see e.g. [59] or [8]) and a particular set representation, which is fundamental to obtain sharp enclosures of the solution. Indeed, the naive representation of sets does not work, due to the huge uncontrolled overestimation of the errors done during the integration: this effect is usually known as *wrapping effect* [80]. Given a set of initial conditions $B \subseteq \mathbb{R}^n$ and a time τ, the C^1-Lohner algorithm produces an enclosure of the solution of the ODE and of its derivatives with respect to the initial conditions at time τ. The C^1-Lohner algorithm, as well as algorithms to rigorously compute Poincaré maps for affine sections, are implemented in the `CAPD` library [58].

We want to use rigorous numerical integration to find an enclosure for the initial condition of a periodic orbit, using the tools described above. Here we suppose that the system has n degrees of freedom and has a Lagrangian L, independent from the time. The system has the Jacobi first integral, defined as

$$E(u, \dot{u}) = \frac{\partial L}{\partial \dot{u}} \cdot \dot{u} - L(u, \dot{u}). \tag{4.26}$$

Since the hypotheses of Theorem 4.1 require the solution to be isolated, first we have to determine a unique initial condition of a periodic orbit: for this purpose we use a Poincaré map. Fixed a value h, we choose a hypersurface $\sigma \subseteq \mathbb{R}^{2n}$ transversal to the flow and, setting $x = (u, \dot{u})$, we define the isoenergetic manifold

$$\Sigma = \{x \in \mathbb{R}^{2n} : x \in \sigma,\, E(x) = h\},$$

and denote with

$$\mathsf{p} : \Sigma \to \Sigma,$$

the associated Poincaré map. The value h of the energy is obtained computing the energy of a non-rigorous solution $x_0 \in \Sigma$, computed with the methods exposed in Section 4.2. If the system does not have any other first integral then, in general, fixed points of the map p are isolated. Now, given a product of intervals $B \subseteq \mathbb{R}^n$ containing x_0, we can apply the algorithm described above to the function

$$\mathsf{f}(x) = \mathsf{p}(x) - x,$$

and, if it is successful, Theorem 4.1 yields the existence of a unique fixed point of the Poincaré map in the set B, and therefore a unique initial condition for the corresponding periodic orbit.

Furthermore, if one wants to study the stability of the periodic orbit, once we have the box B containing the initial condition, we use the C^1-Lohner algorithm to compute an enclosure of the monodromy matrix, since it corresponds to the partial derivatives of the solution with respect to the initial conditions, computed at time $t = T$, where T denotes the period. At this point we have a rigorous estimate on the entries of the monodromy matrix, and one can deduce rigorous enclosures for the Floquet multipliers. In the next chapter we will see how to proceed with this step for the periodic solutions found in Chapter 1.

Chapter 5

Numerical computations in N-body systems

In this chapter we use numerical methods described in Chapter 4. In particular, in the first section we see how to compute periodic orbits with the symmetry of Platonic polyhedra, described in Chapter 1. After the computation of an initial point, we focus on the study of their stability, using rigorous numerical techniques aimed to produce computer-assisted proofs. For a small number of these orbits we were able to rigorously prove their instability. Non-rigorous numerical computations show that all the orbits found with the algorithm in Section 1.3 are unstable, always experiencing a large Floquet multiplier. In the second section we compute periodic orbits in a system composed by charged particles, moving under the Coulomb force. In particular, we take into account the so called Coulomb $(N+1)$-body problem, composed by a positively charged particle, fixed at the origin, and N equally negatively charged particles, surrounding the positive charge. This system reminds the Rutherford model of the atom [92]. Moreover, still using numerical computations, we provide some suggestions about the variational nature of the orbits we compute.

5.1 System of N masses and computer-assisted proof

In this section we compute periodic orbits of the N-body problem with the symmetry of Platonic polyhedra, whose existence has been proved in Chapter 1. In particular, we were able to compute the orbits in the lists produced by the algorithm described in Section 1.3. Videos and other numerical results about them can be found at the website [34].

5.1.1 Computing periodic orbits

The orbits enumerated in Section 1.3 were first computed with non-rigorous numerical methods described in Chapter 4: to this end we used the following strategy.

Step 1: Generate a first guess in the desired free homotopy class, computing the Fourier coefficients of the linear piecewise loop v, travelling along the sides of $\mathcal{Q}_{\mathcal{R}}$, defined by the sequence of vertexes ν. We usually used a number of Fourier modes between 30 and 50.

Step 2: Start the iterations of the gradient method of Section 4.1, using the first guess computed at Step 1. At each step, the Fourier coefficients are changed in order to decrease the value of the action. We stop iterating when the increments $\delta a_k, \delta b_k$ become small enough.

Step 3: Use the loop produced by the last iteration of the gradient method to construct a first guess for the shooting method of Section 4.2, then start its iterations. To make the computation faster, we added to the system (4.10) also the symmetry of the generating particle, given by the choreography condition (1.6). We usually used a number of shooting points between 5 and 20.

Examples of orbits computed are displayed in Figure 5.2. More figures and videos can be found at the website [34].

As further experiment, we also tried to compute the orbits with the same symmetry and topological constraints, but forcing the particles to be constrained on a sphere of fixed radius. We applied the variant of the gradient method described in Section 4.1 to some free-homotopy classes ν, obtaining the convergence of the method. This suggests that these orbits still exist in this setting. Figure 5.1 shows two examples of them. It is worth noting that choreographies have been computed on the sphere and on the hyperbolic plane, see [74, 75]: the authors were able to carry the planar choreographies computed by C. Simó [97, 96], on a non-flat two-dimensional space, using the cotangent potential [14, 32] as interacting force.

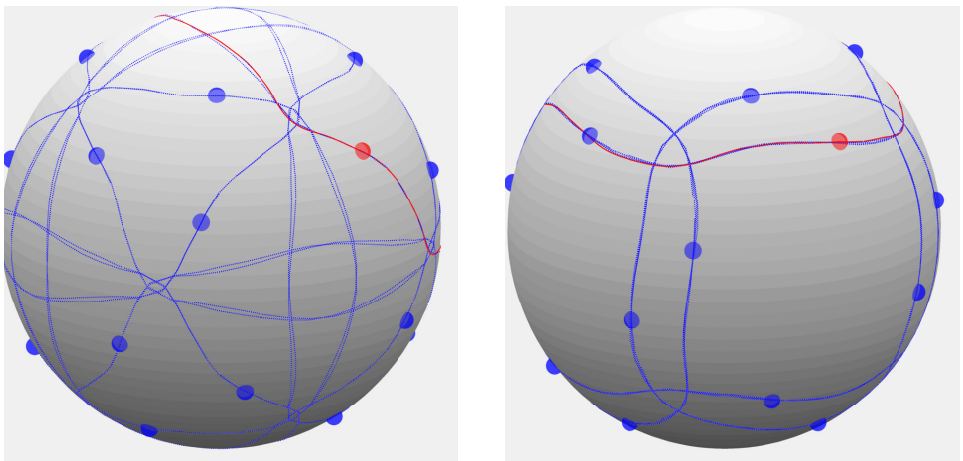

Figure 5.1: Two orbits with the symmetry of the Cube, with the particles constrained to be on a sphere of radius 1. The red curve is the trajectory of the generating particle.

5.1.2 Properties of the monodromy matrix

After the computation of an initial point of the orbit, we studied the stability focusing on the dynamics of the generating particle. This corresponds to study the stability of the periodic orbit of the full N-body problem with respect to symmetric perturbations. However, if the orbit of the generating particle is unstable, also the full orbit of N-body is unstable.

From the standard Floquet theory we know that the monodromy matrix $\mathfrak{M}(T)$ is a 6×6 real symplectic matrix with a double unit eigenvalue, one arising from the periodicity of the orbit and the other one from the energy conservation. Since $\mathfrak{M}(T)$ is symplectic, we have only three possibilities for the remaining eigenvalues $\lambda_1, \lambda_2, \lambda_3, \lambda_4$:

(1) some of them are real and $\lambda_1\lambda_2 = 1, \lambda_3\lambda_4 = 1$;

(2) $\lambda_1, \lambda_2, \lambda_3, \lambda_4 \in \mathbb{C} \setminus \mathbb{R}$ and $\lambda_1 = \lambda_2^{-1} = \bar{\lambda}_3 = \bar{\lambda}_4^{-1}$;

(3) $\lambda_1, \lambda_2, \lambda_3, \lambda_4 \in \mathbb{C} \setminus \mathbb{R}$ and $\lambda_1 = \lambda_2^{-1} = \bar{\lambda}_2, \lambda_3 = \lambda_4^{-1} = \bar{\lambda}_4$.

As in [60], we can give a stability criterion using the values $T_1 = \lambda_1+\lambda_2$ and $T_2 = \lambda_3+\lambda_4$. The characteristic polynomial of the monodromy matrix is

$$\begin{aligned} p(\lambda) &= (\lambda-1)^2(\lambda-\lambda_1)(\lambda-\lambda_2)(\lambda-\lambda_3)(\lambda-\lambda_4) \\ &= (\lambda-1)^2(\lambda^2 - T_1\lambda + 1)(\lambda^2 - T_2\lambda + 1) \\ &= \lambda^6 - (T_1+T_2+2)\lambda^5 + (T_1T_2 + 2(T_1+T_2) + 3)\lambda^4 + \dots \end{aligned} .$$

Let us denote by d_{ij} the generic entry of the monodromy matrix, and set

$$a = \sum_{i=1}^{6} d_{ii}, \qquad b = \sum_{1\le i\le j\le 6} (d_{ii}d_{jj} - d_{ij}d_{ji}).$$

From the expressions of the coefficients of the characteristic polynomial we obtain

$$\begin{cases} T_1 + T_2 + 2 = a, \\ T_1T_2 + 2(T_1+T_2) + 3 = b. \end{cases} \tag{5.1}$$

It turns out that T_1 and T_2 are the roots of the polynomial of degree two

$$q(s) = s^2 - (a-2)s + (b - 2a + 1). \tag{5.2}$$

We use the following result, see [60].

Lemma 5.1. *Let T_1, T_2 the roots of the polynomial* (5.2)*. The eigenvalues of the monodromy matrix lie on the unit circle if and only if*

$$\begin{cases} \Delta = (a-2)^2 - 4(b-2a+1) > 0, \\ |T_1| < 2, \quad |T_2| < 2. \end{cases} \tag{5.3}$$

Proof. The hypothesis $\Delta > 0$ yields that T_1, T_2 are real and distinct. This excludes the possibility (2) above. We also exclude (1), because in this case we have

$$|T_1| = |\lambda_1 + \lambda_2| = |\lambda_1 + \lambda_1^{-1}| > 2, \quad |T_2| = |\lambda_3 + \lambda_4| = |\lambda_3 + \lambda_3^{-1}| > 2.$$

The only possibility left is (3), that is the eigenvalues of the monodromy matrix lie on the unit circle.

□

By this lemma we avoid the numerical computation of the eigenvalues and we can establish the stability of the orbit simply by computing the roots of a polynomial of degree two, whose coefficients depend only on the entries of the monodromy matrix $\mathfrak{M}(T)$. As already explained in Subsection 4.5.1, this lemma permits also to produce a computer-assisted proof, since we can check inequalities (5.3) using a computer.

Moreover, for symmetric periodic orbits we can factorize $\mathfrak{M}(T)$ as in [91]:

$$\mathfrak{M}(T) = (S^T \mathfrak{M}(T/M))^M, \tag{5.4}$$

where $\mathfrak{M}(t)$ is the fundamental solution of the variational equation at time t. Here the matrix $S \in \mathbb{R}^{6\times 6}$ is given by $S = \mathrm{diag}(R, R)$, and $R \in \mathcal{R}$ is the matrix satisfying the choreography condition (1.6). This means that we can integrate the variational equation only over the timespan $[0, T/M]$ and we can study the stability by applying Lemma 5.1 to the matrix $S^T\mathfrak{M}(T/M)$.

Our numerical computations suggest that all the periodic orbits found in Section 1.3 are unstable. Non-rigorous numerical values of Δ, T_1, T_2 for can be found at the website [34]. To make rigorous the results and produce a computer-assisted proof, we have to integrate the equation of motion using interval arithmetic ([80]), as explained in Section 4.5.

label	M	vertexes of $\mathcal{Q}_\mathcal{O}$
ν_1	2	$[1, 3, 8, 10, 16, 5, 1]$
ν_{16}	2	$[1, 3, 8, 18, 13, 12, 4, 9, 2, 19, 11, 14, 1]$
ν_{27}	3	$[1, 3, 7, 20, 18, 8, 15, 4, 6, 10, 16, 5, 1]$
ν_{43}	4	$[1, 3, 8, 15, 4, 9, 2, 5, 1]$

Table 5.1: List of sequences used in the tests. The labels correspond to the enumeration used in the website [34].

5.1.3 Computer-assisted proof of the instability

We have applied the method described in Section 4.5 to produce a rigorous proof of the instability of the periodic orbits corresponding to the free-homotopy classes listed in Table 5.1. As surface of section we choose

$$\Sigma = \{(u, \dot{u}) \in \mathbb{R}^6 : u_3 = 0,\ E(u, \dot{u}) = h\},$$

where u_3 is the third component of u and h is the value of the energy of an approximated initial condition $(u_0, \dot{u}_0) \in \Sigma$. This condition is computed from the solution $\tilde{u}(t)$ obtained with the shooting method, propagated to reach the plane $u_3 = 0$. Note that, up to a rotation $R \in \mathcal{R}$, we can always assume that $\tilde{u}(t)$ passes through this plane.[1] The N-body motion corresponding to the selected cases is displayed in Figure 5.2.

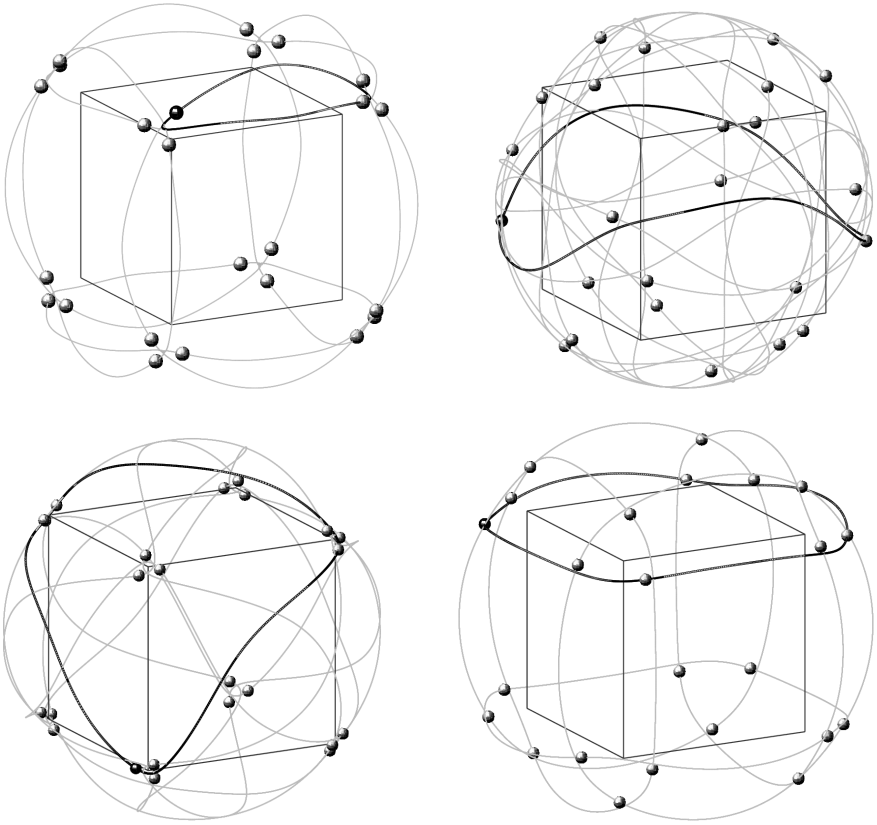

Figure 5.2: Periodic motions of the N bodies corresponding to the sequences listed in Table 5.1. The solid black curve represents the trajectory of the generating particle.

Hereafter we shall use a notation similar to [60, 61] to describe an interval: first we write the digits shared by the interval extrema, then the remaining digits are reported as subscript and superscript. Thus, for instance, we write

$$12.3456789^{5678}_{1234}$$

for the interval

$$[12.34567891234, 12.34567895678].$$

For the four selected cases in Table 5.1 we checked that condition (4.25) holds using multiple precision interval arithmetic. This ensures the existence of an initial condition

[1] For instance, for ν_1 and ν_{43} we rotate the orbit of the generating particle, as it does not pass through the plane $u_3 = 0$.

for the orbits in the selected box B. When the bodies do not undergo close approaches, as in the cases of ν_{16} and ν_{43}, the inclusion can be checked with a much larger box. Using double precision arithmetic, CPU times are quite short: less than a minute in both cases. Multiple precision computations are slower: with the parameters given in Table 5.2 the computer-assisted proof took about 40 minutes for ν_{16} and 60 minutes for ν_{43}. On the other hand, when close approaches occur, as in the cases of ν_1 and ν_{27}, we are forced to use a very tiny box, a longer mantissa and a higher order for the Taylor method (see Table 5.2) and moreover, we need to compute an initial point with the shooting method using quadruple precision. This increases significantly the CPU time: 104 minutes for ν_1 and 190 minutes for ν_{27}. All the tests reported in this section were performed on an AMD FX(tm)-4100 Quad-Core 1.4 GHz Processor.

To show the instability of these orbits we prove that conditions (5.3) are violated. For ν_{16} and ν_{43} these computations are successful even using only double precision interval arithmetic. In the other two cases we need multiple precision and a higher order for the Taylor method. As we can see from Table 5.2, the value of T_1 is well above 2, that yields a computer-assisted proof of the instability of these four test orbits. In Table 5.3 we report also the non-rigorous values of Δ, T_1, T_2, obtained by numerical integration without interval arithmetic. Comparing the values in the two tables, we can see that the non-rigorous ones are in good agreement with the estimates computed with interval arithmetic. Non-rigorous values for several other orbits can be found at [34].

label	mantissa (bits)	size(B)	order	Δ	T_1	T_2
ν_1	100	$2 \cdot 10^{-18}$	30	1488.95^{3031}_{2965}	43.365^{500}_{499}	4.778546^{6}_{1}
ν_{16}	52	$2 \cdot 10^{-14}$	15	90582.1^{30}_{06}	301.0993^{89}_{68}	0.1307^{566}_{359}
	100	$2 \cdot 10^{-14}$	30	90582.1^{22}_{14}	301.0993^{82}_{76}	0.13074^{92}_{33}
ν_{27}	100	$2 \cdot 10^{-25}$	30	5105.47178^{7}_{6}	73.279035^{6}_{5}	1.826451^{4}_{3}
ν_{43}	52	$2 \cdot 10^{-14}$	15	7.0355^{20}_{19}	9.23226^{9}_{1}	6.57980^{1}_{0}
	100	$2 \cdot 10^{-14}$	30	7.0355^{20}_{19}	9.23226^{8}_{3}	6.57980^{1}_{0}

Table 5.2: Enclosures for the values of Δ, T_1, T_2.

label	Δ	T_1	T_2
ν_1	1488.953003	43.365500	4.778546
ν_{16}	90582.118054	301.099379	0.130746
ν_{27}	5105.471786	73.279035	1.826451
ν_{43}	7.035519	9.232260	6.579805

Table 5.3: Non-rigorous values of Δ, T_1, T_2.

5.1.4 Conclusions and further remarks

All the solutions found with the rotation groups $\{\mathcal{T}, \mathcal{O}\}$ appear to be unstable, with a large value of $|T_1|$ or $|T_2|$ (see the website [34] for the results). Using multiple precision interval arithmetic, we were able to make rigorous these results for a few orbits, producing a computer-assisted proof of their instability. From the numerical point of view, the main difficulty is to automatize the choice of the parameters appearing in the computations: the order of the Fourier polynomials, the number of shooting points, the size of the boxes, the order of the Taylor method, the mantissa size for multiple precision computations, etc. Moreover, when the bodies undergo close approaches, a longer computational time is needed to check whether condition (4.25) holds, because a larger size of the mantissa is required. This requires a long computational time. For these reasons we performed interval arithmetic computations only for a few orbits in our list.

We also have to point out that there is no guarantee that the computed periodic solutions correspond to minimizers of the action $\mathcal{A}$, whose existence have been assessed in Sections 1.2, 1.3. Indeed, with the proposed procedure, we first search for a minimizer of $\mathcal{A}$ in a finite dimensional set of Fourier polynomials by a gradient method, decreasing the value of the action; then we refine these solutions by a shooting method. This algorithm is meant to obtain local minima of the action $\mathcal{A}$. However, there is no proof, not even computer-assisted, that the computed solutions minimize the action $\mathcal{A}$ in the cone $\mathcal{K}$. What can be done is to study the variational properties of these solutions with the theory of local minimizers described in Chapter 3, understanding whether they are at least local minimizers of the action. Examples of non-rigorous computations have been proposed in Section 3.5.

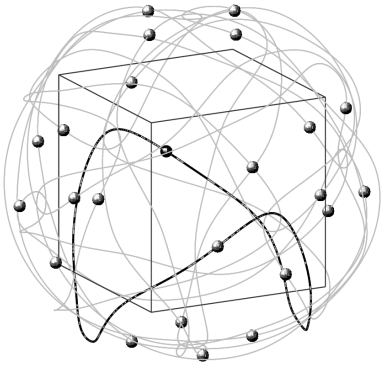

Figure 5.3: Periodic motion with ν not fulfilling condition (1.17).

As a final remark, we observe that the procedure described in Section 4.5 can also be used to prove the existence of periodic orbits not included in our list. For example, the sequence

$$\nu = [1, 3, 7, 18, 20, 24, 12, 4, 9, 17, 19, 21, 23, 14, 1],$$

of vertexes of $\mathcal{Q}_{\mathcal{O}}$ does not satisfy the condition on the maximal length (1.17): in fact it has $M = 2$, $l_{\max}(2) = 12$ and the length of ν is 14. This means that we cannot exclude

total collisions with the estimates of Chapter 1. However, the validity of condition (4.25) can be checked numerically. Using the approximated orbit obtained with multiple shooting, we were able to check that (4.25) holds using a box with size $2 \cdot 10^{-14}$. In this way, we have a computer-assisted proof of the existence of a periodic orbit belonging to $\mathcal{K}(\nu)$, represented in Figure 5.3.

We also found the values

$$\Delta = 4423_{29}^{58}, \quad T_1 = 665.3_{83}^{94}, \quad T_2 = 0._{293}^{305},$$

that yields a rigorous proof of the instability of this orbit.

5.2 System of $N + 1$ charged particles

The connection between the macroscopic scale, i.e. Celestial Mechanics, and the microscopic scale, i.e. atomic mechanics, is given by the Coulomb force, which governs the interaction between charged particles. The Coulomb potential depends on $1/r$, as the Newtonian potential, with the difference that it depends on the charges and not on the masses. However, charges can be also negative, making this force both attractive and repulsive. The most famous connection is given by the Rutherford model of the atom [92], which represents the atom as a miniature Solar System: the nucleus is placed at the center and plays the role of the Sun, while the electrons orbit around it, see Figure 5.4. Since the introduction of quantum mechanics, this model was deprecated. However, despite quantum mechanics provides a more accurate description of nature, classical methods are still useful in studying atomic dynamics [107].

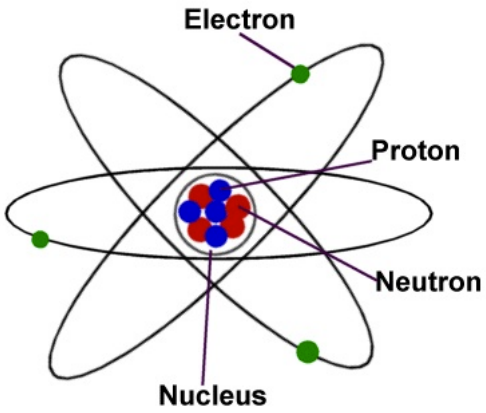

Figure 5.4: A representation of Rutherford's model of the atom.

In more recent years, the Coulomb N-body problem, i.e. the problem of N charged particles which interact through the Coulomb force, was taken into account, and periodic orbits in the Coulomb 3-body problem were found, see for example [86, 93, 57], trying to reproduce some features of the known orbits in the classical Newtonian 3-body problem. On the other hand, some special symmetric solutions were found numerically in [27], for small values of N. The use of the Coulomb force as the only interacting force is motivated by the fact that the gravitational interaction is negligible when the electrostatic force is introduced in the system. Moreover, the Coulomb force by itself amounts to a non-relativistic approximation, which is reliable only when the velocities are small compared to the speed of light [64].

In this section we consider the Coulomb $(N + 1)$-body problem, composed by a positive charged particle and other N negative equally charged particles. We search for

periodic motions sharing the symmetry of Platonic polyhedra, hence N can be either $12, 24$ or 60. Here we have been able to compute a set of periodic orbits similar to the one found in Section 1.3, see the website [36] for animations of these solutions. Our numerical computations also show that these orbits are unstable. Moreover, since the approach used in Chapter 1 for the proof of the existence was the minimization of the action, here we investigated whether this method could still work for the Coulomb $(N+1)$-body problem or not. However, we show numerically that the orbits we compute are not minimizers of the action, not even locally. Finally, we compute other periodic orbits with an even number of electrons, similar to the one found in Section 2.3.

5.2.1 The electrostatic potential

We take into account a system composed by $N+1$ charged particles, one of which has positive charge and the rest have equal negative charges. Despite the Rutherford model [92] turned out to be not valid to represent the physical nature of the atom, for the sake of simplicity we will use terms as *electrons* and *nucleus* in the following.

We denote with $q<0, m>0$ the charge and the mass of the electron respectively, with $Q>0$ the charge of the nucleus, with $u_i \in \mathbb{R}^3, i=1,\dots,N$ the position of the i-th electron and with $u_0 \in \mathbb{R}^3$ the position of the nucleus. The mass of the nucleus is very high compared with the mass of the electrons, so we assume that the nucleus stays fixed at $u_0 \in \mathbb{R}^3$. The particles move under the Coulomb force, and the system of equations that determine the motion is given by

$$m\ddot{u}_i = \kappa q\Big[\sum_{\substack{j=1\\ j\neq i}}^{N} q\frac{u_i-u_j}{|u_i-u_j|^3} + Q\frac{u_i-u_0}{|u_i-u_0|^3}\Big], \quad i=1,\dots,N, \tag{5.5}$$

where $\kappa>0$ is the Coulomb constant.

We choose a reference frame centered at the center of mass, hence from now on we assume that $u_0 \equiv 0$. The system (5.5) is Lagrangian, and the Lagrangian L is given by

$$L = K + U,$$

where

$$K = \frac{1}{2}\sum_{i=1}^{N} m|\dot{u}_i|^2, \tag{5.6}$$

is the kinetic energy and

$$U = -\kappa \sum_{1\le i<j\le N} \frac{q^2}{|u_i-u_j|} - \kappa\sum_{i=1}^{N}\frac{qQ}{|u_i|}, \tag{5.7}$$

is the Coulomb potential. To simplify the computations, we choose the units of charge, mass and distance so that

- the charge of the electron is unitary, hence $q=-1$,

- the mass of the electron is unitary, hence $m = 1$,
- the Coulomb constant is unitary, hence $\kappa = 1$.

Solutions to the equations (5.5) can be found also as stationary points of the Lagrangian action functional, defined as

$$\mathcal{A}(u) = \int_a^b L(u, \dot{u})\, dt. \tag{5.8}$$

The functional (5.8) is defined over a set of curves $\mathcal{K} \subseteq H^1([a,b], \mathbb{R}^{3N})$, which has to be specified, depending on the problem that one wants to study.

5.2.2 Symmetry of the Platonic polyhedra and topological constraints

We want to compute periodic orbits of the system (5.5), imposing both symmetry and topological constraints. As done in Chapter 1, we take into account a Platonic polyhedron and we denote with $\mathcal{R}$ its rotation group. We consider a system composed by $N = |\mathcal{R}|$ electrons, hence N can be either $12, 24$ or 60 and, identifying $\{1, \cdots, N\}$ with the elements of $\mathcal{R}$, we label the positions of the particles with the rotations of the group. Fixed the period $T > 0$, we impose the constraints (a), (b) and (c) of Section 1.2 on the loops. Taking into account the symmetry (a), the action functional writes as

$$\mathcal{A}(u) = N \int_0^T \left(\frac{1}{2}|\dot{u}_I|^2 - \frac{1}{2} \sum_{R \in \mathcal{R} \setminus \{I\}} \frac{1}{|(R-I)u_I|} + \frac{Q}{|u_I|} \right) dt, \tag{5.9}$$

and it is defined on the set of T-periodic loops

$$\mathcal{K} = \{u \in H^1_T(\mathbb{R}, \mathbb{R}^{3N}) : \text{ (a), (b) and (c) hold}\}. \tag{5.10}$$

Since a term with a negative sign appears in the Lagrangian, it is not clear whether this functional is coercive or not, and the search for periodic orbits using the minimization of the action does not apply so easily. For this reason we investigate the existence of periodic orbits with a preliminary numerical study.

Note that (5.9) depends only on the motion of the generating particle u_I. This means that we can reduce the searching for periodic orbits of the full system of charges to the searching of periodic orbits of the generating particle u_I, whose dynamics is defined by the Lagrangian

$$L = \frac{1}{2}|\dot{u}_I|^2 - \frac{1}{2} \sum_{R \in \mathcal{R} \setminus \{I\}} \frac{1}{|(R-I)u_I|} + \frac{Q}{|u_I|}. \tag{5.11}$$

The Euler-Lagrange equations of (5.11), written as first order system, are

$$\begin{cases} \dot{u}_I = v_I, \\ \dot{v}_I = \displaystyle\sum_{R \in \mathcal{R} \setminus \{I\}} \frac{(I-R)u_I}{|(R-I)u_I|^3} - \frac{Q u_I}{|u_I|^3}. \end{cases} \tag{5.12}$$

This system has the advantage that the dimension is much more smaller than the dimension of the system of equations (5.5), 6 compared to $6N$. Moreover, if the periodic orbit of the generating particle u_I is unstable in the system (5.12), also the complete orbit with N electrons is unstable in the system (5.5). On the other hand, the stability in the reduced system leads only to the stability with respect to symmetric perturbations of the complete orbit. To study entirely the stability, we need to solve equations (5.5), together with its variational equation, in order to compute the full $6N \times 6N$ monodromy matrix. Since we do not expect to find many stable orbits for the reduced system, the study of the stability is divided in two steps: at the first step we check whether the generating particle is stable in the reduced system or not and, if it is stable, we proceed in the computation of the full monodromy matrix and get an estimation of the Floquet multipliers.

5.2.3 Computing periodic orbits

As it has been mentioned in Chapter 4, one of the difficulties in computing periodic orbits is to find a good initial guess for the Newton method to converge. To deal with this, we have used two different continuation schemes.

From the physical intuition, if the central charge Q is zero, the electrons only repel each other, and we do not expect to find any periodic solutions. For continuity reasons, if the central charge is too small compared to the number of electrons, a periodic orbit could still not exist. On the contrary, if the positive charge is large enough, the contribution of the electrons in the vector field (5.5) is small, compared to the term given by the positive charge. Indeed, rescaling the loops as $u_i(t) = Q^{1/3} v_i(t),\ i = 1, \ldots, N$ in (5.5), we obtain a differential equation for v_i, which writes as

$$\ddot{v}_i = \mu \sum_{\substack{j=1 \\ j \neq i}}^{N} \frac{v_i - v_j}{|v_i - v_j|^3} - \frac{v_i}{|v_i|^3}, \quad i = 1, \cdots, N, \tag{5.13}$$

where $\mu = 1/Q$. Note that, when the positive charge is ideally "infinite", the interactions between the electrons disappear, and the differential equation that determines the motion of v_i is the equation of the Kepler problem. Intuitively, when the central charge is finite but very large, the solution is close to a circular piecewise loop, composed by Keplerian arcs, joined at points on the collision lines, similarly to what we saw in Chapter 2. For this reason, periodic solutions seem more likely to exist when the central charge is high enough. Therefore, we search for periodic orbits for a high value of the central charge, then we consider Q as a parameter and use the continuation method to lower its value.

To find periodic orbits for large values of Q we use the strategy explained in Section 4.4. Indeed, differently for the case of Section 5.1, the gradient method do not work. This is also a first suggestion that the action is not coercive. Therefore, first we choose a closed curve

$$\varphi : [0, T] \to \mathbb{R}^6, \qquad \varphi(t) = \big(u(t), \dot{u}(t)\big)^T,$$

such that the image of the spatial component $u([0,T])$ belongs to the chosen free-homotopy class of $\mathbb{R}^3 \setminus \Gamma$. Moreover, we can take this spatial component to be on a sphere, since we expect that the final orbit does not have large changes in the radial component. Of course this curve will not solve equation (4.10), but we can perturb the system and define a new differential equation for which φ is a solution. Indeed, if we define

$$\dot{x} = f(x) - \varepsilon\psi(t), \tag{5.14}$$

where

$$\psi(t) = \dot{\varphi}(t) - f(\varphi(t)),$$

then $\varphi(t)$ is a solution of (5.14) for $\varepsilon = 1$. To find the periodic orbit for $\varepsilon = 0$, we consider ε as a parameter and we use the continuation method. In our computations, we decided to stop the continuation when we reach a value of $\varepsilon < 10^{-2}$: this was usually enough to have an initial guess for the shooting method to converge for $\varepsilon = 0$ and compute the periodic orbit.

Summarizing, the approach used to compute the orbits is the divided in three steps.

Step 1: We generate a starting guess for a high value of the central charge Q, with the method described above. In our computations, we decided to choose a value near $2N$, i.e. two times the number of electrons.

Step 2: We compute the solution using the shooting method described in Section 4.2, with the same value of Q used to produce the initial guess, and using continuation w.r.t. ε as explained above, until we reach $\varepsilon = 0$. Using this last solution as starting guess, we compute a second solution for the value of the central charge equal to $Q-1$: this is needed to start the continuation w.r.t. the value of the central charge.

Step 3: Using the two solutions computed at the Step 2, we start the continuation method described in Section 4.3, in order to find solutions for smaller values of Q.

5.2.4 Results of the computations

In Section 1.3, for each Platonic polyhedra, a list of free-homotopy classes of $\mathbb{R}^3 \setminus \Gamma$, each one containing a collision-free minimizer of the N-body problem with equal masses, were provided: these lists are available at [34]. Here we search for symmetric periodic solutions of the system (5.5), in the same free-homotopy classes listed at [34].

In Section 1.3, 9 and 57 homotopically different periodic orbits with the symmetry of the Tetrahedron and the Cube, respectively, were found for the N-body problem with equal masses. The total number of orbits with the symmetry of the Dodecahedron was 1442, but the entire computation of all of them was not done. Here we were able to compute all these orbits also in Coulomb $(N+1)$-body problem, with the symmetry of the Tetrahedron and the Cube, reproducing the list in [34]. For the symmetry of the Dodecahedron only a few number of orbits were computed (a large number of them is expected). Examples of orbits with 24 electrons are displayed in Figure 5.5. More images and videos are available in the webpage [36].

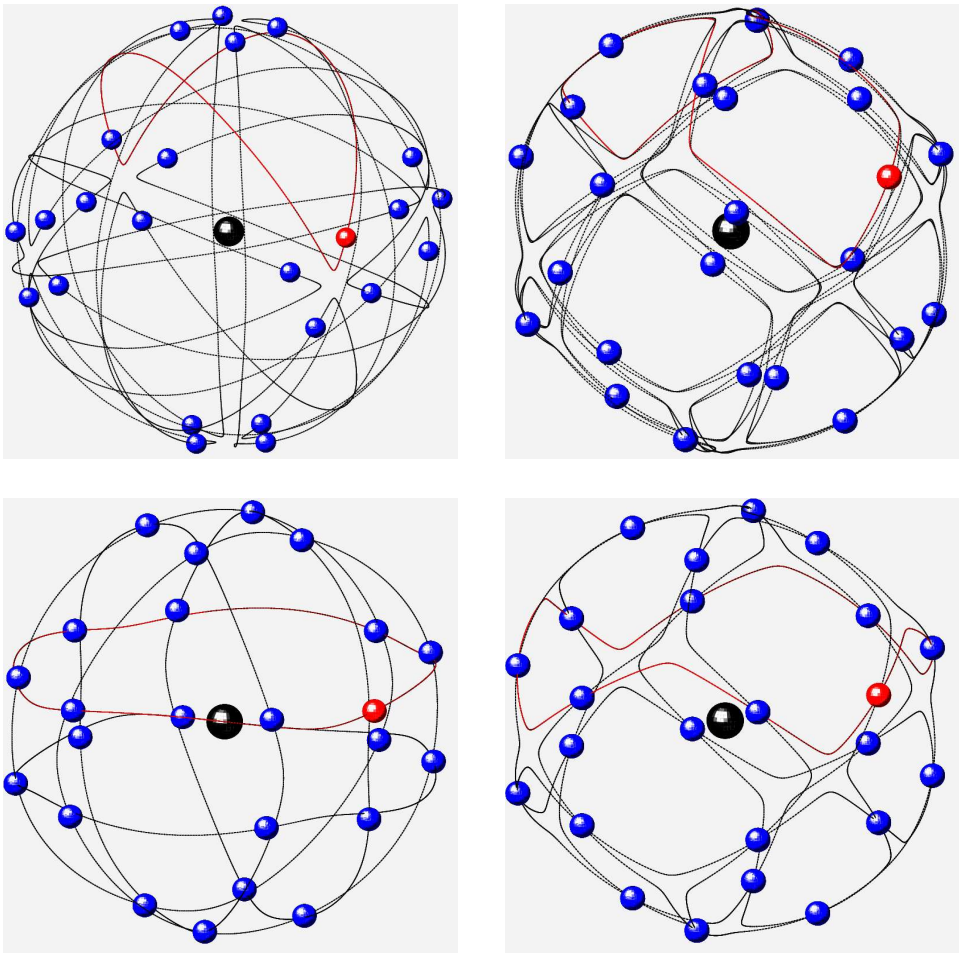

Figure 5.5: Solutions with 24 electrons and the symmetry of the Cube. The value of the central charge is 24 in all the four examples. The homotopy class for the orbits on top is ν_2 and ν_{43} for the orbits on bottom. The enumeration is referred to the website [36]. The red electrons represent the generating particles, and the red curve are their trajectories. The black particle in the middle is the nucleus. The orbits on the right are obtained by the continuation method, starting from the orbits on the left. We reached them after following a turning point on the curve of solutions.

5.2.5 Continuation

In our computations we set the period to be $T = 1$: this is not restricting, since an orbit with an arbitrary period can be found simply by rescaling size and time. During the continuation process we always reached a turning point in Q. This means that, when we were able to reach the physical situation of negative charged ions (i.e. when $Q < N$), we can continue the solutions following the turning point, and find a second orbit in which the system is neutral (i.e. when $Q = N$). This does not happen in all the cases we tried, and it is not clear if there is an additional topological condition to be satisfied in order to have the turning point below $Q = N$.

5.2.6 Stability

As said before, the study of the stability is divided in two steps: first we study the stability of the orbit of the generating particle in the reduced system (5.11), computing a 6×6 monodromy matrix M_6. If the generating particle in unstable, then also the complete orbit in the system (5.5) is unstable, otherwise we proceed in the computation of the complete $6N \times 6N$ monodromy matrix M_{6N}. During the continuation, the six eigenvalues of M_6 move in the complex plane. For the most of the orbits, looking at the eigenvalues of M_6 was enough to conclude the instability, since during the continuation a very large Floquet multiplier (of the order that ranges from 10^6 to 10^{20}, depending on the orbit) appears. However, it can happen that for certain values of the central charge, the eigenvalues of M_6 are all on the unit circle, meaning that the generating particle is stable in the reduced system. In these few cases we computed the matrix M_{6N}, verifying that the complete orbit is in fact unstable, since a large Floquet multiplier arises. An example of this situation is reported in Figure 5.6. More figures of this kind can be found at [36]. From the computations, it results that all the orbits are unstable. Results for the orbits with the symmetry of the Tetrahedron are summarised in Table 5.4.

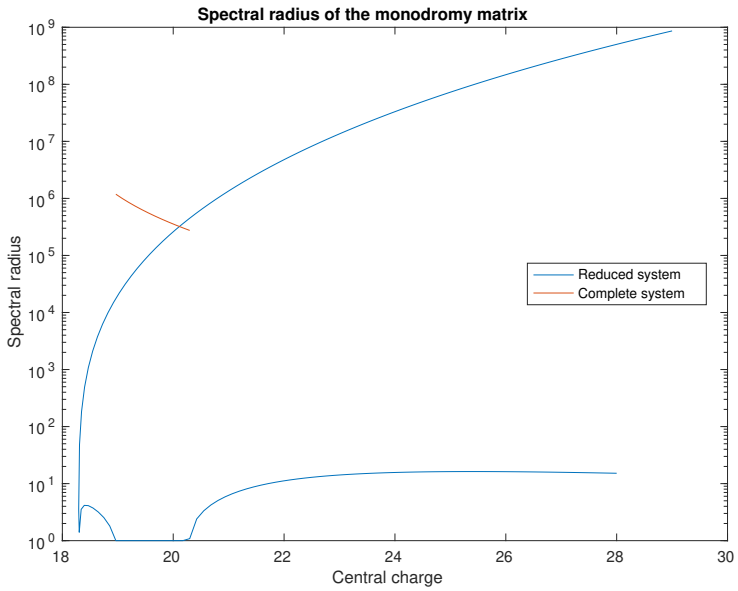

Figure 5.6: The spectral radius of the monodromy matrix. On the x axis is reported the value of the central charge and on the y axis is reported the value of the spectral radius, in logarithmic scale. The blue curve represents the evolution of the spectral radius of the monodromy matrix in the reduced system, while the red curve represents the evolution of the spectral radius in the complete system. During the continuation, the generating particle becomes stable for certain values of Q (near $Q = 20$, blue curve), but in fact the resulting complete orbit is unstable (red curve). This plot is referred to the orbits in Figure 5.5, bottom.

5.2.7 Are these orbits minimizers of the action?

Here we study whether the solutions obtained are local minimizers of the action (5.9) or not. As first indication, we discretize the functional using a space of truncated

label	$\min Q$	$\lvert\lambda\rvert\,(Q=\min Q)$	$\lvert\lambda_{6N}\rvert\,(Q=\min Q)$	$\lvert\lambda\rvert\,(Q=12)$
ν_1	10.346970805	7.3761606	/	$0.18050567\cdot 10^4$
ν_2	8.281250928	2.5911113	/	$0.26940597\cdot 10^4$
ν_3	9.965258217	3.7293607	/	$0.49658024\cdot 10^2$
ν_4	12.905694682	1.0	$0.4930569\cdot 10^5$	/
ν_5	8.720563122	$0.28289539\cdot 10^3$	/	$0.33578812\cdot 10^9$
ν_6	9.546005362	$0.49445974\cdot 10^2$	/	$0.27073516\cdot 10^5$
ν_7	8.076087749	$0.18090607\cdot 10^5$	/	$0.33898930\cdot 10^{13}$
ν_8	12.905977225	2.8508903	/	/
ν_9	12.905656346	1.0	$0.2461446\cdot 10^{10}$	/

Table 5.4: Some numerical values obtained for the orbits with the symmetry of the Tetrahedron. Second column contains an approximation of the minimal value of the central charge Q obtained during the continuation. Third column contains the spectral radius of the monodromy matrix M_6 for $Q=\min Q$. When this value is equal to 1, we report the spectral radius of the complete monodromy matrix M_{6N} in column four. Last column contains the value of the spectral radius of M_6 for $Q=12$, for which the system is neutral. The labels correspond to the enumeration used in the website [36].

Fourier series, as done in Section 4.1. In this manner the discretized action depends only on a finite number of Fourier coefficients. To see if the computed solution $u^*(t)$ is a minimum or not, we can compute the coefficients of its Fourier series and then evaluate the Hessian matrix of the discretized action, using high order numerical differentiation based on Richardson extrapolation (see, for instance, [12] for a detailed treatment about numerical differentiation). To reduce the numerical error, we computed the Hessian matrix increasing the order of truncation, and compare the results. Negative eigenvalues always arise, indicating that the computed solutions are not minima, but indeed saddle points. However, the computation of the numerical Hessian results to be very slow, especially when we use a large number of Fourier modes. Moreover, this method does

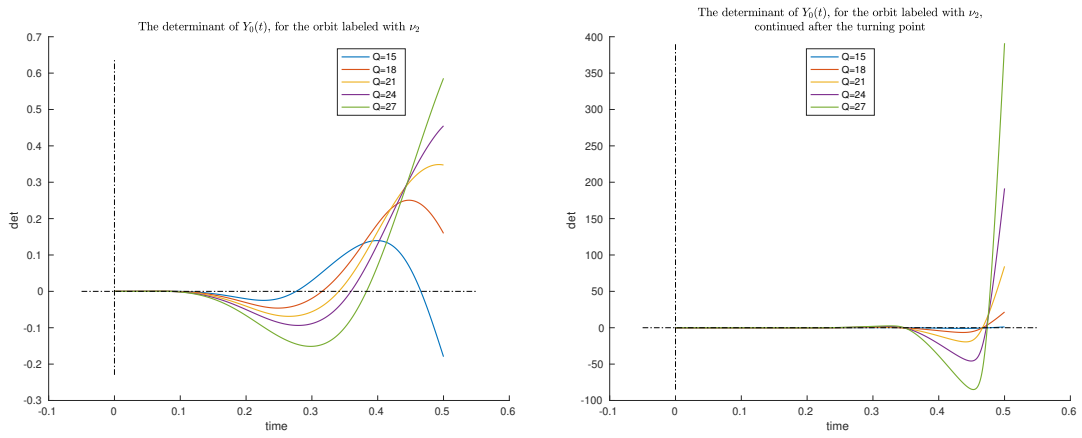

Figure 5.7: The determinant of the matrix $Y_0(t)$ in the fundamental interval $[0,T/M]=[0,1/2]$, for different values of the central charge Q. These plots are referred to the periodic orbits in Figure 5.5, top.

not take into account the symmetries included in the space of loops.

To study better the variational properties, we can use the theory of local minimizers explained in Chapter 3, including also the symmetry constraint as explained in Example 3. First of all, we integrate the Jacobi differential equation and we search for conjugate points in the fundamental interval $[0, T/M]$, simply by plotting the determinant of the matrix $Y_0(t)$. Since the computation is quite fast, we can also see how the determinant changes with respect to the value of the central charge Q, computing it during the continuation process, and see how it behaves after the turning point. Most of the orbits have a behaviour similar to the one shown in Figure 5.7, i.e. they have at least a conjugate point in the interval $[0, T/M]$, indicating that they are not minimizers, not even directional.

However it can occur that, during the continuation process, the determinant of $Y_0(t)$ does not vanish for certain values of the central charge Q. An example of this behaviour is shown in Figure 5.8, where we can see that the determinant is positive for the values $Q = 36, 40$. Continue increasing the value of the charge Q, this behaviour still persists, and it seems that the determinant has a limiting curve that does not vanish in the fundamental interval $(0, 1/4]$. Hence we also have to compute the matrix in (3.36), and verify whether it is positive definite or not. In this case, the eigenvalues of the matrix in (3.36), for $Q = 40$, are computed to be

$$14.723038, \quad 5.5236623, \quad -307.98056,$$

hence this orbit is also not a local minimizer, despite the absence of conjugate points. For values of $Q > 40$, this property still holds, and the negative eigenvalue seems to converge to a value close to -60.757245.

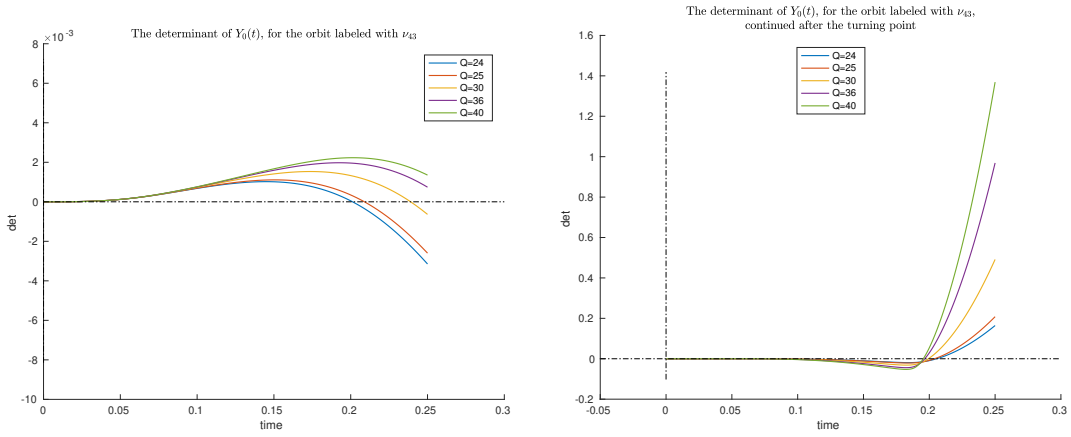

Figure 5.8: The determinant of the matrix $Y_0(t)$ in the fundamental interval $[0, T/M] = [0, 1/2]$, for different values of the central charge Q. These plots are referred to the periodic orbits of Figure 5.5, bottom.

Further computations for the remaining orbits show that the two described behaviours are common to all of them, suggesting that they are not local minimizers, but indeed different kind of stationary points, such as saddles. For this reason the method of minimization of the action does not seem to work for the Coulomb $(N + 1)$-body

problem to find periodic orbits, as it is formulated. A strategy could be to try to find a proper loop set on which the action is coercive, or rather use critical points theorems, see for example [2].

5.2.8 Hip-Hop solutions

In [27], periodic orbits of $2N$ electrons with a positive charged nucleus and the $\mathbb{Z}_{2N}$ symmetry were computed for small values of N (i.e. $N = 2, 3, 4$), for the case of the neutral atom, i.e. $Q = 2N$. Note that the symmetry group is the same of the Hip-Hop solutions of Subsection 2.3.4.

Here we tried to obtain again these orbits, using the computation strategy described above and used for the case of the Platonic polyhedra symmetry. In all the cases we tried, namely $N = 1, \dots, 30$ we were able to obtain periodic orbits in the case of the neutral system, i.e. for $Q = 2N$. Using the continuation method, we also decreased this vale: here, differently from the situation of the symmetry of Platonic polyhedra, we did not observe a turning point in the curve of solutions. Instead, it seems that there is a lower bound of Q for which this value of positive charge is not strong enough to hold the electrons near the nucleus, and therefore everything blows up. In Figure 5.9, periodic orbits with $N = 6$ and displayed for decreasing values of the central charge Q.

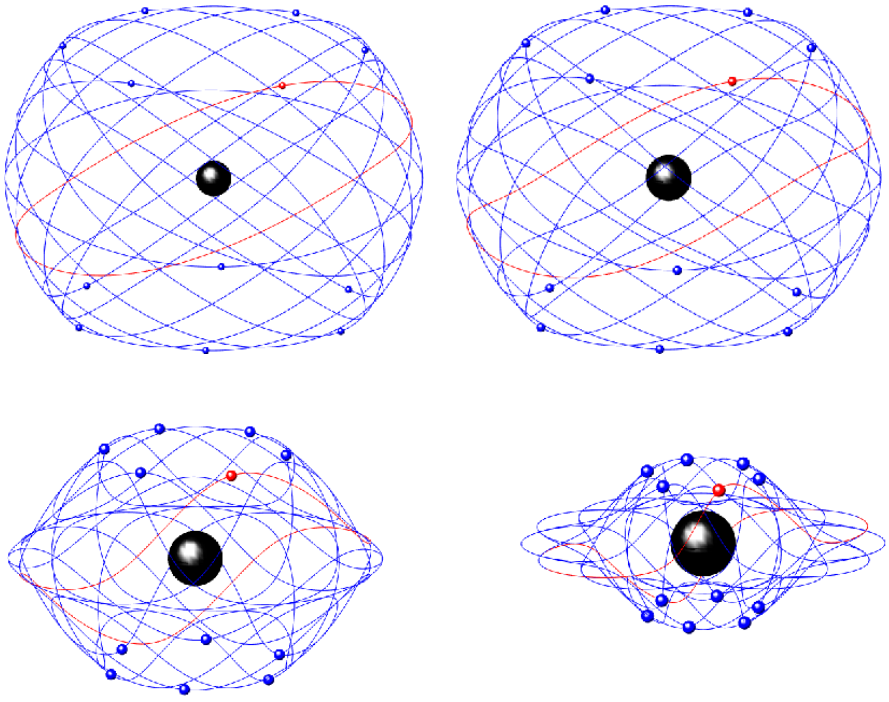

Figure 5.9: Periodic orbits of $2N$ electrons with the $\mathbb{Z}_{2N}$ symmetry, for $N = 6$. The central charge is $Q = 12, 8, 6, 5.5$ (top left, top right, bottom left, bottom right respectively).

As we can see, the orbit of the generating particle tends to flatten to the coordinate

plane $\{x_3 = 0\}$ and there is a small and fast migration from the upper half space $\{x_3 > 0\}$ to the lower half space $\{x_3 < 0\}$. This behaviour could possibly be the explanation of the blow up of the orbit. Indeed, the migration becomes faster and faster as the central charge decreases, and at a certain point the value Q of the central charge it is not able anymore to counteract the repulsion between the electrons, which becomes large during this process. Moreover, the spectral radius of the monodromy matrix grows as

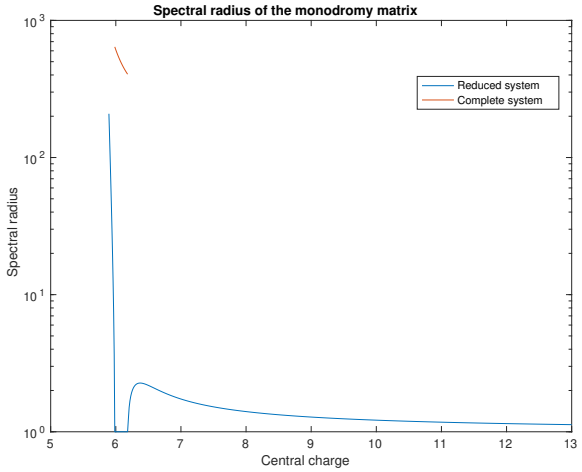

Figure 5.10: Spectral radius of the monodromy matrix for the periodic orbits with $2N$ electrons and the $\mathbb{Z}_{2N}$ symmetry, for $N = 6$.

Q approaches the lower bound, which is another suggestion about the behaviour of of these orbits during the continuation. A plot of the spectral radius of the monodromy matrix can be seen in Figure 5.10, for the example with $N = 6$.

Finally, we note that prove the existence of these orbits seems easier than the case of the symmetry of the Platonic polyhedra. The idea is to use a perturbative approach and use continuation with respect to a parameter (see, for instance, [82] for a deepen explanation) instead of using variational methods. Indeed, if we rescale the loops as $u_i(t) = Q^{1/3} v_i(t)$, $i = 1, \dots, 2N$, we obtain the equations of motion (5.13), which for $\mu = 0$ represent $2N$ uncoupled Kepler problems, where $\mu = 1/Q$. Moreover, if we take into account the $\mathbb{Z}_{2N}$ symmetry, then the motion depends only on the generating particle v_1, and its equation of motion is given by

$$\ddot{v}_1 = -\frac{v_1}{|v_1|^3} + \frac{\partial U}{\partial v_1}, \quad U = -\frac{\mu}{2} \sum_{i=1}^{2N-1} \frac{1}{|(R^i - I)v_1|}. \tag{5.15}$$

Also here, for $\mu = 0$ the generating particle moves with Keplerian motion. Therefore, in this setting, we are able to find a circular orbit with period T with the symmetry

$$v_1(t + T/2) = -v_1(t), \quad t \in \mathbb{R},$$

which is not contained in the plane $\{x_3 = 0\}$. Moreover, since the angular momentum is a first integral, system (5.15) has actually two degrees of freedom. The idea to prove

the existence of these orbits is to construct a Poincaré map, and evaluate its differential for $\mu = 0$ in the point corresponding to the circular orbit, which is a fixed point of the map. Then, if the eigenvalues are not on the unit circle, we can apply the implicit function theorem to prove the existence of a fixed point of the Poincaré map for values $0 < \mu < \mu^*$, for a certain $\mu^* > 0$. Then, a further issue is to estimate the value of μ^*, to state whether $\mu^* > 1/(2N)$ or not. Note that the value $\mu = 1/(2N)$ corresponds to $Q = 2N$, for which we obtain a periodic orbit in a neutral system.

Part II

The full and the averaged CR3BP

Chapter 6

Averaging the restricted 3-body problem

In this chapter we take into account the circular restricted 3-body problem, composed by the Sun, a planet and an asteroid. The planet moves around the Sun on a circular orbit, while the asteroid is allowed to move in the whole three-dimensional space. The long term evolution of the asteroid is obtained averaging the vector field, due to the gravitational attraction of the Sun and the planet, over the two fast angles involved in the problem, i.e. the mean anomalies ℓ, ℓ' of the asteroid and the planet respectively. In Celestial Mechanics, when there are two sets of variables evolving over two different time scales, averaging over the fast ones is a usual procedure. This removes all the fast and small oscillations and captures the relevant long term dynamics. This is commonly known as *averaging principle* and, since it is only a physical principle and not a formal statement neither a theorem, it can not be applied in every situation, see [5].

In the circular restricted 3-body problem, provided that there are no *close encounters* neither *mean motion resonances* between the asteroid and the planet, the semimajor axis of the asteroid is nearly constant. In these conditions, the averaging principle can be applied, the semimajor axis becomes constant and the averaged solution is a good approximation of the original solution.

The averaged vector field becomes singular when the orbits of the planet and the asteroid cross each other, but we can still define a generalized averaged solution that passes through this singularity, see [49, 45, 50]. However, there is no proof that these solutions are close to the solutions of the full circular restricted 3-body problem. This comparison is investigated in Chapter 7. Instead, when there is a mean motion resonance, the semimajor axis changes periodically over a secular timescale. In this situation we can define another model, keeping all the resonant relevant terms, which describes the long term dynamics, see for example [66].

On the other hand, in the circular restricted 3-body problem, the asteroid could undergo close encounters with the planet. Close encounters are a source of numerical instability: indeed, the orbit of the asteroid can vary largely for small perturbations of the initial conditions. Therefore, we have to take care of this problem if we want to

obtain reliable results to make a comparison with the above mentioned models. To this end we use the Kustaanheimo-Stiefel regularization [102, 56].

6.1 The averaged circular restricted 3-body problem

We denote with $\mathcal{X}, \mathcal{X}' \in \mathbb{R}^3$ the heliocentric position of the asteroid and the planet respectively. The equations of motion for the asteroid are

$$\ddot{\mathcal{X}} = -\kappa^2 \frac{\mathcal{X}}{|\,\mathcal{X}\,|^3} + \frac{m_\oplus}{m_\odot}\kappa^2\left(\frac{\mathcal{X}' - \mathcal{X}}{|\,\mathcal{X}' - \mathcal{X}\,|^3} - \frac{\mathcal{X}'}{|\,\mathcal{X}\,|^3}\right), \tag{6.1}$$

where κ is the Gauss constant and $m_\odot$, $m_\oplus$ are the masses of the Sun and the planet, respectively. System (6.1) can be written in Hamiltonian form as

$$\dot{\mathcal{W}} = -\frac{\partial\,\mathcal{H}}{\partial\,\mathcal{X}}, \quad \dot{\mathcal{X}} = \frac{\partial\,\mathcal{H}}{\partial\mathcal{W}} = \mathcal{W},$$

where the Hamiltonian is

$$\mathcal{H}(\mathcal{W}, \mathcal{X}, t) = \frac{|\mathcal{W}|^2}{2} - \frac{\kappa^2}{|\,\mathcal{X}\,|} - \frac{m_\oplus}{m_\odot}\kappa^2\left(\frac{1}{|\,\mathcal{X} - \mathcal{X}'(t)|} - \frac{\mathcal{X}\cdot\mathcal{X}'(t)}{|\,\mathcal{X}'(t)|^3}\right). \tag{6.2}$$

We choose the units so that the radius and the mean motion of the orbit of the Earth are $a' = 1$, $n' = 1$, respectively. Moreover, we can set $G = 1$. Denoting with $\mu = m_\oplus$, from the Third Kepler Law for the Earth, we obtain $m_\odot = 1 - \mu$, and moreover

$$\kappa^2 = G m_\odot = 1 - \mu.$$

The dependence on the time in the Hamiltonian can be written using an angle, say ℓ', identifying the position of the planet, which is

$$\mathcal{X}'(\ell') = \begin{pmatrix} \cos(\ell' + \ell'(0)) \\ \sin(\ell' + \ell'(0)) \\ 0 \end{pmatrix},$$

where $\ell'(0)$ is the initial phase.

To describe the motion, we use Delaunay elements $\mathcal{Y} = (L, G, Z, \ell, g, z)$, defined through the classical Keplerian elements $(a, e, I, \Omega, \omega, \ell)$ as

$$\begin{aligned} L &= \kappa\sqrt{a}, & \ell &= \ell, \\ G &= \kappa\sqrt{a(1-e^2)}, & g &= \omega, \\ Z &= \kappa\sqrt{a(1-e^2)}\cos I, & z &= \Omega. \end{aligned} \tag{6.3}$$

In these coordinates, the Hamiltonian (6.2) becomes

$$\mathcal{H} = \mathcal{H}_0 + \varepsilon\,\mathcal{H}_1, \quad \varepsilon = \frac{m_\oplus}{m_\odot}\kappa^2 = \mu,$$

where

$$\mathcal{H}_0 = -\frac{\kappa^4}{2L^2} \tag{6.4}$$

is the unperturbed Hamiltonian, corresponding to a 2-body problem with the asteroid and the Sun only, and

$$\mathcal{H}_1 = -\Big(\frac{1}{|\,\mathcal{X} - \mathcal{X}'(\ell')|} - \frac{\mathcal{X}\cdot\mathcal{X}'(\ell')}{|\,\mathcal{X}'(\ell')|^3}\Big). \tag{6.5}$$

is the perturbation, where $\mathcal{X}$ is considered as function of $\mathcal{Y}$. Note that

$$\mathcal{H} = \mathcal{H}(L, G, Z, \ell, g, z, \ell').$$

The perturbation $\mathcal{H}_1$ is composed by a sum of two terms: the first is the direct part of the perturbation, due to the attraction of the planet, the second is the indirect perturbation, due to the attraction of the Sun on the planet.

We can reduce the number of degrees of freedom of the system by averaging over the fast angles (ℓ, ℓ'), which are the mean anomalies of the asteroid and the planet respectively. In this way, ℓ is eliminated from the Hamiltonian and the conjugate variable L is an integral of motion in the averaged system, i.e. the semimajor axis a is constant. The averaged equations of motion for the averaged elements $\overline{Y} = (\overline{G}, \overline{Z}, \overline{g}, \overline{z})^T$ are given by

$$\begin{aligned} \dot{\overline{G}} &= -\varepsilon\overline{\frac{\partial\,\mathcal{H}_1}{\partial g}}, \qquad & \dot{\overline{g}} &= \varepsilon\overline{\frac{\partial\,\mathcal{H}_1}{\partial G}}, \\ \dot{\overline{Z}} &= -\varepsilon\overline{\frac{\partial\,\mathcal{H}_1}{\partial z}}, \qquad & \dot{\overline{z}} &= \varepsilon\overline{\frac{\partial\,\mathcal{H}_1}{\partial Z}}, \end{aligned} \tag{6.6}$$

where the bar denotes the average with respect to the variables (ℓ, ℓ'), that is, for example,

$$\overline{\frac{\partial\,\mathcal{H}_1}{\partial g}} = \frac{1}{(2\pi)^2}\int_{\mathbb{T}^2}\frac{\partial\,\mathcal{H}_1}{\partial g}\,d\ell d\ell',$$

where

$$\mathbb{T}^2 = \{(\ell, \ell') : 0 \le \ell \le 2\pi,\ 0 \le \ell' \le 2\pi\}.$$

Here we are assuming that there are no mean motion resonances between the asteroid and the planet, otherwise the solutions of system (6.6) may not be representative of the behaviour of the corresponding components of the solutions of the complete system. We deal with mean motion resonances in Section 6.3.

If no orbit crossing occurs, by the theorem of differentiation under the integral sign, the averaged equations (6.6) are Hamilton equations, defined by the Hamiltonian

$$\overline{\mathcal{H}} = \frac{\varepsilon}{(2\pi)^2}\int_{\mathbb{T}^2}\mathcal{H}_1\;d\ell d\ell' = -\frac{\varepsilon}{(2\pi)^2}\int_{\mathbb{T}^2}\frac{1}{|\,\mathcal{X} - \mathcal{X}'\,|}\,d\ell d\ell'. \tag{6.7}$$

Note that the average in (6.7) of the indirect part of the perturbation vanishes. Note also that the averaged problem is integrable. Indeed, the component Z of the angular

momentum orthogonal to the orbital plane of the planet and the averaged Hamiltonian $\overline{\mathcal{H}}$ are first integral in involution and, generically, independent.

When the orbit of the asteroid crosses the one of the planet, a singularity appears in (6.6), corresponding to a collision for particular values of the mean anomalies (ℓ, ℓ'). A method to extend the solutions also in the case of crossing singularities is explained in the following section. Note that, since in the averaged system the semimajor axis a is constant, we expect that the generalized solutions of the averaged system represent the singular solution of the complete system only when there are no close approaches between the planet and the asteroid, because close encounters may change widely the value of a. However, when we take into account a large number of solutions of the complete system, with the same initial conditions for the slow variables (G, Z, g, z), the generalized solutions can still be reliable in a statistical sense, as long as the changes in semimajor axis are compensated by the large number of solutions taken into account. We will explain better this situation, showing numerical simulations in Chapter 7.

6.2 Averaging in presence of orbit crossings

Here we explain how to deal with the crossing singularity of the averaged problem. In particular, we will see that it is possible to continue an averaged solution beyond a crossing configuration [49, 45, 50]. The main fundamental tool to treat the singularity is the minimum orbit intersection distance (MOID) [46, 47, 63].

6.2.1 The minimum orbit intersection distance

Let $(E_j, v_j) \in \mathbb{R}^6$, $j = 1, 2$ be two sets of orbital elements of two confocal Keplerian orbits. The component $E_j \in \mathbb{R}^5$, $j = 1, 2$ describes the shape of the orbit, while $v_j \in S^1$, $j = 1, 2$ is a parameter along the orbit, i.e. an angle. We denote with $\mathcal{E} = (E_1, E_2) \in \mathbb{R}^{10}$ the couple of the orbit configurations and we set $V = (v_1, v_2) \in \mathbb{T}^2$. We choose a reference frame centered at the common focus and we denote with $\mathcal{X}_j(E_j, v_j)$, $j = 1, 2$ the Cartesian coordinates of the two bodies.

For a given configuration $\mathcal{E}$, we define the *Keplerian distance function* d as

$$d : \mathbb{T}^2 \to \mathbb{R}, \quad d(\mathcal{E}, V) = |\, \mathcal{X}_1 - \mathcal{X}_2 \,|.$$

Local minimum points of d can be found by computing all the critical points of the function d^2. Methods to do this are described for instance in [46, 47].

Let $V_h = V_h(\mathcal{E})$ be a local minimum point of the Keplerian distance function. We consider the maps

$$\mathcal{E} \mapsto d_h(\mathcal{E}) = d(\mathcal{E}, V_h), \quad \mathcal{E} \mapsto d_{\min}(\mathcal{E}) = \min_h d_h(\mathcal{E}, V_h).$$

Note that, fixed the configuration $\mathcal{E}$, $d_{\min}$ gives the minimum orbit distance. Moreover d_h and $d_{\min}$ are singular at crossing configurations, and their derivatives do not exist. We can deal with this singularity and obtain analytic maps in a neighbourhood of a

crossing configuration $\mathcal{E}_c$ by properly choose a sign of these maps. It is worth noting that d_h, $d_{\min}$ have also other type of singularities[1]. In fact d_h has bifurcations, since the number of local minimum points can change. Therefore the maps d_h and $d_{\min}$ are defined only locally.

We say that a configuration $\mathcal{E}$ is *non-degenerate* if all the critical points of the Keplerian distance function are non-degenerate. If $\mathcal{E}$ is non-degenerate, then there exists a neighbourhood $\mathcal{W} \subseteq \mathbb{R}^{10}$ of $\mathcal{E}$ such that the maps d_h, restricted to $\mathcal{W}$, do not have bifurcations. On the other hand, the map $d_{\min}$ can lose regularity when two local minima exchange their role as absolute minimum.

Here we summarize the procedure to deal with the crossing singularity of d_h, the procedure for $d_{\min}$ being the same. We consider the points on the two ellipses corresponding to the local minimum points $V_h = (v_1^{(h)}, v_2^{(h)})$ of d^2

$$\mathcal{X}_1^{(h)} = \mathcal{X}_1(E_1, v_1^{(h)}), \quad \mathcal{X}_2^{(h)} = \mathcal{X}_2(E_2, v_2^{(h)}).$$

We denote with $\tau_1^{(h)}, \tau_2^{(h)}$ the tangent vectors to the trajectories E_1, E_2 at these points, i.e.

$$\tau_1^{(h)} = \frac{\partial \mathcal{X}_1}{\partial v_1}(E_1, v_1^{(h)}), \quad \tau_2^{(h)} = \frac{\partial \mathcal{X}_2}{\partial v_2}(E_2, v_2^{(h)}),$$

and their cross product

$$\tau_3^{(h)} = \tau_1^{(h)} \times \tau_2^{(h)}.$$

We define also

$$\Delta = \mathcal{X}_1 - \mathcal{X}_2, \quad \Delta_h = \mathcal{X}_1^{(h)} - \mathcal{X}_2^{(h)}.$$

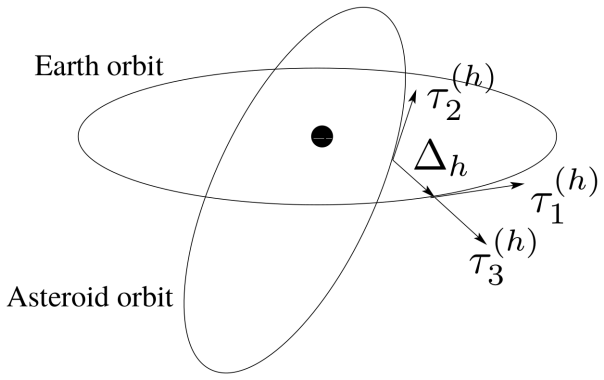

Figure 6.1: The vectors $\tau_1^{(h)}, \tau_2^{(h)}, \tau_3^{(h)}, \Delta_h$.

The vector Δ_h joins the points attaining a local minimum value of d^2, hence $|\Delta_h| = d_h$. From the definition of critical points of d^2, both vectors $\tau_1^{(h)}, \tau_2^{(h)}$ are orthogonal

[1] Actually, this can be done only when the crossing is not tangent, as we are going to see.

to Δ_h, therefore $\tau_3^{(h)}$ and Δ_h are parallel (see Figure 6.1 for a sketch). Denoting with $\hat{\tau}_3^{(h)}, \hat{\Delta}^{(h)}$ the corresponding unit vectors, the distance with sign

$$\tilde{d}_h = (\hat{\tau}_3^{(h)} \cdot \hat{\Delta}^{(h)}) d_h, \tag{6.8}$$

is an analytic function in a neighbourhood of a crossing configuration, provided that $\tau_1^{(h)}$ and $\tau_2^{(h)}$ are not parallel, situation happening only when the trajectories are tangent at the crossing point. A proof of this statement can be found in [50]. Note that to obtain regularity in a neighbourhood of a crossing configuration, we lose continuity at the configurations with $\tau_1^{(h)} \times \tau_2^{(h)} = 0$ and $d_h \neq 0$: this can happen for example when there are symmetries in the spatial configuration of the trajectories.

The derivatives of $\tilde{d}_h$ with respect to the component $\mathcal{E}_k$, $k = 1, \ldots, 10$ of $\mathcal{E}$ are given by

$$\frac{\partial \tilde{d}_h}{\partial \mathcal{E}_k} = \hat{\tau}_3^{(h)} \cdot \frac{\partial \Delta}{\partial \mathcal{E}_k}(\mathcal{E}, V_h). \tag{6.9}$$

We call (signed) orbit distance the map $\tilde{d}_{\min}$.

6.2.2 Extraction of the singularity

With the notations used in Section 6.1, in the restricted 3-body problem (6.1) the elements $\mathcal{E}$ are the Delaunay elements (L, G, Z, g, z) of the asteroid and the planet, and $V = (\ell, \ell')$ are the mean anomalies. Denote by $\mathcal{E}_c$ a non-degenerate crossing configuration with only one crossing point. We choose the index h such that $d_h(\mathcal{E}_c) = 0$. For each $\mathcal{E}$ in a neighborhood of $\mathcal{E}_c$ we consider the Taylor development of $V \mapsto d^2(\mathcal{E}, V) = |\mathcal{X} - \mathcal{X}'|^2$, in a neighborhood of the local minimum point $V_h = V_h(\mathcal{E})$

$$d^2(\mathcal{E}, V) = d_h^2(\mathcal{E}) + \frac{1}{2}(V - V_h) \cdot \mathcal{H}_h(\mathcal{E})(V - V_h) + \mathcal{R}_3^{(h)}(\mathcal{E}, V)\,, \tag{6.10}$$

where

$$\mathcal{H}_h(\mathcal{E}) = \frac{\partial^2 d^2}{\partial V^2}(\mathcal{E}, V_h(\mathcal{E})),$$

is the Hessian matrix of d^2 in $V_h = (\ell_h, \ell'_h)$, and

$$\mathcal{R}_3^{(h)}(\mathcal{E}, V) = \sum_{|\alpha|=3} r_\alpha^{(h)}(\mathcal{E}, V)(V - V_h)^\alpha\,, \tag{6.11}$$

$$r_\alpha^{(h)}(\mathcal{E}, V) = \frac{3}{\alpha!} \int_0^1 (1-t)^2 D^\alpha d^2(\mathcal{E}, V_h + t(V - V_h))\, dt, \tag{6.12}$$

is the Taylor remainder in the integral form. We introduce the approximated distance

$$\delta_h = \sqrt{d_h^2 + (V - V_h) \cdot \mathcal{A}_h (V - V_h)}\,, \tag{6.13}$$

where

$$\mathcal{A}_h = \frac{1}{2}\mathcal{H}_h = \begin{bmatrix} |\tau_h|^2 + \dfrac{\partial^2 \mathcal{X}}{\partial \ell^2}(E, \ell_h) \cdot \Delta_h & -\tau_h \cdot \tau_h' \\ -\tau_h \cdot \tau_h' & |\tau_h'|^2 - \dfrac{\partial^2 \mathcal{X}'}{\partial \ell'^2}(E', \ell_h') \cdot \Delta_h \end{bmatrix},$$

and

$$\Delta_h = \Delta_h(\mathcal{E}), \quad \tau_h = \frac{\partial \mathcal{X}}{\partial \ell}(E, \ell_h), \quad \tau_h' = \frac{\partial \mathcal{X}'}{\partial \ell'}(E', \ell_h') .$$

Note that, if the matrix $\mathcal{A}_h$ is non-degenerate, then it is positive definite since V_h is a minimum point, and this property holds in a suitably chosen neighbourhood $\mathcal{W}$ of $\mathcal{E}_c$. The matrix $\mathcal{A}_h$ is degenerate at the crossing configuration if and only if the tangent vectors τ_h, τ_h' are parallel: in this situation we have seen that we can not even define the signed orbit distance. Therefore, in the following we always assume that the crossing is not tangent.

To extract the singularity at an orbit crossing, we split the integral as

$$\int_{\mathbb{T}^2} \frac{1}{d}\, d\ell d\ell' = \int_{\mathbb{T}^2} \left(\frac{1}{d} - \frac{1}{\delta_h}\right) d\ell d\ell' + \int_{\mathbb{T}^2} \frac{1}{\delta_h} d\ell d\ell'. \tag{6.14}$$

We refer to

$$\frac{1}{d} - \frac{1}{\delta_h},$$

as *reminder function*: first we investigate the behaviour of this term of the splitting. Let us set

$$\Sigma = \{\mathcal{E} \in \mathcal{W} : \, d_h(\mathcal{E}) = 0\}. \tag{6.15}$$

From [50], we have a bound on the reminder function, i.e. there exists a positive C such that

$$\left|\frac{1}{d} - \frac{1}{\delta_h}\right| \leq C, \quad \forall (\mathcal{E}, V) \in (\mathcal{W} \times \mathbb{T}^2) \setminus \mathcal{U}_\Sigma,$$

where

$$\mathcal{U}_\Sigma = \{(\mathcal{E}, V_h(\mathcal{E})) : \mathcal{E} \in \Sigma\},$$

therefore this function is integrable. Moreover, we also have a bound on the derivatives. In fact, there exists a positive constant C' such that, if we denote with y_k one of the Delaunay elements, we have

$$\left|\frac{\partial}{\partial y_k}\left(\frac{1}{d} - \frac{1}{\delta_h}\right)\right| \leq \frac{C'}{d_h + |V - V_h|}, \quad \forall (\mathcal{E}, V) \in (\mathcal{W} \times \mathbb{T}^2) \setminus \mathcal{U}_\Sigma.$$

Hence the derivatives are integrable and it follows that the map

$$\mathcal{W} \setminus \Sigma \ni \mathcal{E} \mapsto \int_{\mathbb{T}^2} \frac{\partial}{\partial y_k}\left(\frac{1}{d} - \frac{1}{\delta_h}\right) d\ell d\ell', \tag{6.16}$$

can be extended continuously to the whole set $\mathcal{W}$. To compute the derivatives in (6.16) we can use

$$\frac{\partial}{\partial y_k}\left(\frac{1}{\delta_h}\right) = -\frac{1}{2\delta_h^3}\frac{\partial \delta_h^2}{\partial y_k}.$$

From (6.10) we obtain the derivatives of the approximated distance as

$$\frac{\partial \delta_h^2}{\partial y_k} = \frac{\partial d_h^2}{\partial y_k} - 2\frac{\partial V_h}{\partial y_k}\cdot \mathcal{A}_h(V - V_h) + (V - V_h)\cdot \frac{\partial \mathcal{A}_h}{\partial y_k}(V - V_h). \tag{6.17}$$

The derivatives of V_h are computed differentiating the relation

$$\frac{\partial}{\partial y_k} d_h^2(\mathcal{E}, V_h(\mathcal{E})) = 0,$$

which holds since $(\mathcal{E}, V_h(\mathcal{E}))$ is a stationary point of d^2. Hence

$$\frac{\partial V_h}{\partial y_k}(\mathcal{E}) = -[\mathcal{H}_h(\mathcal{E})]^{-1}\frac{\partial}{\partial y_k}\nabla_V d^2(\mathcal{E}, V_h(\mathcal{E})). \tag{6.18}$$

On the other hand, the average over $\mathbb{T}^2$ of the derivatives of $1/\delta_h$ are non-convergent integrals for $\mathcal{E} \in \Sigma$: for this reason the averaged vector field is not defined at orbit crossings, and this term is the source of the singularity: let us discuss better its behaviour.

6.2.3 Integration of $1/\delta_h$ and its derivatives

Let $(\mathcal{E}_c, V_h(\mathcal{E}_c))$ be the crossing configuration and consider the translation

$$\mathcal{T}_h : \mathbb{R}^2 \to \mathbb{R}^2, \qquad V \mapsto \mathcal{T}_h(V) = V + V_h.$$

We consider also the linear map given by the matrix

$$\mathcal{L}_h = \sqrt{\mathcal{A}_h},$$

defined as the unique positive definite matrix such that

$$\mathcal{L}_h^2 = \mathcal{A}_h. \tag{6.19}$$

Using these transformations to change the coordinates in the integral, we get that

$$\int_{\mathbb{T}^2} \frac{1}{\delta_h} d\ell d\ell' = \int_{\mathcal{T}_h(\mathbb{T}^2)} \frac{1}{\delta_h} dV = \frac{1}{\det\sqrt{\mathcal{A}_h}} \int_{\mathcal{L}_h(\mathbb{T}^2)} \frac{1}{\sqrt{d_h^2 + |W|^2}} dW$$

where

$$W = \mathcal{L}_h \circ \mathcal{T}_h^{-1}(V) = \mathcal{L}_h(V - V_h).$$

Let us denote with

$$\mathcal{L}_h = \begin{bmatrix} a_{11} & a_{12} \\ a_{12} & a_{22} \end{bmatrix},$$

and compute the coefficients a_{ij} of this matrix as function of the coefficients A_{ij} of $\mathcal{A}_h$. From (6.19) we obtain the system

$$a_{11}^2 + a_{12}^2 = A_{11}, \tag{6.20}$$
$$a_{11}a_{12} + a_{12}a_{22} = A_{12}, \tag{6.21}$$
$$a_{12}^2 + a_{22}^2 = A_{22}. \tag{6.22}$$

Set

$$\alpha = \sqrt{\det \mathcal{A}_h}.$$

We search for the coefficients a_{ij} so that $\mathcal{L}_h$ is positive definite. From

$$\det \sqrt{\mathcal{A}_h} = \sqrt{\det \mathcal{A}_h}$$

we get

$$a_{12}^2 = a_{11}a_{22} - \alpha.$$

Inserting this relation in (6.20), (6.22) and summing we have

$$(a_{11} + a_{22})^2 - 2\alpha = A_{11} + A_{22}.$$

Since by assumption the trace of $\mathcal{L}_h$ is positive, we get

$$a_{11} + a_{22} = \sqrt{2\alpha + A_{11} + A_{22}}.$$

Inserting this relation in (6.21) we obtain

$$a_{12} = \frac{A_{12}}{\sqrt{2\alpha + A_{11} + A_{22}}}.$$

Then, from (6.20), (6.22), taking into account that $a_{11}, a_{22} > 0$, we get

$$a_{11} = \frac{\alpha + A_{11}}{\sqrt{2\alpha + A_{11} + A_{22}}}, \qquad a_{22} = \frac{\alpha + A_{22}}{\sqrt{2\alpha + A_{11} + A_{22}}}.$$

Let us consider the points

$$P_1 \equiv (\pi, \pi), \qquad P_2 \equiv (-\pi, \pi),$$
$$P_3 \equiv (-\pi, -\pi), \quad P_4 \equiv (\pi, -\pi),$$

and their images through the linear map $\mathcal{L}_h$

$$Q_j \equiv (x_j, y_j), \qquad j = 1, \ldots, 4,$$

so that

$$(x_1, y_1) = \pi(a_{11} + a_{12}, a_{12} + a_{22}), \qquad (x_2, y_2) = \pi(-a_{11} + a_{12}, -a_{12} + a_{22}),$$

$$(x_3, y_3) = -(x_1, y_1), \qquad (x_4, y_4) = -(x_2, y_2).$$

Set $P_5 = P_1$ and, for $j = 1, \dots, 4$, let $\mathscr{R}_j$ be the straight line passing through the points P_j, P_{j+1}, whose equation is

$$\xi_j(y - y_j) = \eta_j(x - x_j),$$

with

$$\xi_j = x_{j+1} - x_j, \qquad \eta_j = y_{j+1} - y_j.$$

Note that $(\xi_j, \eta_j) \neq (0, 0)$ unless $\det \mathcal{A}_h = 0$. Introducing polar coordinates (ρ, θ) such that

$$W = (\rho \cos\theta, \rho \sin\theta),$$

we can write these lines in polar form:

$$\mathscr{R}_j = \left\{ (r_j(\theta)\cos\theta, r_j(\theta)\sin(\theta)) : \theta \in (\bar\theta_j, \bar\theta_j + \pi) \right\}$$

with

$$r_j(\theta) = \frac{\xi_j y_j - \eta_j x_j}{\xi_j \sin\theta - \eta_j \cos\theta}$$

and

$$\bar\theta_j = \begin{cases} \arctan(\eta_j/\xi_j), & \xi_j \neq 0, \\ \pi/2, & \xi_j = 0. \end{cases}$$

Note that

$$(\xi_1, \eta_1) = -2\pi(a_{11}, a_{12}), \qquad (\xi_2, \eta_2) = -2\pi(a_{12}, a_{22}),$$
$$(\xi_3, \eta_3) = -(\xi_1, \eta_1), \qquad (\xi_4, \eta_4) = -(\xi_2, \eta_2),$$

so that, for each $j = 1, \dots, 4$,

$$\xi_j y_j - \eta_j x_j = -2\pi^2 \det \mathcal{L}_h$$

and

$$r_1(\theta) = \frac{\pi \det \mathcal{L}_h}{a_{11}\sin\theta - a_{12}\cos\theta}, \qquad r_2(\theta) = \frac{\pi \det \mathcal{L}_h}{a_{12}\sin\theta - a_{22}\cos\theta},$$
$$r_3(\theta) = -r_1(\theta), \qquad r_4(\theta) = -r_2(\theta).$$

Now, taking into account these changes of coordinates, we have

$$\int_{\mathcal{T}_h(\mathbb{T}^2)} \frac{1}{\delta_h} d\ell d\ell' = \frac{1}{\sqrt{\det \mathcal{A}_h}} \left(\sum_{j=1}^{4} \int_{\theta_j}^{\theta_{j+1}} \sqrt{d_h^2 + r_j^2(\theta)}\, d\theta - 2\pi d_h \right) \tag{6.23}$$

with

$$\cos\theta_j = \frac{x_j}{\sqrt{x_j^2 + y_j^2}}, \qquad \sin\theta_j = \frac{y_j}{\sqrt{x_j^2 + y_j^2}},$$

and

$$\theta_1 < \theta_2 < \theta_3 < \theta_4 < \theta_5 = 2\pi + \theta_1.$$

Note that the integrals in (6.23) are bounded, hence they are differentiable functions of the Delaunay elements. Instead, the term $-2\pi d_h/\sqrt{\det \mathcal{A}_h}$ is not differentiable at $\mathcal{E} = \mathcal{E}_c \in \Sigma$, and the loss of regularity is due only to this term.

Exchanging again the integral sign and the derivative in the terms of the sum in (6.23), we can compute the derivatives as

$$\begin{aligned}\frac{\partial}{\partial y_k}\int_{\mathbb{T}^2}\frac{1}{\delta_h}d\ell d\ell' = \Big(\frac{\partial}{\partial y_k}\frac{1}{\sqrt{\det \mathcal{A}_h}}\Big)\Big(\sum_{j=1}^4\int_{\theta_j}^{\theta_{j+1}}\sqrt{d_h^2+r_j^2(\theta)}d\theta - 2\pi d_h\Big)\\ + \frac{1}{\sqrt{\det \mathcal{A}_h}}\Big(\sum_{j=1}^4\int_{\theta_j}^{\theta_{j+1}}\frac{d_h\frac{\partial d_h}{\partial y_k}+r_j(\theta)\frac{\partial r_j}{\partial y_k}(\theta)}{\sqrt{d_h^2+r_j^2(\theta)}}d\theta - 2\pi\frac{\partial d_h}{\partial y_k}\Big),\end{aligned} \tag{6.24}$$

where y_k is one of the Delaunay elements. Note that the above derivatives should contain also the term given by the differentiation of the extrema of the integrals

$$\frac{1}{\sqrt{\det \mathcal{A}_h}}\sum_{j=1}^4\Big(\sqrt{d_h^2+r_j^2(\theta_{j+1})}\frac{\partial\theta_{j+1}}{\partial y_k} - \sqrt{d_h^2+r_j^2(\theta_j)}\frac{\partial\theta_j}{\partial y_k}\Big).$$

However, this term vanishes because

$$r_2(\theta_2) = r_1(\theta_2), \quad r_3(\theta_3) = r_2(\theta_3), \quad r_4(\theta_4) = r_3(\theta_4), \quad r_1(\theta_1) = r_4(\theta_5),$$

and

$$\frac{\partial\theta_5}{\partial y_k} = \frac{\partial\theta_1}{\partial y_k}.$$

Moreover, in (6.24) we have that

$$\begin{aligned}\frac{\partial r_1}{\partial y_k}(\theta) &= \frac{1}{(a_{11}\sin\theta - a_{12}\cos\theta)}\Big[\pi\Big(\frac{\partial}{\partial y_k}\det\mathcal{L}_h\Big) - r_1(\theta)\Big(\frac{\partial a_{11}}{\partial y_k}\sin\theta - \frac{\partial a_{12}}{\partial y_k}\cos\theta\Big)\Big],\\ \frac{\partial r_2}{\partial y_k}(\theta) &= \frac{1}{(a_{12}\sin\theta - a_{22}\cos\theta)}\Big[\pi\Big(\frac{\partial}{\partial y_k}\det\mathcal{L}_h\Big) - r_2(\theta)\Big(\frac{\partial a_{12}}{\partial y_k}\sin\theta - \frac{\partial a_{22}}{\partial y_k}\cos\theta\Big)\Big].\end{aligned}$$

As said before, the term $-2\pi d_h/\sqrt{\det \mathcal{A}_h}$ is not differentiable at the orbit crossing. However, the derivatives admit two analytic extensions to the whole $\mathcal{W}$ from both sides of the singular set Σ, see [50]. More specifically, we set

$$\mathcal{W}^+ = \mathcal{W}\cap\{\tilde{d}_h > 0\}, \quad \mathcal{W}^- = \mathcal{W}\cap\{\tilde{d}_h < 0\},$$

where $\tilde{d}_h$ is the signed distance given by (6.8). Then we have that the maps

$$\mathcal{W}^+ \ni \mathcal{E} \mapsto \frac{\partial}{\partial y_k}\int_{\mathbb{T}^2}\frac{1}{\delta_h}d\ell d\ell', \quad \mathcal{W}^- \ni \mathcal{E} \mapsto \frac{\partial}{\partial y_k}\int_{\mathbb{T}^2}\frac{1}{\delta_h}d\ell d\ell',$$

can be extended to two different analytic maps defined on $\mathcal{W}$.

When we gather together the terms of the split (6.14), we obtain that the derivatives of $\overline{\mathcal{H}}_1$ with respect to the Delaunay elements can be extended to two Lipschitz-continuous

maps $(\overline{\frac{\partial \mathcal{H}_1}{\partial y_k}})^{\pm}_h$ on a neighbourhood $\mathcal{W}$ of the crossing configuration $\mathcal{E}_c$. These maps, restricted to $\mathcal{W}^+, \mathcal{W}^-$ respectively, correspond to $\overline{\frac{\partial \mathcal{H}_1}{\partial y_k}}$. Moreover, the jump in the derivatives, passing from $\mathcal{W}^+$ to $\mathcal{W}^-$, is given by

$$\begin{aligned} \mathrm{Diff}_h\Big(\overline{\frac{\partial \mathcal{H}_1}{\partial y_k}}\Big) &:= \Big(\overline{\frac{\partial \mathcal{H}_1}{\partial y_k}}\Big)^-_h - \Big(\overline{\frac{\partial \mathcal{H}_1}{\partial y_k}}\Big)^+_h \\ &= \frac{1}{\pi}\Big[\frac{\partial}{\partial y_k}\Big(\frac{1}{\sqrt{\det \mathcal{A}_h}}\Big)\tilde{d}_h + \frac{1}{\sqrt{\det \mathcal{A}_h}}\frac{\partial \tilde{d}_h}{\partial y_k}\Big]. \end{aligned} \tag{6.25}$$

6.2.4 Generalized solutions

Generically, we can uniquely extend the solutions beyond the crossing singularity $d_{\min} = 0$. This is obtained by patching together classical solutions defined on the domain $\mathcal{W}^+$ with solutions defined on $\mathcal{W}^-$ or vice versa. Here we describe how to extend a solution of the averaged equations beyond the crossing singularity.

Let $a > 0$ be the value of the semimajor axis of the asteroid and $\overline{Y} : I \to \mathbb{R}^4$ be a continuous function defined in an open interval $I \subseteq \mathbb{R}$, representing a possible evolution of the Delaunay elements $Y = (G, Z, g, z)$ of the asteroid. Then we set

$$\overline{\mathcal{E}}(t) = (\overline{E}(t), \overline{E}') \in \mathbb{R}^{10},$$

where $\overline{E}' \in \mathbb{R}^5$ are the elements representing the shape and the orientation of the orbit of the planet and

$$\overline{E}(t) = (k\sqrt{a}, \overline{Y}(t)) \in \mathbb{R}^5,$$

are the elements for the asteroid, depending on the time. Let $T(\overline{Y})$ be the set of times $t_c \in I$ such that $d_{\min}(\overline{\mathcal{E}}(t_c)) = 0$, and assume also that each t_c is isolated. Hence

$$I \setminus T(\overline{Y}) = \cup_{j\in\mathcal{N}} I_j,$$

is a disjoint union of open intervals I_j, with $\mathcal{N}$ a countable set. We say that $\overline{Y}$ is a *generalized solution* if its restriction to each I_j, $j \in \mathcal{N}$ is a classical solution of the averaged equations (6.6) and, for each $t_c \in T(\overline{Y})$, there exist the limits

$$\lim_{t\to t_c^+} \dot{\overline{Y}}(t), \qquad \lim_{t\to t_c^-} \dot{\overline{Y}}(t),$$

and they are finite.

Let $Y_0 \in \mathbb{R}^4$ be such that $d_{\min}(\mathcal{E}_0) > 0$, with

$$\mathcal{E}_0 = (E_0, E'), \quad E_0 = (k\sqrt{a}, Y_0).$$

Given a time $t_0 \in \mathbb{R}$, we show how to construct a generalized solution of the Cauchy problem

$$\begin{cases} \dot{\overline{Y}} = \varepsilon \mathbb{J}_2 \overline{\nabla \mathcal{H}_1}, \\ \overline{Y}(t_0) = Y_0, \end{cases} \tag{6.26}$$

where $\mathbb{J}_2 \in \mathbb{R}^{4\times 4}$ is the symplectic identity. Let $\overline{Y}(t)$ be the maximal classical solution of (6.26), defined on the interval $J \subseteq \mathbb{R}$. Assume that

$$t_c = \sup J < +\infty,$$

and

$$\lim_{t\to t_c^-} \overline{\mathcal{E}}(t) = \mathcal{E}_c,$$

with $\mathcal{E}_c$ a non-degenerate crossing configuration, such that $d_{\min}(\mathcal{E}_c) = d_h(\mathcal{E}_c) = 0$ for some h. Let $\mathcal{W}, \mathcal{W}^{\pm}$ be the neighbourhoods of $\mathcal{E}_c$ as defined above and suppose that there exists $\tau \in (t_0, t_c)$ such that $\overline{\mathcal{E}}(t) \in \mathcal{W}^+$ for $t \in (\tau, t_c)$. Let $Y_\tau = \overline{Y}(\tau)$, hence there exists $\dot{Y}_c \in \mathbb{R}^4$ such that

$$\lim_{t\to t_c^-} \dot{\overline{Y}}(t) = \dot{Y}_c. \tag{6.27}$$

In fact (6.27) is fulfilled by the solution of the Cauchy problem

$$\begin{cases} \dot{\overline{Y}} = \varepsilon \mathbb{J}_2 (\overline{\nabla \mathcal{H}_1})_h^+, \\ \overline{Y}(\tau) = Y_\tau, \end{cases} \tag{6.28}$$

and this solution is defined at the crossing time t_c. Then let Y_c be its value at $t = t_c$. We can extend $\overline{Y}(t)$ beyond the crossing singularity by considering the new problem

$$\begin{cases} \dot{\overline{Y}} = \varepsilon \mathbb{J}_2 (\overline{\nabla \mathcal{H}_1})_h^-, \\ \overline{Y}(t_c) = Y_c. \end{cases} \tag{6.29}$$

The solution of (6.29) satisfies

$$\lim_{t\to t_c^+} \dot{\overline{Y}}(t) = \dot{Y}_c + \varepsilon \mathrm{Diff}_h(\overline{\nabla \mathcal{H}_1})(\overline{\mathcal{E}}(t_c)). \tag{6.30}$$

The vector field in (6.29) corresponds to $\varepsilon \overline{\nabla \mathcal{H}_1}$ on $\mathcal{W}^-$, hence we can continue the solution outside $\mathcal{W}$ and this procedure can be repeated at almost every crossing singularities. Indeed, the generalized solution is unique provided that the evolution of $t \mapsto \overline{\mathcal{E}}(t)$ is not tangent to the orbit crossing set Σ. Moreover, recall that if $\det \mathcal{A}_h = 0$, the extraction of the singularity cannot be performed.

Note that, in the case $\overline{\mathcal{E}}(t) \in \mathcal{W}^-$ for $t \in (\tau, t_c)$ the previous discussion still holds if we exchange $(\overline{\nabla \mathcal{H}_{1h}})^+$ with $(\overline{\nabla \mathcal{H}_{1h}})^-$. In this case (6.30) becomes

$$\lim_{t\to t_c^+} \dot{\overline{Y}}(t) = \dot{Y}_c - \varepsilon \mathrm{Diff}_h(\overline{\nabla \mathcal{H}_1})(\overline{\mathcal{E}}(t_c)).$$

6.2.5 Numerical implementation

We describe here the algorithm used to compute the solutions of the averaged equations and extend them towards the crossing singularity. To perform the integration we

use the Runge-Kutta-Gauss scheme, which is an implicit Runge-Kutta method. More specifically, let

$$\dot{x} = f(x,t), \quad x \in \mathbb{R}^n,$$

be a first order differential equation, where $f : \mathbb{R}^n \times \mathbb{R} \to \mathbb{R}^n$ is the vector field. Given a time step $h \in \mathbb{R}$ and $x_m \in \mathbb{R}^n$ an approximation of the solution at time t_m, the approximated solution x_{m+1} at time $t_m + h$ is defined by

$$\begin{cases} x_{m+1} &= x_m + h\sum_{i=1}^{s} b_i k_i, \\ k_i &= f\Big(x_m + h\sum_{j=1}^{s} a_{ij}k_j,\, t_m + hc_i\Big), \quad i = 1,\dots,s. \end{cases} \tag{6.31}$$

Here s is an integer number, $A = (a_{ij}) \in \mathbb{R}^{s\times s}$ is a matrix and $b = (b_1,\dots,b_s)^T, c = (c_1,\dots,c_s)^T \in \mathbb{R}^s$ are vectors such that

$$\sum_{j=1}^{s} a_{ij} = c_i, \quad i = 1,\dots,s, \qquad \sum_{j=1}^{s} b_i = 1. \tag{6.32}$$

The scheme (6.31) is a generic Runge-Kutta method with s stages. Note that, in computing the solution x_{m+1}, the vector field is evaluated in intermediate points between x_m and x_{m+1}. In a Runge-Kutta-Gauss method, which has maximal order $2s$, the matrix A is a full matrix, hence equation (6.31) defines x_{m+1} implicitly and it has to be solved with iterative methods (e.g. using a fixed point method). Coefficients of the Runge-Kutta-Gauss methods can be found in classical books on numerical analysis, such as [6, 67]. Moreover, the Runge-Kutta-Gauss method is very suitable to integrate Hamiltonian systems over long time spans, since it is a symplectic method and it nearly conserves the value of the energy.

During the integration we use an adaptive time step. Away from the orbit crossing, we use a larger step. Instead, when approaching the orbit crossing, the time step is decreased, in order to reach exactly the crossing condition. To compute the solution beyond the singularity, we use the formula (6.25) that gives the difference between the two different extensions of the vector field. We compute the intermediate values of the extended vector field just after the crossing, then we correct these values by (6.25) and use them as approximations of the averaged vector field at the intermediate points of the solutions, see Figure 6.2. Moreover, when we are close to the crossing, the vector field is computed using the extraction of the singularity explained in Subsection 6.2.2, with the splitting (6.14). After the crossing, the time step is reset to its original maximal value.

6.3 Mean motion resonances

Here we assume that there is resonance between the mean motions of the planet and the asteroid, that is there exists $(\mathtt{h}, \mathtt{h}') \in \mathbb{Z}^2$ such that

$$\mathtt{h}n + \mathtt{h}'n' \simeq 0, \tag{6.33}$$

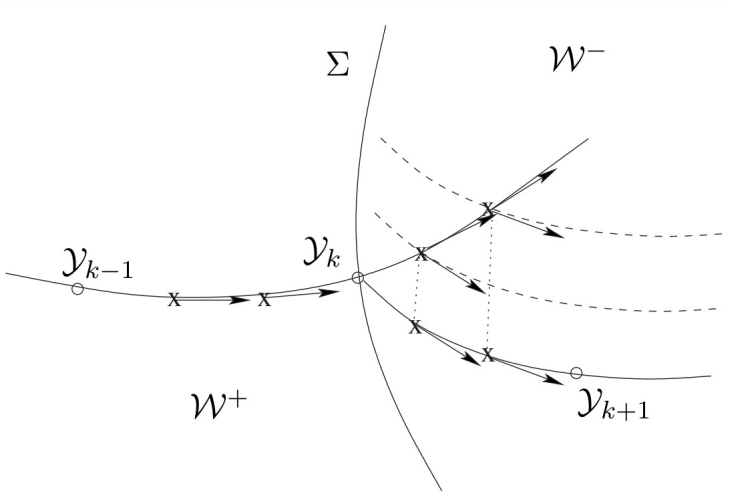

Figure 6.2: The Runge-Kutta-Gauss method and continuation of the solution beyond the singularity

where n, n' are the mean motions of the asteroid and the planet respectively. Note that, since $\dot{\ell} = n$, $\dot{\ell}' = n'$, from (6.33) we get that the *resonant angle*

$$\sigma := \mathtt{h}\ell + \mathtt{h}'\ell', \tag{6.34}$$

is almost constant and may change significantly only over a secular timescale. In this case, σ has to be included in the secular equations. When a mean motion resonance is involved in the dynamics, the averaged problem of Section 6.1 does not represent well the secular dynamics of the asteroid. However, it is still possible to define a system with a long term dynamics that takes into account these effects, using a resonant normal form [81, 66]. In the following we also assume that there are no close approaches between the planet and the asteroid.

6.3.1 Resonance detection

A method to determine whether an asteroid is in mean motion resonance with the planet or not is the following:

(i) first we use the third Kepler's law in a 2-body approximation to check whether the initial mean motions of the planet and the asteroid are commensurable;

(ii) perform a numerical integration and check the behaviour of the critical angle.

Indeed, in a 2-body approximation where we neglect the influence of the planet, the mean motion n of the asteroid is

$$n = \sqrt{\frac{Gm_\odot}{a^3}}, \tag{6.35}$$

which simply becomes

$$n = a^{-3/2},$$

with the units defined in Section 6.1. Inserting this in (6.33) and taking into account that $n' = 1$, we obtain the condition

$$a^{-3/2} = -\frac{\mathtt{h}}{\mathtt{h}'}.$$

Hence, if the initial value a of the semimajor axis is such that $a^{-3/2}$ is close to be a rational number, it is likely that the asteroid is in mean motion resonance with the planet. At this point, to check the resonance condition, we integrate the full circular restricted 3-body problem for a timespan comparable to several orbital periods of the planet, and analyze the behaviour of the resonant angle σ defined by (6.34). If σ librates, it means that a mean motion resonance is involved in the dynamics. As an example, in Figure 6.3 we show the time evolution of the critical angle $\sigma = 5\ell - 2\ell'$ relative to the asteroid 1999 JB_{11}. Here the planet involved is the Earth, and the integration is performed over 3000 years: we can clearly see the libration of σ, with a period of approximately 1000 years. We conclude that the asteroid is in the $2:5$ mean motion resonance with the Earth. This result was obtained in [41]. Note also that the semimajor axis oscillates with a similar period.

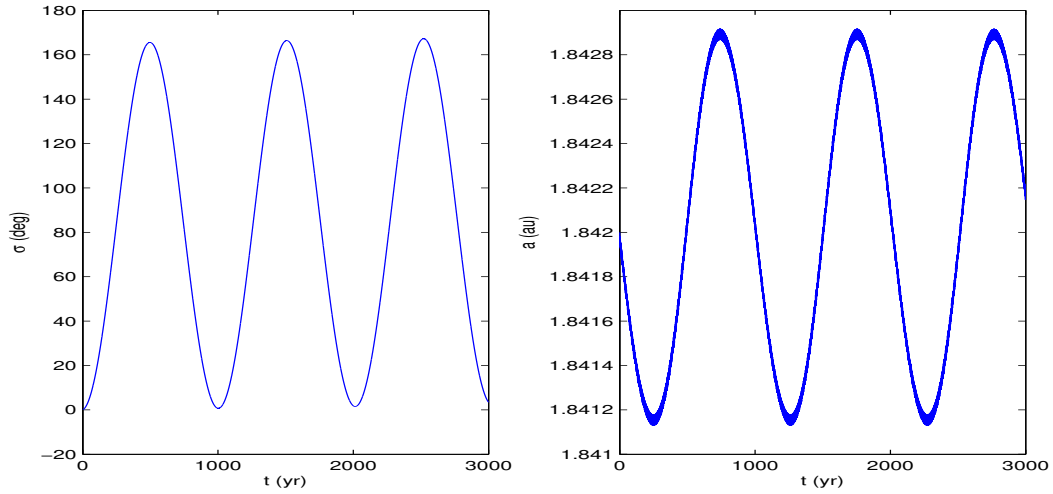

Figure 6.3: Time evolution of the critical angle $\sigma = 5\ell - 2\ell'$ (left) and the semimajor axis (right) of the asteroid 1999 JB_{11}.

Another possibility to identify a mean motion resonance, similar to the approach of [100], is to fix a maximal order $\mathtt{K} \in \mathbb{N}$, perform a numerical integration of the full circular restricted 3-body problem for a total time of several orbital periods of the planet and consider the set of all integer combinations of the fast variables (ℓ, ℓ'), up to order $\mathtt{K}$. More specifically, we consider all the combinations

$$\sigma_{(\mathtt{h},\mathtt{h}')} = \mathtt{h}\ell + \mathtt{h}'\ell', \quad \mathtt{h}, \mathtt{h}' \in \mathbb{Z},$$

for which $|\mathtt{h}| + |\mathtt{h}'| \leq \mathtt{K}$ and $\mathtt{h}, \mathtt{h}'$ are relatively prime. Then, we check whether the angle $\sigma_{(\mathtt{h},\mathtt{h}')}$ librates or not. Once we have identified the couples $(\mathtt{h}, \mathtt{h}')$ for which $\sigma_{(\mathtt{h},\mathtt{h}')}$ librates, we can determine the center and the amplitude of the oscillation, in order to detect the strongest resonance involved. Moreover, the time evolution of the semimajor axis is related to the libration of the critical angle. Indeed it is known that, in presence of a resonance, the semimajor axis oscillates with the same period of oscillation of the critical angle, see [84]. This also explains the plot of Figure 6.3.

It is worth saying that, when we consider more than one planet in the system, the identification of resonances becomes more challenging. The detection of 2-body resonances can be done in the same way, with the only difference that we do not know the planet involved. Moreover also 3-body mean motion resonances, involving the asteroid and two planets, can be relevant in the dynamics. Analytical methods to detect 3-body mean motion resonances were developed in [83], and the same authors applied their method to main belt asteroids [84]. A total of 255 objects in 3-body mean motion resonances with Jupiter and Saturn were found. In [42] a semi-analytical method to estimate the strength of the 3-body resonances was developed, producing an atlas of the strongest ones in the Solar System. Another numerical technique was developed in [99], where the authors found 65972 main belt asteroids in a 3-body mean motion resonance with two planets of the Solar System.

6.3.2 The resonant normal form

We describe now how to obtain the *resonant normal form*, as done in [81, 66]. Let $(\mathtt{h}, \mathtt{h}') \in \mathbb{Z}^2$ be the vector satisfying relation (6.33). The orbit of the planet is fixed and its mean anomaly ℓ' grows linearly with time with constant rate n', hence

$$\ell' = n't + \ell'(0).$$

We extend the phase space, introducing a variable L' conjugated to ℓ'. The Hamiltonian in the extended phase space is given by

$$\mathcal{H} = \mathcal{H}_0 + \varepsilon \mathcal{H}_1, \qquad \mathcal{H}_0 = -\frac{\kappa^4}{2L^2} + n'L', \tag{6.36}$$

and $\mathcal{H}_1$ is given by (6.5). It is worth noting that the variable L' is not related[2] to the semimajor axis a' of the planet, since we have assumed that a' has a constant value, but it gives the changing rate of ℓ'. Therefore, the perturbing function $\mathcal{H}_1$ depends on $(L, G, Z, \ell, g, z, \ell')$, but not on L'.

Let us denote with $\varphi \in \mathbb{T}^2$ the fast angles, i.e. $\varphi = (\ell, \ell')$ and let $I \in \mathbb{R}^6$ be the remaining variables, i.e. $I = (L', L, G, Z, g, z)$. We use the Lie series to search for a suitable canonical transformation, close to the identity, that pushes the non-resonant terms to the order ε^2. We search for a function $\chi = \chi(I', \varphi')$ such that the inverse transformation is

$$\phi^{\varepsilon}_{\chi}(I', \varphi') = (I, \varphi),$$

[2] That is, we are not using the relation $L' = \kappa\sqrt{a'}$.

where ϕ_χ^t is the Hamiltonian flow associated to χ. Using a formal expansion in ε we have

$$\begin{aligned}\mathcal{H}' &= \mathcal{H}\circ\phi_\chi^\varepsilon \\ &= \mathcal{H} + \varepsilon\{\mathcal{H},\chi\} + O(\varepsilon^2) \\ &= \mathcal{H}_0 + \varepsilon(\,\mathcal{H}_1 + \{\mathcal{H}_0,\chi\}) + O(\varepsilon^2).\end{aligned} \tag{6.37}$$

In the resonant case, we search for a solution χ of the equation

$$\mathcal{H}_1 + \{\mathcal{H}_0,\chi\} = f, \tag{6.38}$$

where $f = f(I', \mathtt{h}\ell + \mathtt{h}'\ell')$. We suppose that there are no orbit crossings with the planet. We can write the perturbing function $\mathcal{H}_1$ as a Fourier series of the fast angles, hence

$$\mathcal{H}_1 = \sum_{(k,k')\in\mathbb{Z}^2} \hat{\mathcal{H}}_{(k,k')} e^{i(k\ell+k'\ell')},$$

where

$$\hat{\mathcal{H}}_{(k,k')} = \frac{1}{(2\pi)^2}\int_{\mathbb{T}^2} \mathcal{H}_1\, e^{-i(k\ell+k'\ell)} d\ell d\ell', \tag{6.39}$$

are the Fourier coefficients. We also write χ as a Fourier series, hence

$$\chi = \sum_{(k,k')\in\mathbb{Z}^2} \hat{\chi}_{(k,k')} e^{i(k\ell+k'\ell')}. \tag{6.40}$$

Inserting these series in the left hand side of (6.38) we obtain

$$\begin{aligned}\mathcal{H}_1 + \{\mathcal{H}_0,\chi\} &= \mathcal{H}_1 - \frac{\partial\,\mathcal{H}_0}{\partial I}\cdot\frac{\partial\chi}{\partial\varphi} \\ &= \sum_{(k,k')\in\mathbb{Z}^2}\Big(\hat{\mathcal{H}}_{(k,k')} - i(kn+k'n')\hat{\chi}_{(k,k')}\Big)e^{i(h\ell+h'\ell')}.\end{aligned} \tag{6.41}$$

Hence we choose

$$\chi_{(k,k')} = \frac{\hat{\mathcal{H}}_{k,k'}}{i(kn+k'n')}, \tag{6.42}$$

when the denominator does not vanish, and zero otherwise: in this manner we eliminate as many terms as possible from equation (6.41). Therefore, the term with $(k,k') = (0,0)$ and the resonant terms with $(k,k') = m(\mathtt{h},\mathtt{h}')$, $m\in\mathbb{Z}\backslash\{0\}$ are excluded in the expression (6.40) of χ. With this choice, we have that

$$f = \hat{\mathcal{H}}_{(0,0)} + \sum_{m\in\mathbb{Z}\backslash\{0\}} \hat{\mathcal{H}}_{(m\mathtt{h},m\mathtt{h}')} e^{im(\mathtt{h}\ell+\mathtt{h}'\ell')}. \tag{6.43}$$

The function f contains only resonant terms and we rename it $\mathcal{H}_{\rm res}$. Thus the new Hamiltonian, which is obtained from (6.37), has the form

$$\mathcal{H}' = \mathcal{H}_0 + \varepsilon\,\mathcal{H}_{\rm res}, \tag{6.44}$$

and it is called *resonant normal form*.

To deal with the Fourier series expansion, since the coefficients decay exponentially, it is natural to truncate $\mathcal{H}_{\rm res}$ up to a certain order. This is also useful in numerical computations. To this end, we introduce the *resonant set*, which contains all the integer multiples of $(\mathtt{h},\mathtt{h}')$, that is

$$\mathcal{R} := \{(k,k') \in \mathbb{Z}^2 : \text{ there exists } m \in \mathbb{Z} : (k,k') = m(\mathtt{h},\mathtt{h}')\}. \tag{6.45}$$

Then the resonant normal form to order $N \in \mathbb{N}$ is given by

$$\mathcal{H}^{\rm N}_{\rm res} = \sum_{\substack{(k,k')\in\mathcal{R},\\ |k|+|k'|\le N}} \hat{\mathcal{H}}_{(k,k')} e^{i(k\ell+k'\ell')}, \tag{6.46}$$

where $\hat{\mathcal{H}}_{(k,k')}$ are defined in (6.39). We can also write (6.46) as

$$\mathcal{H}^{\rm N}_{\rm res} = \frac{1}{(2\pi)^2}\int_{\mathbb{T}^2} D_N\big((\mathtt{h}\bar\ell + \mathtt{h}'\bar\ell') - (\mathtt{h}\ell+\mathtt{h}'\ell')\big)\,\mathcal{H}_1\, d\bar\ell d\bar\ell', \tag{6.47}$$

where D_N is the *Dirichlet kernel*, defined by

$$D_N(x) = \sum_{|x|\le N} e^{inx} = \frac{\sin\big((N+1/2)x\big)}{\sin(x/2)}. \tag{6.48}$$

We introduce the resonant angle σ through the canonical transformation Ψ defined as

$$\begin{pmatrix}\sigma\\ \sigma'\end{pmatrix} = A\begin{pmatrix}\ell\\ \ell'\end{pmatrix}, \qquad \begin{pmatrix}S\\ S'\end{pmatrix} = A^{-T}\begin{pmatrix}L\\ L'\end{pmatrix}, \tag{6.49}$$

where

$$A = \begin{pmatrix}\mathtt{h} & \mathtt{h}'\\ 0 & 1/\mathtt{h}\end{pmatrix}, \qquad A^{-T} = \begin{pmatrix}1/\mathtt{h} & 0\\ -\mathtt{h}' & \mathtt{h}\end{pmatrix}. \tag{6.50}$$

Using the new canonical variables $\mathcal{Y} = (S,G,Z,\sigma,g,z)$, the terms $\mathcal{H}_0$ and $\mathcal{H}^{\rm N}_{\rm res}$ of the Hamiltonian become

$$\begin{aligned}\mathcal{H}_0 &= -\frac{\kappa^4}{2(\mathtt{h}S)^2} + n'\Big(\mathtt{h}'S + \frac{S'}{\mathtt{h}}\Big),\\ \mathcal{H}^{\rm N}_{\rm res} &= \frac{1}{(2\pi)^2}\int_{\mathbb{T}^2} D_N(\mathtt{h}\ell+\mathtt{h}'\ell'-\sigma)\,\mathcal{H}_1\, d\ell d\ell'.\end{aligned} \tag{6.51}$$

Note that, since $\mathcal{H}_0, \mathcal{H}^{\rm N}_{\rm res}$ do not depend on σ', the value of S' is constant. The equations of motion are given by

$$\begin{cases}\dot S = & -\varepsilon\dfrac{\partial\,\mathcal{H}^{\rm N}_{\rm res}}{\partial\sigma},\\ \dot G = & -\varepsilon\dfrac{\partial\,\mathcal{H}^{\rm N}_{\rm res}}{\partial g},\\ \dot Z = & -\varepsilon\dfrac{\partial\,\mathcal{H}^{\rm N}_{\rm res}}{\partial z},\end{cases} \qquad \begin{cases}\dot\sigma = & \dfrac{h\kappa^4}{(hS)^3} + n'\mathtt{h}' + \varepsilon\dfrac{\partial\,\mathcal{H}^{\rm N}_{\rm res}}{\partial S},\\ \dot g = & \varepsilon\dfrac{\partial\,\mathcal{H}^{\rm N}_{\rm res}}{\partial G},\\ \dot z = & \varepsilon\dfrac{\partial\,\mathcal{H}^{\rm N}_{\rm res}}{\partial Z}.\end{cases} \tag{6.52}$$

As we have seen in Section 6.1 for the non-resonant case, also the truncated resonant normal form $\mathcal{H}^{\mathrm{N}}_{\mathrm{res}}$ is singular at orbit crossings. The extraction of the singularity can be performed in a similar way, still using the MOID, see [66]. It turns out that the vector field has two different Lipschitz-continuous extensions $(\frac{\partial \mathcal{H}^{\mathrm{N}}_{\mathrm{res}}}{\partial y_i})^{\pm}_h$ in a neighbourhood of each non-degenerate crossing configuration $\mathcal{E}_c$. Moreover, in this neighbourhood, the difference between the two extensions is

$$\begin{aligned}\mathrm{Diff}\left(\frac{\partial \mathcal{H}^{\mathrm{N}}_{\mathrm{res}}}{\partial y_i}\right)_h &:= \varepsilon\left[\left(\frac{\partial \mathcal{H}^{\mathrm{N}}_{\mathrm{res}}}{\partial y_i}\right)^{-}_h - \left(\frac{\partial \mathcal{H}^{\mathrm{N}}_{\mathrm{res}}}{\partial y_i}\right)^{+}_h\right] \\ &= -\frac{\varepsilon}{\pi} D_N\big(\sigma - (\mathtt{h}\ell_h + \mathtt{h}'\ell'_h)\big)\left[\frac{\partial}{\partial y_i}\left(\frac{1}{\sqrt{\det \mathcal{A}_h}}\right)\tilde{d}_h + \frac{1}{\sqrt{\det \mathcal{A}_h}}\frac{\partial \tilde{d}_h}{\partial y_i}\right].\end{aligned} \tag{6.53}$$

It is worth noting that the component $\frac{\partial \mathcal{H}^{\mathrm{N}}_{\mathrm{res}}}{\partial \sigma}$ is always regular, since σ appears only in the Dirichlet kernel, and not in the perturbing function $\mathcal{H}_1$.

As a final remark, we point out that, setting $\sigma_c = \mathtt{h}\ell_h - \mathtt{h}'\ell'_h$, we have

$$\lim_{N\to\infty} D_N(\sigma - \sigma_c) = \delta_{\sigma_c},$$

that is, for $N \to \infty$, the Dirichlet kernel converges in the sense of distributions to the Dirac delta centered at σ_c.

6.3.3 Dynamical protection from collisions

When the orbit of the asteroid crosses the orbit of the planet, the resonance protects the asteroid from close encounters with the planet itself. This was already known before, see for instance [71], but it was obtained by using another perturbative approach. Indeed, we can choose to perform a canonical transformation that brings the couple of fast angles (ℓ, ℓ') in the couple (σ, τ), where σ is the slow critical angle and τ evolves much faster that σ.

More precisely, we define a canonical transformation $(\ell, \ell', L, L') \to (\sigma, \tau, S, T)$, which leaves the other variables unchanged, through the unimodular matrix

$$A = \begin{pmatrix} \mathtt{h} & \mathtt{h}' \\ \mathtt{a} & \mathtt{b} \end{pmatrix},$$

where $\mathtt{a}, \mathtt{b}$ are integer numbers such that $\mathtt{bh} - \mathtt{ah}' = 1$. Then, the canonical transformation Ψ is defined by

$$\begin{pmatrix} \sigma \\ \tau \end{pmatrix} = A \begin{pmatrix} \ell \\ \ell' \end{pmatrix}, \quad \begin{pmatrix} S \\ T \end{pmatrix} = A^{-T} \begin{pmatrix} L \\ L' \end{pmatrix}.$$

The average is done over the fast angle τ, and we get the Hamiltonian

$$\overline{\mathcal{K}}(\sigma, S, T; X) = \frac{1}{2\pi}\int_0^{2\pi} \mathcal{H}_1 \circ \Psi^{-1}(\sigma, \tau, S, T; X) d\tau, \tag{6.54}$$

where we denote with X the remaining variables.

With the notations above, we also have

$$\lim_{N\to\infty} \mathcal{H}^{\mathrm{N}}_{\mathrm{res}} = \mathcal{H}_{\mathrm{res}}\,.$$

We introduce the functions

$$\begin{aligned}\mathscr{K}^{\mathrm{N}}_{\mathrm{res}}(\sigma,S,T;X) &= \mathcal{H}^{\mathrm{N}}_{\mathrm{res}}\circ\Psi^{-1}(\sigma,\tau,S,T;X),\\ \mathscr{K}_{\mathrm{res}}(\sigma,S,T;X) &= \mathcal{H}_{\mathrm{res}}\circ\Psi^{-1}(\sigma,\tau,S,T;X).\end{aligned}$$

Moreover, $\overline{\mathcal{K}}$ can be defined as pointwise limit for $N\to\infty$ of the partial Fourier sum

$$\overline{\mathcal{K}}^{\mathrm{N}}(\sigma,S,T;X) = \frac{1}{2\pi}\int_0^{2\pi} D_N(\tilde\sigma-\sigma)\overline{\mathcal{K}}(\tilde\sigma,S,T;X)d\tilde\sigma.$$

Assume now that $\mathcal{E}_c$ is a non-degenerate crossing configuration, i.e. $d_h = 0$, and let $\sigma_c = \mathtt{h}\ell_h + \mathtt{h}'\ell'_h$, where (ℓ_h,ℓ'_h) are the values of the mean anomalies corresponding to the collision. Let us also denote with $Y = Y(\mathcal{E})$ the vector of the elements different from σ and let $Y_c(\mathcal{E}_c)$ be its value at the crossing configuration. It turns out (see [66]) that, at every non-crossing configuration, $\overline{\mathcal{K}}^{\mathrm{N}}$ coincides with $\mathscr{K}^{\mathrm{N}}_{\mathrm{res}}$ for every N and $\overline{\mathcal{K}}$ coincides with $\mathscr{K}_{\mathrm{res}}$. On the other hand, for $\mathcal{E} = \mathcal{E}_c$ we have

(i) $\mathscr{K}^{\mathrm{N}}_{\mathrm{res}}(\sigma;Y_c) = \overline{\mathcal{K}}^{\mathrm{N}}(\sigma;Y_c)$ for all $N\in\mathbb{N}$, for all σ,

(ii) $\mathscr{K}_{\mathrm{res}}(\sigma;Y_c) = \overline{\mathcal{K}}(\sigma;Y_c)$ for all $\sigma\neq\sigma_c$, and

(iii) $\lim_{\sigma\to\sigma_c}\mathscr{K}_{\mathrm{res}}(\sigma;Y_c) = \lim_{\sigma\to\sigma_c}\overline{\mathcal{K}}(\sigma;Y_c) = +\infty$.

Moreover, the derivatives with respect to any one of the elements y_j in Y of the truncated Hamiltonians $\overline{\mathcal{K}}^{\mathrm{N}}$ and $\mathscr{K}^{\mathrm{N}}_{\mathrm{res}}$ generically do not exists at a crossing configuration $\mathcal{E}_c$, while the derivatives of $\overline{\mathcal{K}}$ and $\mathscr{K}_{\mathrm{res}}$ exist and are continuous for $\sigma\neq\sigma_c$. However, the derivatives of these truncated Hamiltonians fulfill

$$\lim_{\mathcal{E}\to\mathcal{E}_c^{\pm}} \frac{\partial\mathscr{K}^{\mathrm{N}}_{\mathrm{res}}(\sigma;Y)}{\partial y_i} = \lim_{\mathcal{E}\to\mathcal{E}_c^{\pm}} \frac{\partial\overline{\mathcal{K}}^{\mathrm{N}}(\sigma;Y)}{\partial y_i},$$

and the difference between the two limits converges, in the sense of distributions for $N\to\infty$, to a Dirac delta. Therefore, averaging over a single fast variable produces a well defined vector field, provided that $\sigma\neq\sigma_c$. Moreover, the fact that at the crossing configuration $\mathcal{E}_c$ the single averaged Hamiltonian $\overline{\mathcal{K}}$ has a pole of order one at the collision configuration $\sigma=\sigma_c$, has a consequence on the dynamics. Indeed, the averaged solution cannot pass through this collision configuration in the resonant averaged model.

6.4 Integration of the full problem

The full circular restricted 3-body problem has to be integrated to make a comparison with the averaged system. Since we want to investigate the connection between these

two problems in a statistical sense, we have to perform numerical integrations of the full problem using several different initial conditions. Among them, it can happen that we choose an initial condition leading to a collision, or to a close encounter with the planet. For this reason, we have to properly integrate the problem near the collisions, in order to prevent as much as possible the effects of close encounters in the numerical propagation. To this end we use the Kustaanheimo-Stiefel regularization [39, 102, 56, 16, 101].

6.4.1 The problem in synodic coordinates

We take into account a Cartesian reference frame centered at the center of mass of the system Sun-Planet. The units of mass and distance are chosen so that

$$m_\odot + m_\oplus = 1, \quad |x_\odot - x_\oplus| = 1,$$

where $x_\odot$, $x_\oplus$ are the positions of the Sun and the planet, respectively. The unit of time is chosen so that the angular velocities of the planet and the Sun are equal to 1. We denote with ε the mass of the planet, since it is small compared to the mass of the Sun. In a uniformly rotating reference frame, called *synodic reference frame*, the positions of the Sun and the planet are fixed, and their coordinates are $(-\varepsilon, 0, 0)^T$, $(1-\varepsilon, 0, 0)^T$ respectively. Denote with $(x, y, z)^T, (\dot{x}, \dot{y}, \dot{z})^T \in \mathbb{R}^3$ the coordinates of the position and velocity of the asteroid, respectively. The Lagrangian of the problem is given by

$$L = \frac{1}{2}(\dot{x}^2 + \dot{y}^2 + \dot{z}^2) + (x\dot{y} - x\dot{y}) + U, \quad U = \frac{1}{2}(x^2 + y^2) + \frac{1-\varepsilon}{r_1} + \frac{\varepsilon}{r_2}, \tag{6.55}$$

where r_1, r_2 are the distances from the Sun and the planet respectively, i.e.

$$r_1 = \sqrt{(x+\varepsilon)^2 + y^2 + z^2}, \quad r_2 = \sqrt{(x-1+\varepsilon)^2 + y^2 + z^2}. \tag{6.56}$$

The equations of motion in this reference frame are

$$\begin{cases} \ddot{x} - 2\dot{y} &= \dfrac{\partial U}{\partial x} = x - (1-\varepsilon)\dfrac{x+\varepsilon}{r_1^3} - \varepsilon\dfrac{x-1+\varepsilon}{r_2^3}, \\ \ddot{y} + 2\dot{x} &= \dfrac{\partial U}{\partial y} = y - (1-\varepsilon)\dfrac{y}{r_1^3} - \varepsilon\dfrac{y}{r_2^3}, \\ \ddot{z} &= \dfrac{\partial U}{\partial z} = -(1-\varepsilon)\dfrac{z}{r_1^3} - \varepsilon\dfrac{z}{r_2^3}. \end{cases} \tag{6.57}$$

System (6.57) has the first integral C, usually called *Jacobi integral*, defined by

$$\frac{C}{2} = -\frac{1}{2}(\dot{x}^2 + \dot{y}^2 + \dot{z}^2) + \frac{1}{2}(x^2 + y^2) + \frac{1-\varepsilon}{r_1} + \frac{\varepsilon}{r_2}, \tag{6.58}$$

C corresponds to the opposite of the doubled total energy.

6.4.2 Kustaanheimo-Stiefel regularization

It is possible to gain in computation time and accuracy regularizing the problem, that is changing the space and time variables in order to eliminate the singularity of the collision with a body. For this purpose we use the Kustaanheimo-Stiefel regularization, which generalizes the Levi-Civita regularization for the planar circular restricted 3-body problem, having in mind that we want to regularize the collisions with the planet. First we perform a time transformation and later a coordinate one. We define the *fictitious time* τ by

$$\frac{dt}{d\tau} = r_2, \quad r_2 = \sqrt{(x-x_0)^2 + y^2 + z^2}, \tag{6.59}$$

where $x_0 = 1 - \varepsilon$. Note that, when we are close to the collision, this change of time has the effect of slowing down the dynamics. The relation between the second derivatives is given by

$$\frac{d^2}{dt^2} = \frac{d}{dt}\left(\frac{1}{r_2}\frac{d}{d\tau}\right) = \frac{1}{r_2}\frac{d}{d\tau}\left(\frac{1}{r_2}\frac{d}{d\tau}\right) = \frac{1}{r_2^2}\frac{d^2}{d\tau^2} - \frac{1}{r_2^3}\frac{dr_2}{d\tau}\frac{d}{d\tau}.$$

Denoting with a prime the derivative with respect to the fictitious time τ, the equations of motion (6.57) are written as

$$\begin{cases} \dfrac{1}{r_2^2}x'' - \dfrac{r_2'}{r_2^3}x' - \dfrac{2}{r_2}y' &= x - \dfrac{1-\varepsilon}{r_1^3}(x+\varepsilon) - \dfrac{\varepsilon}{r_2^3}(x-1+\varepsilon), \\ \dfrac{1}{r_2^2}y'' - \dfrac{r_2'}{r_2^3}y' + \dfrac{2}{r_2}x' &= y - \dfrac{1-\varepsilon}{r_1^3}y - \dfrac{\varepsilon}{r_2^3}y, \\ \dfrac{1}{r_2^2}z'' - \dfrac{r_2'}{r_2^3}z' &= -\dfrac{1-\varepsilon}{r_1^3}z - \dfrac{\varepsilon}{r_2^3}z, \end{cases}$$

which are equivalent to

$$\begin{cases} x'' - 2r_2y' &= \dfrac{r_2'}{r_2}x' + r_2^2F_1 - \dfrac{\varepsilon}{r_2}(x-1+\varepsilon), \\ y'' + 2r_2x' &= \dfrac{r_2'}{r_2}y' + r_2^2F_2 - \dfrac{\varepsilon}{r_2}y, \\ z'' &= \dfrac{r_2'}{r_2}z' + r_2^2F_3 - \dfrac{\varepsilon}{r_2}z, \end{cases} \tag{6.60}$$

where

$$\begin{aligned} F_1 &= x - \frac{(1-\varepsilon)}{r_1^3}(x+\varepsilon), \\ F_2 &= y - \frac{(1-\varepsilon)}{r_1^3}y, \\ F_3 &= -\frac{(1-\varepsilon)}{r_1^3}z. \end{aligned} \tag{6.61}$$

Let $Q = (x - x_0, y, z, 0)^T \in \mathbb{R}^4$ and $F = (F_1, F_2, F_3, 0)^T \in \mathbb{R}^4$, then equations (6.60) are written as

$$\begin{aligned} Q'' &= \frac{r_2'}{r_2} Q' + r_2^2 F + r_2 B Q' - \varepsilon \frac{Q}{r_2} \\ &= \frac{Q \cdot Q'}{Q \cdot Q} Q' + |Q|^2 F + |Q| B Q' - \varepsilon \frac{Q}{|Q|}, \end{aligned} \tag{6.62}$$

where

$$B = \begin{pmatrix} 0 & 2 & 0 & 0 \\ -2 & 0 & 0 & 0 \\ 0 & 0 & 0 & 0 \\ 0 & 0 & 0 & 0 \end{pmatrix}.$$

Let $u = (u_1, u_2, u_3, u_4)^T \in \mathbb{R}^4$, we consider the transformation

$$Q = L(u)u, \tag{6.63}$$

where $L(u)$ is the matrix of the K-S transformation

$$L(u) = \begin{pmatrix} u_1 & -u_2 & -u_3 & u_4 \\ u_2 & u_1 & -u_4 & -u_3 \\ u_3 & u_4 & u_1 & u_2 \\ u_4 & -u_3 & u_2 & -u_1 \end{pmatrix}. \tag{6.64}$$

Note that the change of coordinates (6.63) can be written also as

$$\begin{cases} x - x_0 &= u_1^2 - u_2^2 - u_3^2 + u_4^2, \\ y &= 2(u_1 u_2 - u_3 u_4), \\ z &= 2(u_1 u_3 + u_2 u_4), \end{cases} \tag{6.65}$$

since the last equation is trivially zero. Moreover, we have that

$$r_2^2 = (x - x_0)^2 + y^2 + z^2 = (u_1^2 + u_2^2 + u_3^2 + u_4^2)^2 = |u|^4. \tag{6.66}$$

The matrix $L(u)$ has the following properties

(1) $L^T(u)L(u) = |u|^2 I$.

(2) $L'(u) = L(u')$.

(3) $L(u)u' = L(u')u$, provided that $u_4 u_1' - u_3 u_2' + u_2 u_3' - u_1 u_4' = 0$. This last relation is also called *bilinear relation*.

(4) If u, u' satisfy the bilinear relation, then

$$|u|^2 L(u')u' - 2u \cdot u' L(u)u' + |u'|^2 L(u)u = 0.$$

From (6.63) and properties (2) and (3) we have

$$\begin{aligned} Q' &= 2L(u)u', \\ Q'' &= 2L(u)u'' + 2L(u')u'. \end{aligned} \tag{6.67}$$

Combining (6.67) with (6.62), and changing the coordinates, we get

$$2L(u)u'' + 2L(u')u' = 4\frac{u \cdot u'}{|u^2|}L(u)u' + |u|^4 F + 2|u|^2 BL(u)u' - \frac{\varepsilon}{|u|^2}L(u)u.$$

Using property (4), the above equation becomes

$$L(u)u'' - \frac{|u'|^2}{|u|^2}L(u)u = \frac{|u|^4}{2}F + |u|^2 BL(u)u' - \frac{\varepsilon}{2|u|^2}L(u)u. \tag{6.68}$$

Using property (1), the inverse of $L(u)$ is $L(u)^{-1} = L^T(u)/|u|^2$, hence (6.68) becomes

$$u'' + \left(\frac{\varepsilon}{2|u|^2} - \frac{|u'|^2}{|u|^2}\right)u = \frac{|u|^2}{2}L^T(u)F + L^T(u)BL(u)u', \tag{6.69}$$

and this defines the equation of motion in the K-S variables u. This equation is well defined at the collision with the planet, i.e. when $u = 0$. Indeed, we define

$$h = \frac{\dot{Q} \cdot \dot{Q}}{2} - \frac{\varepsilon}{r_2}. \tag{6.70}$$

In the u coordinates and with the new time τ we have

$$\frac{\dot{Q} \cdot \dot{Q}}{2} = 2\frac{|u'|^2}{|u|^2},$$

hence

$$h = \frac{|u'|^2}{|u|^2} - \frac{\varepsilon}{|u^2|}. \tag{6.71}$$

Combining (6.71) with the equation of motion (6.69), we obtain

$$u'' - \frac{h}{2}u = \frac{|u|^2}{2}L^T(u)F + L^T(u)BL(u)u'. \tag{6.72}$$

Moreover, using the expression (6.58) of the Jacobi constant C, we have that

$$h = \frac{1}{2}(x^2 + y^2) + \frac{1-\varepsilon}{r_1} - \frac{C}{2}, \tag{6.73}$$

hence in this term the singularity of the collision with the planet is removed. Since also the right hand side of equation (6.72) is smooth at $u = 0$, we conclude that there is

no singularity at the origin. The expressions of r_1, h, F_1, F_2, F_3 in the new variables u, appearing in the equation of motion (6.72) and (6.73), are given by

$$\begin{aligned}
r_1 &= \sqrt{(1+u_1^2-u_2^2-u_3^2+u_4^2)^2+4(u_1u_2-u_3u_4)^2+4(u_1u_3+u_2u_4)^2)},\\
F_1 &= (u_1^2-u_2^2-u_3^2+u_4^2+1-\varepsilon)-\frac{(1-\varepsilon)(1+u_1^2-u_2^2-u_3^2+u_4^2)}{r_1^3},\\
F_2 &= 2(u_1u_2-u_3u_4)-\frac{2(1-\varepsilon)(u_1u_2-u_3u_4)}{r_1^3},\\
F_3 &= -\frac{2(1-\varepsilon)(u_1u_3+u_2u_4)}{r_1^3},\\
h &= \frac{1}{2}((u_1^2-u_2^2-u_3^3+u_4^2+1-\varepsilon)^2+4(u_1u_2-u_3u_4)^2)+\frac{1-\varepsilon}{r_1}-\frac{C}{2}.
\end{aligned} \tag{6.74}$$

Note that, when we integrate numerically equation (6.72), we also add to the system the equation (6.59) defining the fictitious time τ, in order to recover the original time t.

Moreover, given the initial conditions $(x,y,z)^T, (\dot{x},\dot{y},\dot{z})^T \in \mathbb{R}^3$ for the problem in the synodic reference frame, we have to find the initial conditions $(u_1,u_2,u_3,u_4)^T$, $(u_1',u_2',u_3',u_4')^T \in \mathbb{R}^4$ in the K-S variables. To do that, note that equations (6.65) define a map from $\mathbb{R}^4$ to $\mathbb{R}^3$, thus the inverse transformation is undetermined, since we have three equations and four variables. Therefore, we can set arbitrarily one of the four variables equal to zero as done in [102]. It is convenient to distinguish between the cases $x < x_0$ and $x \geq x_0$: in the first case we set $u_3 = 0$, in the second case $u_4 = 0$. Therefore, the inverse relations are

$$u_3 = 0, \quad u_2 = \sqrt{\frac{r-x+x_0}{2}}, \quad u_1 = \frac{y}{2u_2}, \quad u_4 = \frac{z}{2u_2}, \tag{6.75}$$

if $x < x_0$, and

$$u_4 = 0, \quad u_1 = \sqrt{\frac{r+x-x_0}{2}}, \quad u_2 = \frac{y}{2u_1}, \quad u_3 = \frac{z}{2u_1}, \tag{6.76}$$

if $x \geq x_0$. Finally, to compute the initial derivatives u' we can simply invert the first equation in (6.67).

Chapter 7

Comparison between the systems

In science, an experiment is a test used to support or confute a hypothesis or, in general, a theory. Due to the large distances involved in astronomical motions, the most common way of performing experiments on existing objects is by means of observations. However, depending on the problem, large evolution timescales are also involved. Thus, performing experiments on real astronomical objects is not always trivial. Nowadays in Celestial Mechanics, thanks to the available computational power, the role of experiments is played by accurate numerical simulations.

In this chapter we investigate the relation between the solutions of the circular restricted 3-body problem and the solution of the equations given by the non-resonant or the resonant normal form. Using the tools introduced in Chapter 6, we perform numerical experiments in the cases of regular dynamics, orbit crossings and mean motion resonances.

When there are neither close encounters nor mean motion resonances between the planet and the asteroid, the averaging principle is valid and the solution of the averaged problem is a good approximation of the original solution for a large timespan. However, if no mean motion resonances are involved but the solution of the averaged equations passes through an orbit crossing, then the classical averaging principle cannot be applied. Indeed, it may happen that the solution of the full problem undergoes close approaches with the planet, which usually produce large changes in the semimajor axis.

Here we tried to interpret the solution of the averaged problem using a large set of solutions of the full problem, computed varying only the initial fast angles involved. Numerical simulations suggest that the solution of the averaged problem gives information on the solutions of the full circular restricted 3-body problem, in a statistical sense. Indeed, it seems that the large number of solutions taken into account compensate the changes in semimajor axis produced by close encounters, whose effects almost cancel out when we consider their arithmetic mean. This behaviour seems to be valid also when the asteroid and the planet are in mean motion resonance, provided that the comparison is done on the solutions of the full problem having the same initial resonant angle.

Some of these experiments were already present in [48, 50, 66], performed for some particular known objects in the Solar System. However, the dynamics in that case is

more complicated, due to the presence of several planets. Here we used the simple model of the circular restricted 3-body problem, for a better understanding of the results.

7.1 Arithmetic mean and standard deviation

The circular restricted 3-body problem (6.57) is integrated in Cartesian Coordinates, using the Kustaanheimo-Stiefel regularization near close approaches between the planet and the asteroid. Then the Cartesian coordinates $(x, y, z, \dot{x}, \dot{y}, \dot{z})$ are converted into the set of action-angle coordinates used for the averaged problem, i.e. Delaunay elements (L, G, Z, ℓ, g, z) if there are no mean motion resonances, or the elements (S, G, Z, σ, g, z) in case of mean motion resonances. Here we discuss the setting of the averaged problem without mean motion resonances, pointing out later the differences arising in the second setting. This allows to compare the solution of the averaged equations (6.6) with the solutions of the full equations (6.1).

To make a statistical comparison, we proceed in the following way. We fix the initial shape and orientation of the orbit of the asteroid, i.e. we provide the initial Keplerian elements $(a, e, i, \Omega, \omega)$ at time $t = 0$. Then we perform several numerical integrations, changing the initial values of the fast angles (ℓ, ℓ'). More specifically, fixed a positive integer $M \in \mathbb{N}$, we take the angles

$$\begin{cases} \ell_{j_1} = \dfrac{2\pi}{M} j_1, \\ \ell'_{j_2} = \dfrac{2\pi}{M} j_2, \end{cases} \qquad j_1, j_2 = 1, \dots, M. \tag{7.1}$$

Then, for every index $j_1, j_2 = 1, \dots, M$, we integrate numerically the full problem with initial Keplerian elements

$$(a, e, i, \Omega, \omega, \ell_{j_1}, \ell'_{j_2}), \quad j_1, j_2 = 1, \dots, M, \tag{7.2}$$

which have to be converted in Cartesian coordinates, for a timespan $[0, T]$, obtaining M^2 different solutions. In the following, we will also use the term *clones* to refer to these solutions. Let $y \in \{G, Z, g, z\}$ be one of the relevant Delaunay elements for the averaged problem, and denote with $y_{j_1,j_2}(t)$, $j_1, j_2 = 1, \dots, M$ the evolution of this element in the circular restricted 3-body problem, obtained with the initial condition (7.2) corresponding to the couple (j_1, j_2). Then we consider the arithmetic mean

$$\hat{y}_M(t) = \frac{1}{M^2} \sum_{j_1,j_2=1}^{M} y_{j_1,j_2}(t), \quad t \in [0, T], \tag{7.3}$$

and the standard deviation

$$\hat{\sigma}_M(t) = \sqrt{\sum_{j_1,j_2=1}^{M} \frac{\left(y_{j_1,j_2}(t) - \hat{y}_M(t)\right)^2}{M^2 - 1}}, \quad t \in [0, T]. \tag{7.4}$$

To investigate the relation between the solutions of the full equations and the solution of the averaged equations, we compare the averaged solution to the arithmetic mean $\hat{y}_M(t)$ and use also the standard deviation $\hat{\sigma}_M(t)$ to understand a possible statistical connection.

Note that, to integrate the circular restricted 3-body problem, we use an explicit Runge-Kutta of order 7 with adaptive step-size, namely the `DOP853` integrator (see [52] for a description) available at [51]. Therefore, every computed solution is discretized at different times. Moreover, also the solution of the averaged problem is computed using another different time discretization, since the Runge-Kutta-Gauss method explained in Subsection 6.2.5 is also step-size adaptive. However, the comparison has to de done using the same time for the averaged solution and the arithmetic mean. To this end, we discretize the integration interval $[0, T]$ using $K + 1$ equispaced points, that is we set

$$t_k = \frac{T}{K}k, \quad k = 0, \dots, K.$$

Hence $y_{j_1,j_2}(t_k)$, $j_1, j_2 = 1, \dots, M$ is obtained using cubic splines, based on the output of the numerical integration. The same is done for the solution of the averaged equations.

7.2 Non-resonant case

As already remarked, the averaged system (6.6) is integrable, since Z and the averaged Hamiltonian $\overline{\mathcal{H}}$ itself are first integrals in involution and generally independent. Therefore, to understand the flow of the averaged problem, we can look at the level curves of $\overline{\mathcal{H}}(\cdot, Z(0), \cdot, z(0))$, as function of the remaining Delaunay elements (G, g). Level curves for $Z(0)$ computed from

$$a = 1.8, \quad e = 0.15, \quad i = 45^\circ,$$

and $z(0) = 10^\circ$ are represented in Figure 7.1.

Due to the planet crossing singularity, some level curves of the averaged Hamiltonian are non-smooth. In particular, non-smooth level curves correspond to solutions passing through an orbit crossing. Since, as explained before, the vector field has a jump at the crossing, these level curves define only piecewise smooth solutions. Instead, if the chosen initial condition corresponds to a smooth level curve, then there are no orbit crossings during the evolution and the solution is smooth. Let us first discuss this case.

7.2.1 Smooth evolution

In this first experiment, the value of the mass of the planet is chosen to be $\mu = 10^{-4}$. We compute the initial Delaunay elements from the initial Keplerian elements

$$a = 1.8, \quad e = 0.15, \quad i = 45^\circ, \quad \Omega = 10^\circ, \quad \omega = 60^\circ.$$

From Figure 7.1 we see that the value (ω, e) belongs to a domain on which the level curves of $\overline{\mathcal{H}}$ are smooth, hence we do not expect crossings during the evolution. The averaged problem is integrated for a total time of 400 planet periods.

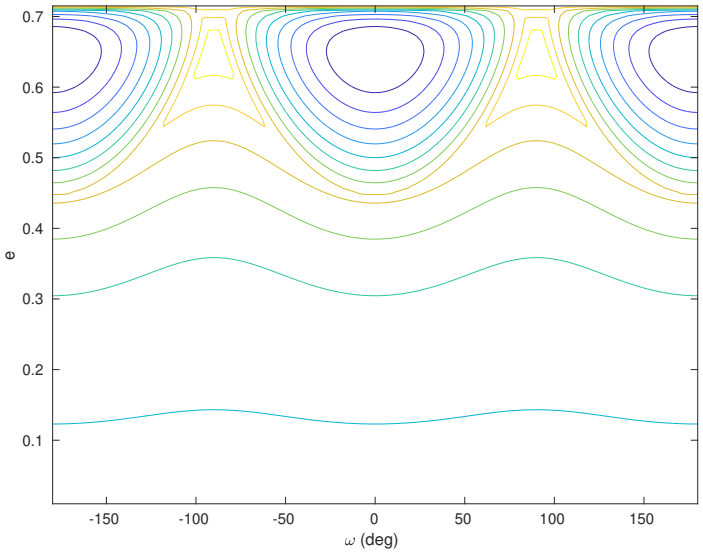

Figure 7.1: The level curves of the averaged Hamiltonian.

The full circular restricted 3-body problem has been integrated using the procedure explained in Section 7.1, using $M = 8, 100$, producing 64 and 10000 different clones respectively. Then the arithmetic mean and the standard deviation have been computed using cubic spline.

In Figure 7.2, the results of these integrations are shown. The green curve represents the solution of the averaged problem, while the black solid curve is the evolution of the arithmetic mean $\hat{y}_M$ for the elements e, i, Ω, ω. The gray filled area represents the points which are closer than the standard deviation to the arithmetic mean, at each time. As we can see, already with $M = 8$ we obtain a good correspondence between the averaged solution and the arithmetic mean. Increasing M to 100, we do not see any significant improvement in the approximation. This is explained by the fact that, in these conditions, the averaging principle can be applied, then any solution is well approximated by the solution of the averaged problem, independently from the initial values of the fast angles ℓ, ℓ'. It is important to note that the value of the standard deviation is small, because the dynamics is smooth in this part phase space: indeed, in this situation, small changes in the initial conditions produce small changes in the solutions. Moreover, we recognize fast and small oscillations in the arithmetic mean, which are persistent also for large values of M. This is due to the fact that every solution has fast and small oscillations, produced by the perturbation of the planet, and they do not cancel out when we consider the arithmetic mean $\tilde{y}_M$. In particular, we cannot conclude the convergence of $\hat{y}_M$ to the solution of the averaged problem, as $M \to +\infty$. We expect that $\hat{y}_M$ is close to the solution of the averaged problem up to some order in ε.

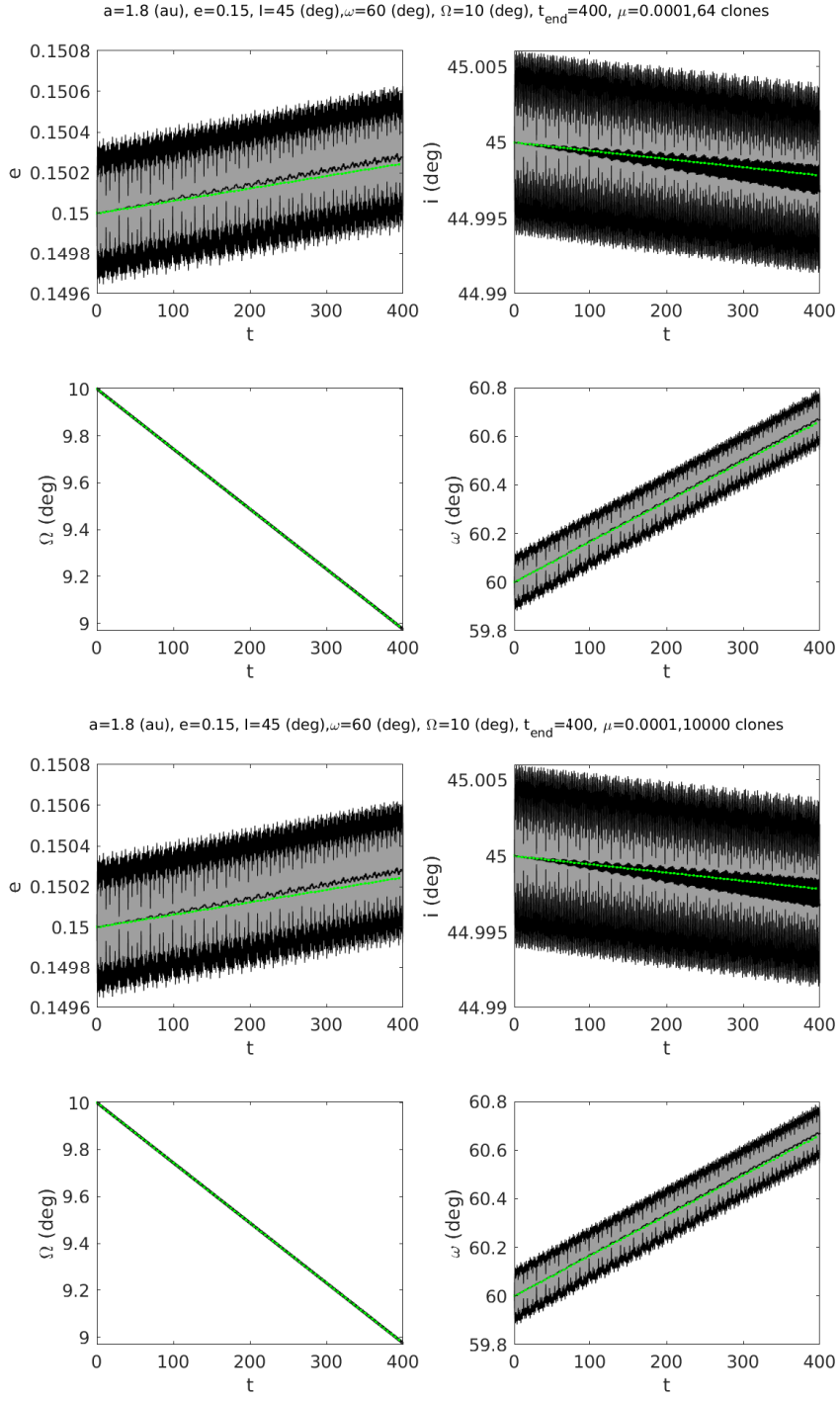

Figure 7.2: A smooth solution of the averaged circular restricted 3-body problem. The green curve represents the averaged solution, while the black solid curve represents the evolution of the arithmetic mean $\hat{I}_M(t)$. The gray filled area is the standard deviation from the mean. The plot on the top is produced using $M = 8$, the plot on the bottom using $M = 100$.

7.2.2 Non-smooth evolution

Here we search for an initial condition which produces a crossing configuration in the solution of the averaged equations. The value of the mass of the planet is chosen to be $\mu = 10^{-4}$, as in the previous experiment. We compute the initial Delaunay elements from the Keplerian elements

$$a = 1.8, \quad e = 0.75, \quad i = 45^\circ, \quad \Omega = 10^\circ, \quad \omega = 75^\circ.$$

From Figure 7.1 we see that the value (ω, e) corresponds to a non-smooth level curve of $\overline{\mathcal{H}}$, hence we expect an orbit crossing during the secular evolution. Therefore, the solution of the averaged equations is integrated using the Runge-Kutta-Gauss scheme explained in Subsection 6.2.5, for a total time of 400 orbital periods of the planet.

The full circular restricted 3-body problem has been integrated using the procedure explained in Section 7.1, using $M = 8,100$, producing 64 and 10000 different clones respectively. Then the arithmetic mean and the standard deviation have been computed using cubic splines.

In Figure 7.4 the results of these integrations are shown. The green curve represents the solution of the averaged problem, while the black solid curve is the evolution of the arithmetic mean $\hat{y}_M$, for the elements e, i, Ω, ω. The gray filled area represents the points which are closer than the standard deviation to the arithmetic mean, at each time. As we can see, near the time $t_c = 210$ the solution of the averaged problem (green line) has a corner, meaning that at this epoch the orbit of the asteroid crosses the orbit of the planet.

On the other hand, from the time evolution of the arithmetic mean (black solid curve) and the standard deviation (gray area), computed from whole set of solutions with different initial conditions for the fast angles, we understand that some of them undergo close approaches with the planet. Indeed, near the crossing time t_c, the arithmetic mean changes its approximated linear behaviour and moreover, the standard deviation has an evident large grow in the elements e, i, ω. When we increase the number of clones to $M = 100$ (see Figure 7.4, bottom), we see this large grow also in the longitude of the ascending node Ω, meaning that strong close approaches occurred in some of these solutions.

As we said in Chapter 6, the averaged equations of motion represents well enough the long term behaviour of the full system as long as there are no close approaches. However, from the plots of Figure 7.4 we can see that there is a relation between the solution of the averaged problem passing through an orbit crossings and the arithmetic mean introduced in Section 7.1. Indeed, the solution of the averaged problem always remains confined in the region defined by the arithmetic mean $\hat{y}_M$ and its standard deviation $\hat{\sigma}_M$. Moreover, passing from $M = 8$ to $M = 100$, the arithmetic mean does not have quick changes, suggesting that the effects of close approaches are canceled when we take into account the arithmetic mean of the elements. Furthermore, in the plot with $M = 100$, near the crossing time t_c, we can clearly see a change of direction in the evolution of the arithmetic mean, which tends to follow the solution of the averaged equations, and the two curves get closer. As before, we cannot have a convergence as $M \to \infty$, but we

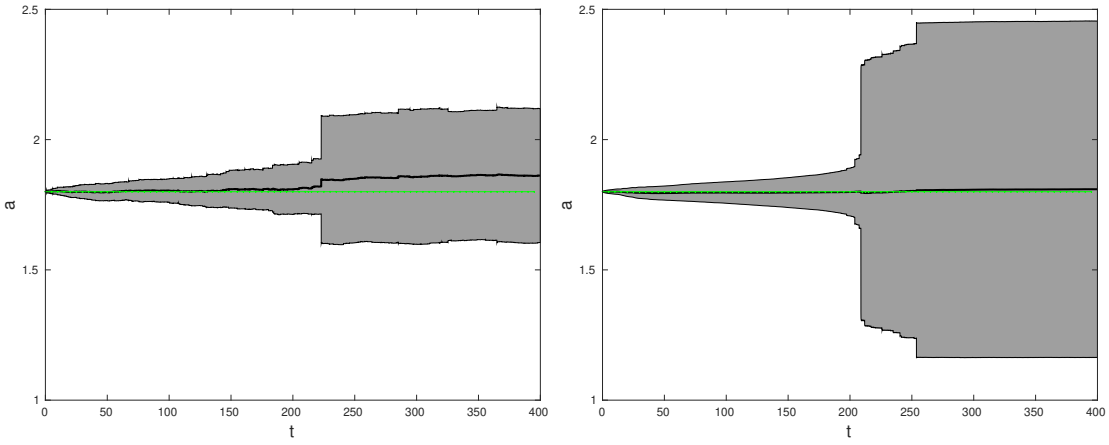

Figure 7.3: Comparison between the constant value of the semimajor axis a (green line) and the arithmetic mean (black solid curve) computed with $M = 8$, on the left, and $M = 100$, on the right. The gray filled area represents the standard deviation from the mean value.

expect that the arithmetic mean and the solution of the averaged problem are close up to some order in ε, for large values of M. These facts suggest that the solutions of the averaged problem give information on the whole set of solutions of the full equations of motion of the restricted 3-body problem, in the sense that they are confined in a *confidence region* defined by the arithmetic mean and its standard deviation.

Furthermore, we stress the fact that close approaches generally produce a wide change in the value of the semimajor axis, while we know that it remains constant in the averaged problem. For this reason, when we integrate the full problem, we also compute the arithmetic mean and the standard deviation for this element. Comparison between these two quantities is shown in Figure 7.3. As we can see, near the crossing time t_c, the standard deviation grows largely, confirming that close approaches occurred in some solutions. However, when we take into account a large number of solutions with different initial fast angles, as in the case $M = 100$, these large changes are compensated by the large number of solutions. Indeed, despite the large standard deviations, we see that the arithmetic mean remains close to the initial value.

7.3 Resonant case

When a mean motion resonance between the asteroid and the planet is involved in the dynamics, we have to modify the procedure to compute the arithmetic mean. Indeed, initial conditions (7.1) for the fast angles ℓ, ℓ' give rise to different initial conditions for the secular angle σ. To make a reliable comparison between the model given by the truncated resonant normal form $\mathcal{H}^{\mathrm{N}}_{\mathrm{res}}$ and the full circular restricted 3-body problem, we have to define initial conditions that keep the initial value of σ unchanged. In this manner, the corresponding solution of the resonant model does not change.

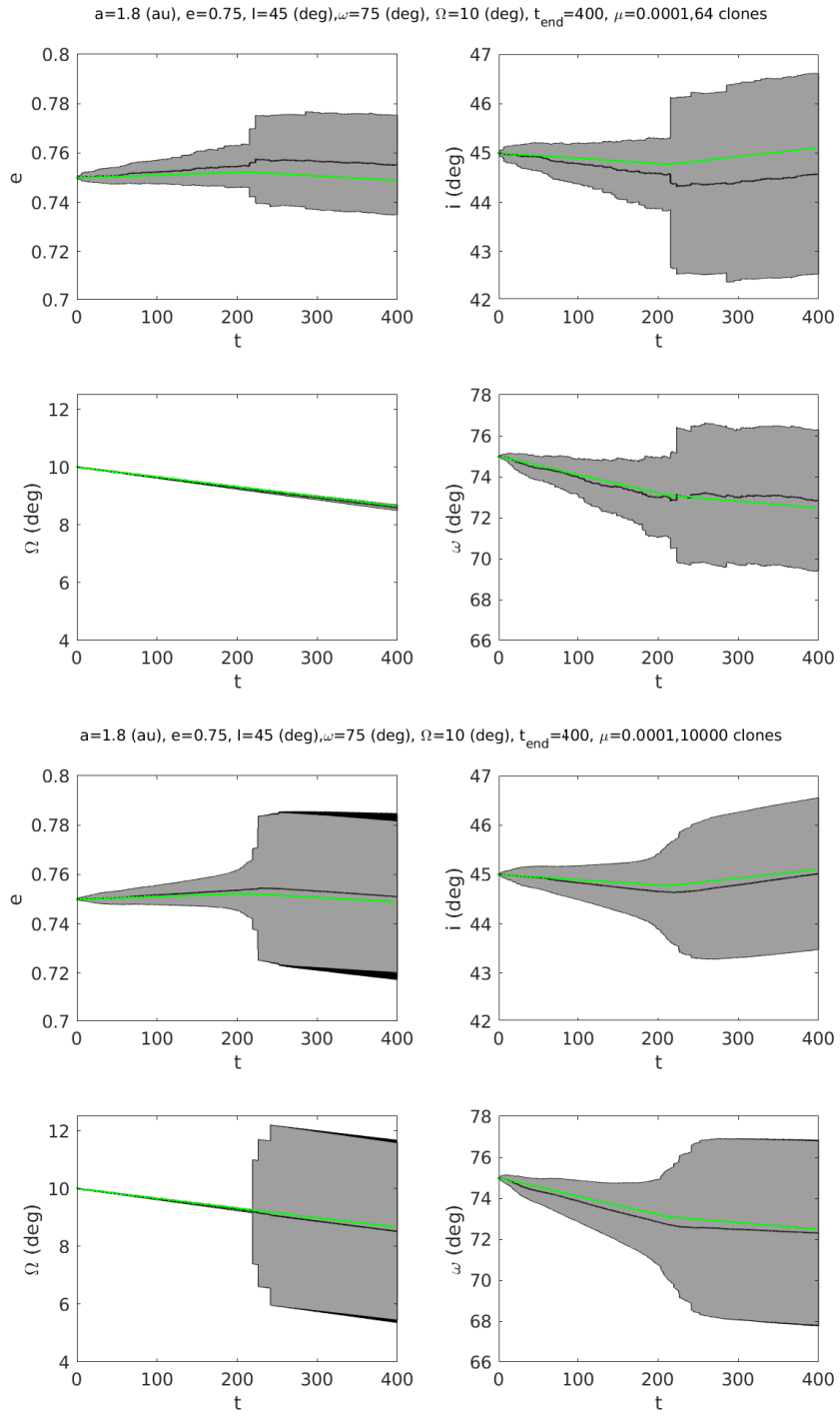

Figure 7.4: An orbit crossing solution of the averaged circular restricted 3-body problem. The green curve represents the averaged solution, while the black solid curve represents the evolution of the arithmetic mean $\hat{I}_M(t)$. The gray filled area is the standard deviation from the mean. The plot on the top is produced using $M = 8$, the plot on the bottom using $M = 100$.

7.3.1 Arithmetic mean

Let us suppose that we have detected a resonant dynamics using the method of Subsection 6.3.1. Let $(a, e, i, \Omega, \omega, \ell)$ be the initial Keplerian elements of the asteroid and ℓ' be the initial phase of the planet, that we used to integrate the full circular restricted 3-body problem in order to detect the resonance. Let $(\mathtt{h}, \mathtt{h}') \in \mathbb{Z}^2$ be the resonant vector of integer numbers. Let

$$\sigma = \mathtt{h}\ell + \mathtt{h}'\ell'$$

be the initial value of the secular angle. Then, fixed a positive integer number $M \in \mathbb{N}$, we take the initial conditions

$$\begin{cases} \ell_j = \dfrac{2\pi}{M} j, \\ \ell'_j = \dfrac{\sigma - \mathtt{h}\ell_j}{\mathtt{h}'}, \end{cases} \qquad j = 1, \dots, M. \tag{7.5}$$

Therefore, for every index $j = 1, \dots, M$, we integrate numerically the circular restricted 3-body problem with initial Keplerian elements

$$(a, e, i, \Omega, \omega, \ell_j, \ell'_j), \quad j = 1, \dots, M. \tag{7.6}$$

which have to be converted into Cartesian coordinates, for a timespan $[0, T]$, obtaining M different clones instead of M^2, as for the non-resonant case. Then, the Cartesian coordinates in output are converted into the resonant variables (S, G, Z, σ, g, z), then the arithmetic mean $\hat{y}_M$ and its standard deviation $\hat{\sigma}_M$ are computed as before at equispaced time points, using a cubic spline interpolation.

7.3.2 Numerical simulations

We perform a test using the initial conditions of the asteroid 1999 JB_{11}, which we found to be in the 5 : 2 resonance with the Earth. The mass of the planet used in the test is chosen to be $\mu = 10^{-4}$. This value is slightly larger than the mass parameter of the Earth used to perform the resonance detection in Subsection 6.3.1, however the resonance still persists. We compute the initial resonant elements from the initial Keplerian elements

$$a = 1.842, \quad e = 0.25, \quad i = 37.1^\circ, \quad \Omega = 10^\circ, \quad \omega = 31^\circ, \quad \ell = 0^\circ,$$

which are taken from [41]. Therefore, the solution of the resonant model is integrated using the Runge-Kutta-Gauss scheme explained in Subsection 6.2.5, for a total time of 400 orbital periods of the planet. We performed two numerical tests, using $N = 3$ and $N = 15$ for the truncation order of the truncated resonant normal form $\mathcal{H}^{\mathrm{N}}_{\mathrm{res}}$.

The full circular restricted 3-body problem has been integrated using the procedure explained in Subsection 7.3.1, keeping the initial value of the resonant angle σ constant, with $M = 300$ different clones. Then the arithmetic mean and the standard deviation have been computed using the cubic spline.

In Figure 7.5 the results of these integrations are shown. The green curve represents the solution of the resonant model, while the black solid curve is the evolution of the arithmetic mean $\hat{y}_M$. The gray filled area represents the points which are closer than the standard deviation to the arithmetic mean, at each time. As we can see from the plot on the top, which is produced using a truncation order equal to $N = 3$ for the resonant normal form, the solution of the resonant model exits out from the standard deviation area, after about 270 orbital periods of the planet. However, this is explained by the fact that, when the truncation order is small, the truncated resonant normal form does not represent well the solutions of the full problem after some libration periods. Indeed, increasing the truncation order to $N = 15$, this problem disappears, as we can see from the plot in Figure 7.5, bottom: here the solution of the resonant model stays very close to the arithmetic mean over the entire propagation timespan.

Moreover, we do not notice any orbit crossing during the evolution in the resonant model, and furthermore we do not see any evidence of the presence of close encounters between the planet and the asteroid in the 300 clones, since we do not see any large grow in the standard deviation. This still has the consequence that small changes in the initial conditions produce small changes in the solutions, and this can be noticed in the sharp standard deviation. Moreover, fast and small oscillations due to the perturbation of the planet are still persistent.

From these plots, it seems that the solutions of the resonant model give information about the solutions of the full circular restricted 3-body problem in a statistical sense, as in the case without mean motion resonances, provided that we consider only the solutions with the same initial condition for the resonant angle σ.

We did not perform any test in the case of mean motion resonances and orbit crossings, which is the last possible setting in this framework. We plan to investigate better this setting with further numerical experiments. However, the results presented in [66] suggest that, using a large order of truncation for the resonant Hamiltonian, the jumps in the derivatives due to the crossing singularity are as small as the rounding off error, therefore they cannot be perceived in the numerical simulations and they do not have any effect on the dynamics.

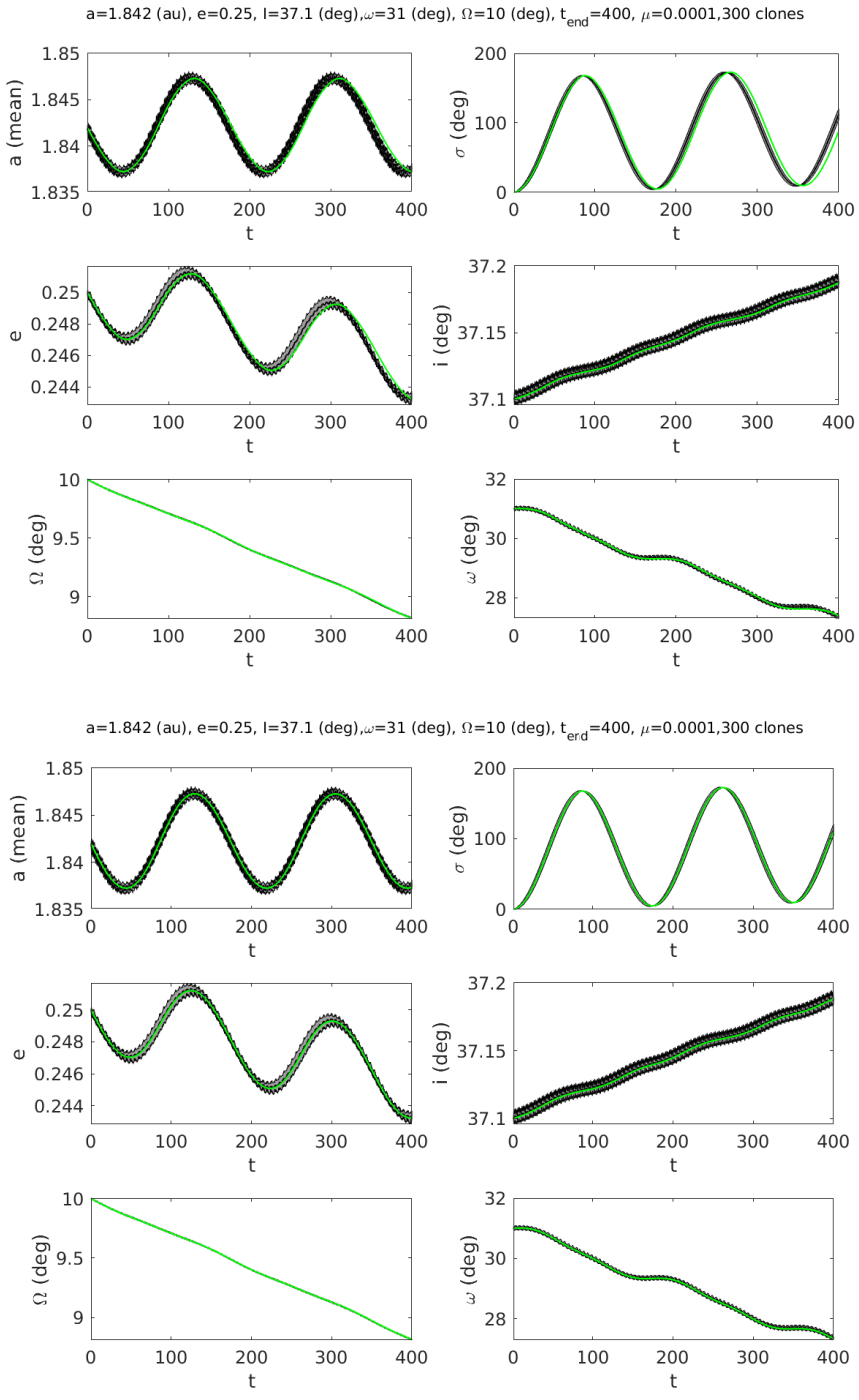

Figure 7.5: Comparison between the averaged resonant solution (green line) and the arithmetic mean computed (black solid line), computed using $M = 300$ clones. The gray region represents the standard deviation from the mean. The plot on the top is produced using truncation order equal to $N = 3$, the plot on the bottom using truncation order equal to $N = 15$.

Appendix A

The Marchal Lemma

A.1 Weak force potential

We consider a unitary mass particle, moving under the central force defined by the α-homogeneous potential energy

$$V(x) = -\frac{1}{|x|^\alpha}, \tag{A.1}$$

where $x \in \mathbb{R}^2 \setminus \{0\}$ and $\alpha \in [1, 2)$. The Lagrangian is

$$L(x, \dot{x}) = \frac{|\dot{x}|^2}{2} + \frac{1}{|x|^\alpha}, \tag{A.2}$$

and the equations of motion are

$$\ddot{x} = -\alpha \frac{x}{|x|^{\alpha+2}}. \tag{A.3}$$

The problem has the first integrals of the energy, which is defined as

$$E(x, \dot{x}) = \frac{|\dot{x}|^2}{2} - \frac{1}{|x|^\alpha}, \tag{A.4}$$

and the total angular momentum

$$c(x, \dot{x}) = x_1 \dot{x}_2 - x_2 \dot{x}_1, \tag{A.5}$$

where $x = (x_1, x_2)$, $\dot{x} = (\dot{x}_1, \dot{x}_2)$. In polar coordinates (ρ, θ), defined through

$$\begin{cases} x_1 = \rho \cos\theta, \\ x_2 = \rho \sin\theta, \end{cases}$$

the equations of motion (A.3) are written as

$$\begin{cases} \rho^2 \dot{\theta} = c, \\ \\ \ddot{\rho} = -\dfrac{\alpha}{\rho^{\alpha+1}} + \dfrac{c^2}{\rho^3}. \end{cases} \tag{A.6}$$

The first equation represents the conservation of the angular momentum, while the second depends only on the variable ρ and can be written as

$$\ddot{\rho} = -\frac{d}{d\rho} V^c_{\text{eff}}(\rho), \tag{A.7}$$

where V^c_{eff} is the *effective potential*, defined as

$$V^c_{\text{eff}}(\rho) := -\frac{1}{\rho^\alpha} + \frac{c^2}{2\rho^2}. \tag{A.8}$$

System (A.7) has a first integral, corresponding to the total energy (A.4) written using the conservation of the angular momentum, which results to be

$$E^c_{\text{eff}}(\rho, \dot{\rho}) = \frac{\dot{\rho}^2}{2} + V^c_{\text{eff}}(\rho). \tag{A.9}$$

Therefore, system (A.7) is integrable and the phase portrait can be deduced from the level curves of V^c_{eff}. An example of phase portrait for specific values of α and c is shown in Figure A.1.

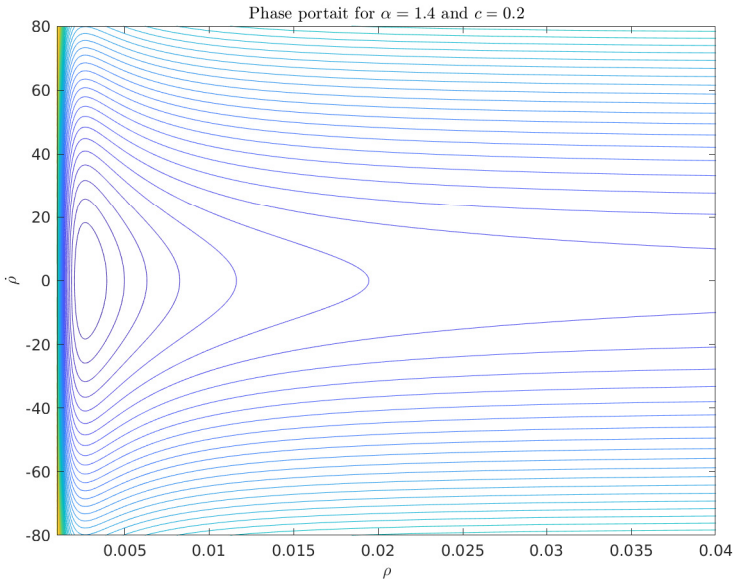

Figure A.1: The phase portrait of (A.7) in the plane $(\rho, \dot{\rho})$, for $\alpha = 1.4$ and $c = 0.2$.

A.2 Collision-ejection solutions

Let $\bar{\rho} > 0$ be a positive value and $h \in \mathbb{R}$ such that $h \geq h_{\min}(\bar{\rho})$, where

$$h_{\min}(\bar{\rho}) = -\frac{1}{\bar{\rho}^\alpha}.$$

Note that $h_{\min}(\bar{\rho})$ is the minimal value of the energy which allows a solution of (A.7) to pass from the value $\bar{\rho}$. A *collision-ejection solution* is a solution passing through the origin, connecting two points in the plane at distance $\bar{\rho}$ from the origin. Note that for $\alpha \in [1, 2)$, collision solutions are possible only when $c = 0$, see [69].

We search for the collision-ejection orbit with energy h. We can study only half of this solution, for example the ejection one. Moreover, since the angular momentum is zero, the motion takes place on a line. The time needed for the ejection solution to go from the origin to the point at distance $\bar{\rho}$ is recovered from the conservation of the energy, and it is given by

$$\begin{aligned} \tau(h) &= \int_0^{\bar{\rho}} \frac{\rho}{\sqrt{2h\rho^2 + 2\rho^{2-\alpha}}} d\rho \\ &= \frac{1}{\sqrt{2}} \int_0^{\bar{\rho}} \frac{\rho^{\alpha/2}}{\sqrt{h\rho^\alpha + 1}} d\rho. \end{aligned} \tag{A.10}$$

Denote with $x_h : [-\tau(h), \tau(h)] \to \mathbb{R}^2$ the collision-ejection solution in the plane and let $\rho_h(t)$ be its radial component. The action of the collision-ejection solution is given by

$$\mathcal{A}(x_h) = 2 \int_0^{\tau(h)} \left(\frac{\dot{\rho}_h^2(t)}{2} + \frac{1}{\rho_h^\alpha(t)} \right) dt. \tag{A.11}$$

From the conservation of the energy, we have that

$$\frac{d\rho_h}{dt} = \sqrt{2\left(h + \frac{1}{\rho_h^\alpha}\right)}. \tag{A.12}$$

We can express the integral (A.11) using ρ as parameter instead of t and, dropping the subscript h for the sake of simplicity, we obtain

$$\begin{aligned} \mathcal{A}(x_h) &= 2 \int_0^{\tau(h)} \left(h + \frac{2}{\rho^\alpha} \right) dt \\ &= 2h\tau(h) + 2\sqrt{2} \int_0^{\bar{\rho}} \frac{1}{\rho^\alpha \sqrt{h + 1/\rho^a}} d\rho \\ &= 2h\tau(h) + 2\sqrt{2} \int_0^{\bar{\rho}} \frac{1}{\rho^{\alpha/2} \sqrt{h\rho^\alpha + 1}} d\rho. \end{aligned} \tag{A.13}$$

Parabolic collision-ejection When the value of the energy is $h = 0$, we have the so called *parabolic collision-ejection solution*: we have seen in Chapters 1 and 2 that it plays an important role in excluding partial collisions. In this case we can solve explicitly the above integrals. The time needed to arrive at the collision is

$$\tau(0) = \frac{\sqrt{2}}{2 + \alpha} \bar{\rho}^{\frac{\alpha+2}{2}}, \tag{A.14}$$

and the action is given by

$$\mathcal{A}(x_0) = \frac{4\sqrt{2}}{2 - \alpha} \bar{\rho}^{\frac{2-\alpha}{2}}. \tag{A.15}$$

We can also explicitly compute the collision solution. Indeed, searching for a solution of the form

$$\rho(t) = \gamma t^{\beta},$$

and imposing that it solves equation (A.7) with $c = 0$, we get

$$\begin{cases} \beta = \dfrac{2}{2+\alpha}, \\ \gamma = \left(\dfrac{(\alpha+2)^2}{2}\right)^{\frac{1}{\alpha+2}}. \end{cases} \tag{A.16}$$

A.3 Marchal's Lemma for α-homogeneous potentials

Results present in the literature In the literature, Marchal's Lemma is often referred to the following result (see for example [65, 19, 38, 76] for a proof).

Lemma A.1 (Marchal's Lemma)**.** *Let $\tau > 0$, $\alpha \in [1, 2)$ and $x_A, x_B \in \mathbb{R}^2 \setminus \{0\}$ be two points in the space. Then any minimizer of the action*

$$\mathcal{A}(x) = \int_0^\tau \left(\frac{|\dot{x}|^2}{2} + \frac{1}{|x|^\alpha}\right) dt, \tag{A.17}$$

which is defined on the set of curves $x : [0, \tau] \to \mathbb{R}^2$ such that $x(0) = x_A$, $x(\tau) = x_B$, is free of interior collisions.

In the Keplerian case, the method used in [19] to prove this lemma is the following: take a solution connecting x_A and x_B which has a collision and perturb it in all the possible directions. Then, average the actions of the perturbed paths over a small circle: it turns out that this average is less than the action of the collision path. Therefore, there exists a perturbing direction which lowers the action of the collision path, so that it cannot be a minimizer. However, this version of the lemma does not provide any information about how many minimizers exist and, more in general, it does not relate the action of other stationary points to the action of the collision-ejection solution.

Another version of Marchal's Lemma, stated for the Keplerian case $\alpha = 1$, can be found in [40]. We have reported this version in Chapter 1, Lemma 1.8. Here, only the parabolic collision-ejection solution is taken into account and it states that there are actually two solutions of the Keplerian equations of motion, connecting any two different points (at the same distance from the origin), whose action is lower than the action of the parabolic collision-ejection solution itself. Moreover, if the ending points coincide, there is only one non-collision connecting solution. In general, the action of these two arcs is different, hence we conclude that any non-collision stationary point has action lower than the action of the parabolic collision-ejection solution. Furthermore, the number of stationary points is related to the angle between x_A and x_B: this is also important in the proof of the exclusion of partial collisions given in Subsection 1.2.3. However, the proof in [40] of this version of the lemma is done by using the explicit form of the solutions of the Kepler problem, hence it cannot be adapted to the case $\alpha \in (1, 2)$.

A more general statement is contained in [10], and it holds for potential depending also on the angle (e.g. for the anisotropic Kepler potential). In the case of α-homogeneous potential, the result can be summarized as follows.

Theorem A.2. *Let $x_A = r_A(\cos\varphi_A, \sin\varphi_A)$, $x_B = r_B(\cos\varphi_B, \sin\varphi_B) \in \mathbb{R}^2 \setminus \{0\}$ and $\tau > 0$. Given an integer $k \in \mathbb{Z}$ such that*

$$|\varphi_A - (\varphi_B + 2k\pi)| < \frac{2\pi}{2-\alpha},$$

define

$$\mathcal{G} = \big\{x \in H^1([-\tau,\tau],\mathbb{R}^2) : x(-\tau) = x_A,\, x(\tau) = x_B \\ \text{and the total angle swept by } x \text{ is } \varphi_B + 2k\pi - \varphi_A\big\}.$$

Then any minimizer of the action

$$\mathcal{A}(x) = \int_{-\tau}^{\tau} \left(\frac{|\dot{x}|^2}{2} + \frac{1}{|x|^\alpha}\right) dt.$$

in the class $\mathcal{G}$ is free of collisions.

This version of the theorem gives informations not only on the minimizer, but also on other stationary points of the fixed-ends problem. The strategy used to prove this lemma is the following. A disk of radius $\varepsilon > 0$ centered at the origin is cut out from the plane and an obstacle problem is introduced. If the minimizer in $\mathcal{G}$ has a collision, then the minimizers x_ε^* of the obstacle problem touch the border of the disk, for every $\varepsilon > 0$. Using a blow-up, it can be proven that x_ε^* is composed by two parabolic arcs, connected by an arc on the circle of radius ε. Then, the total variation of the angle can be computed and it results to be greater than $2\pi/(2-\alpha)$: this is in contradiction with the arcs in the class $\mathcal{G}$, hence the minimizer is collision free.

Marchal's Lemma for the parabolic collision-ejection solution A version of Marchal's Lemma (analogous to Lemma 1.8 in the Keplerian case) which is suitable for our purposes of Chapter 2, can be stated as follows.

Lemma A.3. *Let $\alpha \in (1,2)$ and $\bar{\rho} > 0$. Let $\tau(0)$ be the time needed for the parabolic collision-ejection solution, starting at distance $\bar{\rho}$, to arrive at the collision. Let $\varphi \in [0, 2\pi)$ and set*

$$\begin{cases} x_A = (0, \bar{\rho}), \\ x_B = \bar{\rho}(\cos\varphi, \sin\varphi). \end{cases}$$

Let $\bar{x} : [-\tau(0), \tau(0)] \to \mathbb{R}^2$ be any non-collision solution of equation (A.3) *connecting x_A to x_B in time $2\tau(0)$, i.e. such that*

$$\bar{x}(-\tau(0)) = x_A, \quad \bar{x}(\tau(0)) = x_B,$$

and denote with $x_0 : [-\tau(0), \tau(0)] \to \mathbb{R}^2$ *the parabolic collision-ejection solution with the same boundary conditions. Then we have that*

$$\mathcal{A}(\bar{x}) < \mathcal{A}(x_0), \tag{A.18}$$

where

$$\mathcal{A}(x) = \int_{-\tau(0)}^{\tau(0)} \left(\frac{|\dot{x}|^2}{2} + \frac{1}{|x|^\alpha} \right) dt.$$

Moreover, the total number of connecting arcs is a function of the angle φ between the points and the exponent $\alpha \in (1, 2)$.

Lemma A.4. *In the hypotheses of Lemma A.3, connecting arcs all have a different winding number with respect to the zero. In particular, the total angle swept by each arc is*

$$\varphi + 2\pi k, \quad k = k_{min}, \dots, k_{max},$$

where

$$k_{min} = \begin{cases} -\left[\dfrac{1}{2-\alpha} + \dfrac{\varphi}{2\pi} \right] & \text{if } \dfrac{1}{2-\alpha} + \dfrac{\varphi}{2\pi} \notin \mathbb{Z}, \\ -\left(\dfrac{1}{2-\alpha} + \dfrac{\varphi}{2\pi} \right) + 1 & \text{if } \dfrac{1}{2-\alpha} + \dfrac{\varphi}{2\pi} \in \mathbb{Z}, \end{cases} \tag{A.19}$$

$$k_{max} = \begin{cases} \left[\dfrac{1}{2-\alpha} - \dfrac{\varphi}{2\pi} \right] & \text{if } \dfrac{1}{2-\alpha} - \dfrac{\varphi}{2\pi} \notin \mathbb{Z}, \\ \left(\dfrac{1}{2-\alpha} - \dfrac{\varphi}{2\pi} \right) - 1 & \text{if } \dfrac{1}{2-\alpha} - \dfrac{\varphi}{2\pi} \in \mathbb{Z}, \end{cases} \tag{A.20}$$

and $[\,\cdot\,]$ *denotes the integer part. Moreover, the total number of arcs is given by*

$$k_{tot}(\alpha, \varphi) = k_{max} - k_{min} + 1.$$

Remark A.5. Note that Lemma A.4 matches with the Keplerian case $\alpha = 1$. Indeed, the value

$$\frac{1}{2-\alpha} + \frac{\varphi}{2\pi} = 1 + \frac{\varphi}{2\pi}$$

is an integer number if and only if $\varphi = 0$, since $\varphi \in [0, 2\pi)$. Hence, for $\varphi \neq 0$, we always have

$$k_{\min} = -1, \quad k_{\max} = 0,$$

and there are exactly two connecting arcs, one sweeping a total angle of φ and the other one sweeping a total angle of $\varphi - 2\pi$, see Figure A.2 for an example. For $\varphi = 0$ we have that $k_{\min} = k_{\max} = 0$, therefore there is only one connecting arc and it lies on the half line connecting the origin to the point itself.

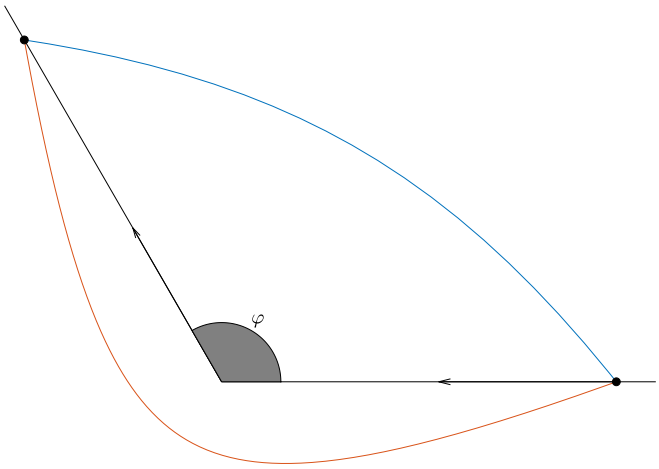

Figure A.2: Example of Keplerian connecting arcs. The ending points are at distance 1 from the origin, the angle between them is $\varphi = 120°$. The blue arc is the direct arc (which is also the minimizer of the action) and the red arc is the indirect arc.

This version of the lemma follows immediately from Theorem A.2. In the following sections, we report our idea to prove Lemma A.3, which is supported by numerical computation. This work has been done before our knowledge of the existence of Theorem A.2.

A.4 Connecting arcs

Let $\alpha \in [1, 2)$, $\tau > 0$, $\bar{\rho} > 0$ and let $\varphi \in [0, 2\pi)$ be an angle. Given the values (h, c) of the energy and the angular momentum respectively, we define two functions, computing the time passed and the angle swept by an arc which starts at distance $\bar{\rho}$ from the center and ends at the same distance $\bar{\rho}$. Moreover, we assume that these arcs pass only through the pericenter or the apocenter.

Properties of the effective potential Note that the derivative of the effective potential V^c_{eff} is

$$\frac{d}{d\rho} V^c_{\text{eff}} = -\frac{c^2}{\rho^3} + \frac{\alpha}{\rho^{\alpha+1}},$$

hence there exists a unique point $\rho_m(c)$ such that V^c_{eff} attains its minimum at $\rho_m(c)$, and it is given by

$$\rho_m(c) = \left(\frac{c^2}{\alpha}\right)^{\frac{1}{2-\alpha}}. \tag{A.21}$$

Moreover, we have that

$$\lim_{\rho \to 0^+} V^c_{\text{eff}}(\rho) = +\infty, \quad \lim_{\rho \to +\infty} V^c_{\text{eff}}(\rho) = 0^-.$$

The typical graph of the function V^c_{eff} is shown in Figure A.3. Hence, given $h \in \mathbb{R}$, the motion is possible only when $h - V^c_{\text{eff}}(\rho) \geq 0$, and the equation

$$h - V^c_{\text{eff}}(\rho) = 0$$

has

(i) two solutions $0 < \rho_-(h,c) < \rho_+(h,c)$ for $h < 0$;

(ii) one solution $0 < \rho_-(h,c)$ for $h \geq 0$.

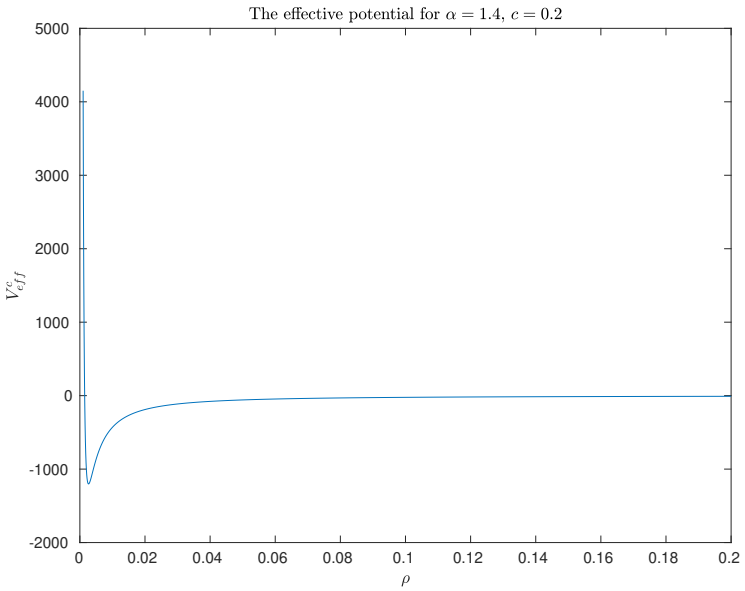

Figure A.3: The graphic of the effective potential V^c_{eff}.

The domain of definition Note that an arc can pass through the value $\bar{\rho}$ only if the values (h,c) of the first integrals satisfy

$$h - V^c_{\text{eff}}(\bar{\rho}) \geq 0.$$

The border of this region in the (h,c) plane is given by the equation

$$V^c_{\text{eff}}(\bar{\rho}) = h, \tag{A.22}$$

which can be written as

$$c^2 = 2h\bar{\rho}^2 + 2\bar{\rho}^{2-\alpha}. \tag{A.23}$$

This is a parabola in the (h,c) plane, whose axis of symmetry corresponds to the energy axis. We define then the region

$$\mathcal{D} := \{(h,c) \in \mathbb{R}^2 : h - V^c_{\text{eff}}(\bar{\rho}) \geq 0\}.$$

Note that $(h,c) \in \mathcal{D}$ if and only if

(i) $h < 0$ and $\rho_-(h,c) \le \bar\rho \le \rho_+(h,c)$ or

(ii) $h \ge 0$ and $\rho_-(h,c) \le \bar\rho$,

where $\rho_\pm(h,c)$ are the solutions of equation (A.22). Moreover, the border $\partial\mathcal{D}$ corresponds to the union of the two curves

$$\mathcal{C}^- := \{(h,c) \in \mathbb{R}^2 : \rho_-(h,c) = \bar\rho\},$$
$$\mathcal{C}^+ := \{(h,c) \in \mathbb{R}^2 : \rho_+(h,c) = \bar\rho\}.$$

These two curves join at two symmetric points $(h_s, \pm c_s)$, for which equation (A.22) has only a solution and $\bar\rho$ is a minimum of V^c_{eff}. With easy computations, we get

$$\begin{cases} h_s = \dfrac{\alpha-2}{2}\dfrac{1}{\bar\rho^\alpha}, \\ c_s = \sqrt{\alpha}\bar\rho^{\frac{2-\alpha}{2}}. \end{cases} \tag{A.24}$$

Note that $h_s < 0$.

Arcs passing through the pericenter The function $\rho_-(h,c)$ defining the minimum positive solution of $h - V^c_{\text{eff}}(\rho) = 0$ is well defined in $\mathcal{D}$ and it is continuous and differentiable. This value corresponds to the pericenter of the orbit with energy h and angular momentum c, and moreover $\rho_-(h,c) \le \bar\rho$. We define then

$$\mathsf{T} : \mathcal{D} \to \mathbb{R}, \qquad \Phi : \mathcal{D} \to \mathbb{R},$$

as

$$\mathsf{T}(h,c) = 2\int_{\rho_-(h,c)}^{\bar\rho} \frac{\rho}{\sqrt{2h\rho^2 + 2\rho^{2-\alpha} - c^2}} d\rho, \tag{A.25}$$

$$\Phi(h,c) = 2\int_{\rho_-(h,c)}^{\bar\rho} \frac{c}{\rho\sqrt{2h\rho^2 + 2\rho^{2-\alpha} - c^2}} d\rho. \tag{A.26}$$

The function T associates to the orbit with energy h and angular momentum c the time needed to go from a point at distance $\bar\rho$ from the center to return at the same distance, passing through the pericenter. The function Φ associates the total angle swept by this arc in time $\mathsf{T}(h,c)$.

With the same notations used to state Lemma A.3, the arcs connecting the points x_A, x_B in a fixed time τ, passing through the pericenter, are found as intersections of the level curves

$$\begin{cases} \mathsf{T}(h,c) = \tau, \\ \Phi(h,c) \equiv \varphi \pmod{2\pi}. \end{cases} \tag{A.27}$$

Level curves of these functions, computed numerically, are shown in Figure A.4, for $\alpha = 1.4$.

Therefore, to study the existence and the number of connecting arcs, we have to study the intersections between the level curves of the above functions. Note that on

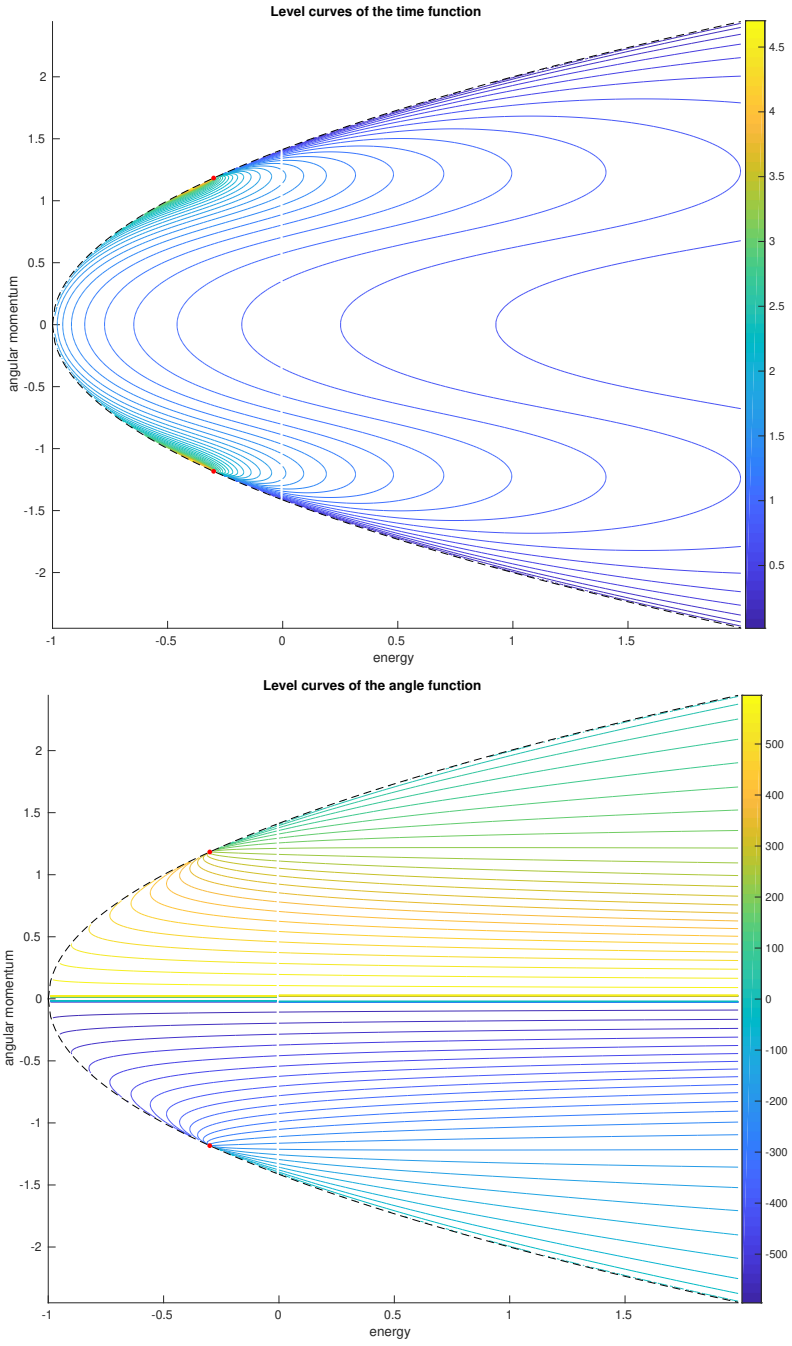

Figure A.4: The level curves of the functions T (top) and Φ (bottom) for $\alpha = 1.4$. The red points correspond to the points $(h_s, \pm c_s)$ of equation (A.24) where the two branches of the border join.

the border $\partial\mathcal{D}$, the function Φ computing the angle swept is 0 on the branch $\mathcal{C}^-$ and corresponds to the precession angle of the pericenter on the branch $\mathcal{C}^+$, hence

$$2\pi \leq \Phi|_{\mathcal{C}^+\cap\{c>0\}} \leq \frac{2}{2-\alpha}\pi, \quad -2\pi \geq \Phi|_{\mathcal{C}^+\cap\{c<0\}} \geq -\frac{2}{2-\alpha}\pi, \quad \Phi|_{\mathcal{C}^-} = 0.$$

In a similar way, the function T computing the time, is 0 on the branch $\mathcal{C}^-$ and corresponds to the time of passage between two pericenters $\mathtt{P}(h,c)$ on the branch $\mathcal{C}^+$, i.e.

$$\mathsf{T}|_{\mathcal{C}^+} = \mathtt{P}(h,c), \quad \mathsf{T}|_{\mathcal{C}^-} = 0.$$

Note also that we are interested in finding arcs connecting in the time of the parabolic collision-ejection solution $x_0(t)$, which we denoted by $2\tau(0)$. Therefore, it is clear that

$$\mathsf{T}(0,0) = 2\tau(0),$$

i.e. the point $(0,0) \in \mathcal{D}$ lies on the level curve of T we are interested in.
Asymptotic properties can be deduced for these functions. For instance, for the time function T we have that

$$\lim_{h\to+\infty} \mathsf{T}(h,c) = 0,$$

for every c. Indeed, we have the estimate

$$\begin{aligned}
0 &\leq \mathsf{T}(h,c) \\
&= \int_{\rho_-(h,c)}^{\bar\rho} \frac{\rho}{\sqrt{2h\rho^2 + 2\rho^{2-\alpha} - c^2}} d\rho \\
&\leq \int_{\rho_-(h,c)}^{\bar\rho} \frac{4\rho + \frac{2(2-\alpha)}{h}\rho^{1-\alpha}}{\sqrt{2h\rho^2 + 2\rho^{2-\alpha} - c^2}} d\rho \\
&= \frac{1}{h}\sqrt{2h\rho^2 + 2\rho^{2-\alpha} - c^2}\Big|_{\rho_-(h,c)}^{\bar\rho} \\
&= \frac{\sqrt{2h\bar\rho^2 + 2\bar\rho^{2-\alpha} - c^2}}{h}.
\end{aligned}$$

and the last term goes to 0 as $h \to +\infty$.

Moreover for negative energies, it is known (see [15]) that the angle of precession of the pericenter, defined by

$$\Delta\theta(h,c) = 2\int_{\rho_-(h,c)}^{\rho_+(h,c)} \frac{c}{\rho\sqrt{2h\rho^2 + 2\rho^{2-\alpha} - c^2}} d\rho,$$

satisfies

$$\lim_{c\to 0^\pm} \Delta\theta(h,c) = \pm\frac{2}{2-\alpha}\pi.$$

Hence we can write

$$\Delta\theta(h,c) = \Phi(h,c) + \Phi'(h,c),$$

where

$$\Phi'(h,c) = 2\int_{\bar\rho}^{\rho_+(h,c)} \frac{c}{\rho\sqrt{2h\rho^2 + 2\rho^{2-\alpha} - c^2}} d\rho.$$

and we get

$$\lim_{c\to 0^\pm} \Phi(h,c) = \pm\frac{2}{2-\alpha}\pi + \lim_{c\to 0^\pm} \Phi'(h,c).$$

Now, we note that

$$\begin{aligned}\lim_{c\to 0^\pm} \Phi'(h,c) &= 2\lim_{c\to 0^\pm} \int_{\bar\rho}^{\rho_+(h,c)} \frac{c}{\rho\sqrt{2h\rho^2 + 2\rho^{2-\alpha} - c^2}} d\rho \\ &= 2\lim_{c\to 0^\pm} \int_{\mathbb{R}} \frac{c}{\rho\sqrt{2h\rho^2 + 2\rho^{2-\alpha} - c^2}} \mathbb{1}_{[\bar\rho,\rho_+(h,c)]} d\rho \\ &= 0,\end{aligned}$$

where $\mathbb{1}_{[\bar\rho,\rho_+(h,c)]}$ denotes the characteristic function of the interval. The last equality follows from the Lebesgue theorem of dominated convergence. Indeed, the functions in the integral are all integrable, hence we can compute the limit as the integral of the pointwise limit function. To this end, we can compute that

$$\lim_{c\to 0^\pm} \rho_+(h,c) = \left(\frac{-1}{h}\right)^{\frac{1}{\alpha}},$$

and in particular it is bounded, thus the functions in the integral converge to 0 almost everywhere. Then, for negative energies, it follows that

$$\lim_{c\to 0^\pm} \Phi(h,c) = \pm\frac{2}{2-\alpha}\pi. \tag{A.28}$$

We can arrive to the same conclusion also for positive values of the energy. In this case, the total angle swept by the orbit is given by

$$\Delta\theta(h,c) = 2\int_{\rho_-(h,c)}^{\infty} \frac{c}{\rho\sqrt{2h\rho^2 + 2\rho^{2-\alpha} - c^2}} d\rho,$$

and we can still prove that

$$\lim_{c\to 0^\pm} \Delta\theta(h,c) = \pm\frac{2}{2-\alpha}\pi. \tag{A.29}$$

Indeed, assume that $c > 0$ (the case $c < 0$ is analogous), with the variable change $\rho = 1/u$ we get

$$\Delta\theta(h,c) = 2\int_0^{u_-(h,c)} \frac{1}{\sqrt{\frac{2h}{c^2} + \frac{2}{c^2}u^\alpha - u^2}} du,$$

where $u_-(h,c) = 1/\rho_-(h,c)$. With the variable change $s = u/u_-(h,c)$, and using the equation

$$h = \frac{c^2}{2}u_-(h,c)^2 - u_-(h,c)^\alpha, \tag{A.30}$$

we get that

$$\Delta\theta(h,c) = 2\int_0^1 \frac{1}{\sqrt{s(1-s)}} \frac{1}{\sqrt{1+\frac{1}{s}+a(h,c)\frac{1-s^\alpha}{s(1-s)}}} ds, \tag{A.31}$$

where

$$a(h,c) = \frac{2}{c^2} u_-(h,c)^{\alpha-2}.$$

Now, using (A.30), we can write

$$a(h,c) = 1 - \frac{2h}{c^2 u_-(h,c)^2}. \tag{A.32}$$

Since $h \geq 0$, then $\rho_-(h,c)$ is lower than the zero of V^c_{eff}, i.e.

$$\rho_-(h,c) \leq \rho_0 := \left(\frac{c^2}{2}\right)^{\frac{1}{2-\alpha}}.$$

Therefore

$$c^2 u_-(u,c)^2 \geq 2^{\frac{2}{2-\alpha}} c^{-\frac{2\alpha}{2-\alpha}},$$

hence

$$\frac{1}{c^2 u_-(u,c)^2} \leq 2^{-\frac{2}{2-\alpha}} c^{\frac{2\alpha}{2-\alpha}},$$

In particular, from (A.32) it follows that

$$\lim_{c\to 0^+} a(h,c) = 1.$$

Moreover, the functions in the integral in (A.31) are all uniformly bounded, then we can pass to the limit for $c \to 0^+$. In this manner, we obtain

$$\lim_{c\to 0^+} \Delta\theta(h,c) = 2\int_0^1 \frac{1}{\sqrt{s(1-s)}} \frac{1}{\sqrt{1+\frac{s-s^\alpha}{s^2-s}}} ds = \frac{2}{2-\alpha}\pi.$$

Still splitting the integral, we have that

$$\begin{aligned} \lim_{c\to 0^+} \Phi(h,c) &= \frac{2}{2-\alpha}\pi + 2\lim_{c\to 0^+} \int_{\bar\rho}^\infty \frac{c}{\rho\sqrt{2h\rho^2 + 2\rho^{2-\alpha} - c^2}} d\rho \\ &= \frac{2}{2-\alpha}\pi, \end{aligned} \tag{A.33}$$

where the last equality still follows from the dominated convergence theorem. In particular, the function Φ is discontinuous on the line $c = 0$.

Arcs passing through the apocenter On the other hand, similar functions can be defined considering the arcs passing through the apocenter. Of course, to do that the pericenter has to exist, hence we can define them only for $h < 0$, in such a way that $\rho_+(h,c)$ exists. Therefore we set

$$\mathcal{D}' := \mathcal{D} \cap \{(h,c) \in \mathbb{R}^2 : h < 0\}.$$

Then we define the functions

$$\mathsf{T}' : \mathcal{D}' \to \mathbb{R}, \qquad \Phi' : \mathcal{D}' \to \mathbb{R},$$

as

$$\mathsf{T}'(h,c) = 2\int_{\bar\rho}^{\rho_+(h,c)} \frac{\rho}{\sqrt{2h\rho^2 + 2\rho^{2-\alpha} - c^2}} d\rho, \tag{A.34}$$

$$\Phi'(h,c) = 2\int_{\bar\rho}^{\rho_+(h,c)} \frac{c}{\rho\sqrt{2h\rho^2 + 2\rho^{2-\alpha} - c^2}} d\rho, \tag{A.35}$$

which have the same meaning as before, but instead of taking the arc passing through the pericenter, we take the arc passing through the apocenter. Connecting arcs are still found as intersections between the level curves

$$\begin{cases} \mathsf{T}'(h,c) = \tau, \\ \Phi'(h,c) \equiv \varphi \pmod{2\pi}. \end{cases} \tag{A.36}$$

Level curves of these functions are represented in Figure A.5, in an example with $\alpha = 1.4$. Here the behaviour on the border is different. Indeed, for T' we have that

$$\mathsf{T}'|_{\mathcal{C}^+} = 0, \quad \mathsf{T}'|_{\mathcal{C}^-} = \mathsf{P}(h,c),$$

and moreover, since $\rho_+(h,c) \to +\infty$ for every admissible c as $h \to 0^-$, we have that

$$\lim_{h\to 0^-} \mathsf{T}'(h,c) = +\infty.$$

For the angle function Φ', we have that

$$2\pi \le \Phi'|_{\mathcal{C}^- \cap \{c>0\}} \le \frac{2}{2-\alpha}\pi, \quad -2\pi \ge \Phi'|_{\mathcal{C}^- \cap \{c<0\}} \ge -\frac{2}{2-\alpha}\pi, \quad \Phi'|_{\mathcal{C}^+} = 0.$$

Moreover, Φ' is continuous on the line $\{c = 0\}$ and

$$\Phi'(h,0) = 0,$$

for every admissible h, as we have seen before.

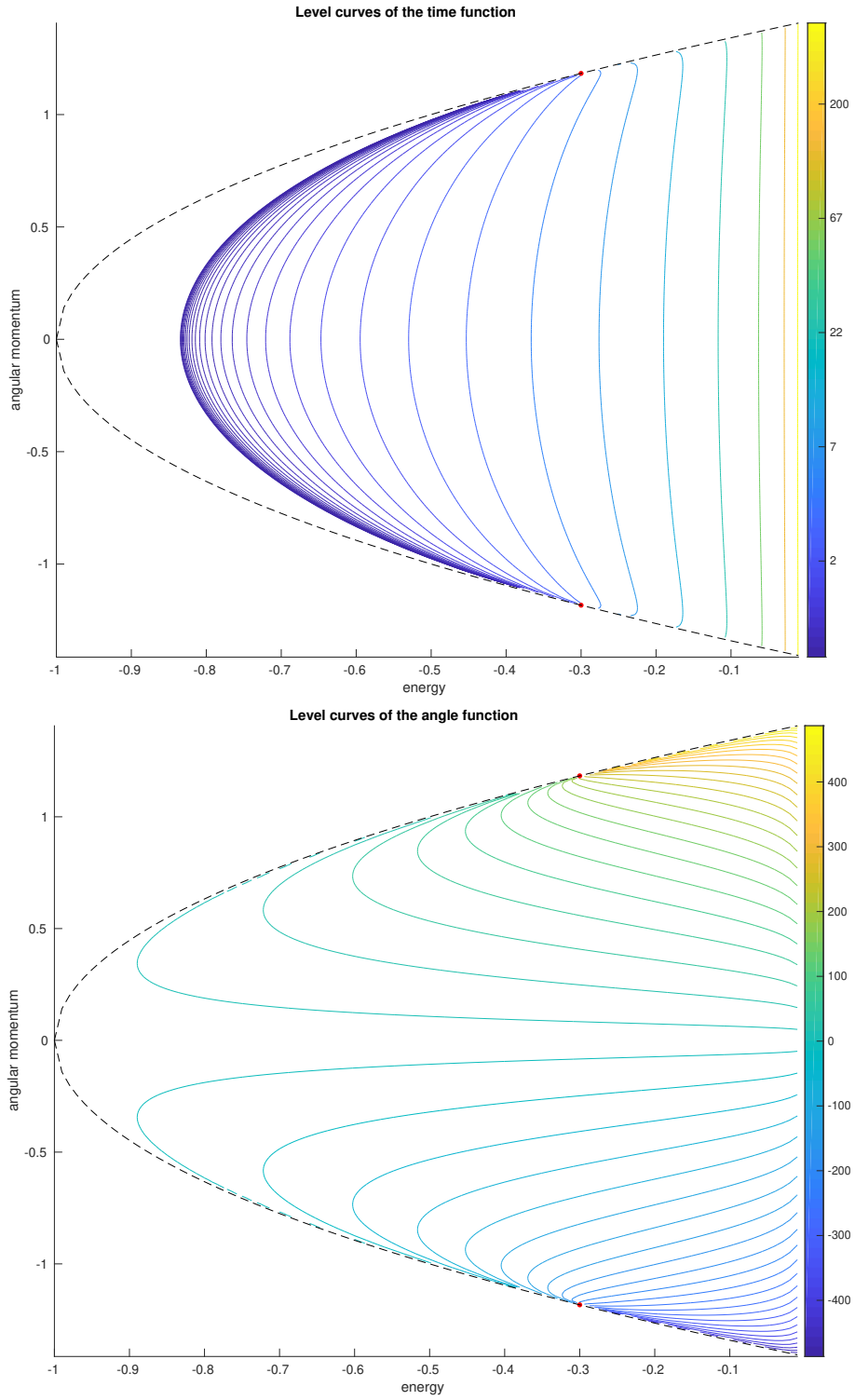

Figure A.5: The level curves of the functions T' (top) and Φ' (bottom) for $\alpha = 1.4$. The red points correspond to the points $(h_s, \pm c_s)$ of equation (A.24) where the two branches of the border join.

A.5 Action of connecting arcs

For a connecting arc $\bar{x}(t)$ with energy h and angular momentum c, using polar coordinates, the action becomes

$$\begin{aligned}\mathcal{A}(\bar{x}) &= \int_0^\tau \left(\frac{\dot\rho^2}{2} + \frac{c^2}{2\rho^2} + \frac{1}{\rho^\alpha}\right)dt \\ &= 2\int_0^{\frac{\tau}{2}} \left(\frac{\dot\rho^2}{2} + \frac{c^2}{2\rho^2} + \frac{1}{\rho^\alpha}\right)dt,\end{aligned}$$

where the last equation follows from the fact that connecting arcs defined above are symmetric. Using the conservation of the energy (A.9), we can write

$$\mathcal{A}(\bar{x}) = 2\int_0^{\frac{\tau}{2}} \left(h + \frac{2}{\rho^\alpha}\right)dt.$$

Still from the conservation of the energy, we can use ρ as independent variable instead of the time t, through the coordinate change

$$\frac{d\rho}{dt} = \pm\sqrt{2\left(h - \frac{c^2}{2\rho^2} + \frac{1}{\rho^\alpha}\right)}, \tag{A.37}$$

where the sign is $-$ if the arc passes through the pericenter and $+$ if it passes through the apocenter. Let us assume, for instance, that the arc passes through the pericenter, then the action becomes

$$\begin{aligned}\mathcal{A}(\bar{x}) &= 2\int_{\rho_-(h,c)}^{\bar\rho} \left(h + \frac{2}{\rho^\alpha}\right)\frac{d\rho}{\sqrt{2(h - \frac{c^2}{2\rho^2} + \frac{1}{\rho^\alpha})}} \\ &= 2\int_{\rho_-(h,c)}^{\bar\rho} \left(h + \frac{2}{\rho^\alpha}\right)\frac{\rho\, d\rho}{\sqrt{2h\rho^2 + 2\rho^{2-\alpha} - c^2}} \\ &= 2\int_{\rho_-(h,c)}^{\bar\rho} \frac{\rho\, d\rho}{\sqrt{2h\rho^2 + 2\rho^{2-\alpha} - c^2}} h + 4\int_{\rho_-(h,c)}^{\bar\rho} \frac{d\rho}{\rho^{\alpha-1}\sqrt{2h\rho^2 + 2\rho^{2-\alpha} - c^2}} \\ &= h\mathsf{T}(h,c) + 4\int_{\rho_-(h,c)}^{\bar\rho} \frac{d\rho}{\rho^{\alpha-1}\sqrt{2h\rho^2 + 2\rho^{2-\alpha} - c^2}}.\end{aligned} \tag{A.38}$$

Using the fact that for a connecting arc $\mathsf{T}(h,c) = \tau$, then we can write

$$\mathcal{A}(\bar{x}) = h\tau + 4\int_{\rho_-(h,c)}^{\bar\rho} \frac{d\rho}{\rho^{\alpha-1}\sqrt{2h\rho^2 + 2\rho^{2-\alpha} - c^2}}.$$

If the arc $\bar{x}$ passes through the apocenter, with similar computations we get that the action can be written as

$$\mathcal{A}(\bar{x}) = h\mathsf{T}'(h,c) + 4\int_{\bar\rho}^{\rho_+(h,c)} \frac{d\rho}{\rho^{\alpha-1}\sqrt{2h\rho^2 + 2\rho^{2-\alpha} - c^2}}. \tag{A.39}$$

A.6 Numerical examples

Here we show some numerical evidences, which can help in complete the proof of Lemmas A.3 and A.4 with the approach used above. In particular, Lemma A.4 is motivated by the fact that the total angle swept by an arc defined above cannot exceed the value

$$\frac{2\pi}{2-\alpha},$$

and moreover this is reached only in limit cases, either on the border $\partial\mathcal{D}$, or for $c \to 0^{\pm}$ where $\Phi(h,c)$ is discontinuous. Therefore, we expect that level curves of Φ, Φ' exist only for integer values k for which

$$-\frac{2\pi}{2-\alpha} < \varphi + 2k\pi < \frac{2\pi}{2-\alpha}.$$

These inequalities lead to the bounds

$$k_{\min} \le k \le k_{\max},$$

where $k_{\min}$ and $k_{\max}$ are defined by A.19 and A.20, respectively. Then, one have to prove that such level curves exist and intersect the level curve of the time function T only once, for each admissible value of k.

We see here numerical examples in which we discuss the behaviour of the level curves. To produce some tests we choose $\alpha = 1.4$, which allows a maximal deflection angle equals to

$$\frac{2\pi}{2-\alpha} = \frac{10}{3}\pi.$$

We use different values for the angle $\varphi \in [0, 2\pi)$ between the two ending points. These values are chosen in order to take into account also the particular cases in which the expressions

$$\frac{1}{2-\alpha} + \frac{\varphi}{2\pi}, \quad \frac{1}{2-\alpha} - \frac{\varphi}{2\pi},$$

assume an integer value. The values of φ and $k_{\min}$, $k_{\max}$ computed by (A.19), (A.20) respectively, are reported in Table A.1. In three cases, we expect three different connecting arcs, while in one case we expect four connecting arcs. Moreover, for $\varphi = 11\pi/9$, $4\pi/3$ we expect to have two connecting arcs with negative angular momentum. To actually find the connecting arcs, we numerically compute the functions T, Φ for the arcs passing through the pericenter and the function T', Φ' for the arcs passing through the apocenter. The value chosen for the distance is $\bar{\rho} = 1$ and the total time for the parabolic collision-ejection solution to go from the starting point to the ending point is

$$\mathsf{T}(0,0) \simeq 0.8318903.$$

We plot then the level curve of T corresponding to the value $\mathsf{T}(0,0)$, and the level curves of Φ corresponding to the values $\varphi \pmod{2\pi}$. Plots of these curves are reported

φ	$\frac{1}{2-\alpha}+\frac{\varphi}{2\pi}$	$\frac{1}{2-\alpha}-\frac{\varphi}{2\pi}$	$k_{\min}$	$k_{\max}$
$\frac{1}{3}\pi$	$\frac{11}{6}$	$\frac{3}{2}$	-1	1
$\frac{2}{3}\pi$	2	1	-1	1
$\frac{11}{9}\pi$	$\frac{41}{11}$	$\frac{18}{11}$	-2	1
$\frac{4}{3}\pi$	$\frac{7}{3}$	1	-2	0

Table A.1: Values of $k_{\min}$, $k_{\max}$ obtained from (A.19), (A.20) respectively, for some values of the angle $\varphi \in [0, 2\pi)$, computed for $\alpha = 1.4$.

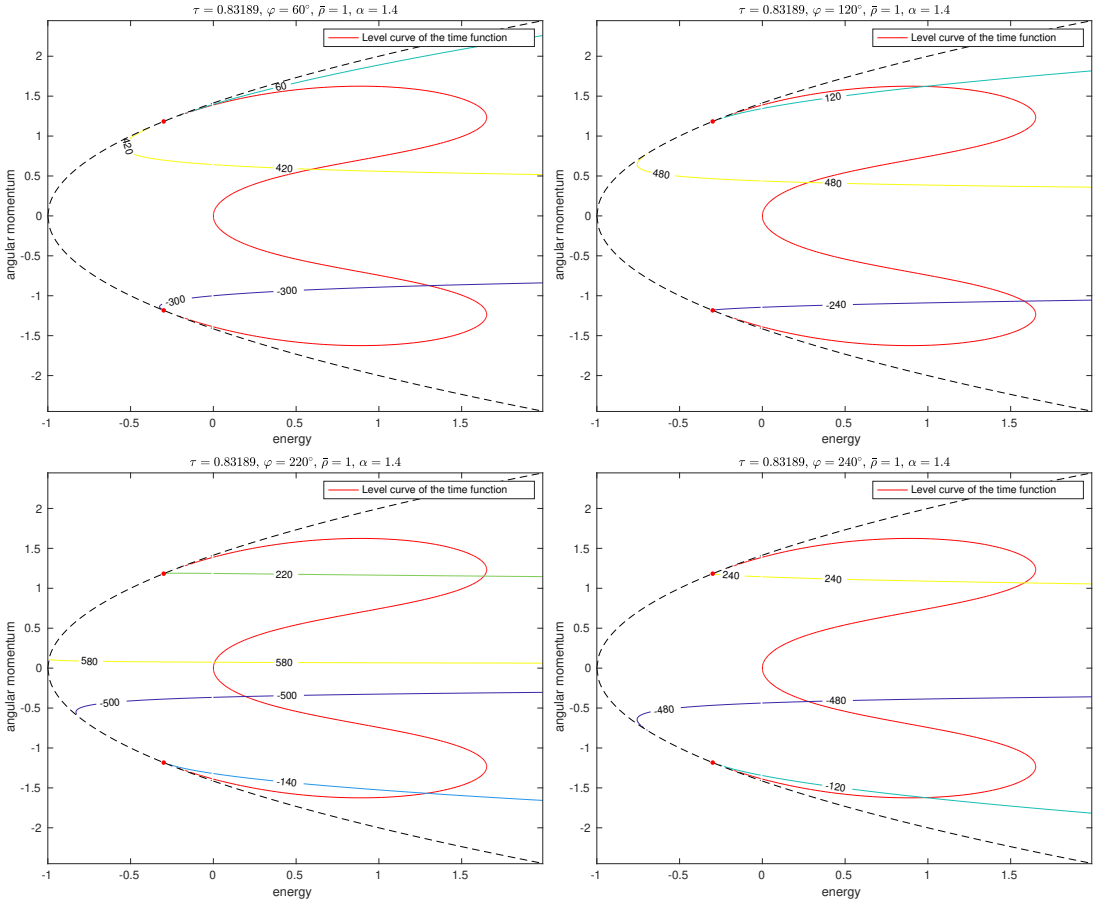

Figure A.6: Intersections between the level curves of the function T and Φ. The red curve is the level curve of T corresponding to time needed for the parabolic collision-ejection solution to go from the starting point to the ending point. The other curves correspond to level curves of $\Phi(h, c) = \varphi \pmod{2\pi}$. The values used are $\varphi = \pi/3$, $2\pi/3$, $11\pi/9$, $4\pi/3$ to produce the figures top left, top right, bottom left, bottom right, respectively.

in Figure A.6. As we can see from these figures, we can recover the number of arcs computed from Table A.6.

Indeed, for the case $\varphi = \pi/3$, we recognize three different intersections between the curves, corresponding to three different connecting arcs passing through the pericenter. Moreover, only one of them has negative angular momentum, in agreement with the values of $k_{\min}$ and $k_{\max}$. The case $\varphi = 2\pi/3$ is similar to the previous one.

When we increase the angle between the points, we see that another connecting arc appears, as in the case $\varphi = 11\pi/9$: here in fact there are four intersection points. Moreover, two of them have negative angular momentum.

Increasing again the angle, one of the arcs with positive angular momentum disappear, as in the case $\varphi = 4\pi/3$, and the total number of connecting arcs is again three.

From these figures (and also from Figure A.4), it seems that every level curve of T is bounded and they end in the singular points $(h_s, \pm c_s)$. These points seem to be focal points also for the level curves of Φ, as we can see from Figure A.4, bottom. Instead, looking at the level curves of the function T' and Φ', represented in Figure A.5, we see that T' is very flat for energies $h \leq h_s$. Since we are interested in the level curve of value $\mathsf{T}(0,0)$ reported above, we expect this curve to lie in this region. Level curves of Φ' passing in $h \leq h_s$ have a moderate level value. Therefore, we expect to find connecting arcs passing through the apocenter only for small values of φ.

Indeed, in the above examples, we plotted also the level curves of T' and Φ', but we did not find any intersection between them, suggesting that all the connecting arcs pass through the pericenter in these case.

Using a shooting method, we were able to compute accurate initial velocity needed to obtain the connecting arcs. From these values, we computed the energy and the angular momentum: in this way we found the intersection points that we see in the plots of Figure A.6. Then, integrating numerically the equation of motion, we obtained the entire time evolution of the connecting arcs (which are shown in Figure A.7), and we also computed the corresponding values of the action. These values are all reported in Table A.2. The action of the parabolic collision-ejection solution is computed through (A.15) and it results to be

$$\mathcal{A}(x_0) = 9.42809.$$

As we can see from the values reported in the table, the action of the connecting arcs is always lower than the action of the parabolic collision-ejection solution.

As we have seen, the intersection of the level curve of the time function T with the level curve of the angle function Φ is used to recover the number of connecting arcs. However, from the examples above we understand that, to prove Lemma A.3, what is important is only the value of the action along the level curve of T. Indeed, it seems that the intersections can take place at any point of this curve, since we have to take into account any angle $\varphi \in [0, 2\pi)$ between the two ending points. To this end, we can define two additional functions

$$\mathsf{A} : \mathcal{D} \to \mathbb{R}, \qquad \mathsf{A}' : \mathcal{D}' \to \mathbb{R},$$

using formulas (A.38) and (A.39), respectively. The function $\mathsf{A}(h,c)$ (resp. $\mathsf{A}'(h,c)$) computes the action of an arc passing through the pericenter (resp. apocenter), connecting two points at a distance $\bar{\rho}$ from the origin, in time $\mathsf{T}(h,c)$. Therefore, Marchal's

φ	h	c	action
$\frac{1}{3}\pi$	-0.2321566	1.2378042	1.49036
	0.5943874	0.5838823	8.44843
	1.3033445	-0.8734238	6.92642
$\frac{2}{3}\pi$	0.9838781	1.6217948	3.07209
	0.2782592	0.4184355	8.97619
	1.5813843	-1.0677468	5.91637
$\frac{11}{9}\pi$	1.2891075	-1.5677844	3.63051
	0.1941770	-0.3554013	9.11137
	0.0077296	0.0739359	9.41517
	1.6347522	1.1523729	5.52925
$\frac{4}{3}\pi$	0.9838781	-1.6217948	3.07209
	0.2782592	-0.4184355	8.97619
	1.5813843	1.0677468	5.91637

Table A.2: The values of the energy and angular momentum corresponding to the intersection points, for the cases analyzed above. In the last column we report also the value of the action of the arc.

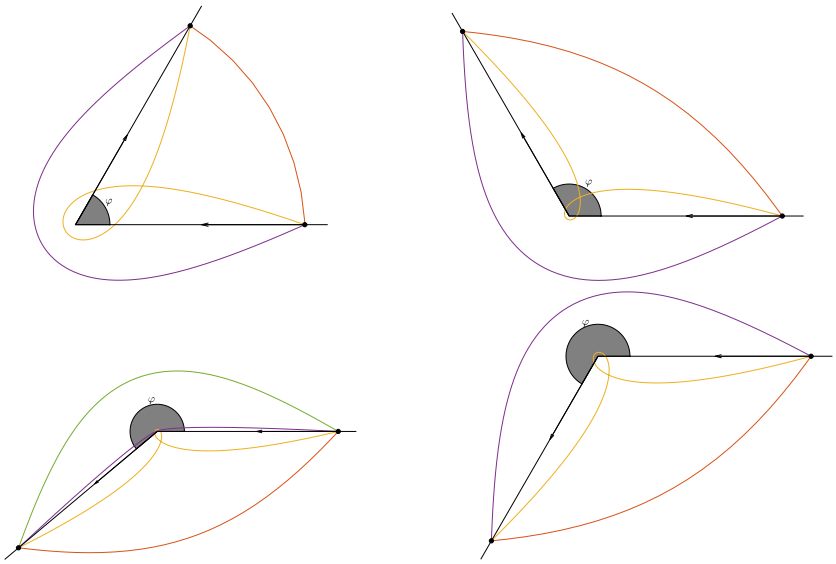

Figure A.7: The connecting arcs in the cases analyzed above.

Lemma traduces in the inequality

$$\mathsf{A}(h,c)\Big|_{\left\{(h,c)\in\mathcal{D}:\,\mathsf{T}(h,c)=\mathsf{T}(0,0)\right\}} \leq \mathsf{A}(0,0),$$

where the equal sign holds if and only if $(h,c)=(0,0)$, for the arcs passing through the

pericenter. For the arcs passing through the apocenter, it becomes

$$\mathsf{A}'(h,c)\Big|_{\left\{(h,c)\in\mathcal{D}':\,\mathsf{T}'(h,c)=\mathsf{T}(0,0)\right\}} < \mathsf{A}(0,0).$$

In Figure A.8 we show example with the level curves of A, numerically computed for

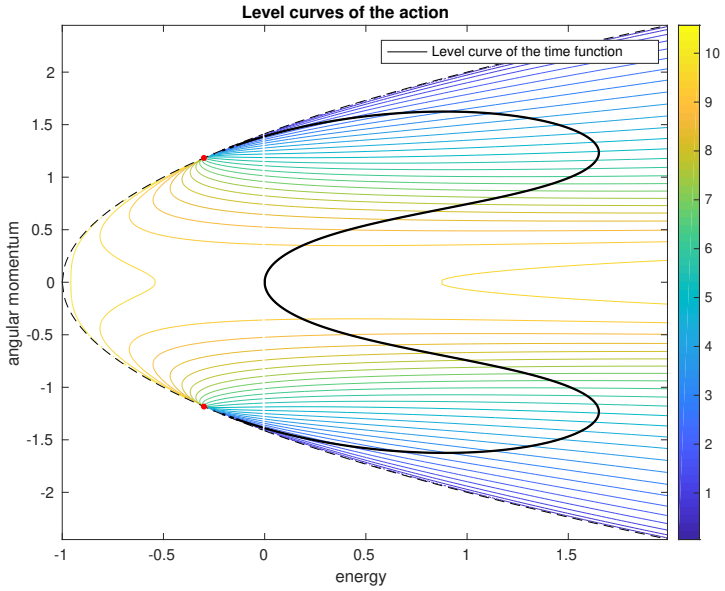

Figure A.8: Level curves of the function A. The black curve passing through $(0,0)$ is $\{(h,c) : \mathsf{T}(h,c) = \mathsf{T}(0,0)\}$.

$\alpha = 1.4$ and $\bar{\rho} = 1$. In the same plot, we reported also the level curve

$$\{(h,c) \in \mathcal{D} : \mathsf{T}(h,c) = \mathsf{T}(0,0)\}$$

of the time function, corresponding to the black thick curve. Recall that the values (h,c) belonging to this curve correspond to possible connecting arcs passing through the pericenter. Stating from the point $(0,0)$ and following the black curve, we can see that the value of A decreases, suggesting that $(0,0)$ is actually the maximum on this curve. Since the point $(0,0)$ corresponds to the parabolic collision-ejection solution, this would prove that any other connecting arc has action lower than the collision solution, as stated in Lemma A.3.

Appendix B

Properties of solutions with partial collisions

We recall here the uniqueness result of [40] and propose an extension to $\alpha \in (1,2)$. Suppose that $w : (0,\bar{t}) \to \mathbb{R}^3$ is a maximal ejection solution of (1.13) (or (2.48) for $\alpha \in (1,2)$), having a collision on an axis r for $t = 0$. We denote with $\mathtt{e}_r$ the unit vector parallel to r and with R_π the rotation of an angle π around r. Then, we have that there exist $b \in \mathbb{R}$ and a unit vector $\mathtt{n}$ orthogonal to r such that

$$\lim_{t\to 0^+} \frac{\dot{w}(t) + R_\pi \dot{w}(t)}{2} = b\mathtt{e}_r, \tag{B.1}$$

$$\lim_{t\to 0^+} \frac{w(t) - R_\pi w(t)}{|w(t) - R_\pi w(t)|} = \lim_{t\to 0^+} \frac{w(t)}{|w(t)|} = \mathtt{n}. \tag{B.2}$$

The unit vector $\mathtt{n}$ is the ejection direction we used in Chapters 1 and 2. The following result generalizes Proposition 5.6 in [40] to the case of α-homogeneous potentials. We omit the proof, that can be derived from the results in [38], [9].

Proposition B.1. *Let $w : (0,\bar{t}) \to \mathbb{R}^3$ be a maximal solution of (2.49). Assume that*

$$\lim_{t\to 0^+} w(t) = 0. \tag{B.3}$$

Then
(i) there exist $b \in \mathbb{R}$ and a unit vector $\mathtt{n}$, orthogonal to r, such that

$$\lim_{t\to 0^+} \frac{\dot{w}(t) + R_\pi \dot{w}(t)}{2} = b\mathtt{e}_r, \tag{B.4}$$

$$\lim_{t\to 0^+} \frac{w(t) - R_\pi w(t)}{|w(t) - R_\pi w(t)|} = \lim_{t\to 0^+} \frac{w(t)}{|w(t)|} = \mathtt{n}. \tag{B.5}$$

(ii) The rescaled function $w^\lambda : [0,1] \to \mathbb{R}^3$ defined by $w^\lambda(0) = 0, w^\lambda(\tau) = \lambda^{2/(2+\alpha)} w(\tau/\lambda), \lambda > 1/\bar{t}$, satisfies

$$\begin{aligned} &\lim_{\lambda\to+\infty} w^\lambda(\tau) = s^\alpha(\tau)\mathtt{n} \text{ uniformly in } [0,1], \\ &\lim_{\lambda\to+\infty} \dot{w}^\lambda(\tau) = \dot{s}^\alpha(\tau)\mathtt{n} \text{ uniformly in } [\delta,1], 0 < \delta < 1, \end{aligned} \tag{B.6}$$

where

$$s^\alpha(\tau) = \frac{(2+\alpha)^{2/(2+\alpha)}}{2} c_\alpha^{1/(2+\alpha)} \tau^{2/(2+\alpha)}, \tau \in [0, +\infty)$$

is the parabolic ejection motion, that is the solution of

$$\dot{s} = (c_\alpha/2^\alpha)^{1/2} s^{-\alpha/2}$$

that satisfies $\lim_{\tau \to 0^+} s(\tau) = 0$.
(iii) The following estimates hold for positive constants t_0, ρ_0, x_0, C_j, $j = 1, .., 7$ *that depend only on* b *and on the energy constant* h.

$$\begin{cases} C_1 t^{2/(2+\alpha)} \le \rho(t) \le C_2 t^{2/(2+\alpha)}, & \\ C_3 t^{-\alpha/(2+\alpha)} \le \dot{\rho}(t) \le C_4 t^{-\alpha/(2+\alpha)}, & t \in (0, t_0], \\ |\frac{dx}{d\rho} - 1| \le C_5 \rho^{1+\alpha}, & \rho \in (0, \rho_0], \\ |y'| \le C_6 x^{\alpha/2}, \qquad |z'| \le C_7 x^{1+\alpha}, & x \in (0, x_0], \end{cases} \tag{B.7}$$

where $\rho = \frac{1}{2}|(R_\pi - I)w|$ *and* x, y, z *are the components of* w *on* n, e_r, $\mathsf{e}_\perp = \mathsf{e}_r \times \mathsf{n}$ *and* $'$ *denotes differentiation with respect to* x.

The same result stated in Proposition 5.9 of [40] holds also in the case of α-homogeneous potentials. We recall the statement below.

Proposition B.2. *Let* $w_i : (0, \bar{t}_i) \to \mathbb{R}^3$, $\bar{t}_i > 0$, $i = 1, 2$ *be two maximal solutions of* (2.48) *such that*

$$\lim_{t \to 0^+} w_i(t) = 0, \quad i = 1, 2.$$

If $h_i, b_i, \mathtt{n}_i$, $i = 1, 2$ *are the corresponding values of the energy and the values of* b *and* $\mathtt{n}$ *given by* (B.1) *and* (B.2)*, respectively, then*

$$\begin{cases} h_1 = h_2, \\ b_1 = b_2, \\ \mathtt{n}_1 = \mathtt{n}_2, \end{cases} \implies \begin{cases} \bar{t}_1 = \bar{t}_2, \\ w_1 = w_2. \end{cases}$$

Proof. The proof follows exactly the same steps as in the case $\alpha = 1$. Here we recall the main points. Projecting the equation of motion (2.49) onto the basis $\mathsf{n}, \mathsf{e}_r, \mathsf{e}_\perp$ and setting

$$w = x\mathsf{n} + y\mathsf{e}_r + z\mathsf{e}_\perp$$

we get

$$\begin{cases} \ddot{x} = -\dfrac{\alpha c_\alpha}{(2x)^{1+\alpha}(1 + \frac{z^2}{x^2})^{\frac{2+\alpha}{2}}} + V_1 \cdot \mathsf{n} \\ \ddot{y} = V_1 \cdot \mathsf{e}_r \\ \ddot{z} = -\dfrac{\alpha c_\alpha z}{2^{1+\alpha} x^{2+\alpha}(1 + \frac{z^2}{x^2})^{\frac{2+\alpha}{2}}} + V_1 \cdot \mathsf{e}_\perp \end{cases} . \tag{B.8}$$

We take x as independent variable and write the energy equation (2.50) as

$$\dot{x}^2(1+|y'|^2+|z'|^2)=\frac{c_\alpha}{(2x)^\alpha(1+\frac{z^2}{x^2})^{\frac{\alpha}{2}}}+V+h, \tag{B.9}$$

where $'$ denotes differentiation with respect to x. Setting

$$x=e^s, \qquad s\in(-\infty,s_0], \tag{B.10}$$

where $s_0<0$ is chosen later, and introducing the variables

$$\eta=\frac{dy}{ds}, \qquad \zeta=\frac{dz}{ds}$$

we can write the first order system

$$\begin{cases} \dfrac{dy}{ds}=\eta, \quad \dfrac{d\eta}{ds}=\Big(\dfrac{2+\alpha}{2}+\dfrac{\alpha}{2}\mathcal{U}\Big)\eta+e^{(2+\alpha)s}\mathcal{A} \\ \dfrac{dz}{ds}=\zeta, \quad \dfrac{d\zeta}{ds}=\Big(\dfrac{2+\alpha}{2}+\dfrac{\alpha}{2}\mathcal{U}\Big)\zeta-\Big(\dfrac{\alpha}{2}+\dfrac{\alpha}{2}\mathcal{V}\Big)z+e^{(2+\alpha)s}\mathcal{B} \end{cases}, \tag{B.11}$$

where $\mathcal{U},\mathcal{A},\mathcal{V},\mathcal{B}$ are defined by relations

$$\begin{aligned}
1+\mathcal{U}&=\frac{(1+|y'|^2+|z'|^2)}{(1+\frac{z^2}{x^2})^{\frac{2+\alpha}{2}}}\frac{\Big(1-(2x)^{1+\alpha}(1+\frac{z^2}{x^2})^{\frac{2+\alpha}{2}}\frac{V_1\cdot\mathsf{n}}{\alpha c_\alpha}\Big)}{\Big(1+(2x)^\alpha(1+\frac{z^2}{x^2})^{\frac{\alpha}{2}}\frac{V+h}{c_\alpha}\Big)},\\
1+\mathcal{W}&=\frac{(1+|y'|^2+|z'|^2)(1+\frac{z^2}{x^2})^{\frac{\alpha}{2}}}{1+(2x)^\alpha(1+\frac{z^2}{x^2})^{\frac{\alpha}{2}}\frac{V+h}{c_\alpha}},\\
\mathcal{A}&=\frac{2^\alpha}{c_\alpha}V_1\cdot\mathsf{e}_r(1+\mathcal{W}),\\
1+\mathcal{V}&=\frac{1}{(1+\frac{z^2}{x^2})^{\frac{2+\alpha}{2}}}(1+\mathcal{W}),\\
\mathcal{B}&=\frac{2^\alpha}{c_\alpha}V_1\cdot\mathsf{e}_\perp(1+\mathcal{W}).
\end{aligned}$$

System B.11 can be written in compact form as

$$\frac{d\gamma}{ds}=M\gamma+\mathcal{N}(\gamma,s) \tag{B.12}$$

where $\gamma=(y,z,\eta,\zeta)^T$,

$$\mathcal{N}(\gamma,s)=\Big(0,0,\frac{\alpha}{2}\mathcal{U}\eta+e^{(2+\alpha)s}\mathcal{A},\frac{\alpha}{2}\mathcal{U}\zeta-\frac{\alpha}{2}\mathcal{V}z+e^{(2+\alpha)s}\mathcal{B}\Big)^T$$

and M is the constant matrix

$$M=\begin{bmatrix} 0 & 0 & 1 & 0 \\ 0 & 0 & 0 & 1 \\ 0 & 0 & \frac{2+\alpha}{2} & 0 \\ 0 & -\frac{\alpha}{2} & 0 & \frac{2+\alpha}{2} \end{bmatrix}.$$

To each solution w of (2.49) satisfying (B.3) there corresponds a solution γ_w of (B.12) and this correspondence is 1–1. Moreover, from the estimates (B.7), we can find a constant $C_0 > 0$, depending only on h, b, such that

$$|\gamma_w(s)| \leq C_0 e^{\frac{2+\alpha}{2}s}, \qquad s \in (-\infty, s_0]. \tag{B.13}$$

Computing explicitly the eigenvalues

$$\lambda_1 = 0, \qquad \lambda_2 = \frac{\alpha}{2}, \qquad \lambda_3 = 1, \qquad \lambda_4 = \frac{2+\alpha}{2},$$

and the eigenvectors

$$\rho_1 = (1,0,0,0)^T, \quad \rho_2 = (0,1,0,\tfrac{\alpha}{2})^T, \quad \rho_3 = (0,1,0,1)^T, \quad \rho_4 = (1,0,\tfrac{2+\alpha}{2},0)^T,$$

of the matrix M, we find that there exists a constant $C_1 > 0$ such that

$$|e^{Ms}| \leq C_1 e^{\frac{2+\alpha}{2}s}, \quad s \in [0, +\infty). \tag{B.14}$$

Let us consider a solution of the homogeneous equation $\frac{d\gamma}{ds} = M\gamma$ of the form

$$\gamma_\delta(s) = e^{\frac{2+\alpha}{2}s}\delta\rho_4, \qquad \delta \in \mathbb{R}. \tag{B.15}$$

Given $K > 0$ and $c \in (0, \frac{\alpha}{2}]$, consider the complete metric space of the continuous maps

$$X = \{\gamma : (-\infty, s_0] \to \mathbb{R}^4 : |(\gamma - \gamma_\delta)(s)| \leq K e^{(1+c)s}\}, \tag{B.16}$$

endowed with the distance

$$d(\gamma, \tilde{\gamma}) = \max_{s \in (-\infty, s_0]} |\gamma(s) - \tilde{\gamma}(s)| e^{-s}. \tag{B.17}$$

For each fixed δ and for K large enough we have

$$\gamma_w \in X$$

for all solutions w of (2.49), (B.3) corresponding to given values of h, b, n. Moreover, solutions of (2.49) correspond to continuous solutions $\gamma : (-\infty, s_0] \to \mathbb{R}^4$ of the nonlinear integral equation

$$\gamma(s) = \gamma_\delta(s) + \int_{-\infty}^{s} e^{M(s-r)} \mathcal{N}(\gamma(r), r) dr. \tag{B.18}$$

We can show that the map

$$(T\gamma)(s) = \gamma_\delta(s) + \int_{-\infty}^{s} e^{M(s-r)} \mathcal{N}(\gamma(r), r) dr \tag{B.19}$$

defines a contraction on X for $-s_0 > 0$ sufficiently large, implying that equation (B.18) has a unique solution for each $\delta \in \mathbb{R}$. Moreover, the choice of δ is uniquely determined by the value of b in (B.4).

From the estimates

$$\mathcal{U}, \mathcal{V}, \mathcal{W} = O(e^{\alpha s}), \qquad \mathcal{A}, \mathcal{B} = O(1) \quad s \in (-\infty, s_0] \tag{B.20}$$

and, for the gradients,

$$\mathcal{U}_\gamma, \mathcal{V}_\gamma, \mathcal{A}_\gamma, \mathcal{B}_\gamma = O(e^{-\frac{(2-\alpha)}{2}s}), \qquad s \in (-\infty, s_0], \tag{B.21}$$

we get

$$|\mathcal{N}(\gamma(s), s)| \leq Ce^{\frac{2+3\alpha}{2}s} \qquad |\mathcal{N}(\gamma(s), s) - \mathcal{N}(\tilde{\gamma}(s), s)| \leq Ce^{(1+\alpha)s} d(\gamma, \tilde{\gamma}) \tag{B.22}$$

and, by (B.14),

$$|(T\gamma)(s) - \gamma_\delta(s)| \leq Ce^{\frac{2+3\alpha}{2}s}, \quad s \in (-\infty, s_0], \tag{B.23}$$

and

$$d(T\gamma, T\tilde{\gamma}) \leq Ce^{\alpha s_0} d(\gamma, \tilde{\gamma}), \qquad \forall \gamma, \tilde{\gamma} \in X. \tag{B.24}$$

Relation (B.24) shows that the map $T : X \to X$ is a contraction, provided $-s_0 > 0$ is sufficiently large.

If $\gamma = (y, z, \eta, \zeta)^T$ is the fixed point of T, (B.23) implies that

$$\lim_{s \to -\infty} |\gamma(s) - \gamma_\delta(s)| e^{-\frac{2+\alpha}{2}s} = 0. \tag{B.25}$$

Proposition B.1 and the variable change (B.10) imply the asymptotic estimates

$$t \propto \frac{2}{2+\alpha} \sqrt{\frac{2^\alpha}{c_\alpha}} e^{\frac{2+\alpha}{2}s}, \qquad \frac{dt}{dx} \propto \sqrt{\frac{2^\alpha}{c_\alpha}} e^{\frac{\alpha}{2}s}. \tag{B.26}$$

From these asymptotic formulas and (B.25) it follows that

$$\delta = \frac{2}{2+\alpha} \sqrt{\frac{2^\alpha}{c_\alpha}} b.$$

□

Bibliography

[1] A. Abad, R. Barrio, and Á. Dena. Computing periodic orbits with arbitrary precision. *Phys. Rev. E*, 84:016701, 2011.

[2] A. Ambrosetti and V. Coti-Zelati. *Periodic Solutions of Singular Lagrangian Systems*. Progress in Nonlinear Differential Equations and Their Applications. Birkhäuser Boston, 1993.

[3] K. Appel and W. Haken. Every planar map is four colorable. Part I: Discharging. *Illinois J. Math.*, 21(3):429–490, 09 1977.

[4] K. Appel, W. Haken, and J. Koch. Every planar map is four colorable. Part II: Reducibility. *Illinois J. Math.*, 21(3):491–567, 09 1977.

[5] V.I. Arnold. *Mathematical Methods of Classical Mechanics*. Graduate Texts in Mathematics. Springer New York, 1978.

[6] U. M. Ascher and L. R. Petzold. *Computer Methods for Ordinary Differential Equations and Differential-Algebraic Equations*. Society for Industrial and Applied Mathematics, Philadelphia, PA, USA, 1st edition, 1998.

[7] E. Barrabés, J. M. Cors, C. Pinyol, and J. Soler. Hip-hop solutions of the $2N$-body problem. *Celestial Mechanics and Dynamical Astronomy*, 95(1):5–66, May 2006.

[8] R. Barrio, M. Rodríguez, A. Abad, and F. Blesa. Breaking the limits: The Taylor series method. *Appl. Math. Comput.*, 217(20):7940–7954, 2011.

[9] V. Barutello, D. L. Ferrario, and S. Terracini. On the singularities of generalized solutions to n-body type problems. *Int. Math. Res. Not.*, ??:1–78, 2008.

[10] .V Barutello, S. Terracini, and G. Verzini. Entire minimal parabolic trajectories: The planar anisotropic kepler problem. *Archive for Rational Mechanics and Analysis*, 207(2):583–609, Feb 2013.

[11] U. Bessi and V. Coti Zelati. Symmetries and noncollision closed orbits for planar N-body-type problems. *Nonlinear Anal.*, 16(6):587–598, 1991.

[12] R. Bevilacqua, D. Bini, M. Capovani, and O. Menchi. *Metodi Numerici*. Zanichelli, 1992.

[13] A. Braides. *Gamma-convergence for Beginners*. Oxford Lecture Series in Mathe. Oxford University Press, 2002.

[14] J. F. Cariñena, M. F. Rañada, and M. Santander. Central potentials on spaces of constant curvature: The Kepler problem on the two-dimensional sphere S^2 and the hyperbolic plane H^2. *Journal of Mathematical Physics*, 46(5), 2005.

[15] R. Castelli. *On the variational approach to the one and N-center problem with weak forces*. PhD thesis, Università degli Studi di Milano-Bicocca, 2009.

[16] A. Celletti. *The Levi-Civita, KS and Radial-Inversion Regularizing Transformations*, pages 25–48. Springer Berlin Heidelberg, Berlin, Heidelberg, 2002.

[17] K.-C. Chen. Binary decompositions for planar N-body problems and symmetric periodic solutions. *Arch. Ration. Mech. Anal.*, 170(3):247–276, 2003.

[18] K. C. Chen. Existence and minimizing properties of retrograde orbits to the three-body problem with various choices of masses. *Annals of Mathematics*, 167(2):325–348, 2008.

[19] A. Chenciner. Action minimizing solutions of the newtonian n-body problem: from homology to symmetry. In *Proceedings of the International Congress of Mathematicians, Vol. III (Beijing, 2002)*, pages 279–294. Higher Ed. Press, Beijing, 2002.

[20] A. Chenciner and R. Montgomery. A remarkable periodic solution of the three-body problem in the case of equal masses. *Annals of Mathematics*, 152(3):881–901, 2000.

[21] A. Chenciner and A. Venturelli. Minima de l'intégrale d'action du problème newtonien de 4 corps de masses égales dans $\mathbf{R}^3$: orbites "hip-hop". *Cel. Mech. Dyn. Ast.*, 77(2):139–152, 2000.

[22] F. Clarke. *Functional Analysis, Calculus of Variations and Optimal Control*. Graduate Texts in Mathematics. Springer London, 2013.

[23] F. H. Clarke and V. Zeidan. Sufficiency and the Jacobi condition in the calculus of variations. *Canad. J. Math.*, 38(5):1199–1209, 1986.

[24] V. Coti Zelati. Periodic solutions for N-body type problems. *Annales de l'I.H.P. Analyse non linéaire*, 7(5):477–492, 1990.

[25] B. Dacorogna. *Introduction to the Calculus of Variations*. Imperial College Press, 2004.

[26] G. Dal Maso. *An Introduction to Gamma-convergence*. Progress in nonlinear differential equations and their applications. Birkhäuser, 1993.

[27] I. Davies, A. Truman, and Z. Williams. Classical periodic solutions of the equal-mass $2n$-body problem, $2n$-ion problem and the n-electron atom problem. *Physics Letters A*, 99(1):15 – 18, 1983.

[28] E. De Giorgi. Sulla convergenza di alcune successioni d'integrali del tipo dell'area. *Rend. Mat. (6)*, 8:277–294, 1975.

[29] E. De Giorgi. Γ-convergenza e G-convergenza. *Boll. Un. Mat. Ital. A (5)*, 14(2):213–220, 1977.

[30] E. De Giorgi and T. Franzoni. Su un tipo di convergenza variazionale. *Atti Accad. Naz. Lincei Rend. Cl. Sci. Fis. Mat. Natur. (8)*, 58(6):842–850, 1975.

[31] M. Degiovanni and F. Giannoni. Dynamical systems with Newtonian type potentials. *Ann. Scuola Norm. Sup. Pisa Cl. Sci. (4)*, 15(3):467–494, 1988.

[32] F. Diacu. *Relative Equilibria of the Curved N-Body Problem*. Atlantis Studies in Dynamical Systems. Atlantis Press, 2012.

[33] Z. Došlá and O. Došlý. Quadratic functionals with general boundary conditions. *Appl. Math. Optim.*, 36(3):243–262, 1997.

[34] M. Fenucci. `http://adams.dm.unipi.it/~fenucci/research/nbody.html`.

[35] M. Fenucci. `http://adams.dm.unipi.it/~fenucci/research/gammaconv.html`.

[36] M. Fenucci. `http://adams.dm.unipi.it/~fenucci/research/coulomb.html`.

[37] M. Fenucci and G. F. Gronchi. On the stability of periodic N-body motions with the symmetry of Platonic polyhedra. *Nonlinearity*, 31(11):4935, 2018.

[38] D. L. Ferrario and S. Terracini. On the existence of collisionless equivariant minimizers for the classical n-body problem. *Inventiones mathematicae*, 155(2):305–362, 2004.

[39] C. Froeschle. Numerical study of dynamical systems with three degrees of freedom. *Astronomy and Astrophysics*, 5:177–183, apr 1970.

[40] G. Fusco, G. F. Gronchi, and P. Negrini. Platonic polyhedra, topological constraints and periodic solutions of the classical N-body problem. *Inventiones mathematicae*, 185(2):283–332, 2011.

[41] T. Gallardo. Atlas of the mean motion resonances in the solar system. *Icarus*, 184(1):29 – 38, 2006.

[42] T. Gallardo. Atlas of three body mean motion resonances in the Solar System. *Icarus*, 231:273 – 286, 2014.

[43] M. Giaquinta and S. Hildebrandt. *Calculus of Variations I*. Grundlehren der mathematischen Wissenschaften. Springer Berlin Heidelberg, 2004.

[44] W. B. Gordon. A minimizing property of Keplerian orbits. *Amer. J. Math.*, 99(5):961–971, 1977.

[45] G. F. Gronchi. Generalized averaging principle and the secular evolution of planet crossing orbits. *Celestial Mechanics and Dynamical Astronomy*, 83(1):97–120, May 2002.

[46] G. F. Gronchi. On the stationary points of the squared distance between two ellipses with a common focus. *SIAM Journal on Scientific Computing*, 24(1):61–80, 2002.

[47] G. F. Gronchi. An algebraic method to compute the critical points of the distance function between two keplerian orbits. *Celestial Mechanics and Dynamical Astronomy*, 93(1):295–329, Sep 2005.

[48] G. F. Gronchi and P. Michel. Secular orbital evolution, proper elements, and proper frequencies for near-earth asteroids: A comparison between semianalytic theory and numerical integrations. *Icarus*, 152(1):48 – 57, 2001.

[49] G. F. Gronchi and A. Milani. Averaging on earth-crossing orbits. *Celestial Mechanics and Dynamical Astronomy*, 71(2):109–136, Jun 1998.

[50] G. F. Gronchi and C. Tardioli. The evolution of the orbit distance in the double averaged restricted 3-body problem with crossing singularities. *Discrete and Continuous Dynamical Systems - B*, 18:1323, 2013.

[51] E. Hairer. `http://www.unige.ch/~hairer/software.html`.

[52] E. Hairer, S.P. Nørsett, and G. Wanner. *Solving Ordinary Differential Equations I: Nonstiff Problems*. Springer Series in Computational Mathematics. Springer Berlin Heidelberg, 2009.

[53] T. C. Hales. A computer verification of the kepler conjecture. *Proceedings of the International Congress of Mathematicians*, 2:795–804, 05 2003.

[54] T. C. Hales. A proof of the Kepler conjecture. *Ann. of Math. (2)*, 162(3):1065–1185, 2005.

[55] M.R. Hestenes. *Calculus of Variations and Optimal Control Theory*. Applied mathematics series. John Wiley & Sons, 1966.

[56] K. C. Howell and J. V. Breakwell. Almost rectilinear halo orbits. *Celestial Mechanics*, 32:29–52, 1984.

[57] M. Šindik, A. Sugita, M. Šuvakov, and V. Dmitrašinović. Periodic three-body orbits in the Coulomb potential. *Phys. Rev. E*, 98:060101, Dec 2018.

[58] Computer Assisted Proofs in Dynamics (CAPD), a package for rigorous numerics. `http://capd.ii.uj.edu.pl/`.

[59] À. Jorba and M. Zou. A software package for the numerical integration of odes by means of high-order taylor methods. *Experimental Mathematics*, 14(1):99–117, 2005.

[60] T. Kapela and C. Simó. Computer assisted proofs for nonsymmetric planar choreographies and for stability of the eight. *Nonlinearity*, 20:1241–1255, 2007.

[61] T. Kapela and C. Simó. Rigorous KAM results around arbitrary periodic orbits for Hamiltonian systems. *Nonlinearity*, 30(3):965–986, 2017.

[62] T. Kapela and P. Zgliczynski. The existence of simple choreographies for the N-body problem - a computer assisted proof. *Nonlinearity*, 16(6):1899–1918, 2003.

[63] K. V. Kholshevnikov and N. N. Vassiliev. On the distance function between two keplerian elliptic orbits. *Celestial Mechanics and Dynamical Astronomy*, 75(2):75–83, Oct 1999.

[64] L. D. Landau and E. M. Lifshitz. *The Classical Theory of Fields*. Butterworth-Heinemann, 4 edition, 1980.

[65] C. Marchal. How the method of minimization of action avoids singularities. *Celestial Mech. Dynam. Astronom.*, 83(1-4):325–353, 2002. Modern celestial mechanics: from theory to applications (Rome, 2001).

[66] S. Marò and G. F. Gronchi. Long term dynamics for the restricted N-body problem with mean motion resonances and crossing singularities. *SIAM Journal on Applied Dynamical Systems*, 17(2):1786–1815, 2018.

[67] R. M. M. Mattheij and J. Molenaar. *Ordinary differential equations in theory and practice*. Classics in applied mathematics. Society for Industrial and Applied Mathematics (SIAM), 2002.

[68] J.C. Maxwell. *On the stability of the motion of Saturn's Rings*. Macmillan & Company, 1859.

[69] R. McGehee. Double collisions for a classical particle system with nongravitational interactions. *Commentarii Mathematici Helvetici*, 56(1):524–557, Dec 1981.

[70] K. R. Meyer and D. S. Schmidt. Librations of central configurations and braided Saturn rings. *Celestial Mechanics and Dynamical Astronomy*, 55:289–303, 1993.

[71] A. Milani and S. Baccili. Dynamics of Earth-crossing asteroids: the protected Toro orbits. *Celestial Mechanics and Dynamical Astronomy*, 71(1):35–53, May 1998.

[72] K. Mischaikow and M. Mrozek. Chaos in the Lorenz equations: a computer-assisted proof. *Bull. Amer. Math. Soc. (N.S.)*, 32(1):66–72, 1995.

[73] R. Moeckel. Linear stability of relative equilibria with a dominant mass. *Journal of Dynamics and Differential Equations*, 6:37–51, 1994.

[74] H. Montanelli. Computing hyperbolic choreographies. *Regul. Chaotic Dyn.*, 21(5):522–530, 2016.

[75] H. Montanelli and N. I. Gushterov. Computing planar and spherical choreographies. *SIAM J. Appl. Dyn. Syst.*, 15(1):235–256, 2016.

[76] R. Montgomery. Metric cones, n-body collisions, and marchal's lemma. *arXiv e-prints*, page arXiv:1804.03059, Apr 2018.

[77] C. Moore. Braids in classical dynamics. *Phys. Rev. Lett.*, 70(24):3675–3679, 1993.

[78] C. Moore and M. Nauenberg. New periodic orbits for the n-body problem. *Journal of Computational and Nonlinear Dynamics*, 1(4):307–311, 2006.

[79] G. E. Moore. Cramming more components onto integrated circuits. *Electronics*, 38(8), April 1965.

[80] R. E. Moore, R. B. Kearfott, and M. J. Cloud. *Introduction to Interval Analysis*. Society for Industrial and Applied Mathematics, Philadelphia, PA, USA, 2009.

[81] A. Morbidelli. *Modern celestial mechanics: aspects of Solar System dynamics*. Advances in astronomy and astrophysics. Taylor & Francis, 2002.

[82] J. Moser and E. Zehnder. *Notes on Dynamical Systems*. Courant Lecture Notes. Courant Institute of Mathematical Sciences, New York University, 2005.

[83] D. Nesvorný and A. Morbidelli. An analytic model of three-body mean motion resonances. *Celestial Mechanics and Dynamical Astronomy*, 71(4):243–271, Aug 1998.

[84] D. Nesvorný and A. Morbidelli. Three-Body mean motion resonances and the chaotic structure of the asteroid belt. *The Astronomical Journal*, 116(6):3029–3037, dec 1998.

[85] L.A. Pars. *An introduction to the calculus of variations*. Wiley, 1962.

[86] F. Pérez and J. Mahecha. Classical trajectories in Coulomb three body systems. *Rev. Mexicana Fís.*, 42(6):1070–1086, 1996.

[87] H. Poincaré. Sur les solutions périodiques et le principe de moindre action. *C. R. Acad. Sci.*, 123:915–918, 1896.

[88] H. Poincaré. Sur les solutions périodiques et le principe de moindre action. *Comptes rendus hebdomadaires de l'Académie des sciences de Paris*, 124:713–716, 1897.

[89] W.H. Press, S.A. Teukolsky, W.T. Vetterling, and B.P. Flannery. *Numerical Recipes 3rd Edition: The Art of Scientific Computing*. Cambridge University Press, 2007.

[90] M. Ramos and S. Terracini. Noncollision periodic solutions to some singular dynamical systems with very weak forces. *Journal of Differential Equations*, 118(1):121 – 152, 1995.

[91] G. E. Roberts. Linear stability analysis of the figure-eight orbit in the three-body problem. *Ergodic Theory and Dynamical Systems*, 27:1947–1963, 2007.

[92] E. Rutherford. The scattering of α and β particles by matter and the structure of the atom. *Philosophical Magazine*, 21(125):669–688, 1911.

[93] A. Santander, J. Mahecha, and F. Pérez. Rigid-rotator and fixed-shape solutions to the Coulomb three-body problem. *Few-Body Systems*, 22(1):37–60, Feb 1997.

[94] C. Simó. `http://www.maia.ub.es/dsg/3body`.

[95] C. Simó. `http://www.maia.ub.es/dsg/nbody`.

[96] C. Simó. New families of solutions in N-body problems. In Carles Casacuberta, Rosa Maria Miró-Roig, Joan Verdera, and Sebastià Xambó-Descamps, editors, *European Congress of Mathematics: Barcelona, July 10–14, 2000, Volume I*, pages 101–115, Basel, 2001. Birkhäuser Basel.

[97] C. Simó. *Periodic orbits of the planar N-body problem with equal masses and all bodies on the same path*, pages 265–284. IoP Publishing, 2001.

[98] S. Smale. Mathematical problems for the next century. *The Mathematical Intelligencer*, 20(2):7–15, Mar 1998.

[99] E. A. Smirnov. Asteroids in three-body mean-motion resonances with jupiter and mars. *Solar System Research*, 51(2):145–149, Mar 2017.

[100] E. A. Smirnov and I. S. Dovgalev. Identification of asteroids in two-body resonances. *Solar System Research*, 52(4):347–354, Jul 2018.

[101] V. K. Srivastava, J. Kumar, P. Mishra, and B. S. Kushvah. Halo orbit of regularized circular restricted three-body problem with radiation pressure and oblateness. *Journal of Astrophysics and Astronomy*, 39(5):63, Oct 2018.

[102] E.L. Stiefel and G. Scheifele. *Linear and regular celestial mechanics*. Grundlehren der mathematischen Wissenschaften. Springer-Verlag, 1971.

[103] S. Terracini. On the variational approach to the periodic n-body problem. *Celestial Mechanics and Dynamical Astronomy*, 95:3–25, 2006.

[104] S. Terracini and A. Venturelli. Symmetric trajectories for the $2N$-body problem with equal masses. *Arch. Ration. Mech. Anal.*, 184(3):465–493, 2007.

[105] W. Tucker. The lorenz attractor exists. *C. R. Acad. Sci. Paris*, 328:1197–1202, 1999.

[106] W. Tucker. A rigorous ode solver and smale's 14th problem. *Foundations of Computational Mathematics*, 2(1):53–117, Jan 2002.

[107] T. Uzer, D. Farrelly, J. A. Milligan, P. E. Raines, and J. P. Skelton. Celestial mechanics on a microscopic scale. *Science*, 253(5015):42–48, 1991.

[108] A. Venturelli. *Application de la minimisation de l'action au Problème de N corps dans le plan e dans l'espace*. PhD thesis, University of Paris VII, 2002.

[109] R.J. Wilson. *Four Colors Suffice: How the Map Problem was Solved*. Princeton Paperbacks. Princeton University Press, 2002.

[110] A. Wintner. *The Analytical Foundation of Celestial Mechanics*. Princeton mathematical series. H. Milford, Oxford University Press, 1941.

[111] V. Zeidan. Sufficient conditions for variational problems with variable endpoints: Coupled points. *Applied Mathematics and Optimization*, 27(2):191–209, 1993.

[112] V. Zeidan. New second-order optimality conditions for variational problems with C^2-Hamiltonians. *SIAM Journal on Control and Optimization*, 40(2):577–609, 2001.

[113] V. Zeidan and P. Zezza. Coupled points in the calculus of variations and applications to periodic problems. *Trans. Amer. Math. Soc.*, 315(1):323–335, 1989.

[114] P. Zgliczynski. C^1 Lohner Algorithm. *Foundations of Computational Mathematics*, 2(4):429–465, 2002.